USING SCRAP TIRES AS AN AGGREGATE IN CHIP SEAL

PHASE II

Final Report	Project No. xxxxxxxxxxxxxxxxx
April 2020	MDNR-SWMP and MS&T cooperative agreement: FY 2017-2019

PREPARED BY:

Alireza Pourhassan, M.S.

Ahmed Gheni, Ph.D.

Mohamed ElGawady, Ph.D.

Missouri University of Science and Technology

PREPARED FOR:

Solid Waste Management Program

Missouri Department of Natural Resources

TECHNICAL REPORT DOCUMENTATION

1. Report No.:	2. Government Accession No.:	3. Recipient's Catalog No.:
4. Title and Subtitle: Using Scrap Tires as an Aggregate in Chip Seal - Phase II		5. Report Date: April 2020 6. Performing Organization Code:
7. Author(s): Alireza Pourhassan, https://orcid.org/0000-0001-5095-5567 Ahmed Gheni, Ph.D. https://orcid.org/0000-0001-9042-869X Mohamed ElGawady, Ph.D. https://orcid.org/0000-0001-5095-5567		8. Performing Organization Report No.:
9. Performing Organization Name and Address: Department of Civil, Architectural and Environmental Engineering Missouri University of Science and Technology 1401 N. Pine St., Rolla, MO 65409		10. Work Unit No.: 11. Contract or Grant No.:
12. Sponsoring Agency Name and Address: Solid Waste Management Program Missouri Department of Natural Resources		13. Type of Report and Period Covered: Final Report 14. Sponsoring Agency Code:
15. Supplementary Notes:		

16. Abstract:

Chip seals are one of the most cost and performance effective pavement preservation treatments commonly used in the United States. An eco-friendly chip seal pavement, in which the natural aggregate was replaced by crumb rubber obtained from scrap tires, was recently developed by the research team at Missouri S&T creating rubberized chip seal. This project investigated and optimized performance of rubberized chip seal under different scenarios. During this project, laboratory chip seal specimens with different sizes were prepared and tested under simulated traffic load with different loading parameters and environmental conditions. Also, the feasibility of the implementation and performance of rubberized chip seal in the field was investigated in two different field sections. Test results indicated that a crumb rubber replacement ratio up to 50% is appropriate for low traffic roads with 0.25 gal/yd^2 emulsion rate and aggregate with a low flakiness index. 100% rubberized chip seal was also performed considerably better for high-speed traffic, snowplowing action, and high-temperature environment. Also, a highly reliable water film depth prediction model was proposed for conventional and rubberized chip seal. Field implementation projects indicated that using up to 50% rubberized chip seal could be successfully implemented in the field using conventional chip sealing

17. Key Words:	18. Distribution Statement:
Chip seal; seal coat; rubber; scrap tires; recycling; traffic load; water film depth; raveling; bleeding	

19. Security Classif. (of this report):	20. Security Classif. (of this page):	21. No. of Pages:	22. Price:
Unclassified	Unclassified	305	

FINAL REPORT

Using Scrap Tires as an Aggregate in Chip Seal

Phase II

Prepared for

Solid Waste Management Program
Missouri Department of Natural Resources

April 2020

The opinions, findings, and conclusions expressed in this publication are those of the principal investigators. They are not necessarily those of the Missouri Department of Natural Resources. This report does not constitute a standard or regulation.

ACKNOWLEDGMENTS

The authors would like to acknowledge the many individuals and organizations that made this research project possible. The authors wish to extend a very sincere thank you to the Missouri Department of Natural Resources (MoDNR). In addition to their financial support, the authors appreciate MoDNR's vision and commitment to innovative concepts and pushing the boundaries of current practice. In particular, the success of this project would not have been possible without the support, encouragement, and patience of Messrs Chris Nagel, Richard Kempker, and Kirk Mitchell.

The authors would also like to thank Mr. Mike Mitchell, Gary Lyons and Adam Hahs from Vance Brothers for coordinating the donation of the emulsion used during the laboratory investigation during this study. The authors want to thank the Digital Surf sales and support team especially Anne Berger for providing the Mountains Map software for the research team. Finally, the authors would like to thank the many undergraduate and graduate students that contributed to this project including but not limited to Jonathan Curenton, Elizabeth Borgmeyer, Hani Alowaymir, Jacob Fitzpatrick, Alexander Gibson, Ali Alwael, Tousif Mahmood, Binod Shrestha, Mohanad Abdulazeez, and especially Md. Mashfiqul Islam of Missouri S&T.

The authors also appreciate the tireless staff of the Department of Civil, Architectural, and Environmental Engineering. Their assistance both inside and out of the various laboratories was invaluable to the successful completion of this project.

EXECUTIVE SUMMARY

Chip seals are one of the most cost and performance effective pavement preservation treatments commonly used in the United States. After an eco-friendly chip seal pavement, in which the natural aggregate was replaced by crumb rubber obtained from scrap tires, was recently developed by the research team at Missouri S&T, this project investigates and optimize its performance under different scenarios. During this project, 55 laboratory chip seal specimens with different sizes from 8 ft by 4 ft to 1 ft by 1 ft were prepared using different asphalt emulsion rates and two different natural aggregates, i.e. trap rock and creek gravel, along with crumb rubber. Different loading and environmental simulating tests including small wheel traffic simulation (SWTS) test with different loading parameters such as traffic speed, number, and magnitude, as well as different temperatures representing Missouri summer and winter, drainage capability of different chip seal samples, mechanical snowplowing test, freeze-thaw resistance of chip seal in the presence of deicing chemicals, and aggregate soundness test. The macrotexture of the chip seal specimens was examined using a 3D surface scanning during this study. Also, the feasibility of the implementation and performance of rubberized chip seal in the field was investigated in two different field sections.

SWTS test results indicated that a crumb rubber replacement ratio up to 50% is appropriate for low traffic roads, while more rubber will reduce the raveling and freeze-thaw resistance under low traffics. Using a binder application rate of more than 0.25 gal/yd^2 is recommended for emulsified asphalt since less binder rate will not provide enough raveling resistance for the conventional nor rubberized chip seal. Using flaky aggregate, whether crumb rubber or natural aggregate, is not recommended since lower fakeness was proved to provide better stability and retention under traffic. Also, flaky aggregate will be more exposed to snowplow blade in nontraffic areas leading to more aggregate loss. 100% rubberized chip seal was also performed considerably better than other aggregates for high-speed traffic, snowplowing action, and high-temperature environment, all due to the inherent characteristics of rubber, i.e., elasticity, hysteresis, and low thermal conductivity, respectively. Also, a highly reliable water film depth (WFD) prediction model was proposed for conventional and rubberized chip seal based on 1784 WFD readings.

Field implementation projects indicated that using up to 50% rubberized chip seal could be successfully implemented in the field using conventional chip sealing procedures and equipment. Also, one year filed macrotexture and skid resistance assessment showed that rubberized chip seals had a higher raveling resistance and final skid resistance than conventional chip seal.

Table of Contents

Chapter 1: Literature Review and Project Significance 1
1.1. Rubberized Chip Seal 1
1.2. Soundness of Aggregates 3
1.3. In Situ Chip Seal Assessment 5
1.4. Laboratory Chip Seal Assessment 7
1.4.1. Aggregate Loss and Bleeding 7
1.4.2. Aggregate Polishing and Skid Resistance Loss 11
1.5. 3D Scanning Technique for Macrotexture measurement 14
1.6. Chip Seal Surface Water Drainage 15
1.7. Effect of Mechanical Snow Removal 16
1.8. Effect of Chemical De-Icing on Chip Seal 17
1.9. Project Significance 19
1.10. Project Organization 21
Chapter 2: Soundness of Aggregate 23
2.1. Introduction 23
2.1.1. Soundness Test 23
2.1.2. Sulfate Soundness 24
2.2. Experimental Program 24
2.2.1. Material Properties 24
2.2.2. Test Procedure 26
2.3. Test Results 27
2.4. Conclusion 29
Chapter 3: Manufacturing the Traffic Load Simulating Machine 31
3.1. Introduction 31
3.2. SWTS Machine Fabrication 32
3.3. SWTS Applied Load 38
3.4. Macrotexture and Skid-resistance Measurements 39
Chapter 4: Construction of the Chip Seal Specimens 41
4.1. Introduction 41

4.2. Material Properties 41
4.2.1. Aggregate 41
4.2.2. Emulsified asphalt (Emulsion) 44
4.3. Design of Test Specimens 46
4.3.1. McLeod method (Single application design with one-size aggregate) 46
4.3.2. Kearby method 49
4.3.3. Modified Kearby method 49
4.4. Chip Seal Test Specimens 53
4.5. Specimen Preparation 56
Chapter 5: Effect of Traffic Load on Conventional and Rubberized Chip Seal 62
5.1. Introduction 62
5.2. Experimental Program 63
5.2.1. Test Specimens and Matrix 63
5.2.2. SWTS Test 66
5.2.3. Macrotexture Evaluation 67
5.2.4. Microtexture Evaluation 70
5.4. Macrotexture Assessment Results 72
5.4.1. Overall performance 72
5.4.2. Effect of Rubber Content 75
5.4.3. Effect of Binder Application Rate 83
5.4.4. Effect of Aggregate Type 88
5.4.5. Effect of Load Magnitude 93
5.4.6. Effect of Traffic Speed 98
5.4.2. Microtexture Evaluation 102
5.5. Conclusions 109
Chapter 6: Hybrid Traffic-Temperature Effects on Conventional and Rubberized Chip Seal Performance 112
6.1. Introduction 112
6.2. Experimental Program 112
6.2.1. Test Specimens and Matrix 112
6.2.2. Traffic-Temperature SWTS Test 114

6.2.3. Macrotexture Evaluation 117
6.3. Traffic-Temperature SWTS Test Results 120
6.3.1. Low Temperature Performance 120
6.3.2. High Temperature Performance 126
6.4. Conclusions 132
Chapter 7: Effect of Crumb Rubber on Rainfall Water Drainage 134
7.1. Introduction 134
7.2. WFD Contributing Factors 135
7.3. Experimental Program 136
7.3.1. Test Setup 137
7.3.2. Test Matrix 139
7.3.3. Test Procedure 142
7.3.4. Water Film Depth Measurement 142
7.3.5. Mean Texture Depth Measurement 143
7.4. Results and Discussion 145
7.4.1. Existing WFD Prediction Models 145
7.4.2. New WFD Prediction Model Development 146
7.5. Conclusion 154
Chapter 8: Effect of Mechanical Snow Removal 156
8.1. Introduction 156
8.2. Experimental Program 157
8.2.1. Test Specimens 157
8.2.2. Snowplowing Test 158
8.2.3. Macrotexture Evaluation 160
8.3. Snowplowing Test Results 163
8.4. Conclusions 170
Chapter 9: Effect of Freezing and Thawing Cycles with Chemical Deicing on Conventional and Rubberized Chip Seal 172
9.1. Introduction 172
9.2. Experimental Program 172
9.2.1. Test Specimens 173

9.2.2. Freeze-Thaw Test 175
9.2.3. Small-Wheel Traffic Simulation (SWTS) Test 178
9.2.4. Macrotexture Evaluation 180
9.3. Test Results 183
9.3.1. Freeze-Thaw Test 183
9.3.2. SWTS Test 187
9.4. Conclusions 190
Chapter 10: Field Implementation of Rubberized Chip Seal 192
10.1. Introduction 192
10.2. Road Location and Traffic Information 192
10.3. Field Implementation of Rolla Section 195
10.3.1. Material Properties 195
10.3.2. Construction Procedure 197
10.4. Field Implementation of The Boonville Section 200
10.4.1. Material Properties 200
10.4.2. Construction Procedure 202
10.5. Field Investigation of Rolla Section 203
10.5.1. Visual Inspection 204
10.5.2. Macrotexture Measurement Using Sand Patch Test 205
10.5.3. Skid Measurement Following ASTM E303 211
10.5.4. Skid Measurement Following ASTM E274 212
10.6. Conclusions 214
Chapter 11: Findings and Recommendations 216
11.1. Recommendations 224
References 226
Appendix A: Chip Seal Specimens Construction 232
Appendix B: SWTS Test Results for Phase I, II, and III 239
B.1. Phase I SWTS Test Results 239
B.2. Phase II SWTS Test Results 246
B.2. Phase II SWTS Test Results 248
Appendix C: Hybrid Traffic-Temperature effect SWTS test results 250

Appendix D: Rainfall Simulation Test Results 254
Appendix E: Snowplowing Test Results 263
Appendix F: Freezing and Thawing Test Procedure and Results 267
F.1. Freezing and Thawing Test Procedure 267
F.2. Freezing and Thawing Results 269
F.3. SWTS Test Results from 3D Scanning 270
Appendix G: Field Implementation Evaluation Procedure and Results 277
G.1. Construction of The Field Test Sections 277
G.2. Field Investigation of Rolla Section 280
G.3. Sand Patch Test Results of Rolla Section 282

List of Figures

Fig 1.1 – Typical cross-section of chip seal 1
Fig. 1.2 – Microtexture and Macrotexture of chip seal 3
Fig. 1.3 – Laboratory traffic load simulator devices. (a) ZJRL-07a [26], (b) MMLS3 [28], (c) HSKSC [29]. 9
Fig. 1.4 – Modified standard test. (a) modified WTL [31], (b) modified HWT [32]. 11
Fig. 1.5 – Three wheel polishing device (TWPD) (a) made by NCAT [33], (b) used by [34]..... 12
Fig. 2.1 – Used aggregate. 25
Fig. 2.2 – Aggregate soundness test procedure including (a) selected aggregates, (b) washing the test sample, (c) sodium sulfate solution preparation, (d) storage of sample in solution, (e) drying sample after immersion, and (f) weighting the sample after removing the solution. 27
Fig. 2.3 – Aggregate soundness test results. 28
Fig. 2.4 – Weight loss by aggregate soundness test versus (a) water absorption, (b) weight loss by Los Angeles test, and (c) weight loss by Micro Deval test. 29
Fig. 3.1 – SWTS drawings. (a) 3D sketch and (b) dimensions. 33
Fig 3.2 –SWTS (a) schematic and (b) real view. 34
Fig 3.3 – Wheel assembly and wheel pass. 35
Fig 3.4 – Electronic motor, gearbox and speed control unit. 35
Fig 3.5 – Digital energy meter. 36
Fig. 3.6 – Snowplow assembly (a) drawing, and (b) real view. 37
Fig. 3.7 – Snowplow test, (a) drawing showing the cutting angle, and (b) real view. 37
Fig. 3.8 – Weights added on the circular plate of the wheel assembly. 38
Fig 3.9 – Tire footage used for measuring tire contact area. 39
Fig. 3.10 – (a) Handhold portable 3D scanner, (b) basic setup of a structured light triangular system. 40
Fig. 4.1 – Natural and synthetic aggregates (a) creek gravel, (b) crumb rubber, and (c) trap rock. 42
Fig. 4.2 – Sieve analyses of used aggregate (a) batch 1, (b) batch 2. 44
Fig. 4.3 – Emulsion weight loss due to water breakout. 46
Fig. 4.4 – McLeod method: determination of average least dimension of cover aggregate. 47

Fig. 4.5 – Kearby method. 49
Fig. 4.6 – Relation of percent embedment to mat thickness for the modified Kearby method. ... 51
Fig. 4.7 – Chip seal test specimens with different sizes; (a) 8x4 ft, (b) 2x2 ft, and (c) 1x1 ft..... 55
Fig. 4.8 – Different combinations of crumb rubber and mineral aggregates used in this study. .. 55
Fig. 4.9 – Chip seal test specimen bases made of plywood; (a) 8x4 ft, (b) 2x2 ft, and (c) 1x1 ft. 56
Fig. 4.10 – Chip seal test specimen bases covered with asphalt felt; (a) 8x4 ft, (b) 2x2 ft, and (c) 1x1 ft. 57
Fig. 4.11 – Applying and spreading emulsion for making chip seal test specimens; (a) 8x4 ft, (b) 2x2 ft, and (c) 1x1 ft. 58
Fig. 4.12 – Spreading aggregate for making chip seal test specimens; (a) 8x4 ft, (b) 2x2 ft, and (c) 1x1 ft. 59
Fig. 4.13 – Compacting chip seal test specimens; (a) 8x4 ft, (b) 2x2 ft, and (c) 1x1 ft..... 60
Fig. 4.15 – Premature failure and severe bleeding due to not enough curing time. 61
Fig. 5.1 – Small-wheel traffic simulation (SWTS) test machine. 66
Fig. 5.2 – (a) Handhold portable 3D scanner, (b) basic setup of a structured-light triangular system. 68
Fig. 5.3 – 3D surface data from MountainsMap software (a) example chip seal 3D surface, (b) height distribution and Abbott-Firestone curve, (c) Abbott-Firestone curve and volumetric parameters. 69
Fig. 5.4 – Raith scanning electron microscope. 71
Fig. 5.5 – (a) Prepared samples for SEM imaging, and (b) samples on sample holder of the Raith scope. 72
Fig. 5.6 – SWTS test results after 100,000 wheel applications on Phase I specimens including (a) trap rock with 0.25 gal/yd^2 emulsion rate, (b) trap rock with 0.50 gal/yd^2 emulsion rate, (c) creek gravel with 0.25 gal/yd^2 emulsion rate, and (d) creek gravel with 0.50 gal/yd^2 emulsion rate. ... 74
Fig. 5.7 – Vm versus wheel application number for trap rock specimens with different rubber content and (a) 0.25 gal/yd^2 emulsion rate, and (b) 0.50 gal/yd^2 emulsion rate. 76
Fig. 5.8 – SWTS test results for trap rock specimens with 0.25 gal/yd^2 emulsion rate at the end of 100,000 wheel applications. (a) Vm value, (b) Vm loss percentage. 77
Fig. 5.9 – SWTS test results for trap rock specimens with 0.25 gal/yd^2 emulsion rate at the end of 100,000 wheel applications. (a) Vm value, (b) Vm loss percentage. 78

Fig. 5.10 – Vm versus wheel application number for creek gravel specimens with different rubber content and (a) 0.25 gal/yd^2 emulsion rate, and (b) 0.50 gal/yd^2 emulsion rate. 80
Fig. 5.11 – SWTS test results for creek gravel specimens with 0.25 gal/yd^2 emulsion rate at the end of 100,000 wheel applications. (a) Vm value, (b) Vm loss percentage. 81
Fig. 5.12 – SWTS test results for creek gravel specimens with 0.25 gal/yd^2 emulsion rate at the end of 100,000 wheel applications. (a) Vm value, (b) Vm loss percentage. 82
Fig. 5.13 – Microtexture comparison for trap rock specimens with different emulsion rates at the end of 100,000 wheel applications in the SWTS test. (a) Vm value, (b) Vm loss percentage. 84
Fig. 5.14 – Microtexture comparison for creek gravel specimens with different emulsion rates at the end of 100,000 wheel applications in the SWTS test. (a) Vm value, (b) Vm loss percentage. 86
Fig. 5.15 – Microtexture comparison for crumb rubber specimens with different emulsion rates at the end of 100,000 wheel applications in the SWTS test. (a) Vm value, (b) Vm loss percentage. 87
Fig. 5.16 – Bleeding distress observed in phase I tests for (a) 100C50E, (b) 75C50E specimens. 88
Fig. 5.17 – Microtexture comparison for chip seal specimens with 0.25 gal/yd^2 binder rate and different natural aggregate types at the end of 100,000 wheel applications in the SWTS test. (a) Vm value, (b) Vm loss percentage. 90
Fig. 5.18 – Microtexture comparison for chip seal specimens with 0.50 gal/yd^2 binder rate and different natural aggregate types at the end of 100,000 wheel applications in the SWTS test. (a) Vm value, (b) Vm loss percentage. 92
Fig. 5.19 – Real photo and topographic surface showing the final state of trap rock chip seal specimens tested for 100,000 wheel applications in the SWTS test under different load (a)14 psi and (b) 28 psi load pressure. 94
Fig. 5.20 – Vm versus wheel application number for Phase II specimens. 95
Fig. 5.21 – Microtexture comparison for chip seal specimens under different load magnitudes at the end of 100,000 wheel applications in the SWTS test. (a) Vm value, (b) Vm loss percentage. 96

Fig. 5.22 – Real photo and topographic surface showing the final state of trap rock chip seal specimens tested for 100,000 wheel applications in the SWTS test under traffic speed of (a)120 wpm and (b) 160 wpm. 99
Fig. 5.23 – Vm versus wheel application number for Phase III specimens. 100
Fig. 5.24 – Microtexture comparison for chip seal specimens under different load speed at the end of 100,000 wheel applications in the SWTS test. (a) Vm value, (b) Vm loss percentage. 101
Fig. 5.25 – SEM images of trap rock and crumb rubber particles before experiencing any traffic load at different magnification levels of (a) 100X, (b) 1000X, (c) 5000X, and (d) 10000X..... 105
Fig. 5.26 – SEM images of trap rock and crumb rubber particles after experiencing 100,000 wheel applications in the SWTS test at different magnification levels of (a) 100X, (b) 1000X, (c) 5000X, and (d) 10000X. 107
Fig. 5.27 – SEM image of a crumb rubber particle from a chip seal surface with bleeding distress after experiencing 100,000 wheel applications in the SWTS test at different magnification levels of (a) 100X, (b) 1000X, (c) 5000X, and (d) 10000X..... 109
Fig. 6.1 – Small-wheel traffic simulation (SWTS) (a) test machine, and (b) insulated test chamber. 115
Fig. 6.2 – (a) Handhold portable 3D scanner, and (b) basic setup of a structured-light triangular system. 118
Fig. 6.3 – 3D surface data from MountainsMap software (a) example chip seal 3D surface, (b) height distribution and Abbott-Firestone curve, and (c) Abbott-Firestone curve and volumetric parameters. 119
Fig. 6.4 – Low temperature SWTS test results after different wheel applications for (a) 0% rubber content, (b) 25% rubber content, (c) 50% rubber content, and (d) 100% rubber content..... 122
Fig. 6.5 – Vm versus wheel application number for low temperature SWTS test specimens with different rubber content..... 123
Fig. 6.6 – Vm versus wheel application number comparison between the low temperature SWTS and Phase I SWTS test specimens. 124
Fig. 6.7 –SWTS test results comparison for low temperature and Phase I specimens after 40,000 wheel applications. (a) final Vm value, and (b) Vm loss percentage. 125
Fig. 6.8 – High temperature SWTS test results after 3,000 wheel applications for (a) 0% rubber content, (b) 25% rubber content, (c) 50% rubber content, and (d) 100% rubber content..... 128

Fig. 6.9 – Vm versus wheel application number for high temperature SWTS test specimens with different rubber content..... 128
Fig. 6.10 – Vm versus wheel application number comparison between the high temperature SWTS and Phase I SWTS test specimens. 129
Fig. 6.11 –SWTS test results comparison for high temperature and Phase I specimens after 3,000 wheel applications. (a) final Vm value, and (b) Vm loss percentage. 130
Fig. 6.12 – Sevier bleeding and aggregate loss in high temperature SWTS test. (a) wheel path, and (b) tires covered with binder. 132
Fig. 7.1 – Pavement surface and WFD contributing factors. 136
Fig. 7.2 – Advanced rainfall simulation (ARS) machine (a) schematic, (b) real view. 138
Fig. 7.3 – Rainfall simulation test specimens. 140
Fig 7.4 – Rainfall runoff hydrograph. 142
Fig. 7.5 – Chip seal surface and definition of parameters. 143
Fig. 7.6 – Sand patch test on rainfall simulation test specimen. 144
Fig. 7.7 – Evaluating of existing water film depth prediction models with experimental results for (a) Gallaway model, (b) PAVDRN model. 146
Fig. 7.8 – Variation range of test different test parameters and WFD. 147
Fig. 7.9 – Effect of different parameters on WFD. 149
Fig. 7.10 – Evaluation of proposed water film depth prediction models with experimental results for (a) Eq. 7.4 model, and (b) Eq. 7.5 model. 151
Fig. 7.11 – Evaluation of proposed models for considering the effect of rubber content according to (a, b) Eq. 7.4 model, and (c, d) Eq. 7.5 model with 0.05% slope. 153
Fig 7.12 – Residual plots for WFD calculated per (a) Eq. 7.4 model, and (b) Eq. 7.5 model.... 154
Fig. 8.1 – (a) Snowplow damage between the wheel paths in the field implementation study of this project, (b) schematic view of chip seal surface in the wheel path and snowplow path. 157
Fig. 8.2 – Snowplowing assembly, (a) schematic view showing the snowplow cutting angle α, and (b) real view. 159
Fig. 8.3 – (a) Handhold portable 3D scanner, and (b) basic setup of a structured light triangular system. 161

Fig. 8.4 – 3D surface data from MountainsMap software (a) example chip seal 3D surface, (b) height distribution and Abbott-Firestone curve, and (c) Abbott-Firestone curve and volumetric parameters. 163
Fig. 8.5 – Chip seal specimens after the snowplowing test. 165
Fig. 8.6 – 3D scanned surface and Abbott curve of the snowplow path for test specimens after eight snowplow applications. 167
Fig. 8.7 – Vm of snowplow path versus the number of snowplow applications. 168
Fig. 8.8 – Vm loss percentage for different specimens after different snowplow applications.. 168
Fig. 8.9 – Horsepower consumed for snowplowing versus snowplow velocity for various cutting angles. Reproduced from [107]. 170
Fig 9.1 – Different aggregate combinations used. 174
Fig. 9.2 – Freezing and thawing test specimens. 175
Fig. 9.3 – Dike made around the specimens for ponding the deicing solution. 176
Fig. 9.4 – Freeze-thaw test procedure (a) test specimens inside the environmental chamber, (b) surface covered with 1/4 inch of the deicing solution, (c) flushing off the surface, (d) hand examination for loose aggregate, and (e) weighing the aggregate according to the type. 178
Fig. 9.5 – SWTS test machine. 179
Fig. 9.6 – SWTS test specimens made up of specimens subjected to 50 cycles of freezing and thawing with deicing chemicals before the SWTS test. 180
Fig. 9.7 – (a) Handhold portable 3D scanner, (b) basic setup of a structured light triangular system. 181
Fig. 9.8 – 3D surface data from MountainsMap software (a) example chip seal 3D surface, (b) height distribution and Abbott-Firestone curve, and (c) Abbott-Firestone curve and volumetric parameters. 183
Fig. 9.9 – Freeze-thaw test results 184
Fig. 9.10 – Crushed aggregates (circled) after the freeze-thaw test. (a) creek gravel, and (b) trap rock. 185
Fig. 9.11 – Cumulative aggregate loss after 50 cycles of freezing and thawing. 186
Fig. 9.12 – Normalized aggregate loss for (a) T75, (b) T50, (c) C75, and (d) C50 specimens.. 187
Fig. 9.13 – Specimens experienced 50 cycles of freezing and thawing with deicing chemicals after 5,000 wheel applications in the SWTS test (a) real view, and (b) 3D scanned surface. 188

Fig. 9.14 – Vm degradation after 5,000 wheel applications in SWTS for different aggregate types and rubber content..... 190
Fig. 10.1 – Location of the Rolla construction site..... 193
Fig. 10.2 – Location of the Boonville construction site..... 194
Fig. 10.3 – MoDOT three-year cycle traffic volume count map (2016) for the Rolla section... 195
Fig. 10.4 – Sieve analysis of used aggregate in the Rolla section. 197
Fig. 10.5 – Construction of rubberized chip seal using conventional equipment in the Rolla section. (a) spraying the binder, (b) uniform layer of binder sprayed on the surface, (c) spreading the aggregates, and (d) compaction using a steel roller..... 198
Fig. 10.6 – Collecting chip seal samples from the construction site..... 200
Fig. 10.7 – Sieve analysis of used aggregate in the Boonville section. 201
Fig. 10.8 – Construction of rubberized chip seal using conventional equipment including rubber tire compactor in the Boonville section. (a) spraying the binder, (b) spreading the aggregates, (c) compaction using a steel roller, and (d) companion using a rubber tire roller. 202
Fig. 10.9 – Raveling distress due to the snowplowing. 205
Fig. 10.10 – Field sand patch test on (a) visit #2 and (b) visit #5..... 206
Fig 10.11 – Variation of wheel path MTD versus (a) percentage of crumb rubber, and (b) time, from the sand patch test. 208
Fig. 10.12 – Variation of snowplowing path MTD versus (a) percentage of crumb rubber, and (b) time, from the sand patch test. 209
Fig. 10.13 – Effect of snowplowing on the ratio of the MTD on the wheel path to that on the snowplowing path. 210
Fig. 10.14 – Field British pendulum skid resistance test. 211
Fig. 10.15 – BPN versus percentage of rubber. 212
Fig. 10.16 – Locked wheel skid trailer test (LWST) results..... 213
Fig. 10.17 – Comparing LWST results for different percentages of rubber and no chip seal surface. 213
Fig. A.1 – 1 ft by 1 ft chip seal specimens' preparation. 233
Fig. A.2 – 2 ft by 2 ft chip seal specimens' preparation. 235
Fig. A.3 – 2 ft by 2 ft chip seal specimens..... 236
Fig. A.4 – 8 ft by 4 ft chip seal specimens' preparation. 238

Fig. B.1 – Phase I SWTS test results for trap rock chip seal specimens with 0.25 gal/yd^2 binder rate (a)100T25E, (b) 75T25E, and (c) 50T25E. 240
Fig. B.3 – Phase I SWTS test results for creek gravel chip seal specimens with 0.25 gal/yd^2 binder rate (a)100C25E, (b) 75C25E, and (c) 50C25E. 243
Fig. B.4 – Phase I SWTS test results for creek gravel chip seal specimens with 0.50 gal/yd^2 binder rate (a)100C50E, (b) 75C50E, and (c) 50C50E. 244
Fig. B.5 – Phase I SWTS test results for crumb rubber chip seal specimens with (a) 0.25 gal/yd^2, and (b) 0.50 gal/yd^2 binder rate. 245
Fig. B.6 – Phase II SWTS test results for trap rock specimens with 0.50 gal/yd^2. (a) W100T, (b) W75T, (c) W50T, and (d) W100R. 247
Fig. B.7 – Phase III SWTS test results for trap rock specimens with 0.50 gal/yd^2. (a) S100T, (b) S75T, (c) S50T, and (d) S100R. 249
Fig. C1 – Low temperature SWTS test results after 40,000 wheel applications for (a) L100T, (b) L75T, (c) L50T, and (d) L100R. 251
Fig. C2 – High temperature SWTS test results after 3,000 wheel applications for (a) H100T, (b) H75T, (c) H50T, and (d) R100T. 253
Fig. E.1 – 00R specimens surface analysis (a) after three snowplow applications, (b) after eight snowplow applications, and (c) outside the snowplow path. 263
Fig. E.2 – 25R specimens surface analysis (a) after three snowplow applications, (b) after eight snowplow applications, and (c) outside the snowplow path. 264
Fig. E.3 – 50R specimens surface analysis (a) after three snowplow applications, (b) after eight snowplow applications, and (c) outside the snowplow path. 265
Fig. E.4 – 100R specimens surface analysis (a) after three snowplow applications, (b) after eight snowplow applications, and (c) outside the snowplow path. 266
Fig. F.1 – Freezing and thawing test procedure. 268
Fig. F.2 – SWTS test results for 50C specimen. 270
Fig. F.3 – SWTS test results for 50T specimen. 271
Fig. F.4 – SWTS test results for 75C specimen. 272
Fig. F.5 – SWTS test results for 75T specimen. 273
Fig. F.6 – SWTS test results for 100C specimen. 274
Fig. F.7 – SWTS test results for 100T specimen. 275

Fig. F.8 – SWTS test results for 100R specimen. 276
Fig. G.1 – Construction of the Rolla field test sections. 277
Fig. G.3 – Field investigation visits. 281

List of Tables

Table 2.1 – Aggregate Properties 25
Table 4.1 – Aggregate Properties 43
Table 4.2 – Asphalt Emulsion Properties 45
Table 4.3 – Summary of Chip Seal Design Methods 52
Table 4.4 – Chip Seal Test Specimens 53
Table 5.1 – Polishing Test Matrix 65
Table 6.1 – Traffic-Temperature SWTS Test Matrix 113
Table 6.2 – Batch 1 and Batch 2 Aggregate Comparison 117
Table 7.1 – Test matrix 141
Table 7.2 – Mean texture depth values of the test specimens 144
Table 8.1 – Snowplowing Test Specimens 158
Table 9.1 – Deicing Test Specimens 175
Table 9.2 – SWTS Test Results from 3D Scanned Surface 189
Table 10.1 – The Rolla Section Aggregate Properties 196
Table 10.2 – The Boonville Section Aggregate Properties 201
Table 10.3 – Summary of Field Investigation Visits 204
Table D.1 – Total Water Depth Readings for Rainfall Simulation Test with 0.5% Slope 254
Table D.2 – Total Water Depth Readings for Rainfall Simulation Test with 1.5% Slope 257
Table D.3 – Total Water Depth Readings for Rainfall Simulation Test with 2.5% Slope. 259
Table D.4 – Mean Texture Depth Readings for Rainfall Simulation Test Specimens 261
Table F.1 – Volume of Aggregate Loss for Each Test Specimen after Every 5 Cycles. 269
Table G.1 – Sand Patch Test Results at the Wheel Path 282
Table G.2 – Sand Patch Test Results at the Snowplowing Path 283

Chapter 1: Literature Review and Project Significance

1.1. Rubberized Chip Seal

Chip seal is a single layer of bitumen binder, typically followed by a single layer of embedded aggregate (Fig. 1.1). Using chip seal is one of the most common and cost-effective maintenance treatment approaches to improve the life-time of pavements [1]. It is mainly used to seal the fine cracks on the surface of the pavement, which leads to avoiding water penetration into the underlying layers. Moreover, chip seals are applied as the primary pavement in low traffic volume roads. The practice of this kind of pavement is becoming more widespread as the need for maintaining the current roads increased and the funds allocated for this purpose were not sufficient; since chip seals provide a comparatively inexpensive permanent pavement surface [2].

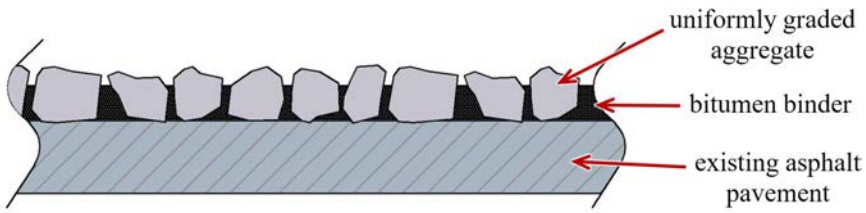

Fig 1.1 – Typical cross-section of chip seal

Used for almost every road, building, and infrastructure element all over the world, civil engineering works consume a huge amount of stone aggregates. More than 16 billion tons of aggregate is produced globally each year and it is rapidly increasing [3]. The excavation, processing, and transporting procedures relating such large amounts of aggregate, consume significant amounts of energy which leads to CO_2 emission, and also apply negative environmental impacts on forested areas and riverbeds [4, 5].

On the other hand, there is a serious environmental problem regarding scrap tires in the world. Only during 2017, more than four million tons of scrap tires were generated in the U.S. This huge number of scrap tires occupy vast landfills and waste precious resources of rubber material each year. During 2017, about 43% of scrap tires in the U.S. were used as tire-derived fuel mainly in cement kilns, while burning the tires will release hazardous substances in air and groundwater resources. The contribution of civil engineering, which is a cleaner recycle for scape tires, was only 8% [6].

Researches show that rubber is a viable option for partial or full substitute of stone aggregates to obtain an eco-friendly chip seal. Crumbed rubbers obtained from recycled tries enhanced the macrotexture, as well as, the micro-texture of the chip seal (Fig. 1.2). Rubberized chip seal is also capable of resisting high temperatures without a substantial decrease in friction resistance [7]. The scrap rubber behavior regarding aggregate retention is also better than the mineral aggregates [8, 9]. This fact also addresses the issue of dislodging of the aggregate that can be dangerous for passing vehicles and humans. The leaching behavior of rubberized chip seal under different conditions was also found to be safe according to EPA drinking water standards [10]. Other issues addressed by using the rubberized chip seal are the roadway noise and the rocky color associated with the conventional chip seal. Since a fog seal is commonly applied to finished conventional chip seal to display a dark color while rubberized chip seal will provide a black surface. The last two factors help for a better perception of the chip seal pavement by the public.

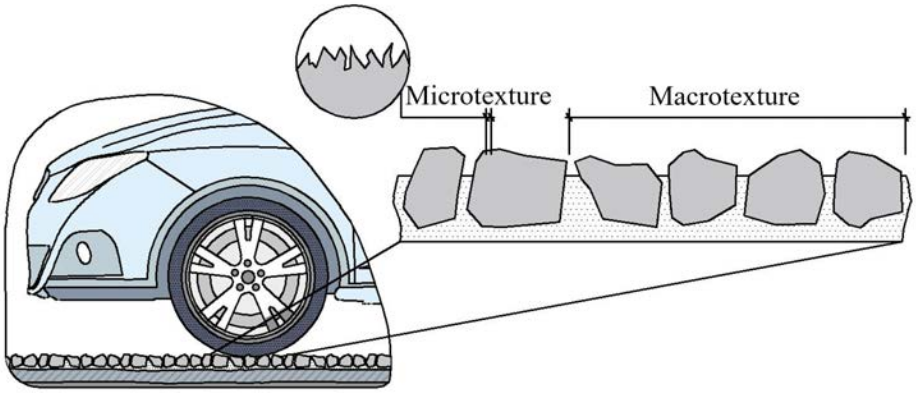

Fig. 1.2 – Microtexture and Macrotexture of chip seal

This project assesses different parameters that affect the design and performance of conventional and rubberized chip seal, i.e., traffic characteristics, seasonal climate conditions, snowplowing effect and rainwater drainage. An extensive literature review on the impact of freezing and thawing on different aggregate types, the performance assessment of chip seal in the field and the laboratory, using 3D scanning techniques for macrotexture measurements, chip seal surface water drainage, the effect of de-icing chemicals and freezing and thawing cycles on chip seal, and effect of snow plowing on chip seal is presented in this chapter. Finally, the significance of this project is briefly discussed and the report organization is presented.

1.2. Soundness of Aggregates

A national survey of specifications shows that 53 percent of the states have requirements for sodium sulfate soundness, 19 percent magnesium sulfate soundness, 10 percent a freeze-thaw loss requirement, 2 percent (1 state) the Durability Index Test, and 16 percent no soundness requirement. Maximum allowable sodium sulfate soundness loss ranges from 5 to 25 percent with an average of about 14 percent. Range and average for magnesium sulfate soundness are 10 to 30 percent and 16 percent, respectively [11].

In the National Cooperative Highway Research Program (NCHRP) report 453, the magnesium soundness test was recommended as one of the performance-base tests for selecting aggregates for use in unbound pavement layers. Aggregates used by state DOTs in highway construction projects were selected for this study composed of limestone, granite, trap rock, sandstone, and naturally occurring river gravels and glacial deposits. The Magnesium Sulfate Soundness test results for the coarse fraction correlated well with the rating, and other test parameters were selected to represent the category in further analysis. It was recommended that only the magnesium sulfate test be used since it provides more precise values than the sodium sulfate [12]. Another study also conducted sodium sulfate and magnesium sulfate soundness tests on different types of natural aggregate form different resources. The soundness test results showed a more severe effect with magnesium sulfate compared to sodium sulfate. Also, it was concluded that Micro-Deval and magnesium sulfate soundness tests were able to separate good and fair aggregates from poor aggregate [13].

The sulfate soundness test has come under scrutiny because of its lack of precision [14, 15] and poor correlation between the sulfate soundness test results and the actual performance were reported [16, 17]. However, some other studies [18, 19] found a good correlation between the sulfate soundness test and the filed performance of asphalt concrete for characterizing aggregate soundness.

Despite the abundant use of the ASTM C88 sulfate and magnesium soundness test, there is no soundness test in the literature being conducted for crumb rubber particles. Therefore, there is a pressing need to fill the gap in the literature for the prediction of the freeze-thaw durability of rubber particles.

1.3. In Situ Chip Seal Assessment

Characteristics of the chip seal surface vary by time as the traffic load passes on the pavement. Chip seal major distress by time are oxidation, aggregate wear, aggregate polishing, bleeding and aggregate loss [1]. The most common practice to evaluate the performance of chip seal is by surveying and mostly visual inspection. Two thousand lane-feet of test areas were constructed using good quality and local low-quality aggregate on two low volume state highways. The roads were monitored by visual condition surveys for three years and results indicated no significant difference in performance between the aggregates. Distress in both pavements was limited to a return of transverse and longitudinal cracks, but with low percentages of chip loss. Some limited areas of the pavements also contained longitudinal flushing streaks where distributor nozzles may not have been adjusted correctly and higher quantities of asphalt were applied [20].

The effect of construction parameters such as emulsion application rate, rolling patterns, and curing time on the aggregate retention was monitored over one year by visual assessments. The results indicated that macrotexture loss is the most important deterioration factor in chip-sealed pavements; initial texture depth is also important concerning the long-term performance of chip-sealed pavements. Rolling operations are another important factor for the performance of chip seal. If rolling operations are performed at high ambient temperatures, the percent embedment of the aggregate will increase, causing the chip seal to deteriorate more rapidly. Consequently, the ambient temperature during the construction of chip seal is important; thus, chip seal should not be constructed at ambient temperatures lower than 30 C or higher than 43.5 C [21].

A road sections constructed using four variables of emulsion rate, number of roller passes, existing pavement surface condition, and time of traffic control. The road was monitored for 1 year by visual inspection, measuring skid resistance (ASTM E274) and mean texture depth (sand patch).

It was concluded that the emulsion application rate was the most influential factor in the long-term performance of a chip seal where a higher emulsion application rate up to 0.41 gal/yd^2 was more appropriate [22].

Eight different chip seal test sections were constructed on existing asphalt concrete as the pavement preservation technique using two different binder types. The road was monitored for 1.5 years by sand-patch test and visual evaluations. The results showed that CRS-2L emulsified asphalt performed better than B100/150 penetration hot asphalt cement as a binder. Also, it was concluded that the loss of aggregate on the passing lane, i.e., left lane, of the road was much higher than that on the right lane because of traffic speed, acceleration, and deceleration [23].

A comprehensive study was conducted to evaluate the performance of chip seals applied on Kansas highways from 1992 to 2006. Profilometer equipment with laser sensors was used to collect roughness, a rut bar profilometer used to measure the rutting depth, and fatigue and transverse crackings were measured manually. It was concluded that chip seal can effectively mitigate the progression of distresses such as transverse and fatigue cracking and rutting. Also, the results showed a similar service life for chip seal as thin overlay treatments. The average service life of chip seals in Kansas was about four years [24].

Finally, a study applied a traffic loading using a five-axle tractor semi-trailer truck loaded to 80,000 lb and 102,500 lb on two different lanes of a chip seal road. It was concluded that the long-term performance of a chip seal is more dependent on the number of trucks passes rather than the truck loading [25].

As it is observed in the literature, the long-term monitoring of implemented chip seal is crucial, but time-consuming which takes years. Besides, there is no control over the type and number of traffic loads during this long period of time. Since the traffic load varies significantly

by different vehicle weight, axle configuration, and speed. There is a pressing need to fill the gap in the literature by investigating the impact of different traffic load parameters under different conditions. Besides, it is required to isolate the effect of each parameter from the others since this was not clear in the literature.

1.4. Laboratory Chip Seal Assessment

1.4.1. Aggregate Loss and Bleeding

In order to evaluate aggregate retention performance of chip seal surfaces, sweeping test, Vialit test, and Pennsylvania Aggregate Retention Test are widely used in the literature. Each of these tests has a different sample preparation process and applies various types of mechanical energy to evaluate the bond between the aggregate and binder. However, none of these methods applies a mechanical wheel load simulating real traffic conditions. Moreover, since chip seal consists only of a surface layer with binder and aggregate and not a strong structural layer, the effects of heavy traffic are magnified. Therefore, there is a need to develop a test protocol that requires chip seal specimens to be subjected to relatively heavy loading conditions.

Beside aggregate retention, bleeding, i.e., the rise of asphalt binder to the surface is another major chip seal distress. The binder fills the voids in the aggregate and spreads on the surface which leads to lower skid resistance. It is usually observed in the wheel path and areas of frequent loading such as intersections where slow traffic and turning movements cause a higher stress condition at the chip seal surface. Also, at elevated temperatures, binder might be picked up by the tires and lead to catastrophic failures in chip seals. Few studied have focused on studying bleeding of chip seal in the laboratory since there is no standard test for this means and the common tests mentioned earlier are not capable of characterizing the bleeding distress.

Few studies found in the literature which applied a simulated wheel loading on chip seal specimens. A pavement surface wear tester namely “ZJRL-07a” was used in China to evaluate the aggregate loss of rubber asphalt chip seal samples under different temperatures, loading speeds, and binder rates (Fig. 1.3a) [26]. Temperatures ranging from 32˚F to 86˚F, loading speeds from 12 to 37 miles per hour, and rubber asphalt quantities from 2.9 to 4.4 lb/yd^2 were tested. The results showed no aggregate loss at 86˚F and the aggregate loss was increased with the reduction of the temperature. Also, the aggregate loss increased with increasing the loading speed.

In North Carolina State University, a third-scale model mobile loading simulator (MMLS3) was developed (Fig. 1.3b). It was consist of four bodies each with a tire with one-third the diameter of a standard truck tire. MMLS3 was deployed to evaluate the performance of hot-mix asphalt pavement. However, it was also used to study the effect of emulsion and aggregate application rates, aggregate gradation, source, and fines content on aggregate loss [27]. MMLS3 was used with a wheels travel speed of 5,500 wheel applications per hour (1.53 Hz) with surface contact stress of about 152 psi. The results showed that the aggregate loss can be reduced by decreasing the aggregate application rate, increasing the emulsion application rate, decreasing fines content, and using uniform aggregate gradation. The aggregate loss criterion used in this study was the percentage of the weight loss of the chip seal sample before and after applying the traffic load. This study also showed a better aggregate retention performance for the lightweight aggregate compared to the normal weight aggregate. However, another study using MMLS3 showed a higher rate of aggregate loss for lightweight aggregate compared to normal weight aggregate [28]. The mean profile depth (MPD) for the specimens that experienced traffic loading in the field and MMLS3 was compared [25]. It was found that the MPD values obtained from MMLS3 and filed traffic loading are similar. Also, from the comparison of two field traffic loaded samples, it was

observed that higher traffic volume at the same number of equivalent wheel passes, resulted in more reduction of MPD.

(a) (b)

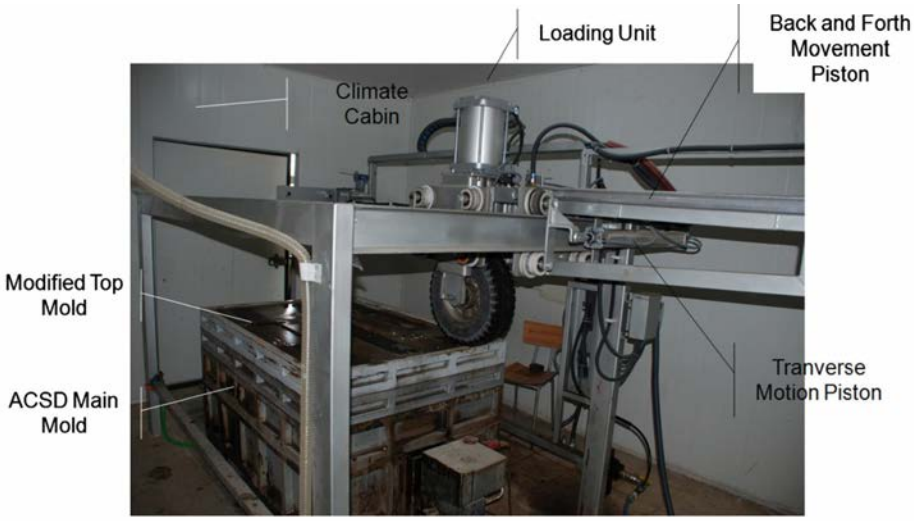

(c)

Fig. 1.3 – Laboratory traffic load simulator devices. (a) ZJRL-07a [26], (b) MMLS3 [28], (c) HSKSC [29].

An accelerated chip seal simulation device namely “HSKSC” was used in Turkey to study the retention performance of chip seal with different binder types and different aggregate types and conditions, i.e., clean, dusty, and precoated (Fig. 1.3c) [29]. HSKSC was used to simulate the

traffic load using a 5.5 inches wide tire moving back and forth on the pavement surface. Chip seal samples were tested under a load of approximately 1100 lbs and a wheel travel speed of about 1,500 wheel applications per hour (0.42 Hz). It was found that most of the aggregate loss occurs during the initial wheel loading and logarithmic functions express the aggregate loss trend. Precoated aggregate found to perform better than clean aggregate and clean aggregate performed better than dusty aggregates in terms of aggregate retention. Also, they found that using the modified binder improved the adhesion between the binder and aggregate compared to the neat binder. The aggregate loss criterion used in this study was the percentage of the weight loss of the chip seal sample before and after applying the traffic load.

Due to the high manufacturing costs of the proposed devices, in some studies, the standard devices were modified to evaluate chip seal performance including the ASTM D6372 [30] standard Loaded Wheel Test (LWT) [31] and Hamburg Wheel Tracking device (HWT) [32] (Fig. 1.4). LWT was used with a modified base plate and supports. Also, a neoprene foam was used between the chip seal sample and the base steel plate to represent existing flexible pavement. The presence of the neoprene foam provided less aggregate loss and more bleeding for the chip seal compared to the case that chip seal was only steel plate as the base. Also, the steel tire of LWT was replaced with a rubber tire and a rubber mat was placed between the wheel and the tire in order to distribute the load on the surface. The percentage of bleeding was calculated using an image processing method. Modified LWT test results showed that increasing the temperature, loading cycle, and contact stress will increase the percentage of bleeding.

HWT was modified by using a rubber tire and a load of 125 lbs. Bleeding susceptibility was evaluated at 54˚C under a wet condition and 2500 HWT cycles. Aggregate loss susceptibility was evaluated at 19˚C under the dry condition and 10 HWT cycles. Using these two tests and

image analysis techniques, the percent of embedment limits were evaluated for two different types of aggregate sources and two different types of emulsions. Based on the test results obtained from modified HWT and image analysis, the embedment limits of a minimum of 58% to a maximum 70% were established.

(a) (b)

Fig. 1.4 – Modified standard test. (a) modified WTL [31], (b) modified HWT [32].

1.4.2. Aggregate Polishing and Skid Resistance Loss

Also, very few studies have implemented wheel loading simulator machines to study the polishing wear of aggregate. In a study conducted at the National Center for Asphalt Technology (NCAT), an accelerated polishing device namely three-wheel polishing device (TWPD) was developed (Fig. 1.5a) [33]. TWPD was initially developed to evaluate the friction resistance of hot

mixed asphalt mixtures (HMA) and was widely used for HMA and concrete pavement slabs. However, few studies used TWPD for chip seal. TWPD was tried to be affordable and it was capable of providing different normal load and speed. Three tires polishing the pavement slabs on a circular path of 11.18 inches diameter which matched with the circular motion path of dynamic friction tester (DFT). The NCAT test protocol for TWPD was a 91 lb load, 60 rpm operational speed and 50 psi tire pressure. However, it was used with diverse loads, tire pressures, tire types, and rotational speeds in the literature.

(a) (b)

Fig. 1.5 – Three wheel polishing device (TWPD) (a) made by NCAT [33], (b) used by [34].

Chip seal samples with a range of high to low polished stone value aggregates were subjected to polishing via TWPD to equilibrium skid resistance levels and tested with DFT (Fig. 1.5b) [34]. A 125 lb weight and 20 psi tire pressure were used for TWPD. The results showed that

the final equilibrium skid resistance levels for different natural aggregate were very close and the polishing stone value test is not a good indicator of the equilibrium level of skid resistance.

MMLS3 that was described earlier was also used for evaluating the skid resistance of the chip seal specimens made with lightweight and granite aggregate [35]. Skid resistance was measured using the British pendulum test after polishing the samples under simulated traffic load in MMLS3. The British pendulum number (BPN) was obtained after about 2 hours of load application at 77˚ F (aggregate retention test) and then after about 4 more hours of load application at 122˚ F (bleeding test) for each sample. Lightweight aggregate had a higher British pendulum number than granite aggregate before and after the bleeding MMLS3 test; the same trend was found in the results for the double seals using lightweight aggregate. The results after MMLS3 loading were confirming the results obtained from the field loading.

In another study, skid resistance of chip seal produced with different aggregate types including slags and with different aggregate sizes at different polishing levels was investigated using the British pendulum test. Aggregate polishing action was provided by the Micro-Deval test machine [ref] and the polishing level was controlled by its' revolutions. However, it does not represent the real aggregate-wheel interaction condition in the field [36].

Different parameters such as temperature, number, and speed of vehicles and vehicles' load magnitude are influencing different chip seal distresses. Therefore, there is a need to study the individual effect of each parameter under a realistic traffic loading mechanism close to the field condition.

1.5. 3D Scanning Technique for Macrotexture measurement

Pavement macrotexture with a wavelength range of 0.02 to 0.2 in is a critical factor for evaluating the performance of the road surface [1]. The conventional approaches for macrotexture measurement have several limitations. Among others, sand patch is the most common technique of measuring the macrotexture of pavements. Sand patch methods cannot be performed when the road surface is sticky or wet. More importantly, sand patch technique gives only one indication of macrotexture which is the mean profile depth (MTD). However, MTD is not the only contributing factor affecting friction, noise [37] and surface drainage. Texture distribution, size, and spacing are also significant contributing factors.

2D profilers have been used in many studies to evaluate the macrotexture of pavement surfaces [38-44]. In some studies, 3D texture scanners were used to extract sections as texture profile and the 2D profile was used for texture measurements [45]. However, 2D profiles vary a lot within the same pavement and using a 3D surface will obtain more accurate information about the surface compared to a 2D profile [42, 46, 47]. Besides, MTD from sand patch test or MPD (mean profile depth) from laser-based testings could be strongly affected by irregularities in the profile.

Besides the more accurate measurement, a 3D surface texture will provide more detail and additional information about the pavement surface and allow a better understanding of the surface characterizations. An experiment on the use of a triangulating desktop laser scanner on various types of asphalt for texture characterization was proposed in a study [47]. Areal and profiles approaches were compared for various surface roughness parameters of ISO 13473 and ISO 13565. The results indicated a high accuracy and reliability for texture characteristics which can be used for different surface performances. For instance, the previous studies have mostly characterized

the chip seal aggregate loss from an empirical perspective, without direct consideration of the macrotexture variations such as aggregates embedment or reorientation. Other data such as adherence, tire-pavement grip and compressing level could be also obtained from 3D surface texture [48]. A 3D surface texture could be also used to perform different volumetric studies, such as the simulation of the process by which surface voids get filled by water in case of a rainfall event, to evaluate the pavement ability to ensure a dry contact for tires.

In summary, the sand patch test cannot be performed on a wet surface, limited surface area, or windy condition. Using a surface profiler provides more information about the surface macrotexture. However, the 2D profile of the surface can be significantly affected by irregularities in the profile such as an abnormally large or small particle. While a 3D surface texture can provide different volumetric information and details about the surface and is more accurate. 3D scanning will obtain information on the areal surface layer through a single measurement.

1.6. Chip Seal Surface Water Drainage

To estimate the WFD, few models have been developed based on laboratory, field data or hydrodynamic models. In several studies regarding the pavement drainage modeling, the effect of pavement texture was ignored, and the pavement surface was assumed to be smooth [49-52]. Few models considered pavement texture, pavement geometry, rainfall intensity, and even permeability effects [53] or weather conditions [54]. Field test validations showed that Gallaway [55] and PAVDRN [56] models are the most accurate models to predict WFD [57, 58].

Nevertheless, the WFD prediction models presented in the literature are mostly developed not for surfaces with very high texture depth such as chip seal. Gallaway model only includes two chip seal surfaces out of eight tested surfaces while the other six surfaces had a significantly lower

texture depth than chip seal. Even though Gallaway et al. reported a more pronounced effect of texture depth on WFD with texture depths greater than 0.050 inches based on the experimental results; the same equation is proposed for all ranges of macrotextures. Also, the rainfall intensities used in Gallaway method development were in the ranges that do not affect high textured surfaces like chip seal since it will only fill the texture storage and will not usually form a water film, i.e., runoff, over the texture. Moreover, the method used by Gallaway et al. for measuring the macrotexture, i.e., silicon putty impression method, is neither a standard nor common technique nowadays. However, sand patch test is a standard and very common technique for macrotexture measurement in both field and laboratory investigations, the results of macrotexture measurement by different methods do not necessarily agree or correlate [59]. For these three reasons, the results of WFD from the existing methods may not be precise for chip seal surfaces.

1.7. Effect of Mechanical Snow Removal

Mechanical snow removal, i.e., snowplowing action, significantly affecting the chip seal life. Using uniformly graded and crushed aggregate, aggregate with lower flakiness index, and increasing the aggregates embedment rate were considered as factors that reduce the snowplow damage [60]. Since uniformly graded aggregate will provide a more even surface withstanding better against the snowplow action. The higher angularity of the aggregates will provide a better interlock. Less flakiness of the aggregate will lead to less exposure of the aggregate in the areas that do not experience traffic load. Embedment rate of around 70% was found helpful to resist the snowplow damage, therefore, an additional calculation has been added to the McLeod design approach to account for more aggregate embedment rate to reduce snowplow damage. Moreover, the binder elastomer characteristics were found to reduce snowplow damage [61]. Another

founding for reducing the snowplow damage to the chip seal surface was using fog seal. Fog seal has reduced snowplow damage by increasing aggregate embedment by approximately 15% [62]. Another study recommends using aggregate gradation including fine particles to increase the stability of aggregates in chip seal [63].

Although previous studies by the authors have shown better retention of crumb rubber particles in the binder compared to natural aggregate, there is no study in the literature to investigate the effect of a snowplow on crumb rubber particles in chip seal and comparing it with natural aggregates. Also, there was no study including a controlled application of snowplow on a chip seal surface to investigate its effect.

1.8. Effect of Chemical De-Icing on Chip Seal

In cold regions, harsh temperature fluctuation causes freezing and thawing cycles which influence the performance of pavements. Effect of freeze and thaw cycles on asphalt mixtures is studied by many researchers and known as the major cause of asphalt mix deterioration in cold areas [64-72]. These deteriorations are mostly occurring because of the adhesion and cohesion loss in the asphalt mix during freeze-thaw cycles. However, very few studies have been conducted to directly investigate the performance of chip seal pavements under low temperature and freeze-thaw cycles, although the surveys conducted in US and Canada showed that the cold climate considerations including freezing cycles, snowplowing, etc. are the major factors that determine the life span of the chip seal pavements [1].

The binder used in asphalt concrete and chip seal has the same asphalt bases [73], therefore, it is expected that the chip-seal life-time would be affected widely by harsh temperature as asphalt

concretes do. Since deterioration of asphalt mixtures are mainly caused by interface adhesion failure between aggregate and asphalt [74, 75] as well as volume expansion of water [76].

Yazgan [77] proposed a test method of freeze-thaw for chip seal following by imposing impact load at specimens. In their method, the chip seal samples went through different numbers of freeze-thaw cycles followed with soaking and then the specimens were subjected to impact loading three times by MPH. Results showed that not only the numbers of freeze-thaw cycles but also the duration of the soaking process after freeze-thaw cycles increased the aggregate loss. Nazimuddin et al. [78] performed freeze-thaw cycles for chip seal specimens with different emulsion and aggregate types. The freeze-thaw cycles were conducted in the presence of water on the surface. The test was conducted for two cycles and the loose aggregate was collected after each cycle. Significantly better performance for CRS-2P emulsion compared to hot asphalts namely PAC-15 and AC20-5TR was found. Also, both precoated and uncoated expanded shale lightweight aggregate performed comparatively very well against freeze-thaw. You et al. [79] used the Vialit aggregate retention test and interface bond test both at different temperatures and showed the reduction of the bond between the asphalt-emulsion and aggregate in freezing temperature.

In addition to freeze-thaw cycles, in order to provide security and mobility of traffic with an ice-free surface, pavements are exposed to deicing salt during the winter season. This is also the case in coastal roads exposing to salty seawater due to tides and/or storms. Accumulated salt on the asphalt concrete surface can lead to erosion and crystal formation which damages the asphalt material [80]. The existence of deicing agents has proven to intensify the freeze-thaw damage on asphalt concrete [81, 82]. It has also shown that salt affects the rheological properties of asphalt mixtures and asphalt binders leading to degraded service performance and durability [76, 83, 84]. Some studies have been conducted to investigate the effect of different deicing agents on asphalt

concrete [82, 85]. Hassan et al [82] found that for all the used deicers, critical concentration was in the range of 1% to 2%. They also found that quartzite which is alkaline aggregate were more susceptible to deicing agents than limestone as an acidic aggregate. It was also concluded that the durability of different aggregate through the freeze-thaw cycles with deicing agents might not be attributed to the difference in chemical composition, but rather to the difference in the micro-structure and contact area of aggregate subjected to deicing solution.

However, no study has been conducted on chip seal pavement investigating the effect of deicing agents. Also, the immerging sustainable chip seal made of crumb rubber particles is not studied in terms of freeze-thaw and deicing agents. Therefore, freeze-thaw cycles and using a deicing agent may have a significant effect on the performance of chip seal.

1.9. Project Significance

Using crumb rubber as a particle and full replacement of mineral aggregate in chip seal construction with an environmental-friendly approach has been proposed by the authors in the previous studies. However, there are still many uncertainties regarding the performance of the rubberized chip seal which needed to be addressed.

- Despite the abundant use of the ASTM C88 sulfate and magnesium soundness test, there is no soundness test in the literature being conducted for crumb rubber particles. Therefore, there is a need to fill the gap in the literature for the prediction of the freeze-thaw durability of rubber particles.
- The long-term monitoring of the implemented chip seal is crucial, but time-consuming which takes years. Besides, there is no control over the type and number of traffic loads during this long period of time. Since the traffic load varies significantly by different

vehicle weight, axle configuration, and speed. There is a pressing need to fill the gap in the literature by investigating the impact of different traffic load parameters under different conditions.

- Although authors have studied the aggregate retention behavior of crumb rubber as chip seal aggregate, those testes were not applying a similar loading mechanism as it is applying by vehicular wheels in the field. Therefore, a field and a laboratory raveling resistance assessment of the conventional and rubberized chip seal is needed.
- There is no standard test to evaluate the bleeding performance of the chip seal surfaces. Bleeding usually happens in the wheel path due to the traffic load. Chip seal is also more susceptible to bleeding in high temperatures. Therefore, a bleeding resistance assessment of the conventional and rubberized chip seal in normal and high temperature under the traffic load is needed.
- The performance of chip seal surfaces at different temperatures will be different due to the thermo-plastic visco-elastic behavior of asphalt material. Also, the bond between the different particles, i.e., natural aggregate or rubber particles, may be different in different temperatures. No study has been conducted to study the effects of temperature on performance or bond of the rubberized chip seal.
- There is no study regarding the drainage capability of the rubberized chip seal. Existing water film depth prediction models did not include any rubberized surface. Also, they did not include very highly textured surfaces such as chip seal and very high rainfall intensities representing the flash flood condition.

- There is no study in the literature to investigate the effect of a snowplowing action on rubberized chip seal and comparing it with conventional chip seal. Also, there was no study including a controlled application of snowplow on a chip seal surface to investigate its effect.
- No study has been conducted on chip seal pavement investigating the effect of deicing agents. Also, the immerging sustainable chip seal made of crumb rubber particles is not studied in terms of freeze-thaw resistance. Freeze-thaw cycles and using a deicing agent may have a significant effect on the performance of chip seal.
- It was necessary to investigate the applicability and feasibility of the implementation and performance of rubberized chip seal in the field. The feasibility of implementing a rubberized chip seal in the field using conventional machinery and equipment and the field performance of rubberized chip seal with different percentages of rubber is a critical gap which is needed to be addressed.
- There are some limitations to the conventional sand patch test to measure the macrotexture of surfaces. 2D profilers have widely used in the literature as a sand patch replacement, however, the 2D profile of the surface can be significantly affected by irregularities in the profile. A 3D surface texture can provide different volumetric information and more details about the surface while it is more accurate. 3D scanning will obtain information on the areal surface layer through a single measurement.

1.10. Project Organization

This report includes 11 chapters. Chapter 1 presents an introduction to rubberized chip along with a description of the significance of this project with an extensive literature review

within the scope of this work. Chapter 2 presents the soundness test and its results for two natural aggregate and crumb rubber particles. Chapter 3 includes the design and manufacturing details of the small wheel traffic simulator (SWTS) test machine used in this study. Chapter 4 presents the material characterization and chip seal specimens' details and construction process. Chapter 5 presents the SWTS test and results for different chip seal specimens with different aggregate type and emulsion rate along with different loading parameters. Chapter 6 includes the SWTS test for hybrid effects of winter or summer temperatures of Missouri state and traffic load for conventional and rubberized chip seal. Chapter 7 presents a water film depth prediction model for conventional and rubberized chip seal which represents the drainage capability of the surface in different conditions. Chapter 8 presents the snowplowing test and results for conventional and rubberized chip seal. Chapter 9 includes the freeze-thaw test in the presence of deicing chemicals for conventional and rubberized chip seal. Chapter 10 includes two different field implantation projects along with field feasibility and performance assessment of rubberized chip seal. Chapter 11 presents the conclusion and recommendations of this project.

Chapter 2: Soundness of Aggregate

2.1. Introduction

Resistance to degradation by weathering action is a major factor affecting the wear rate of aggregates [86-88]. The sulfate soundness test is one of the most widely used tests for the prediction of freezing and thawing durability of aggregates. The test is conducted in accordance with ASTM C88 [89], and either sodium sulfate or magnesium sulfate may be used. The test was initially developed in 1828, for the purpose of simulating the forces acting on building stone by freezing moisture. In the early nineteenth century, there was no way to freeze water in a controlled laboratory setting, so the growth of salt crystals proved to be a suitable alternative. ASTM adopted magnesium sulfate soundness as a tentative test in 1931, and as a standard test method in 1963.

The objective of this task is to evaluate the resistance of crumb rubber particles to disintegration in a saturated solution of sodium sulfate and compare it to that of different types of aggregate, including trap rock and creek gravel. The results of this task will be helpful in judging the soundness of crumb rubber as well as mineral aggregates subjected to weathering actions.

2.1.1. Soundness Test

The soundness test determines an aggregate's resistance to disintegration by weathering and, in particular, freeze-thaw cycles. Aggregates that are durable, i.e., resistant to weathering, are less likely to degrade in the field and to cause premature pavement distress and potentially, failure.

The soundness test repeatedly submerges an aggregate sample in a sodium sulfate or magnesium sulfate solution. This process causes salt crystals to form in the aggregate's water-

permeable pores. The formation of these crystals creates internal forces that apply pressure on aggregate pores and tend to break the aggregate. After a specified number of submerging and drying repetitions, the aggregate is sieved to determine the percent loss of material.

2.1.2. Sulfate Soundness

A sulfate soundness test is a useful first evaluation of a particular aggregate type. Aggregates in chip seal can contain appreciable water content since they are exposed to surface runoff and rainfall water. Therefore, freezing and thawing conditions can directly affect aggregates.

This test subjects the aggregate samples to repeated immersion in either sodium sulfate or magnesium sulfate solution. Salt crystals that form during this test are intended to mimic ice crystals formed in the normal water freeze-thaw process in the field. It is reported that just over half of the states in the U.S. have a sodium sulfate soundness requirement, while about one-fifth have a magnesium sulfate soundness requirement [11].

2.2. Experimental Program

2.2.1. Material Properties

Three types of aggregate, including two mineral aggregates, i.e., trap rock and creek gravel, and a synthetic aggregate, i.e., crumb rubber, obtained from scrap tires by ambient shredding, were used in this test (Fig. 2.1). All three types of aggregate were used with the size of 1/4 to 3/8 inches since this is the most common aggregate size range for chip seal construction [1]. Different properties of the aggregate used are tabulated in Table 2.1.

Creek gravel Crumb rubber Trap rock

Fig. 2.1 – Used aggregate.

Table 2.1 – Aggregate Properties

Property	Crumbed Rubber	Trap Rock	Creek Gravel
Bulk specific gravity	0.87	2.56	2.38
Water absorption (%)	0.00	2.27	4.67
Loose dry unit weight (lb/ft^3)	26	78	74
Voids in loose aggregates (%)	79.5	43.9	40.8
Los Angeles loss by abrasion and impact (%)	0.37	18.7	22.2
Micro Deval weight loss (%)	0.40	4.1	6.0

Table 2.1 shows that the water absorption of creek gravel is more than two times that of the trap rock with 4.67% and 2.27% for creek gravel and trap rock, respectively, whereas the crumb rubber water absorption was 0.00%. Table 2.1 also shows a noticeably higher abrasion resistance for crumb rubber compared to the mineral aggregates. The Micro-Deval weight loss for crumb rubber was 0.40%, compared to 4.1% and 6.0% for trap rock and creek gravel, respectively. Also, Los Angeles weight loss for crumb rubber was 0.37%, compared to 18.7% and 22.2% for trap rock and creek gravel, respectively.

2.2.2. Test Procedure

The aggregate soundness test has been conducted in accordance with ASTM C88-13 [89]. An aggregate sample is subjected to 5 cycles of submergence in a sodium sulfate, i.e., Na_2SO_4, solution followed by drying in an oven. The sodium solution's specific gravity was between 1.154 to 1.171. This process causes salt crystals to form in the aggregate's water-permeable pores. Crystal formation tends to create internal pressure and break the aggregate. Each cycle involves between 16 and 18 hours of submergence in the sulfate solution followed by 4 or more hours of drying. After a specified number of cycles, aggregate samples are washed and sieved to determine their mass loss. Aggregates should be separated into different size ranges and tested independently during the test. The mass loss of each size rage was then calculated using Eq. 2.1.

$$\text{Loss} = \left(\frac{M_B - M_A}{M_B}\right) 100 \qquad \text{Eq. 2.1}$$

where M_B is the mass before the test and M_A is the mass after the test. The final reported loss value, reported as a percentage of total aggregate mass, is a weighted average of the mass loss of each size range. However, aggregates used in this study were all between 1/4 to 3/8 inches in size, therefore, according to the standard, there was no need to separate them by size and all were considered as one category. Fig. 2.2 shows the used aggregate and test procedure.

(a)

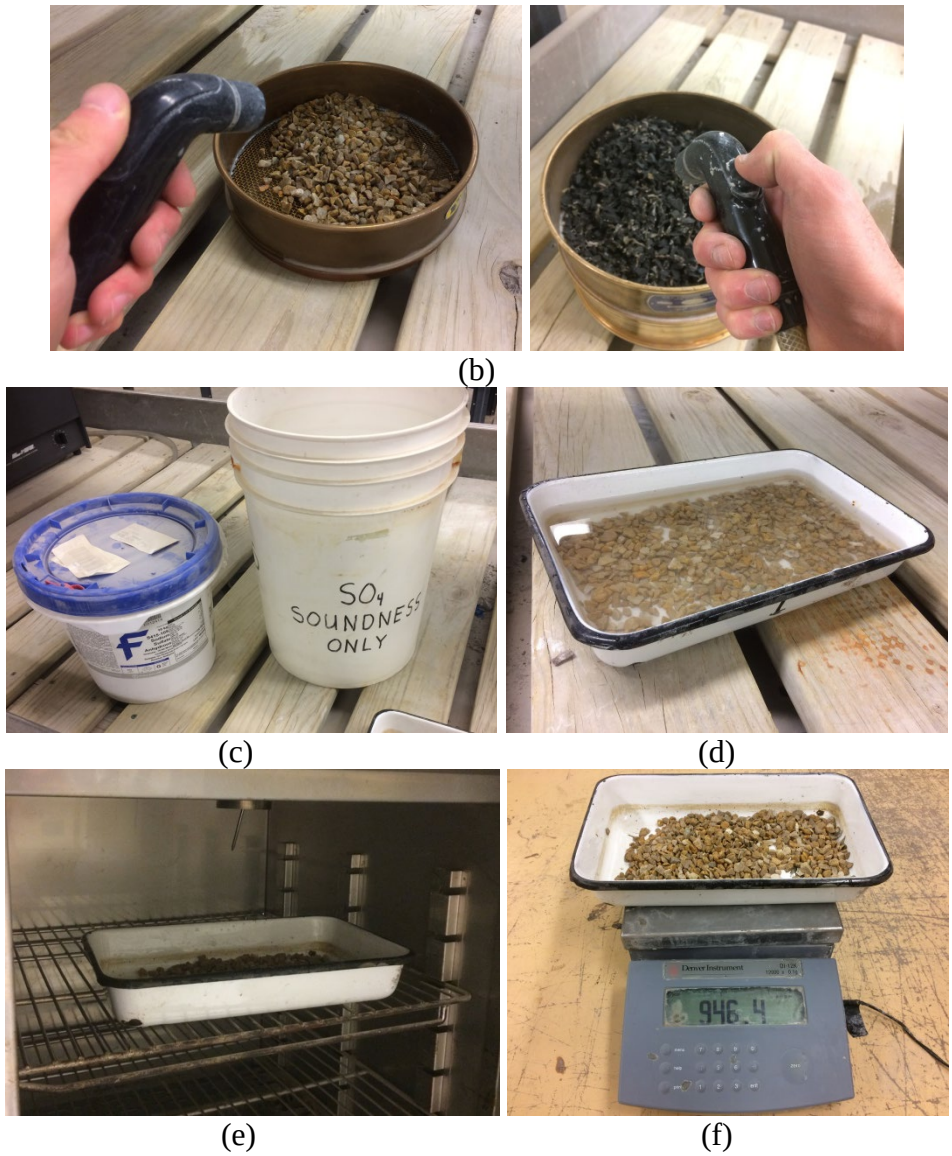

(b) (c) (d) (e) (f)

Fig. 2.2 – Aggregate soundness test procedure including (a) selected aggregates, (b) washing the test sample, (c) sodium sulfate solution preparation, (d) storage of sample in solution, (e) drying sample after immersion, and (f) weighting the sample after removing the solution.

2.3. Test Results

The results of the aggregate soundness test according to ASTM C88-13 is reported in Fig. 2.2. The results show 0% mass loss for crumb rubber particles compared to 2.1% and 4.3% for trap rock and creek gravel, respectively. The reason could be related to the nature of the crumb rubber particles as a synthetic material with a 0% water absorption character. Similarly, the weight

loss for trap rock and creek gravel is proportionate to their water absorption percentage. This relation between the water absorption percentage and the weight loss percentage of the tested aggregates by soundness test is shown in Fig. 2.4(a). Fig. 2.5(b) and 2.5(c) show the relation between the weight loss by the aggregate soundness test versus two common abrasion resistance tests: Los Angeles and Micro Deval. The results from aggregate soundness seem to corollate with weight loss by the Micro Deval test.

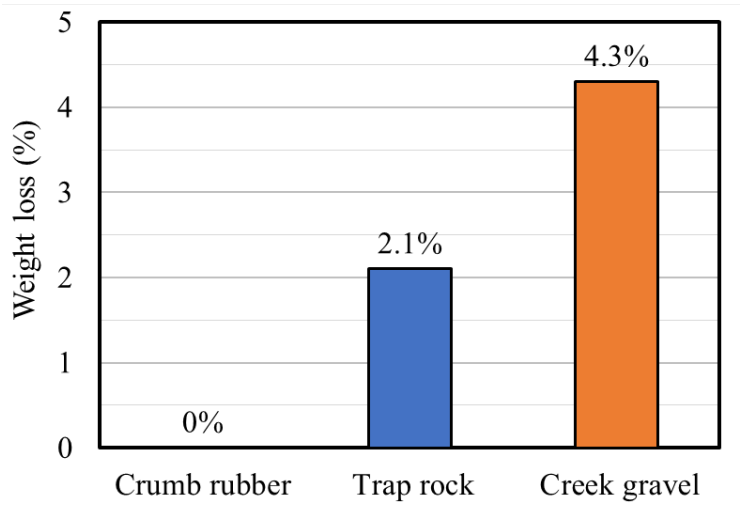

Fig. 2.3 – Aggregate soundness test results.

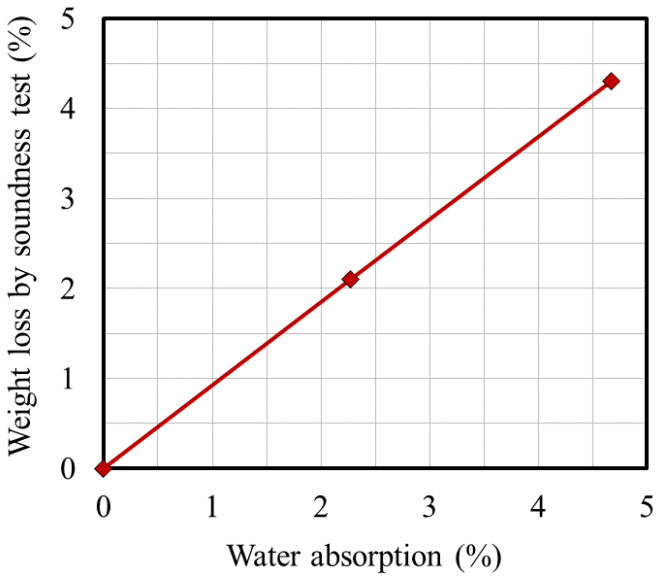

(a)

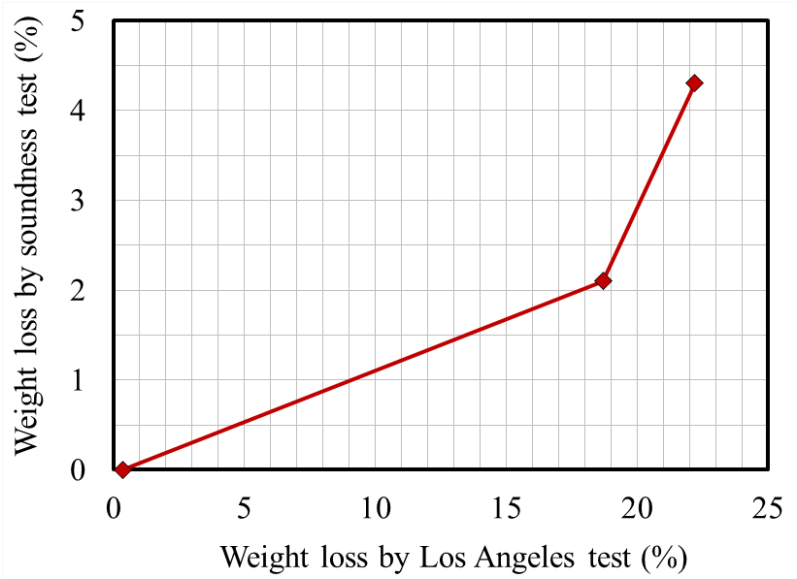

(b)

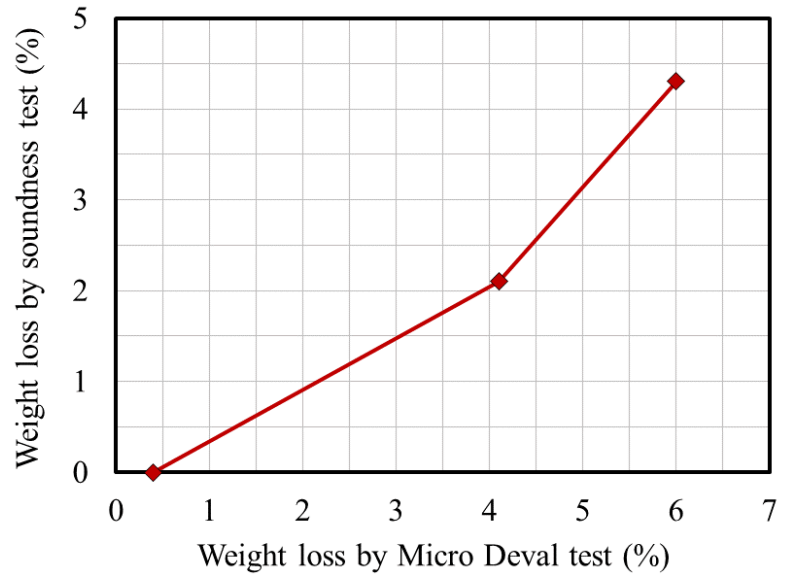

(c)

Fig. 2.4 – Weight loss by aggregate soundness test versus (a) water absorption, (b) weight loss by Los Angeles test, and (c) weight loss by Micro Deval test.

2.4. Conclusion

The sulfate soundness test is widely used for the prediction of freezing and thawing durability of aggregates in the United States. The test is conducted in accordance with ASTM C88. The soundness test results showed that crumb rubber particles are significantly resistant to freezing

and thawing action since they do not absorb any water. Trap rock aggregate also performed better than creek gravel aggregate with more than two times smaller weight loss. It was observed that the weight loss by the soundness test results was proportionate with water absorption of the aggregates and was following the same trend of the Micro Deval abrasion test results.

Chapter 3: Manufacturing the Traffic Load Simulating Machine

3.1. Introduction

One of the major distresses of chip seal that happens under traffic load is aggregate loss or raveling. In order to evaluate the raveling performance of chip seal surfaces, a sweeping test, Vialit test, and Pennsylvania aggregate retention tests are widely used in the literature. Each of these tests has a different sample preparation process and applies various types of mechanical energy to evaluate the bond between the aggregate and binder. However, none of these methods represent the real loading condition that happens in the field.

Beside raveling, bleeding, i.e., the rise of asphalt binder to the surface, is another major chip seal distress. The binder fills the voids in the aggregate and spreads on the surface, which leads to lower skid resistance. It is usually observed in the wheel path and areas of frequent loading such as intersections where slow traffic and turning movements cause a higher stress condition at the chip seal surface. Also, at elevated temperatures, binder might be picked up by the tires and lead to catastrophic failures in chip seals. Few studies have focused on studying bleeding of chip seal in the laboratory since there is no standard test for this means and the common tests mentioned earlier are not capable of characterizing the bleeding distress.

On the other hand, construction and testing multiple field sections will be costly and time-consuming. Besides, controlling the traffic parameters such as load, speed, and the number of vehicles in the field is not practical. Therefore, there is a need to develop a test protocol that applies a mechanical wheel load simulating the loading condition that vehicular tires produce on the

pavement surface in the field. As a result, the raveling and bleeding performance of the chip seal specimens could be evaluated under the loading condition closer to the field condition compared to the existing test methods. In order to fulfill this objective, a small-wheel traffic simulation machine (SWTS) was designed and manufactured.

SWTS could be used to simulate any possible chip seal distress including raveling or bleeding in different temperatures. Moreover, the aggregate wear and polishing susceptibility could be evaluated using SWTS since the wheel's surface friction replicates the load application mechanism of the field on the chip seal sample in the lab. Therefore, the aggregate will go through the same field polishing experience as well as texture loss and texture variation. Other capabilities considered in designing the SWTS were the capability of varying the normal load from 14 psi to 35 psi and speed of polisher from 1 rpm to 80 rpm. Also, the cost of the SWTS was minimized to make it affordable as a piece of laboratory equipment. This chapter presents the manufacturing process and specifications of SWTS.

3.2. SWTS Machine Fabrication

SWTS consisted of a 28 by 28 inch frame with a total height of 70 inches. The main parts were the specimen holder, wheel assembly, and driving system. Fig. 3.1 shows the initial sketch and engineering drawings for SWTS. Also, the schematic and real view of the final product is shown in Fig. 3.2.

The wheel assembly consisted of three pneumatic tires with 8 inch diameters and 2-12 inch widths attached to a circular plate to provide a wheel tracking diameter of 15-3/4 inches center to center (Fig. 3.3). The wheels were equipped with ball bearings in order to make it possible for them to line up with the circular path while the machine is running. The total weight of the wheel

assembly with no additional weight was 87.25 lbs. The normal weight on the wheels could be varied by adding weights on the circular plate. A square tube shaft (central drive shaft) was used to connect the circular plate to the motor shaft. The square tube shaft and the circular plate and wheel assembly were capable of moving freely up and down so that the weight on the circular plate could be transferred to the wheels.

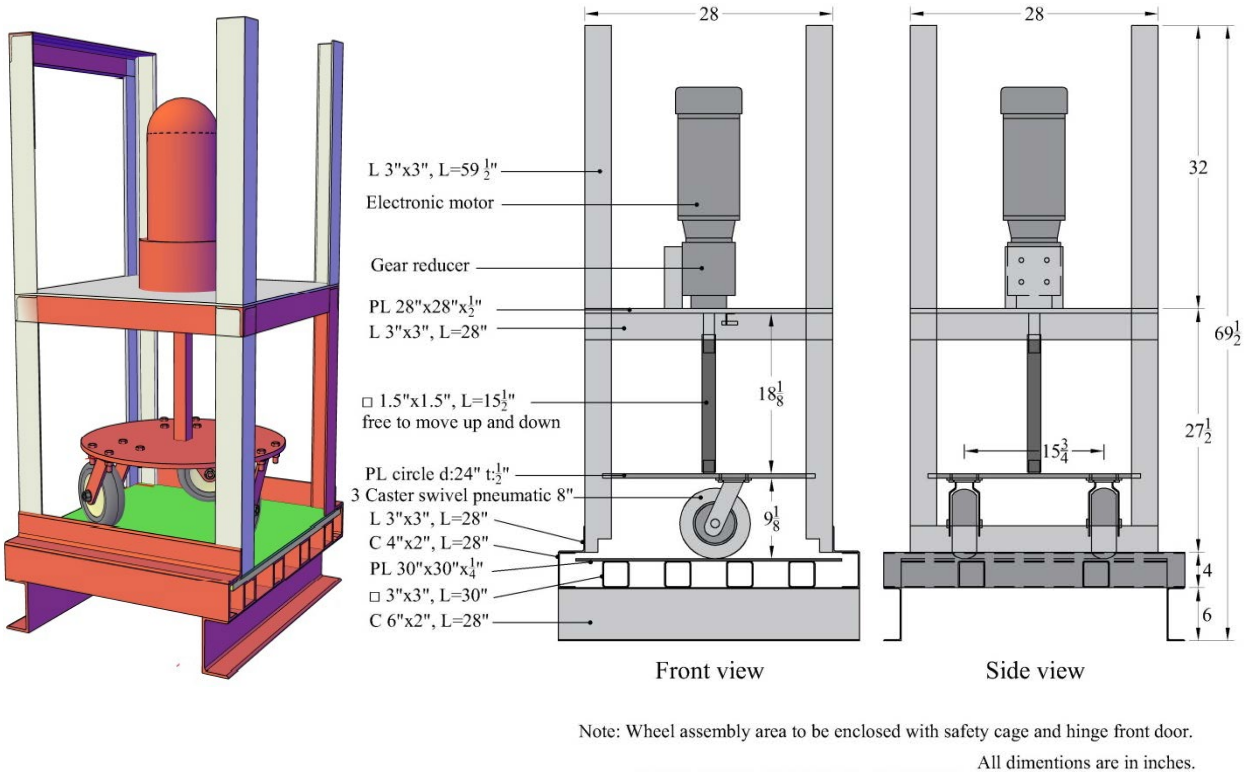

(a) (b)

Fig. 3.1 – SWTS drawings. (a) 3D sketch and (b) dimensions.

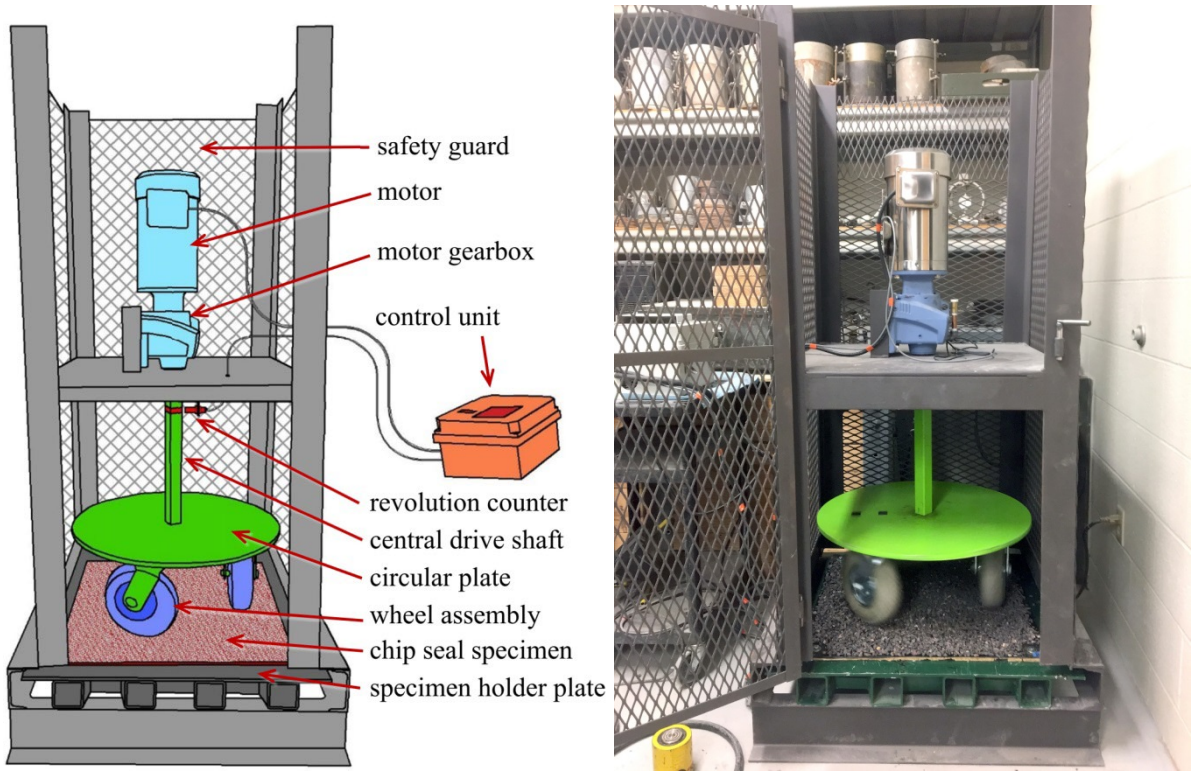

(a) (b)

Fig 3.2 –SWTS (a) schematic and (b) real view.

The driving system provided the torque needed to rotate the wheel assembly. It consisted of an electronic motor of 1/2 horsepower which drove a gearbox that allowed better torque at low speeds (Fig. 3.4). The speed of the motor could be controlled by a digital speed controller shown in Fig. 3.3, so variable speeds could be applied. A digital tachometer sensor was also mounted on the machine to read the revolution per minute (rpm) of the wheel assembly (Fig. 3.2). The specimen holder plate was designed for the 2 ft by 2 ft chip seal specimens to be mounted. The whole frame of the machine was covered with mesh for safety (Fig. 3.2).

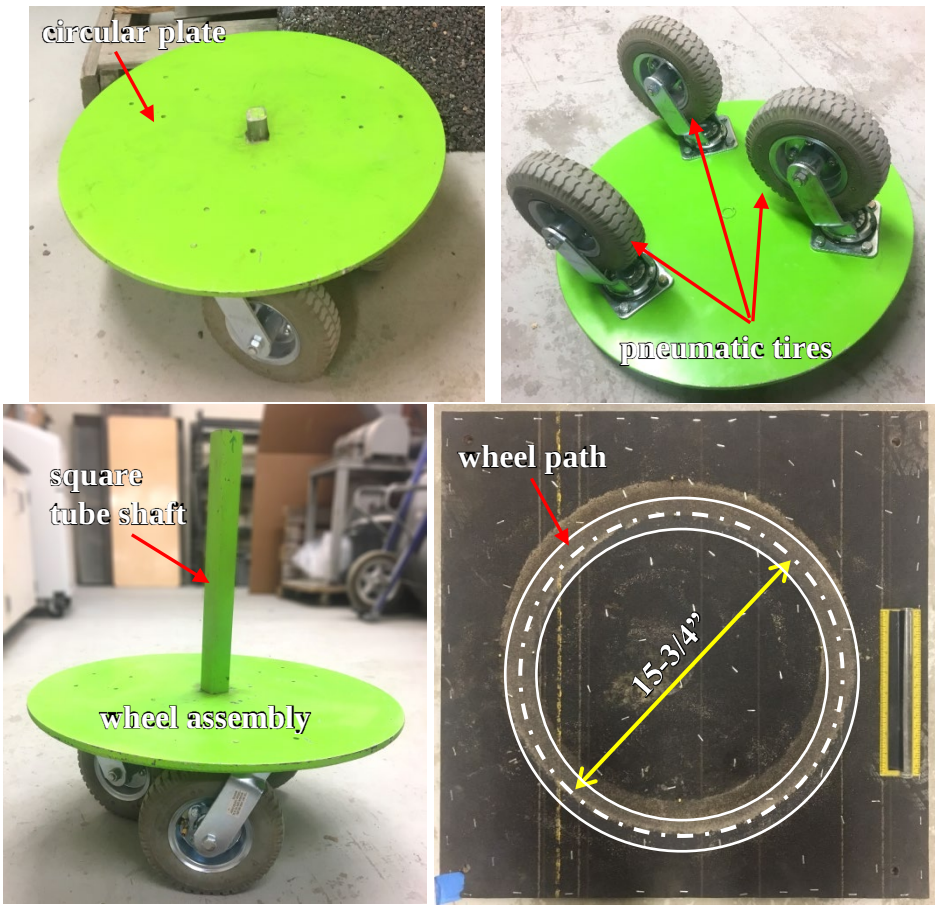

Fig 3.3 – Wheel assembly and wheel pass.

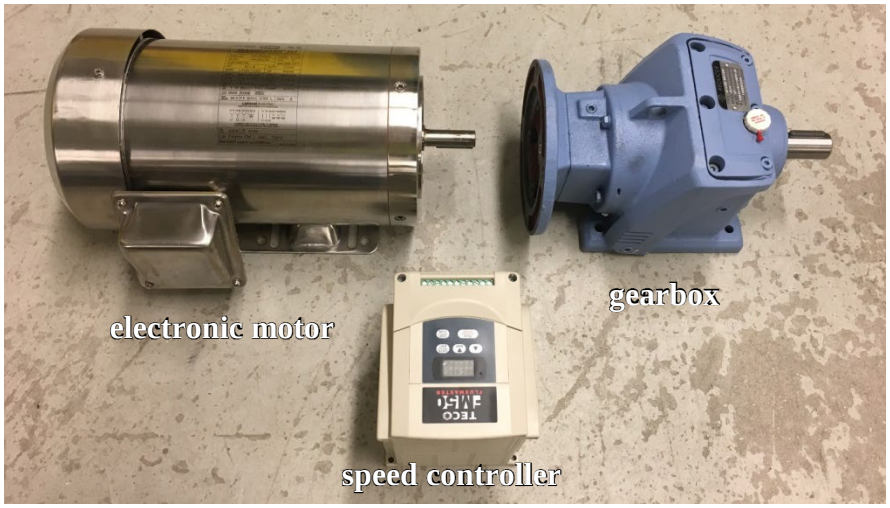

Fig 3.4 – Electronic motor, gearbox and speed control unit.

Moreover, a digital energy meter was installed on the machine to measure the electronic energy consumed by the motor in order to keep the same speed on different chip seal specimens made of different kinds of aggregate (Fig. 3.5). The measured energy consumed by the motor could be an indicator of the energy needed for the motor of a vehicle to ride on the chip seal surface.

Fig 3.5 – Digital energy meter.

In order to investigate the effect of snowplowing on different chip seal samples, as will be discussed in Chapter 8 of this report, a snowplow assembly was also designed and manufactured as shown in Fig. 3.6. The snowplow assembly was designed to be attached to the SWTS wheel assembly (Fig. 3.7). The snowplow assembly consisted of a 3/4 inch thick steel snowplow blade that was cut to 3 by 3 inches from a real scale blade obtained from the Missouri Department of Transportation (MODOT). The snowplow blade was aligned with the wheels in SWTS and was capable of providing different angles between the blade and chip seal surface, called the cutting angle, from 25 to 48 degrees, as shown in Fig. 3.7a. Built-in spring shocks provide performance efficiency with the existing 1/2 horsepower electronic motor, simulating a real mechanism.

During the snowplow test, an additional weight of 90 lbs was added on the wheel assembly to keep the snowplow blade in place and prevent it from raising the wheel assembly. Without this

load, the snowplow blade would stop and raise the wheel assembly due to the interaction between the blade and surface texture. Considering the wheel assembly weight of 87.25 lbs and snowplow assembly weight of 7.33 lbs, the total weight of about 185.6 lbs was imposed on the chip seal surface through the three wheels and the snowplow blade.

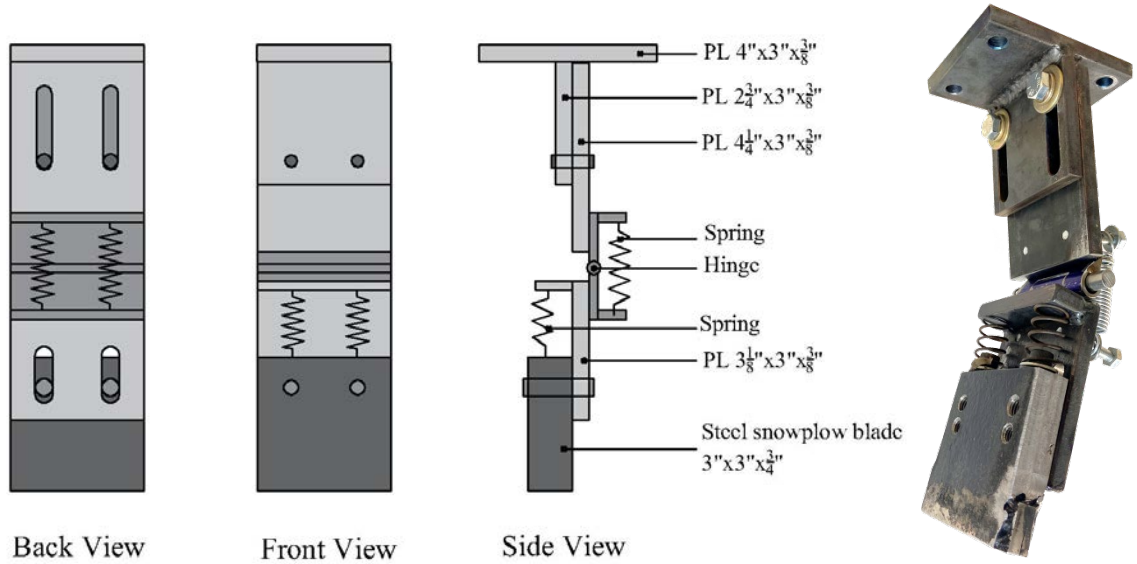

(a) (b)

Fig. 3.6 – Snowplow assembly (a) drawing, and (b) real view.

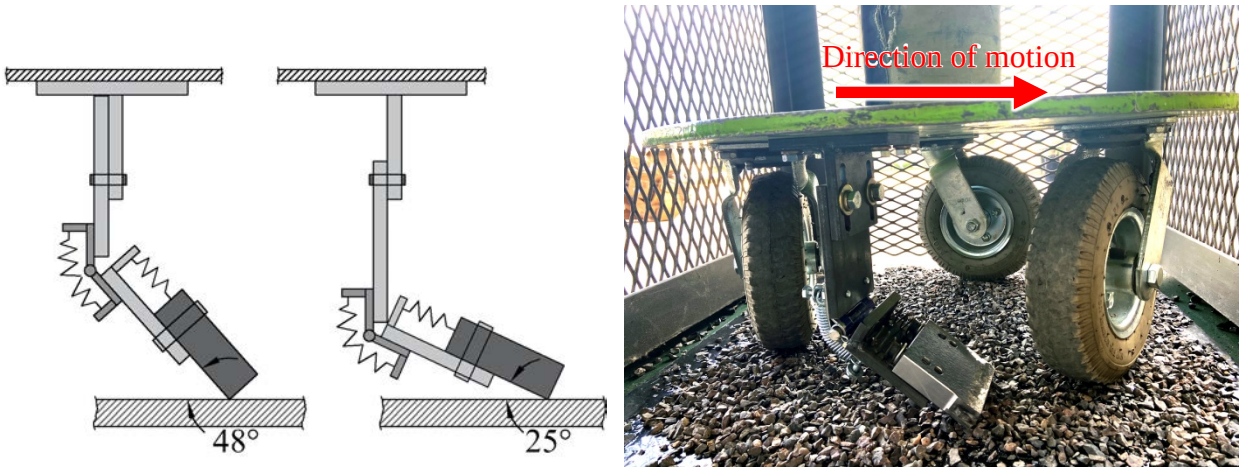

(a) (b)

Fig. 3.7 – Snowplow test, (a) drawing showing the cutting angle, and (b) real view.

3.3. SWTS Applied Load

SWTS was capable of providing different speeds from 3 to 200 wheel applications per minute (wpm). Also, by adding weights on the circular plate of the wheel assembly, different loads from 87.25 lbs to 200 lbs could be provided (Fig. 3.8). In this study, two different traffic speeds of 120 wpm, which corresponds to dynamic loading of 2.00 Hz, and 160 wpm, which corresponds to dynamic loading of 2.67 Hz, was applied on chip seal specimens. Also, two different loading conditions were applied including 87.25 lbs and 172.25 lbs. The same type of pneumatic tires was used through this study, and they were inflated to 290 psi under all loading conditions to keep the same tire-pavement contact area. The tire-pavement contact area was measured as 2.06 in^2 as the average of three different tire footage measurements (Fig. 3.9). Having the tire contact area, the stress applied by each tire was calculated as 14.12 psi and 27.87 psi for 87.25 lbs and 172.25 lbs, respectively.

Fig. 3.8 – Weights added on the circular plate of the wheel assembly.

Fig 3.9 – Tire footage used for measuring tire contact area.

3.4. Macrotexture and Skid-resistance Measurements

In this project, innovative measurement technique were used to record the macrotexture of the chip seal specimens. A non-contact handhold portable 3D scanner was deployed to record the surface texture of specimens before and after the SWTS test. Therefore, the macrotexture variation of the surface could be assessed. The reason for using this technique is the inability to properly use the common method of sand patch [90] for macrotexture measurement due to the circular snowplow path with limited width. A 3D surface scanning technique will also provide more accurate macrotexture measurements [42, 46, 91].

The scanner used in this project was a two-camera structured-light 3D scanner, namely the Thunk3D Fisher (Fig. 3.10a). The manufacturer declared accuracy of 0.04mm to 0.1mm having a scan speed of 1,200,00 points per second and a resolution of 0.2 mm with two 12mm/5mp lenses, two 1.31 mp CMOS sensors, and a 1280x800 LED white light raster. The 3D scanner consists of a downward-looking projector and two cameras at a fixed orientation with respect to the projector. The projector projects a series of black and white patterns onto the scan surface. When light projects onto the object's surface, the patterns become distorted. Two cameras capture these images and calculate the distance from each point in the field of view using the triangulation system (Fig. 3.10b). Having the 3D surface of chip seal specimens, the macrotexture was assessed

using Digital Surf MountainsMap Expert Version 8 surface analysis software [92] which will be discussed in detail in Chapter 5 of this report.

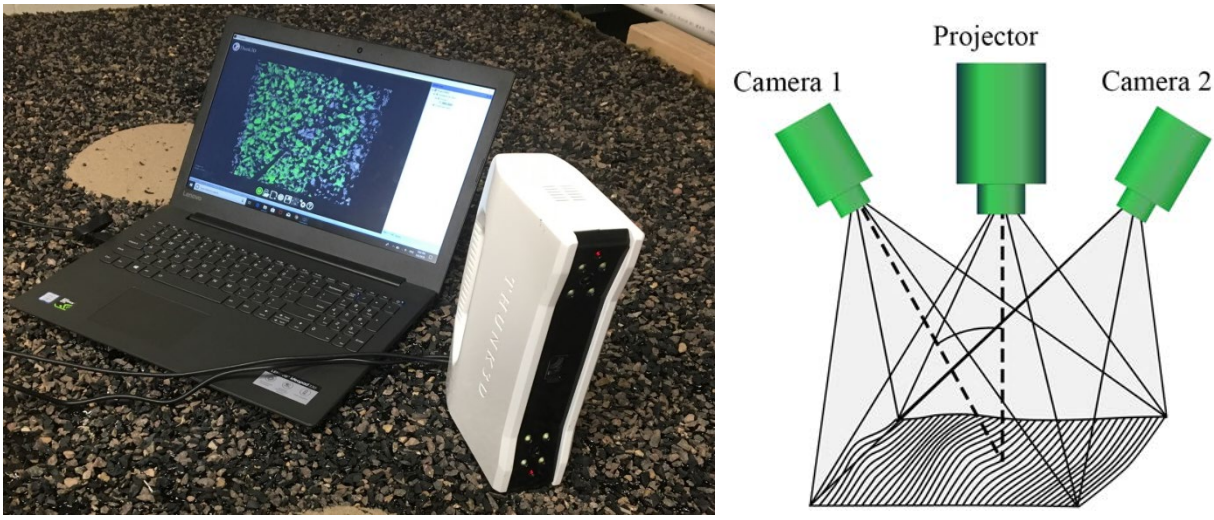

Fig. 3.10 – (a) Handhold portable 3D scanner, (b) basic setup of a structured light triangular system.

Chapter 4: Construction of the Chip Seal Specimens

4.1. Introduction

In this chapter, the specification and preparation process of the chip seal test specimens used for different studies throughout this report is described. Besides the characteristics of different types of aggregate, different chip seal design approaches were reviewed.

4.2. Material Properties

4.2.1. Aggregate

Two different types of mineral aggregate, namely trap rock and crumb rubber, along with a synthetic aggregate, i.e., crumb rubber particles, were used during this study (Fig. 4.1). Ambient shredded crumb rubber was used in this study since the previous study showed that this type has a rougher surface than cryogenic crumb rubber [7]. Also, the ambient shredded crumb rubber could be easily accessed in Missouri.

Since several numbers of specimens were prepared during this study, aggregates were provided in two different batches. Table 4.1 presents the properties of all used aggregates. The aggregate properties for batch 1 and batch 2 were the same except the median particle size and flakiness index. The values mentioned in parentheses in Table 4.1 belong to batch 2. Fig. 4.2 presents the sieve analysis of the aggregates that were used to construct the chip seal specimens. During the lab experiments, it was attempted to use aggregates with the same gradation in order to eliminate the effect of aggregate size on the results [9]. However, in some cases, especially for

crumb rubber particles that were produced in certain sizes, obtaining the same gradation with natural aggregate was not always possible (Fig. 4.2). As reported in Table 4.1, all three types of aggregate in both batches had a nominal maximum size of 3/8 inches. However, the median size was slightly different for different aggregates. It is worth noting that crumb rubber particles initially had a lower percentage of dust, i.e., materials passing through No. 200 sieve, compared to the other two types of aggregate. However, the natural aggregates were washed to remove the excessive amount of dust in order to eliminate the effect of dust on the aggregate bond with the binder.

(a) (b) (c)

Fig. 4.1 – Natural and synthetic aggregates (a) creek gravel, (b) crumb rubber, and (c) trap rock.

Table 4.1 shows higher abrasion resistance for crumb rubber compared to the mineral aggregates. Micro Deval weight loss for crumb rubber was 0.40% compared to 4.1% and 6.0% for trap rock and creek gravel, respectively. Also, Los Angeles weight loss for crumb rubber was 0.37% compared to 18.7% and 22.2% for trap rock and creek gravel respectively. The flakiness index, defined as the percentage by weight of the aggregates whose least dimension is less than three-fifths of its mean dimension, is another important factor in the design of the chip seal. The lower flakiness index represents the more cubic shape of the aggregates. Aggregate with lower

flakiness will provide a more accurate design and a more reliable chip seal surface, since for aggregate with high flakiness, there will be either too much binder in the wheel paths or not enough binder between the wheel paths. Also, higher flakiness will lead to a higher exposure of the aggregate, leading to a higher aggregate loss due to the initial traffic in the wheel paths or due to the snowplow blade in between the wheel paths. Another important parameter for a chip seal surface is the aggregate's fractured faces, which provide the required aggregate interlock. One hundred percent of crumb rubber and trap rock aggregate had two or more fractured faces due to the fracturing and cutting process during the production compering to 93.1% for creek gravel.

Table 4.1 – Aggregate Properties

Property	Crumbed Rubber	Trap Rock	Creek Gravel
Coefficient of uniformity	1.38 (1.28)*	1.82 (1.52)*	2.24
Nominal maximum size (in)	0.38	0.38	0.38
Median particle size (in)	0.24 (0.32)*	0.25 (0.30)*	0.26
Materials passing sieve No. 200 (%)	0.0	0.0	0.0
Bulk specific gravity	0.87	2.56	2.38
Water absorption (%)	0.00	2.27	4.67
Loose dry unit weight (lb/ft^3)	26	78	74
Voids in loose aggregates (%)	79.5	43.9	40.8
Particles with no fractured faces (%)	0.0	0.0	4.6
Particles with one or more fractured faces (%)	100	100	95.4
Particles with two or more fractured faces (%)	100	100	93.1
Los Angeles loss by abrasion and impact (%)	0.37	18.7	22.2
Micro Deval weight loss (%)	0.40	4.1	6.0
Flakiness index (%)	31 (46)*	42 (31)*	15

* Numbers mentioned in parentheses belong to batch 2.

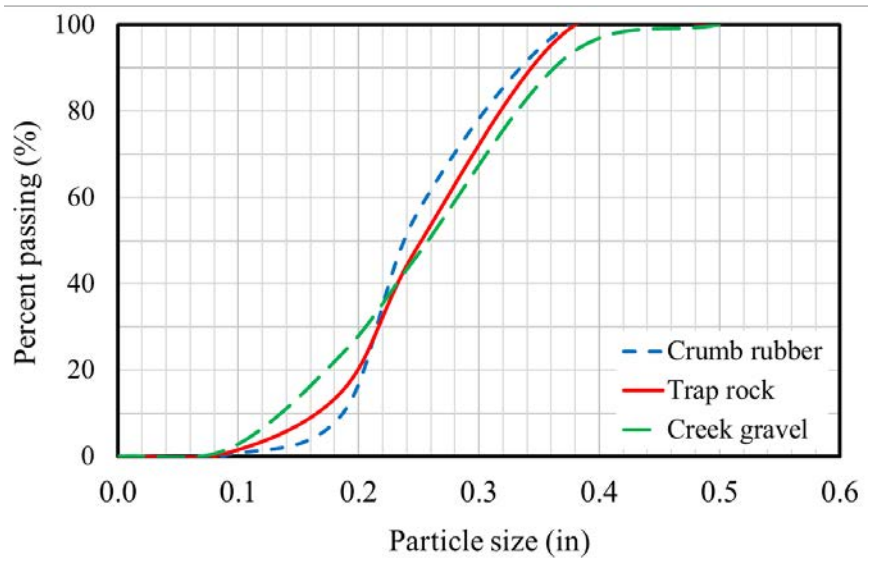

(a)

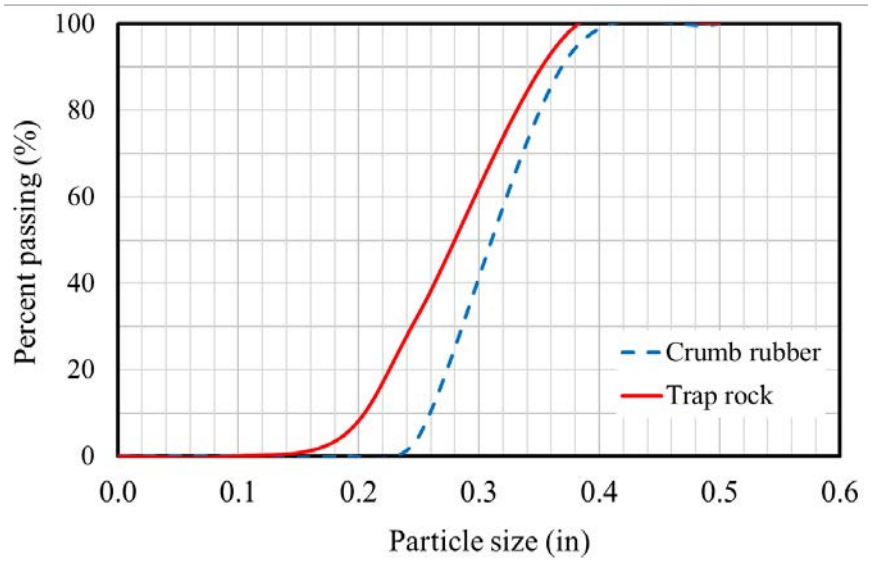

(b)

Fig. 4.2 – Sieve analyses of used aggregate (a) batch 1, (b) batch 2.

4.2.2. Emulsified asphalt (Emulsion)

CRS-2P asphalt emulsion, which is a cationic rapid-setting and high-viscous type, was used during this study per the Missouri Department of Transportation (MoDOT) recommendation. The physical properties of CRS-2P along with the MoDOT specifications [93] are summarized in Table 4.2. The CRS-2P includes 30% water content by weight of the total emulsion. The water breakout

of the emulsion was examined by measuring the weight loss after exposing the emulsion to different temperatures over time (Fig. 4.3). Approximately 81% of the water breakout occurred after 6 hours at a temperature of 95° F, beyond that, there was approximately no evaporation after 24 hours of exposure.

Table 4.2 – Asphalt Emulsion Properties

Parameter	Test Procedure	Result		Required*	
		Min	Max	Min	Max
Tests on emulsion					
Viscosity, Saybolt Furol, 122°F (sec)	ASTM D-7496	100	300	100	400
Sieve test (%)	ASTM D-6933	-	0.3	-	0.3
Demulsibility, 35ml of 0.8% sodium dioctyl sulfosuccinate (%)	ASTM D-6936	40	-	-	-
Storage stability, 1 day (%)	ASTM D-6930	-	1	-	1
Particle charge	ASTM D-7402	Positive		Positive	
Distillation tests					
Residue by distillation (% by weight)	ASTM D-244	65	-	65	-
Oil distillate (% by volume of emulsion)	ASTM D-6997	-	3	-	3
Tests on residue from distillation					
Polymer content, wt. (solids basis) (%)		3	-	3	-
Penetration, 77°F, 100g, 5 sec. (dmm)	ASTM D-5	100	150	100	200
Ductility, 39.2°F, 5 cm/min. (cm)	ASTM D-113	30	-	30	-
Elastic recovery, 50°F (%)	ASTM D-6084	60	-	58	-

* according to the Missouri standard specifications for highway construction, 2019 [93]

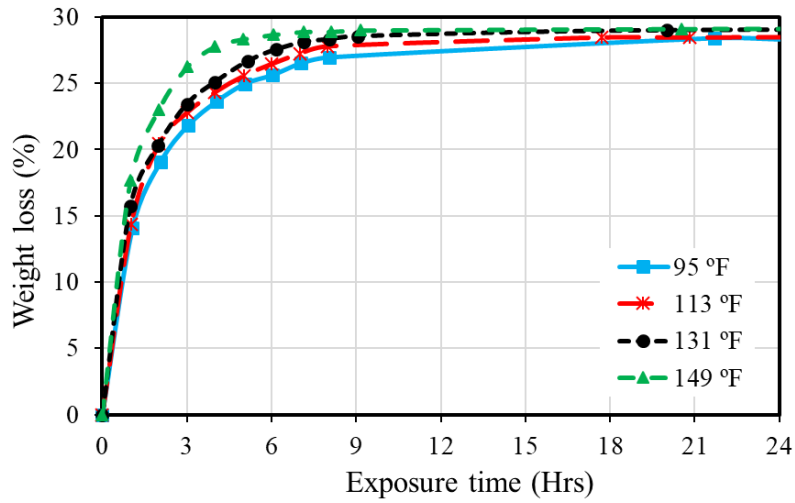

Fig. 4.3 – Emulsion weight loss due to water breakout.

4.3. Design of Test Specimens

There is no consensus in the U.S. on how to design a chip seal. A recent survey including 54 U.S. states and cities showed that only 18% of respondents use McLeod, Kearby, and modified Kearby methods to design a chip seal, while 26% of the respondents do not use a formal design method. The remaining 56% of the respondents use their own local, empirical, or past experience design approach [1]. The design of a chip seal aims to determine the aggregate application rate required to form a blanket of one stone in depth and determine the corresponding asphalt binder application rate to satisfy a given aggregate embedment depth ranging from 50% to 80% of the median aggregate size depending on the design guidelines. The step-by-step design of the test specimens following three different approaches of McLeod, Kearby, and modified Kearby is presented below.

4.3.1. McLeod method (Single application design with one-size aggregate)

According to the McLeod method, the number of pounds of cover aggregate to be applied per square yard (C) can be calculated using Eq. 4.1.

$$C = 37.4HGE \qquad \text{Eq. 4.1}$$

where H is the average least dimension of cover aggregate in inches which can be obtained from Fig. 4.4 (0.19 for rubber, 0.17 for trap rock, and 0.18 for creek gravel). G is the ASTM bulk specific gravity of the cover aggregate (0.87 for rubber, 2.56 for trap rock, and 2.38 for creek gravel). E is the wastage factor due to percent of cover aggregate lost due to the whip-off by traffic and the unevenness of spread. In this study, a waste of 15% was assumed resulting in E = 1.15.

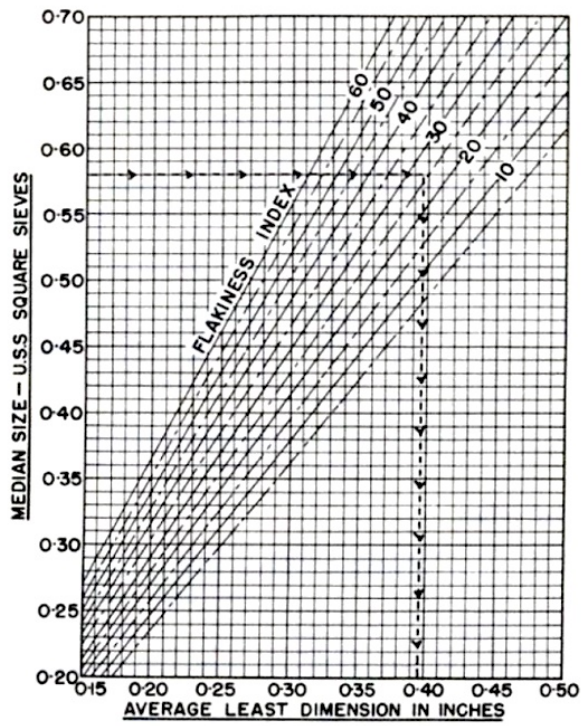

Fig. 4.4 – McLeod method: determination of average least dimension of cover aggregate.

Therefore, using Eq. 4.1,

$$C_r = 37.4 \times 0.19 \times 0.87 \times 1.15 = 7.11 \ \text{lb/yd}^2$$

$$C_t = 37.4 \times 0.17 \times 2.56 \times 1.15 = 18.72 \ \text{lb/yd}^2$$

$$C_c = 37.4 \times 0.18 \times 2.38 \times 1.15 = 18.43 \ \text{lb/yd}^2$$

In other words, McLeod's method resulted in aggregate application rates of 7.11, 18.72, and 18.43 lb/yd^2 for crumb rubber, trap rock, and creek gravel, respectively. The quantity of the asphalt binder to be applied per square yard can be calculated using Eq. 4.2

$$B = \frac{1.122HT + S + A}{R} \qquad \text{Eq. 4.2}$$

where B is the total asphalt binder to be applied in US gallons per square yard. H is the average least dimension of aggregate measured in inches. T is the traffic factor which depends upon the anticipated traffic volume. This study assumed a traffic volume in a range of 100 to 500 vehicles per day and hence T = 0.75. R is fraction of residual asphalt in the asphalt binder selected. This study assumed that the emulsion has 30% water based on its manufacture sheet and hence R = 0.70. S is the surface texture correction in US gallons per square yard measured at 60 °F. Resulting from expected gain or loss of asphalt binder due to the textural characteristics of the existing surface, this study assumed that the texture rating of existing surface is "Hungry 2h" which is the fourth level of roughness out of five and hence S= 0.06. A is the absorption correction in gallons per square yard measured at 60 °F due to loss of asphalt binder by absorption into the particles of the cover. This correction can be neglected for all but unusually absorptive aggregates. When necessary, the Country Roads Board makes an aggregate absorption correction factor of 0.03 US gallon per square yard. Therefore,

$$B_r = \frac{1.122 \times 0.19 \times 0.75 + 0.06 + 0}{0.7} = 0.31\ \frac{\text{gal}}{\text{yd}^2} \quad \text{: for rubber}$$

$$B_t = \frac{1.122 \times 0.17 \times 0.75 + 0.06 + 0}{0.7} = 0.29\ \frac{\text{gal}}{\text{yd}^2} \quad \text{: for trap rock}$$

$$B_c = \frac{1.122 \times 0.18 \times 0.75 + 0.06 + 0}{0.7} = 0.30\ \frac{\text{gal}}{\text{yd}^2} \quad \text{: for creek gravel}$$

4.3.2. Kearby method

There is no difference in determining the required aggregate per the Kearby and modified Kearby methods. Using Fig. 4.5 at the embedment ratio of 50%, which is the maximum embedment ratio that can be assumed based on this method, the following results were obtained for the binder application rate: 0.43 gal/yd^2 for crumb rubber, 0.33 gal/yd^2 for trap rock, and 0.31 gal/yd^2 for creek gravel.

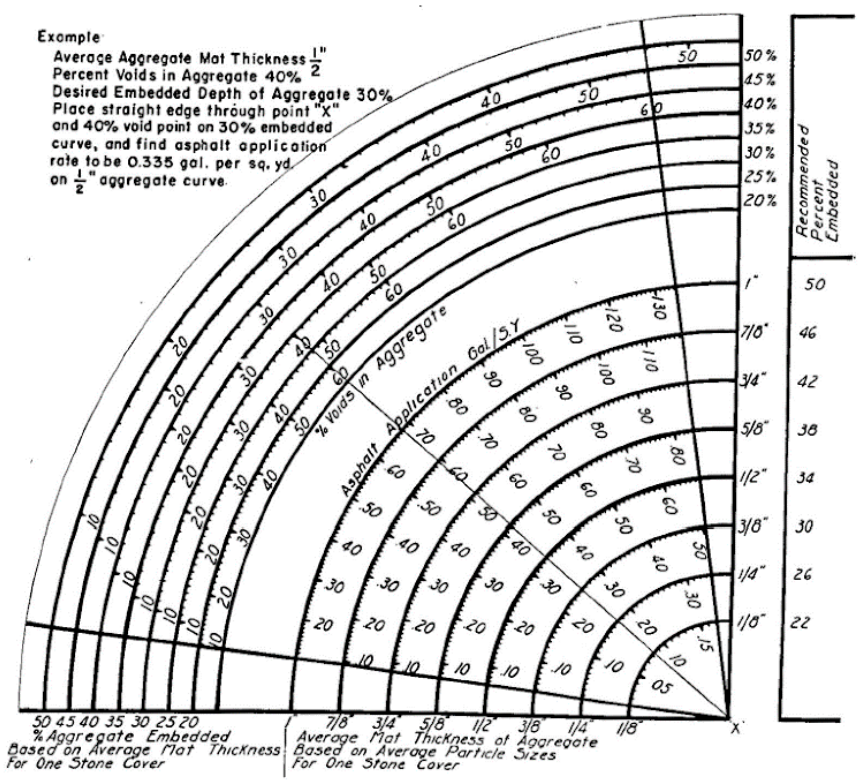

Fig. 4.5 – Kearby method.

4.3.3. Modified Kearby method

The equation utilized to determine asphalt quantity by the existing Modified Kearby seal coat design method is shown below (Eq. 4.3).

$$A = 5.61E * \left(1 - \frac{W}{62.4G}\right) * T + V \qquad \text{Eq. 4.3}$$

where A is the asphalt quantity in gal/yd^2. W is the dry loose unit weight in lb/ft^3 (26 for rubber, 78 for trap rock, and 74 for creek gravel). Q is the aggregate quantity determined from board test, lb/yd^2 (5 for rubber, 15 for trap rock, and 14 for creek gravel). E is the embedment depth =e×d, where e= 0.4 using Fig. 4.6 and d=1.33Q/W, (E=0.102 for rubber, 0.102 for trap rock, and 0.101 for creek gravel). G is the dry bulk specific gravity of aggregate (0.87 for rubber, 2.56 for trap rock, and 2.38 for creek gravel). T is the traffic correction factor. This study assumed a traffic volume in a range of 250 to 500 vehicles per day and hence traffic correction factor equal to 1.1. V is the correction for the surface condition considered equal to zero. It should be noted that asphalt quantities calculated by these methods are for asphalt cement. Appropriate corrections must be made where a cutback or an emulsion is used. Therefore,

$$A_r = 5.61 * 0.102 * \left(1 - \frac{26}{62.4 * 0.87}\right) * 1.1 + 0 = 0.33 \ \text{gal/yd}^2$$

$$A_t = 5.61 * 0.102 * \left(1 - \frac{78}{62.4 * 2.56}\right) * 1.1 + 0 = 0.32 \ \text{gal/yd}^2$$

$$A_c = 5.61 * 0.101 * \left(1 - \frac{74}{62.4 * 2.38}\right) * 1.1 + 0 = 0.32 \ \text{gal/yd}^2$$

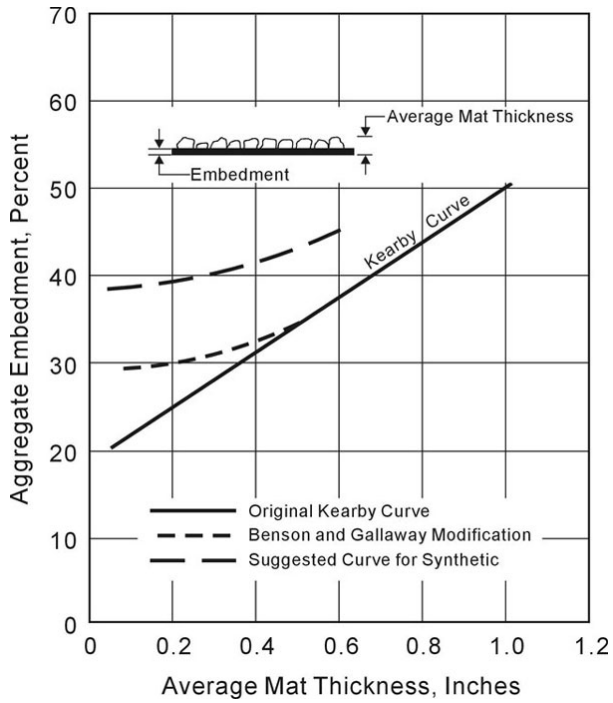

Fig. 4.6 – Relation of percent embedment to mat thickness for the modified Kearby method.

Table 4.3 summarizes the aggregate and binder application rates according to each design method. As shown in Table 4.3, determining the binder rate of application was more challenging, as there were more discrepancies between the results of the different design methods. The main reason behind this discrepancy was the time to achieve the required design aggregate embedment depth. For example, McLeod assumes that the design aggregate embedment depth will be satisfied after two years of service life, while the Kearby and modified Kearby methods assume that the design aggregate embedment depth will be satisfied immediately before opening the road for traffic. This will result in a relatively smaller binder application rate following the McLeod method compared to the Kearby and modified Kearby methods.

The McLeod, Kearby, and modified Kearby design methods resulted in emulsion application rates of 0.31, 0.42, and 0.33 gal/yd^2, respectively, for crumb rubber, 0.29, 0.33, and 0.32 gal/yd^2, respectively, for trap rock, and 0.30, 0.31, and 0.32 gal/yd^2, respectively, for creek

gravel assuming an embedment depth of 67% after two years of service for the McLeod method, 50% for the Kearby method, and 40% for the modified Kearby method, as calculated in earlier.

Table 4.3 – Summary of Chip Seal Design Methods

Aggregate type	Aggregate rate (lb/yd^2)	Emulsion rate (gal/yd^2)		
		McLeod	Kearby	Modified Kearby
Crumb rubber	7.11	0.31	0.43	0.33
Trap rock	18.72	0.29	0.33	0.32
Creek gravel	18.43	0.3	0.31	0.32

4.4. Chip Seal Test Specimens

During this experimental program, a total of 55 laboratory chip seal specimens were made and tested. Different sizes and different combinations of emulsion rate and crumb rubber percentage were used to make the chip seal samples as listed in Table 4.4.

Table 4.4 – Chip Seal Test Specimens

Specimen Size	Test	Binder rate (gal/yd2)	Aggregate type %			No. of similar specimens
			Trap rock	Creek gravel	Crumb rubber	
1 ft by 1 ft	Freez-thaw test	0.25	100	-	-	1
			75	-	25	1
			50	-	50	1
			-	100	-	1
			-	75	25	1
			-	50	50	1
			-	-	100	1
8 ft by 4 ft	Rainfall water drainage test	0.25	100	-	-	1
			75	-	25	1
			50	-	50	1
			-	-	100	1
		0.5	100	-	-	1
			75	-	25	1
			50	-	50	1
			-	-	100	1
2 ft bt 2 ft	Traffic load simulation test (SWTS)	0.25	100	-	-	1
			75	-	25	1
			50	-	50	1
			-	100	-	1
			-	75	25	1
			-	50	50	1
			-	-	100	1
		0.5	100	-	-	8
			75	-	25	7
			50	-	50	7
			-	100	-	1
			-	75	25	1
			-	50	50	1
			-	-	100	8
Total No. of specimens						55

In this study, chip seal specimens in three sizes of 8 ft by 4 ft, 2 ft by 2 ft, and 1 ft by 1 ft were utilized. Fig. 4.7 shows an example of each chip seal test specimen size. Binder application rates of 0.25 gal/yd^2 and 0.50 gal/yd^2 were used. Selected binder rates are about the bottom and top range of the common practice for chip seal applications using emulsified asphalts. Two different natural aggregate types, i.e., trap rock and creek gravel, along with synthetic aggregate, i.e., crumb rubber, was selected. Trap rock and creek gravel are the most common aggregate types which are used for chip sealing in Missouri state. Specimens were made with 100% of each aggregate type and different combinations of natural aggregate with crumb rubber. These combinations included 75% or 50% by volume of natural aggregate combined with 25% or 50% by volume of crumb rubber, respectively. Fig. 4.8 shows an example of different aggregate combinations.

(a)

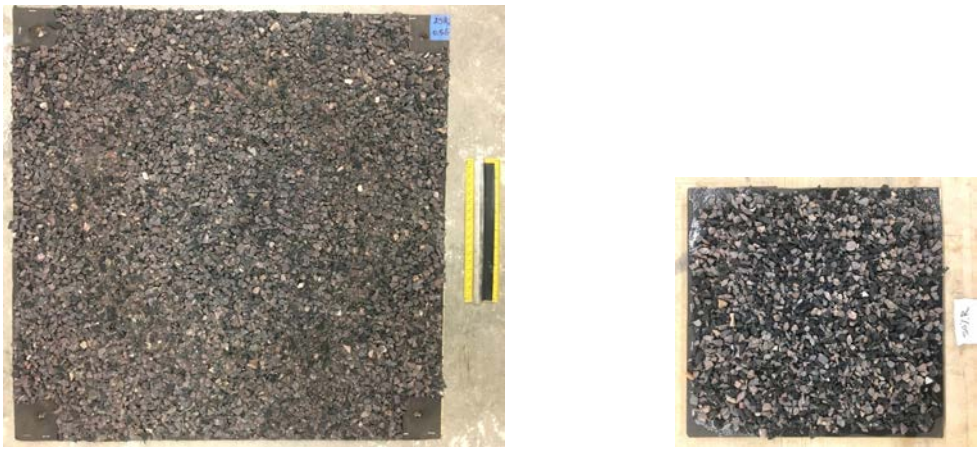

(b) (c)

Fig. 4.7 – Chip seal test specimens with different sizes; (a) 8x4 ft, (b) 2x2 ft, and (c) 1x1 ft.

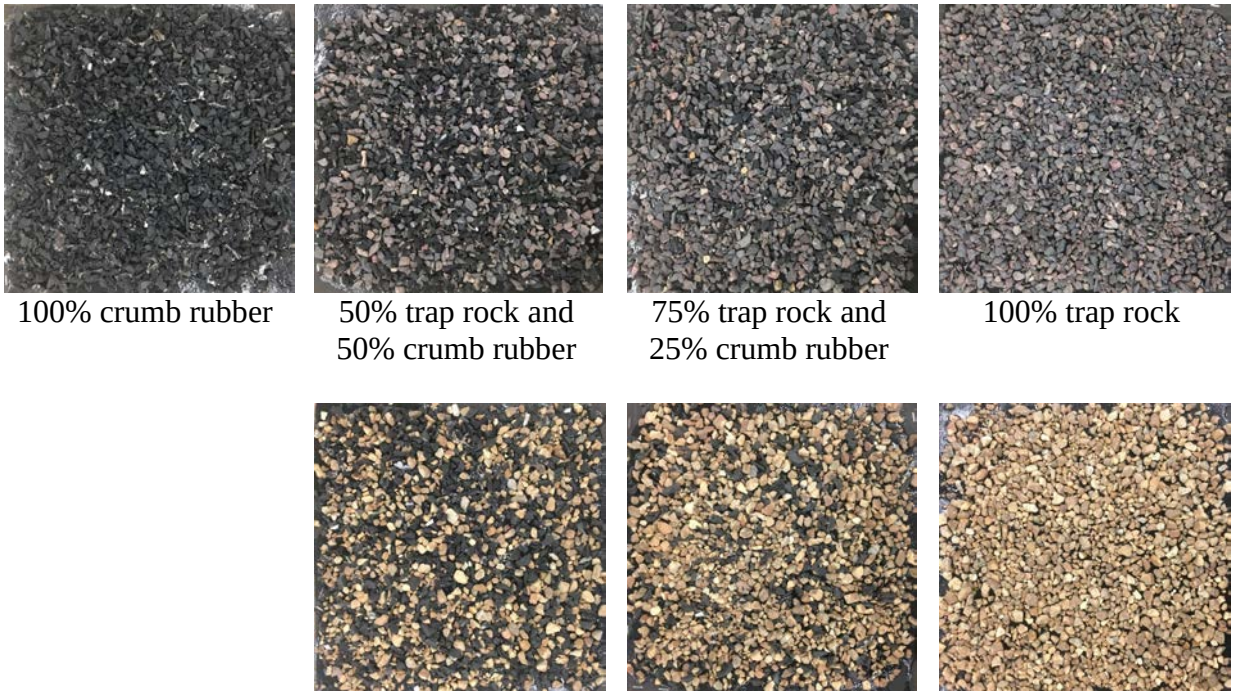

100% crumb rubber | 50% trap rock and 50% crumb rubber | 75% trap rock and 25% crumb rubber | 100% trap rock

50% creek gravel and 50% crumb rubber | 75% creek gravel and 25% crumb rubber | 100% creek gravel

Fig. 4.8 – Different combinations of crumb rubber and mineral aggregates used in this study.

4.5. Specimen Preparation

The chip seal test specimens were all made on a plywood base (Fig 4.9). As learned from the literature, foam or steel bases are too soft or too hard for chip seal application, both resulting in a non-realistic performance. The plywood was covered with an asphalt felt (Fig. 4.10). The asphalt felt was used to provide a proper bond with the chip seal binder, since in the field application, the chip seal is typically applied on an existing asphalt layer.

(a)

(b)

(c)

Fig. 4.9 – Chip seal test specimen bases made of plywood; (a) 8x4 ft, (b) 2x2 ft, and (c) 1x1 ft.

(a)

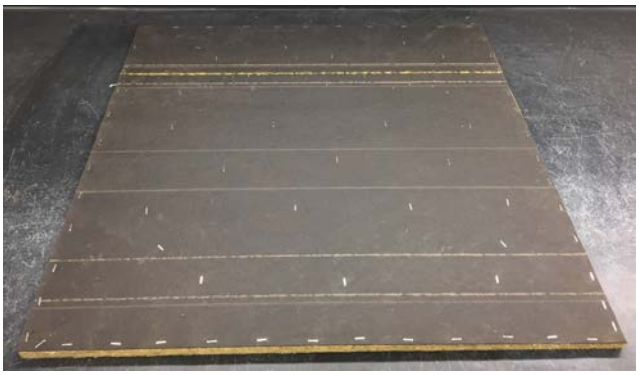

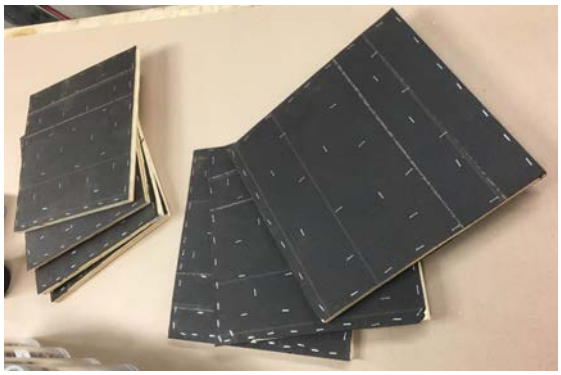

(b) (c)

Fig. 4.10 – Chip seal test specimen bases covered with asphalt felt; (a) 8x4 ft, (b) 2x2 ft, and (c) 1x1 ft.

In order to lay the chip seal, following the field implementation of the chip seal surfaces, the laboratory chip seal specimens were prepared in three main steps. First, a measured amount of binder was applied on the asphalt felt. The CRS-2P emulsified asphalt was preheated to 155˚ F before application. In order to spread the binder uniformly, an aluminum rod was used (Fig. 4.11). Second, a measured amount of aggregate, which was blended before, was manually spread on the

surface (Fig 4.12). The final step, which is compaction, was done using a steel roller (Fig, 4.13). For 1 ft by 1 ft specimens, a rubber roller was used as shown in Fig. 4.13c.

(a)

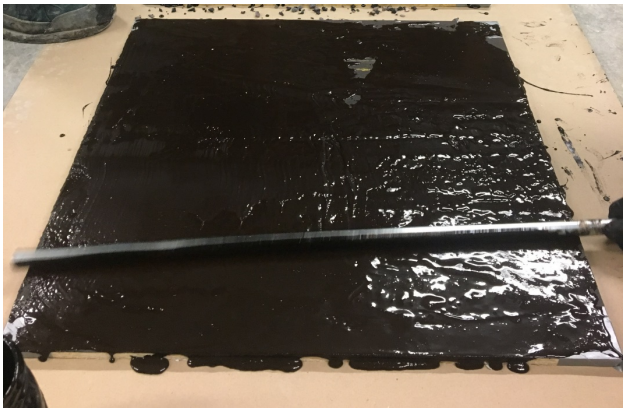

(b)

(c)

Fig. 4.11 – Applying and spreading emulsion for making chip seal test specimens; (a) 8x4 ft, (b) 2x2 ft, and (c) 1x1 ft.

(a)

(b)

(c)

Fig. 4.12 – Spreading aggregate for making chip seal test specimens; (a) 8x4 ft, (b) 2x2 ft, and (c) 1x1 ft.

(a)

(b) (c)

Fig. 4.13 – Compacting chip seal test specimens; (a) 8x4 ft, (b) 2x2 ft, and (c) 1x1 ft.

All specimens were kept for more than 15 days at room temperature for curing. Therefore, insufficient curing time would not influence the test results. The proper amount of curing time was obtained by experience, since the specimens tested earlier showed premature failure accompanied

by severe bleeding under simulated traffic loading (Fig. 4.14). It was observed that the emulsion breakout would take a longer time on the asphalt felt since the asphalt felt acts as an insulation layer. After sufficient curing time, all specimens of any size or type were swept before testing to make sure that all the loose aggregates were removed (Fig. 4.15).

Fig. 4.15 – Premature failure and severe bleeding due to not enough curing time.

(a)

(b)

Fig. 4.15 – Sweeping chip seal test specimens; (a) 8x4 ft, (b) 2x2 ft.

Chapter 5: Effect of Traffic Load on Conventional and Rubberized Chip Seal

5.1. Introduction

Characteristics of the chip seal surface vary by time as the traffic load passes on the pavement. Chip seal major distresses under traffic load are bleeding, i.e., the rise of asphalt binder to the surface, and raveling, i.e., aggregate loss. Aggregate polishing also happens due to traffic load which may reduce the skid resistance of the chip seal surface. Several factors can affect the performance of chip seal regarding these major distresses. The binder application rate, which can provide different embedment and bond for the aggregates can affect both the bleeding and raveling performance of the chip seal. The aggregate bond and polishing highly depend on its origin and inherent characteristics. Another factor that affects raveling, bleeding, and aggregate polishing is the traffic load applied to the chip seal.

In order to evaluate raveling for chip seal surfaces, the sweeping test, Vialit test, and Pennsylvania aggregate retention test have been widely used in the literature. Each of these tests has a different sample preparation process and applies various types of mechanical energy to evaluate the bond between the aggregate and binder. However, none of these methods applies a mechanical wheel load simulating real traffic conditions. Bleeding distress happens when the binder fills the voids in the aggregate and spreads on the surface, which leads to lower skid resistance. It is usually observed in the wheel path and areas of frequent loading, such as intersections, where slow traffic and turning movements cause a higher stress condition at the chip seal surface. There is no standard test for bleeding, and the common tests mentioned earlier are not capable of characterizing the bleeding distress.

Since it would be costly and time consuming to prepare multiple field sections and apply different traffic loads, a laboratory test that simulates field traffic and conditions is necessary. A small wheel traffic simulator (SWTS) is a chip seal testing device which is capable of providing loading mechanism similar to the traffic loading condition through rotating pneumatic tires. The SWTS was manufactured and used in this study to study the performance of chip seal surfaces. Detailed specifications of the SWTS are discussed in Chapter 3 of this report. Besides the main advantage of SWTS, which is proving a more realistic simulation of the traffic loading condition, there are other advantages. Using SWTS, the magnitude, number of cycles, the rate or speed of the applied load, and also the testing temperature can be controlled. Therefore, SWTS makes it possible to evaluate several parameters of chip seal under different conditions.

This chapter evaluates the performance of conventional and rubberized chip seal in terms of raveling, i.e., aggregate loss, and aggregate polishing under a simulated traffic load. The compound effect of using different emulsion application rates, i.e., various percents of embedment of aggregate, using different percentages of crumb rubber particles, and using different types of mineral aggregate were studied. Also, the effect of applied load magnitude and speed, i.e., traffic load and rate, was investigated.

5.2. Experimental Program

5.2.1. Test Specimens and Matrix

A total of 22 chip seal specimens of 2 ft by 2 ft were prepared and tested for the purpose of this chapter. Test specimens were prepared as per the procedure described in Chapter 4 of this report. Three different aggregates with different inherent characteristics including crumb rubber, trap rock, and creek gravel aggregate were used to study the effect of aggregate type. The used

aggregates had a close gradation as presented in Fig. 4.2a. As per Chapter 4 of this report, aggregates of batch 1 were used for all the tests included in this chapter. The characteristics of the aggregate are also reported in Table 4.1. Since aggregate embedment depth is a critical parameter in chip seal performance, the binder application rate was varied to provide different embedment depths for chip seal specimens. Two different binder application rates of CRS-2P emulsified asphalt equal to 0.25 gal/yd^2 and 0.50 gal/yd^2 were used. Test specimens used in this chapter are listed in Table 5.1.

This study was performed in three phases which are described in the next section. Specimens used for Phase I of this study were prepared using two different binder application rates providing different aggregate embedment depths and three different aggregate types along with different combinations of natural aggregate with crumb rubber. The specimens prepared with combined aggregates consisted of 25% and 50% by volume of crumb rubber combined with either of the natural aggregates as listed in Table 5.1. Binder application rates of 0.25 and 0.5 gal/yd^2 were selected, which are near the common minimum and maximum binder rates used by most DOTs. Aggregates used included trap rock and creek gravel, which are the common aggregates used for chip seal in Missouri, along with crumb rubber, which is a green material obtained from scrap tires.

In Phase II and Phase III, the effect of traffic speed and traffic load magnitude were studied, respectively, which will be discussed in the following section. Therefore, similar samples to Phase I were prepared for these phases. A binder application rate of 0.5 gal/yd^2 using trap rock and crumb rubber as aggregate, along with different combinations of trap rock and crumb rubber, were used. The specimens prepared with combined aggregates consisted of 25% and 50% by volume of crumb rubber combined with trap rock aggregates as listed in Table 5.1.

Table 5.1 – Polishing Test Matrix

Test phase	Specimen ID	Emulsion rate (gal/yd^2)	Percentage of Aggregate			Load (lbs)	Speed (wpm)
			Trap rock	Creek gravel	Crumb rubber		
Phase I	100R25E	0.25	-	-	100	87	120
	50T25E	0.25	50	-	50	87	120
	75T25E	0.25	75	-	25	87	120
	100T25E	0.25	100	-	-	87	120
	50C25E	0.25	-	50	50	87	120
	75C25E	0.25	-	75	25	87	120
	100C25E	0.25	-	100	-	87	120
	100R50E	0.50	100	-	-	87	120
	50T50E	0.50	50	-	50	87	120
	75T50E	0.50	75	-	25	87	120
	100T50E	0.50	100	-	-	87	120
	50C50E	0.50	-	50	50	87	120
	75C50E	0.50	-	75	25	87	120
	100C50E	0.50	-	100	-	87	120
Phase II	W100R	0.50	100	-	-	172	120
	W50T	0.50	50	-	50	172	120
	W75T	0.50	75	-	25	172	120
	W100T	0.50	100	-	-	172	120
Phase III	S100R	0.50	100	-	-	87	180
	S50T	0.50	50	-	50	87	180
	S75T	0.50	75	-	25	87	180
	S100T	0.50	100	-	-	87	180

5.2.2. SWTS Test

In order to achieve the objective of this report, a SWTS was developed as described in Chapter 3 (Fig. 5.1). The SWTS was used to apply controlled traffic in terms of number, load, and speed on chip seal specimens. Table 5.1 presents the SWTS test matrix of this study. As mentioned earlier, this testing program was conducted in three phases.

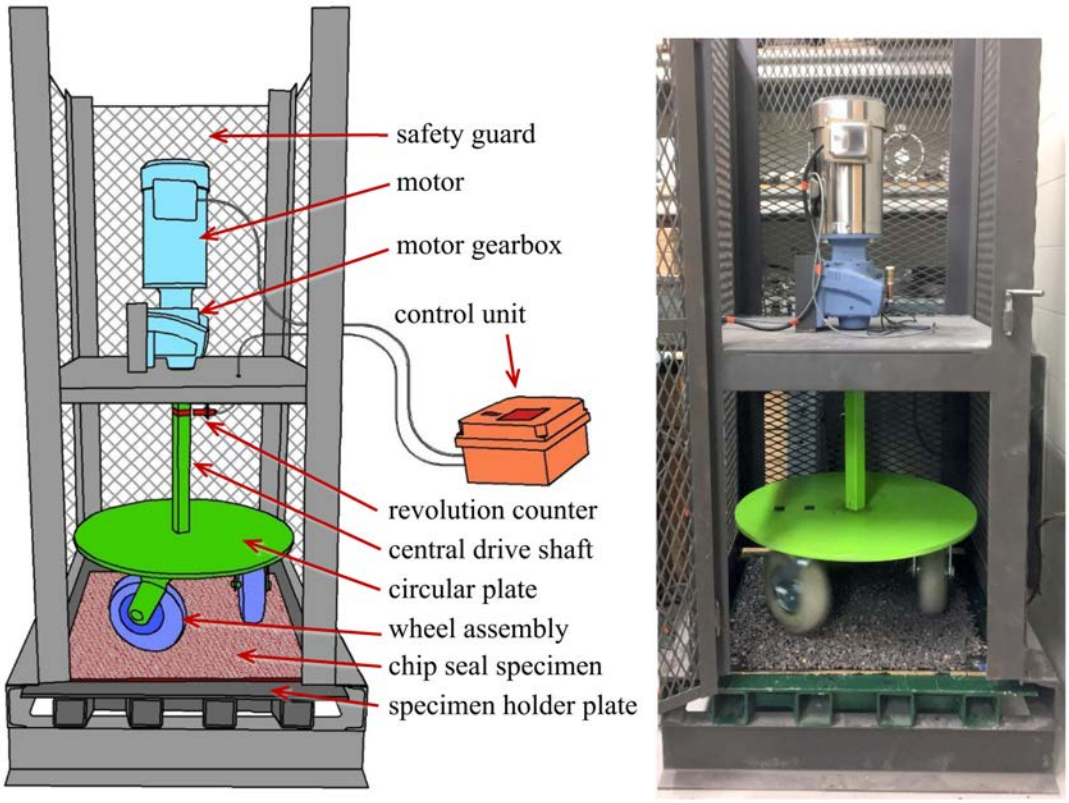

Fig. 5.1 – Small-wheel traffic simulation (SWTS) test machine.

Phase I evaluated the effect of binder application rate and aggregate type along with different combinations of crumb rubber with natural aggregates. For this phase, specimens were subjected to a load of 87.25 lb, which provided a surface contact stress of 14.12 psi under each wheel, considering the contact area of 2.06 in^2 for each wheel. The wheels' travel speed in Phase I

tests was 120 wpm (wheel application per minute), which corresponds to a dynamic loading of 2 Hz on the chip seal surface.

Phase II evaluated the effect of traffic load magnitude. For this phase, the same wheels' travel speed of Phase I was applied on specimens. However, the load magnitude in Phase II was 172.25 lb, which provided a surface contact stress of 27.87 psi under each wheel. Phase III evaluating the effect of traffic speed. For this phase, the same load of Phase I was applied on specimens. However, the wheels' travel speed in Phase III was 160 wpm, which corresponds to a dynamic loading of 2.67 Hz on the chip seal surface.

The SWTS tests for all three phases were conducted in the ambient temperature of 78±4˚F up to 100,000 wheel applications. The test was stopped at different intervals after 5,000, 20,000, 40,000, 70,000, and 100,000 wheel applications, and the macrotexture and skid resistance of specimens were measured. A 3D scanning technique was used for macrotexture measurements, and a modified British pendulum tester was used for skid resistance measurements as will be described in the following sections.

5.2.3. Macrotexture Evaluation

A new non-contact measurement technique using a 3D scanner was used to examine the texture variation and aggregate loss during the SWTS test. The reason for using this technique is not being able to properly use the common method of sand patch [90] for macrotexture measurement due to the circular snowplow path with limited width. The 3D surface scanning technique will also provide more accurate macrotexture measurements [42, 46, 91].

The scanner used in this project was a two-camera structured-light 3D scanner, namely Thunk3D Fisher (Fig. 5.2a). The manufacturer declared accuracy of 0.04mm to 0.1mm having a

scan speed of 1,200,00 points per second and a resolution of 0.2 mm with two 12mm/5mp lenses, two 1.31 mp CMOS sensors, and 1280x800 LED white light raster. The 3D scanner consisted, of a downward-looking projector and two cameras at a fixed orientation with respect to the projector. The projector projects a series of black and white patterns onto the scan surface. When light projects onto the object's surface, the patterns become distorted. Two cameras capture these images and calculate the distance from each point in the field of view using the triangulation system (Fig. 5.2b).

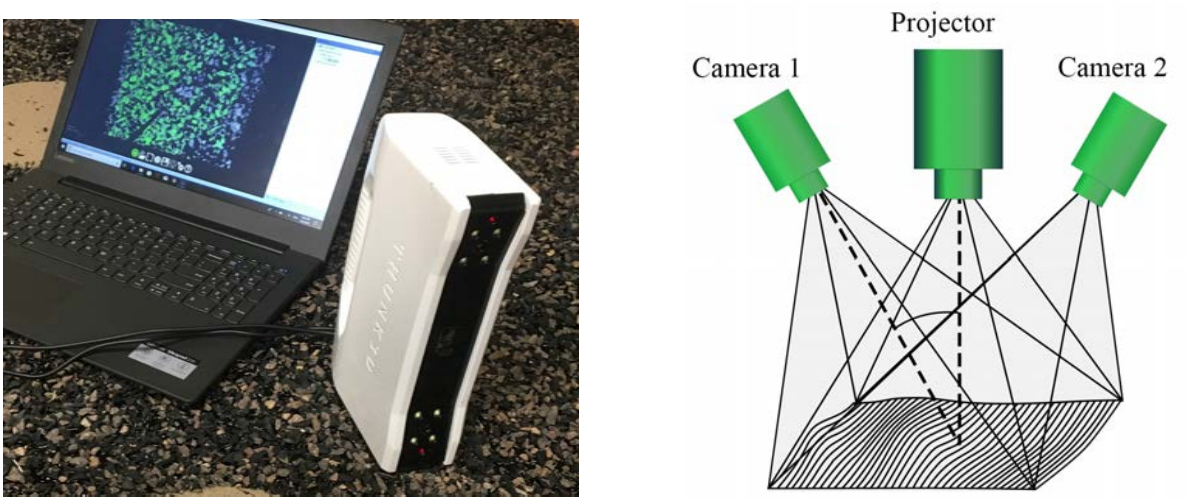

(a) (b)

Fig. 5.2 – (a) Handhold portable 3D scanner, (b) basic setup of a structured-light triangular system.

Having the 3D surface of chip seal specimens, the macrotexture was assessed using Digital Surf MountainsMap Expert Version 8 surface analysis software [92]. Using MountainsMap, a special analysis was conducted in accordance with BS EN ISO 25178-2 [94]. Some post-processing operations such as rotating, leveling and extracting the area of interest, i.e., snowplowing path, were conducted on each surface. Fig. 5.3a shows an example of a chip seal 3D

surface in MountainsMap software. The topographic pseudo-color view of the surface in Fig. 5.3a simply shows the difference in the texture of different spots.

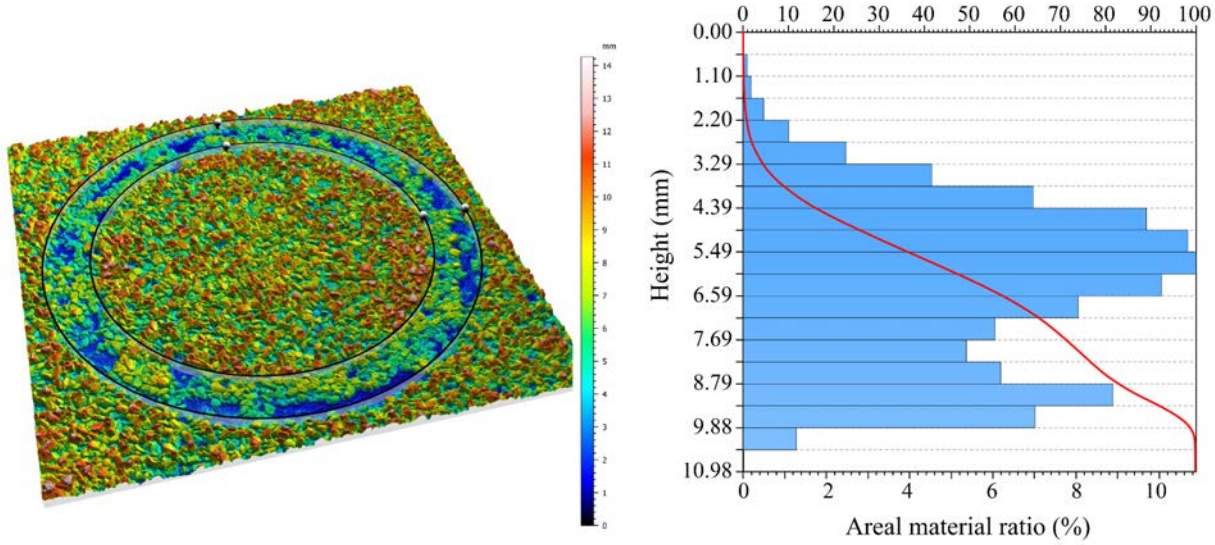

(a) (b)

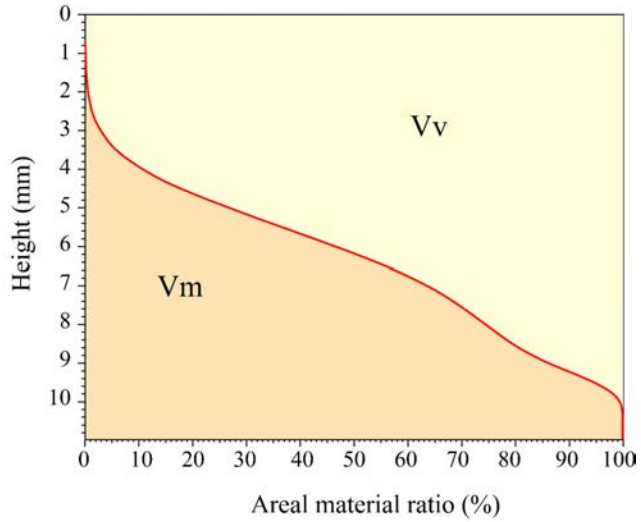

(c)

Fig. 5.3 – 3D surface data from MountainsMap software (a) example chip seal 3D surface, (b) height distribution and Abbott-Firestone curve, (c) Abbott-Firestone curve and volumetric parameters.

The bearing area curve, also known as the Abbott-Firestone curve, which describes the surface texture, was plotted for the surfaces. The Abbott curve, introduced in ISO 13564-2 [95], mathematically represents the cumulative probability density function of the surface profile's height and can be calculated by integrating the profile trace. Fig. 5.3b shows the distribution of heights for the wheel path area of the example chip seal surface shown in Fig. 5.3a. The bars indicate the percentage of surface area at heights within the range of bins (in this case bins of width 0.55 mm between 0 mm and 10.98 mm), and the superimposed line shows the cumulative height distribution. The curve is called the Abbott-Firestone curve, which can be used to calculate two distinct parameters, as shown in Fig. 5.3c. V_m is defined as the area below the Abbott curve, which indicates the volume of material on the surface at various heights from the highest peak to the lowest point on the selected area. V_v is defined as the area above the Abbot curve, which indicates the volume of voids on the surface not occupied by the material on the given area. In other words, V_m represents the volume of material at areal material ratio [95]. The value of V_m in mm^3/mm^2 indicate that a layer of material with V_m mm thickness over the measured area would account for all the material in the given area. Therefore, V_m actually represents the mean texture depth (MTD) of the material in the selected area. In this study, V_m of the wheel path and outside the wheel path was measured to compare the aggregate loss, i.e., texture loss, due to the simulated traffic loading in the SWTS test.

5.2.4. Microtexture Evaluation

The microtexture of trap rock and crumb rubber particles was assessed using a scanning electron microscope (SEM). SEM imaging produces images of a sample by scanning the surface with a focused beam of electrons. The electrons interact with atoms in the sample, producing various signals that contain information about the surface topography. A Raith eLINE SEM (Fig.

5.4) was used to observe and compare the microtexture of trap rock and crumb rubber particles before experiencing any load, i.e., initial microtexture. Also, the microtexture of trap rock and crumb rubber particles detached from the wheel path of chip seal specimens after experiencing 100,000 wheel applications were compared with each other and with their initial microtexture images.

Fig. 5.4 – Raith scanning electron microscope.

In order to acquire an SEM image, the samples should be prepared. Sample preparation in this study included attaching the given particles to a silicon wafer using carbon tape. The samples were grounded using copper tape. To provide a conductive surface and avoid charging, samples were coated with gold/palladium. Fig. 5.5 shows the prepared samples and sample holder of the Raith scope.

In order to acquire the surface features, and also not to charge the originally unconducive samples, SEM images were acquired in a low voltage of 2 kV. The other imaging parameters included 30μm aperture size, SE2 detector, grid voltage of 300 V, and the working distance of

10±0.2 mm. The same imaging parameters were used for all the acquired images provided in this study.

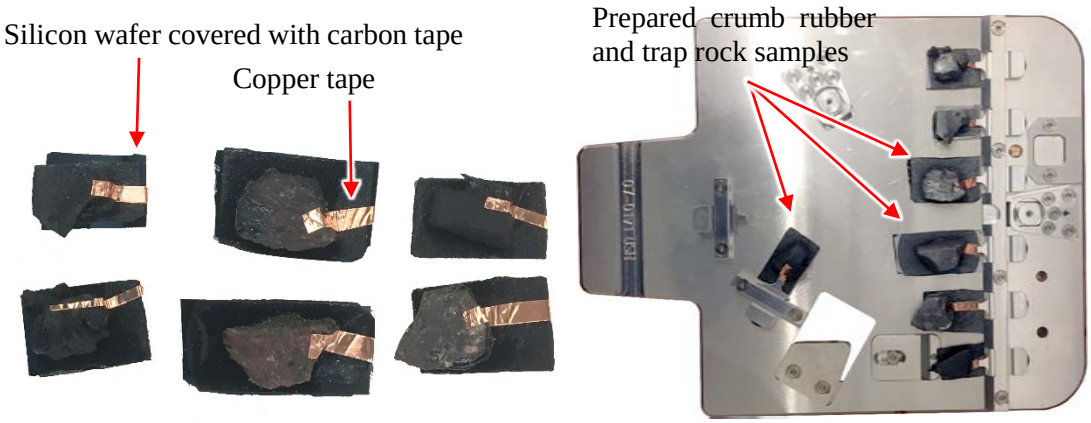

(a) (b)

Fig. 5.5 – (a) Prepared samples for SEM imaging, and (b) samples on sample holder of the Raith scope.

5.4. Macrotexture Assessment Results

5.4.1. Overall performance

Fig. 5.6a to 5.6d show the final state of different chip seal specimens with 0.25 gal/yd^2 or 0.50 gal/yd^2 emulsion rate and different volumetric crumb rubber content from 0% to 100% after the SWTS test. All these specimens have been tested up to 100,000 wheel applications under Phase I test conditions. The topographic pseudo-color view of each surface is also presented in Fig. 5.6 for better visualization of the surface which simply shows the difference in the texture of different spots. In Fig. 5.6, the dark blue color represents the points with the lowest elevation, and the red spots represent the points with the highest elevation on each surface. Also, the wheel path is outlined on the topographic surfaces. Fig. 5.6 provides an overall perception of the SWTS phase I test results. Texture measurements and evaluations are discussed in the following sections.

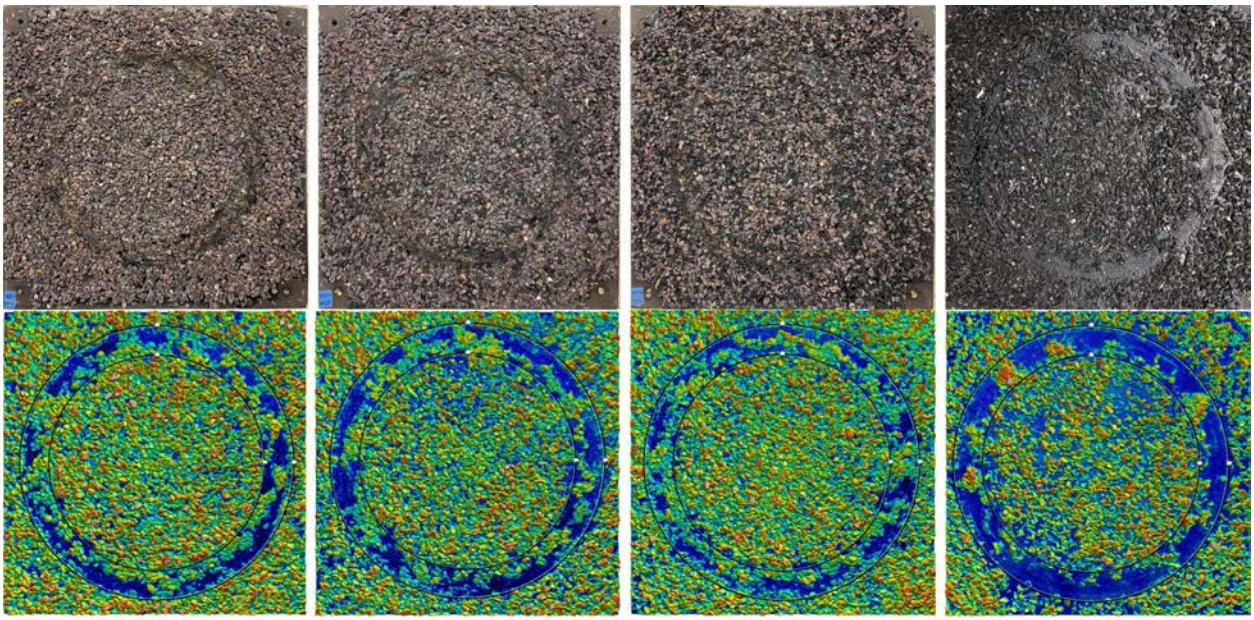

100T25E 75T25E 50T25E 100R25E

(a)

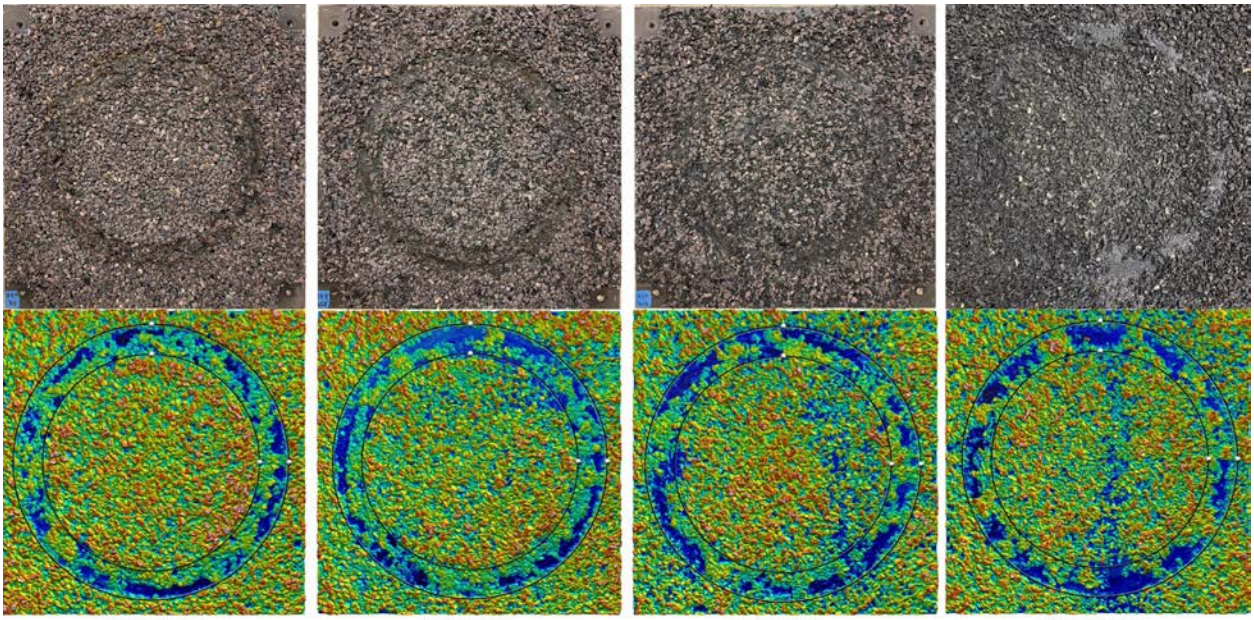

100T50E 75T50E 50T50E 100R50E

(b)

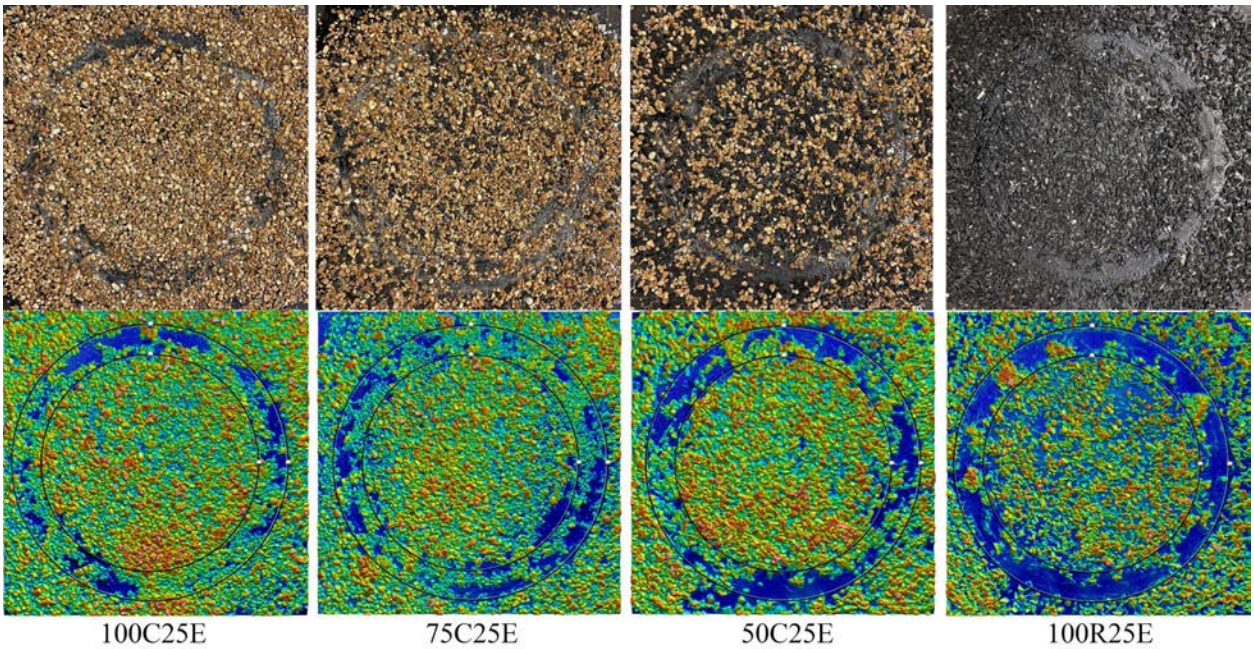

(c)

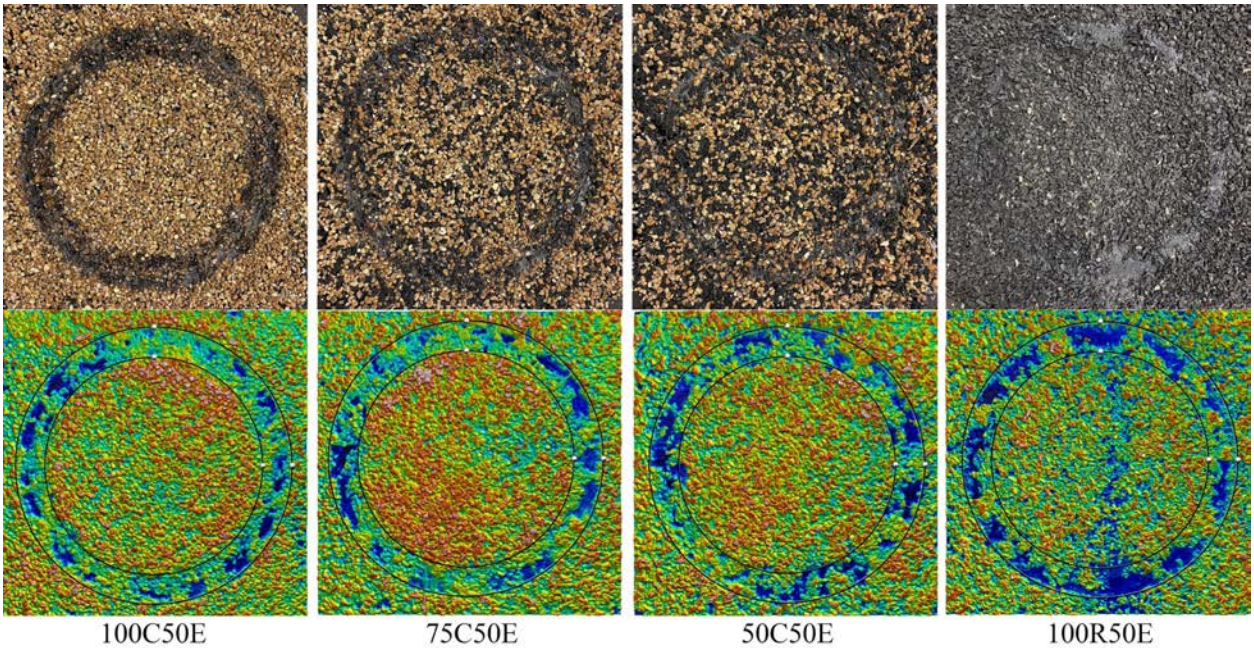

(d)

Fig. 5.6 – SWTS test results after 100,000 wheel applications on Phase I specimens including (a) trap rock with 0.25 gal/yd^2 emulsion rate, (b) trap rock with 0.50 gal/yd^2 emulsion rate, (c) creek gravel with 0.25 gal/yd^2 emulsion rate, and (d) creek gravel with 0.50 gal/yd^2 emulsion rate.

5.4.2. Effect of Rubber Content

Fig. 5.7a and 5.7b show the V_m values versus the number of wheel applications for trap rock chip seal specimens with 0.25 gal/yd^2 and 0.50 gal/yd^2 emulsion rates, respectively. Trap rock specimens showed in Fig. 5.7 had different volumetric crumb rubber content from 0% to 100%. As explained earlier in this chapter, V_m was obtained from the analysis of the 3D scanned surface of chip seal specimens and represents the mean thickness of the macrotexture over the wheel path surface area. As shown in Fig. 5.7, different specimens did not have the same initial V_m. Although the specimens of this study were made with natural aggregate and crumb rubber with close gradation, the initial macrotexture of the specimens before experiencing any traffic load was not the same due to the random orientation of the particles. Fig. 5.7 shows that with increasing the wheel applications on the chip seal surfaces, the specimens experienced more aggregate loss. However, different specimens experienced different amounts of aggregate loss. It can also be observed in Fig. 5.7 that the major macrotexture variation and loss have happened in the first 20,000 wheel applications.

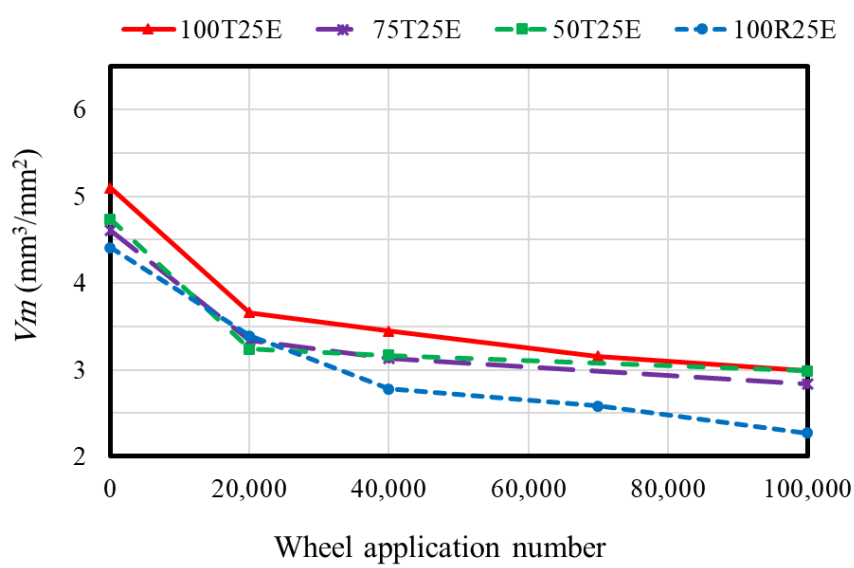

(a)

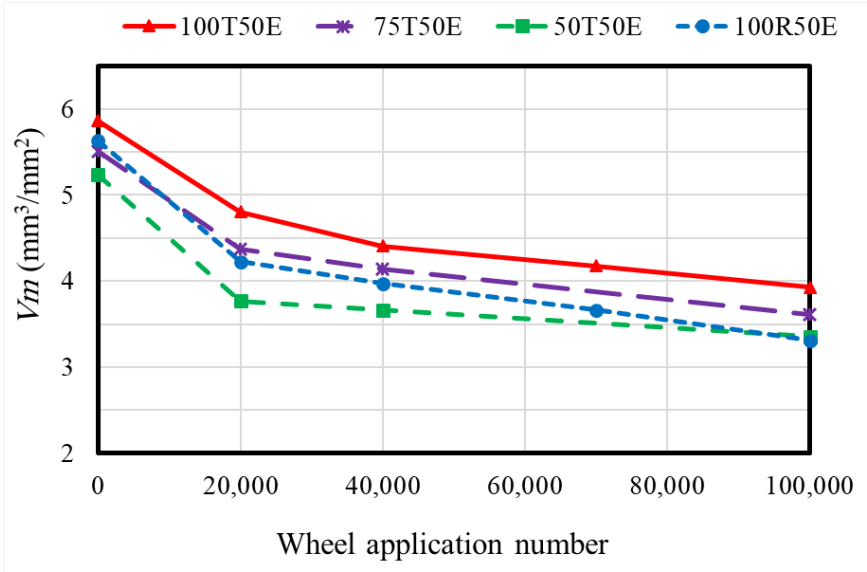

(b)

Fig. 5.7 – V_m versus wheel application number for trap rock specimens with different rubber content and (a) 0.25 gal/yd^2 emulsion rate, and (b) 0.50 gal/yd^2 emulsion rate.

Fig. 5.8 and 5.9 provide a clearer comparison of the V_m values at the end of the SWTS test. Fig. 5.8a and 5.9a present the V_m value at the end of 100,000 wheel applications in the SWTS test for trap rock specimens with emulsion rates of 0.25 gal/yd^2 and 0.50 gal/yd^2, respectively. Fig. 5.8b and 5.9b present the ratio of the V_m value at the end of 100,000 wheel applications to the initial V_m value of the same specimens.

As shown in Fig. 5.8, at the binder application rate of 0.25 gal/yd^2, the specimen with 100% crumb rubber had the V_m of 2.3 mm^3/mm^2 compared to 3.0 mm^3/mm^2 for the specimen with 100% trap rock. Also, considering the initial V_m values, the 100% rubber specimen experienced 49% V_m loss compared to 41% V_m loss for 100% trap rock specimen. 25% and 50% of rubber content also resulted in 2.8 and 3.0 mm^3/mm^2 final V_m corresponding to 38% and 32% V_m loss, respectively. These results indicate that in a low binder rate of 0.25 gal/yd^2, increasing the rubber content up to

50% slightly improved the raveling resistance of the trap rock chip seal. However, using a 100% rubberized chip seal will perform poorly.

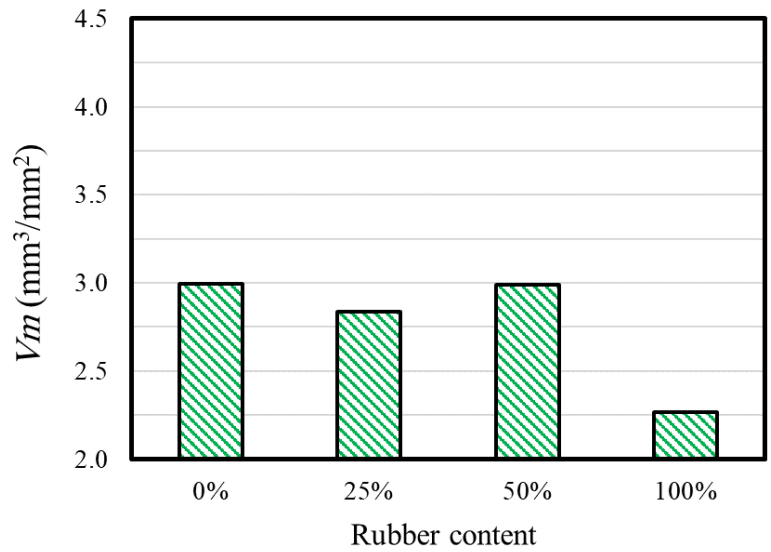

(a)

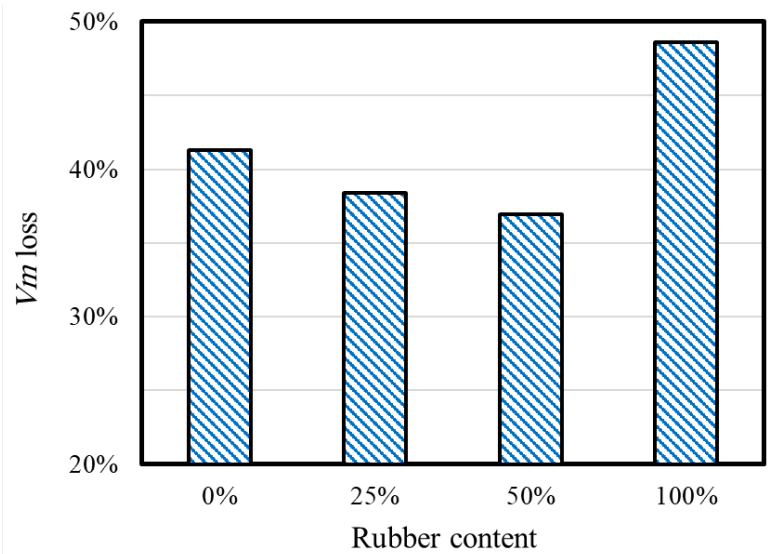

(b)

Fig. 5.8 – SWTS test results for trap rock specimens with 0.25 gal/yd^2 emulsion rate at the end of 100,000 wheel applications. (a) V_m value, (b) V_m loss percentage.

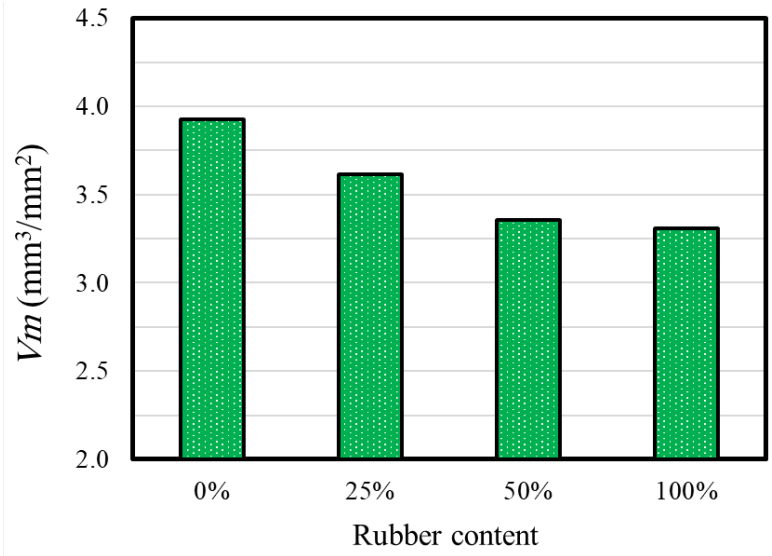

(a)

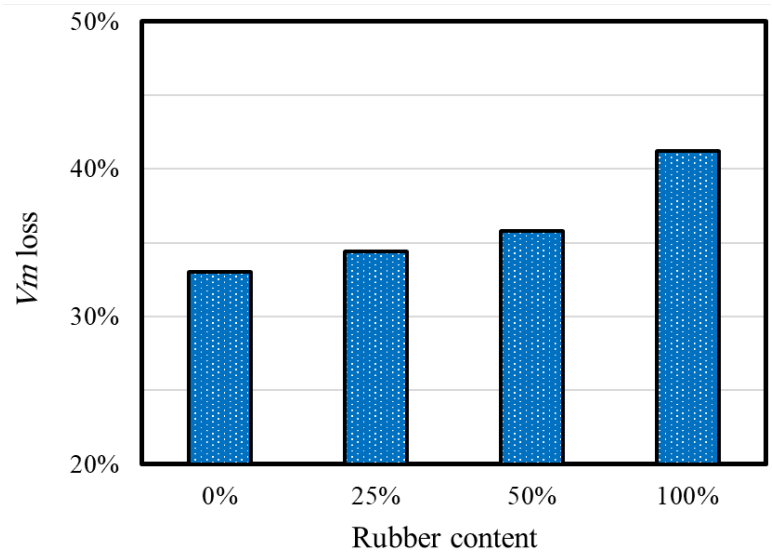

(b)

Fig. 5.9 – SWTS test results for trap rock specimens with 0.25 gal/yd^2 emulsion rate at the end of 100,000 wheel applications. (a) V_m value, (b) V_m loss percentage.

As shown in Fig. 5.9, at the binder application rate of 0.50 gal/yd^2, the specimen with 100% crumb rubber had the V_m of 3.3 mm^3/mm^2 compared to 3.9 mm^3/mm^2 for the specimen with 100% trap rock. Also, considering the initial V_m values, the 100% rubber specimen experienced 41% V_m loss compared to 33% V_m loss for 100% trap rock specimen. 25% and 50% of rubber content also

resulted in 3.6 and 3.4 mm^3/mm^2 final V_m corresponding to 34% and 36% V_m loss, respectively. These results indicated that in a higher binder rate of 0.50 gal/yd^2, increasing the rubber content up to 50% slightly impaired the raveling resistance of the trap rock chip seal.

Fig. 5.10a and 5.10b show the V_m values versus the number of wheel applications for creek gravel chip seal specimens with 0.25 gal/yd^2 and 0.50 gal/yd^2 emulsion rates, respectively. Creek gravel specimens shown in Fig. 5.10 had different volumetric crumb rubber content from 0% to 100%. As shown in Fig. 5.10, different specimens did not have the same initial V_m, which is related to the random orientation of the particles for the specimens before experiencing any traffic load. Fig. 5.10 shows that with increasing the wheel applications on the chip seal surfaces, the specimens experienced more aggregate loss. However, different specimens experienced different amounts of aggregate loss. It can also be observed in Fig. 5.10 that most of the macrotexture variation and loss had happened in the first 20,000 wheel applications.

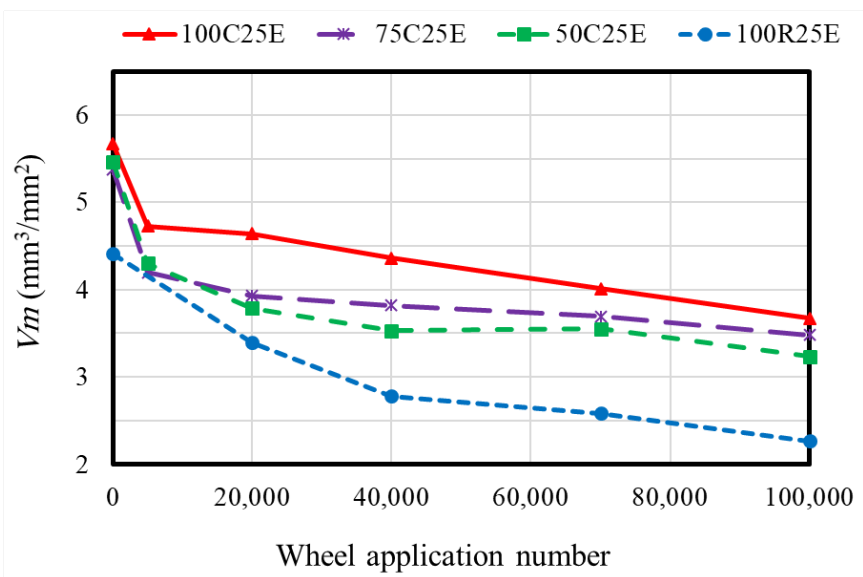

(a)

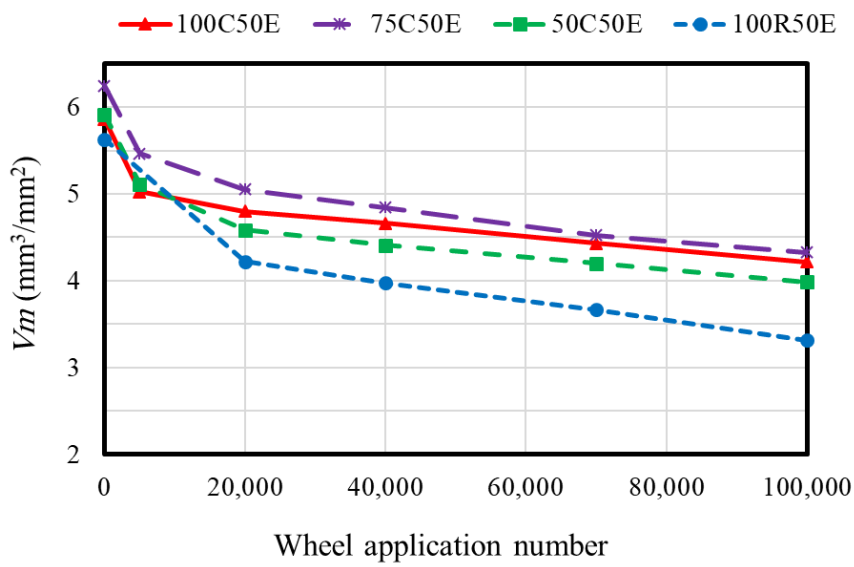

(b)

Fig. 5.10 – V_m versus wheel application number for creek gravel specimens with different rubber content and (a) 0.25 gal/yd^2 emulsion rate, and (b) 0.50 gal/yd^2 emulsion rate.

Fig. 5.11 and 5.12 provide a clearer comparison of the V_m values at the end of the SWTS test. Fig. 5.11a and 5.12a present the V_m value at the end of 100,000 wheel applications in the SWTS test for creek gravel specimens with emulsion rates of 0.25 gal/yd^2 and 0.50 gal/yd^2, respectively. Fig. 5.11b and 5.12b present the ratio of the V_m value at the end of 100,000 wheel applications to the initial V_m value of the same specimens.

As shown in Fig. 5.11, at the binder application rate of 0.25 gal/yd^2, the specimen with 100% crumb rubber had the V_m of 2.3 mm^3/mm^2 compared to 3.7 mm^3/mm^2 for the specimen with 100% creek gravel. Also, compared to the initial V_m values, the 100% rubber specimen experienced 49% V_m loss compared to 35% V_m loss for 100% creek gravel specimen. 25% and 50% of rubber content also resulted in 3.5 and 3.2 mm^3/mm^2 final V_m, corresponding to 35% and 41% V_m loss, respectively. These results indicated that in a low binder rate of 0.25 gal/yd^2, increasing the rubber content up to 25% did not affect the raveling resistance of the creek gravel

chip seal. However, the rubber content of more than 25% impaired the raveling resistance of the creek gravel chip seal.

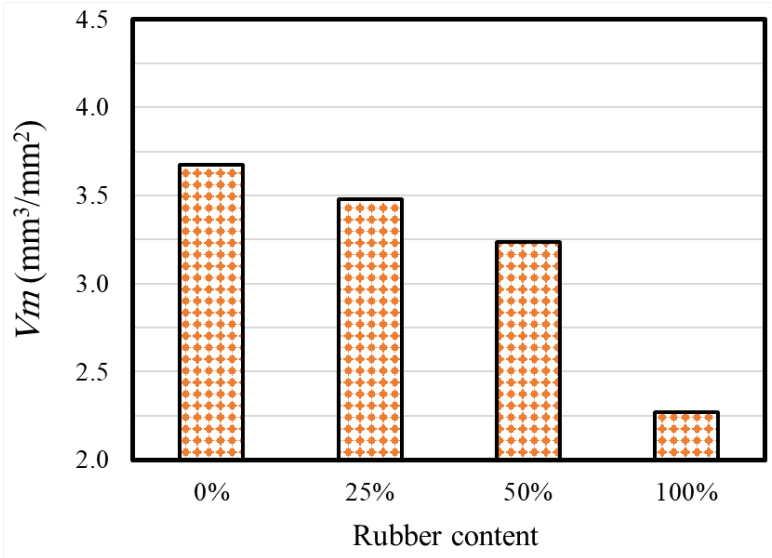

(a)

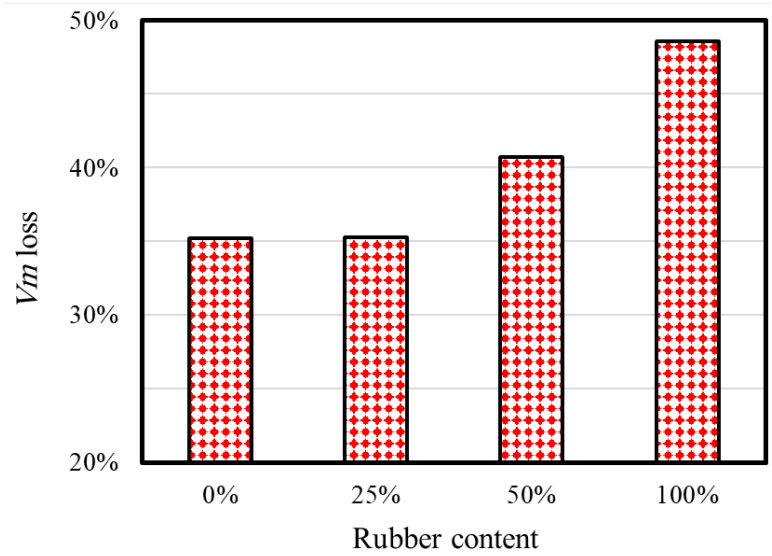

(b)

Fig. 5.11 – SWTS test results for creek gravel specimens with 0.25 gal/yd^2 emulsion rate at the end of 100,000 wheel applications. (a) V_m value, (b) V_m loss percentage.

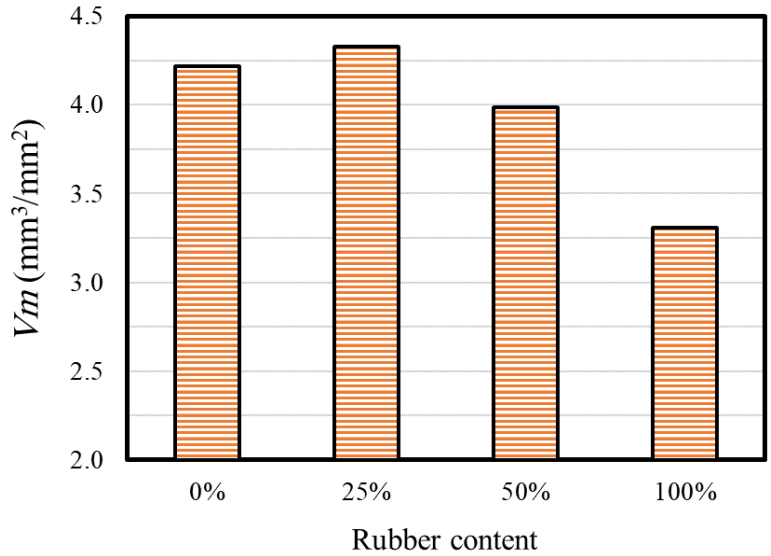

(a)

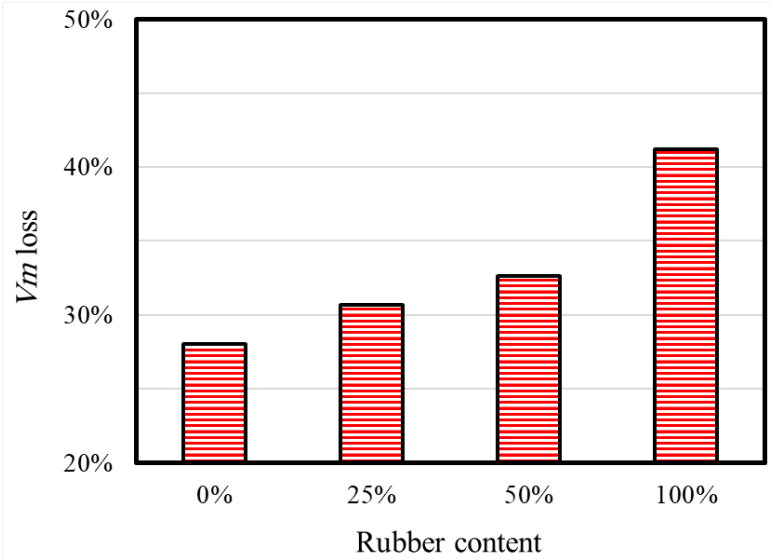

(b)

Fig. 5.12 – SWTS test results for creek gravel specimens with 0.25 gal/yd^2 emulsion rate at the end of 100,000 wheel applications. (a) V_m value, (b) V_m loss percentage.

As shown in Fig. 5.12, at the binder application rate of 0.50 gal/yd^2, the specimen with 100% crumb rubber had the V_m of 3.3 mm^3/mm^2 compared to 4.2 mm^3/mm^2 for the specimen with 100% creek gravel. Also, compared to the initial V_m values, the 100% rubber specimen experienced 41% V_m loss compared to 28% V_m loss for 100% creek gravel specimen. 25% and

50% of rubber content also resulted in 4.3 and 4.0 mm^3/mm^2 final V_m, corresponding to 31% and 33% V_m loss, respectively. These results indicate that in a higher binder rate of 0.50 gal/yd^2, increasing the rubber content up to 50% slightly impaired the raveling resistance of the trap rock chip seal.

In conclusion, for trap rock chip seal specimens, replacing up to 50% of the volume of trap rock aggregate with crumb rubber particles did not significantly affect the raveling resistance of the specimens for both 0.25 and 0.50 gal/yd^2 binder rates. In the case of creek gravel chip seal specimens, replacing up to 25% of the volume of creek gravel aggregate with crumb rubber particles did not significantly affect the raveling resistance of the specimens for both 0.25 and 0.50 gal/yd^2 binder rates. Increasing the rubber content more than 50% and 25% for trap rock and creek gravel chip seal, respectively, impaired the raveling resistance of the specimens.

The chip seal specimens with 100% crumb rubber as aggregate performed poorly, especially with the lower binder application rate of 0.25 gal/yd^2. Similar results were obtained for crumb rubber chip seal compared to trap rock and creek gravel chip seal specimens in another study conducted by the authors using the standard sweeping test [8]. The performance can be attributed to a weaker bond of the crumb rubber particles with the emulsified asphalt binder due to the low water absorption of the rubber particles.

5.4.3. Effect of Binder Application Rate

Fig. 5.13, 5.14, and 5.15 provide a comparison of the V_m values for specimens with different binder rates at the end of the SWTS test for trap rock, creek gravel, and crumb rubber specimens, respectively. Fig. 5.13a, 5.14a, and 5.15a present the V_m value at the end of 100,000 wheel applications in the SWTS test for specimens with different binder rates made of trap rock, creek gravel, and crumb rubber, respectively. Fig. 5.13b, 5.14b, and 5.15b present the ratio of the

V_m value at the end of 100,000 wheel applications to the initial V_m value of the same specimens for trap rock, creek gravel, and crumb rubber specimens, respectively.

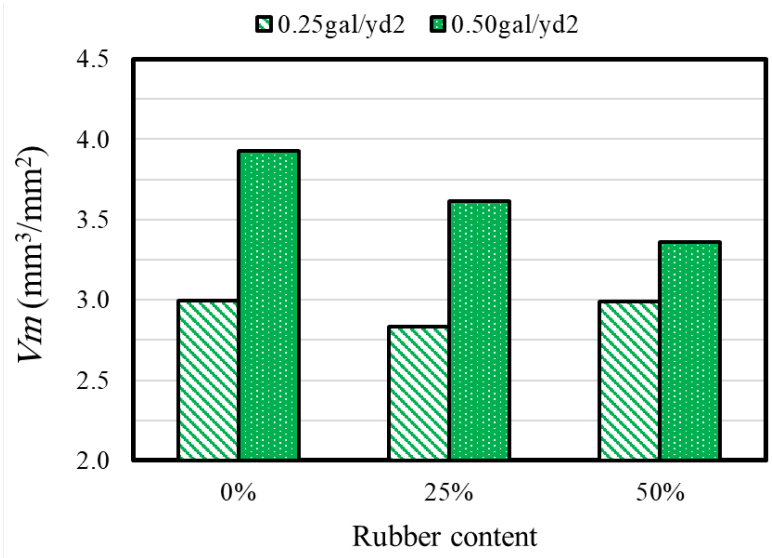

(a)

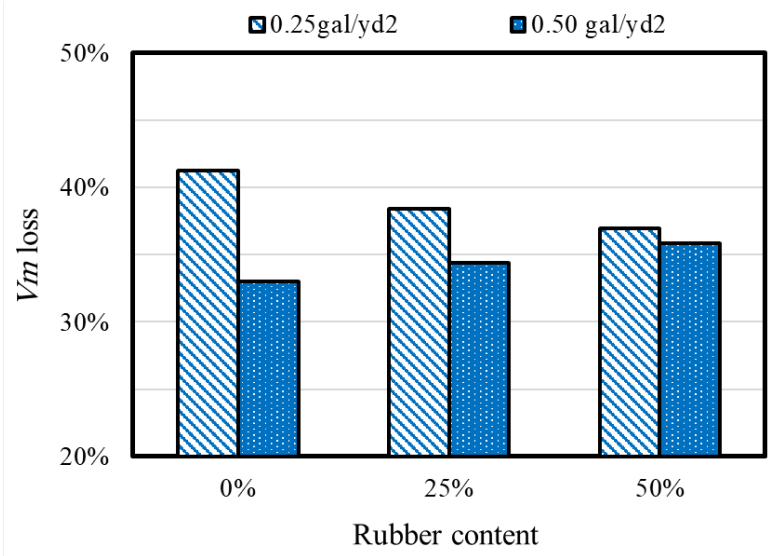

(b)

Fig. 5.13 – Microtexture comparison for trap rock specimens with different emulsion rates at the end of 100,000 wheel applications in the SWTS test. (a) V_m value, (b) V_m loss percentage.

As shown in Fig. 5.13, increasing the binder application rate from 0.25 gal/yd^2 to 0.50 gal/yd^2 increased the final V_m value between 0.9 to 0.4 mm^3/mm^2 for trap rock specimens with 0% to 50% rubber content, respectively. Also, compared to the initial V_m values, increasing the binder application rate from 0.25 gal/yd^2 to 0.50 gal/yd^2 reduced the V_m loss between 8 to 1% for trap rock specimens with 0% to 50% rubber content, respectively.

As shown in Fig. 5.14, increasing the binder application rate from 0.25 gal/yd^2 to 0.50 gal/yd^2 increased the final V_m value between 0.5 to 0.8 mm^3/mm^2 for creek gravel specimens with 0% to 50% rubber content, respectively. Also, compared to the initial V_m values, increasing the binder application rate from 0.25 gal/yd^2 to 0.50 gal/yd^2 reduced the V_m loss between 7 to 8% for creek gravel specimens with 0% to 50% rubber content, respectively.

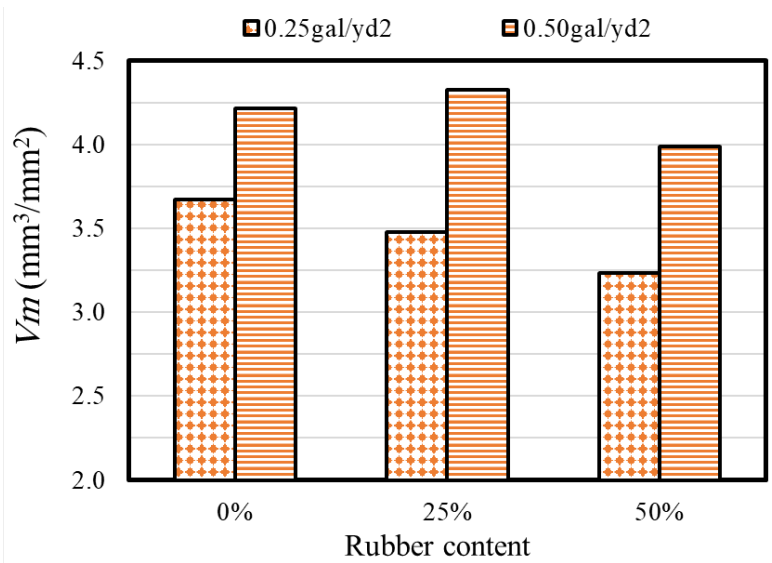

(a)

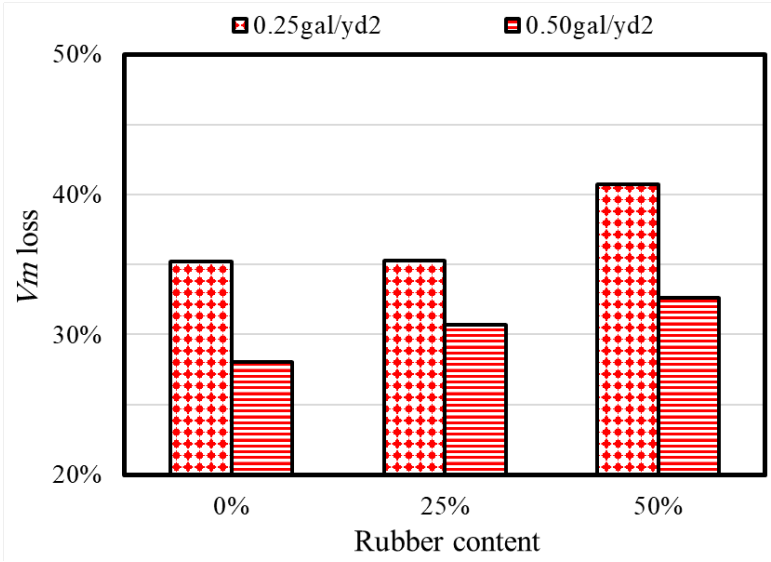

(b)

Fig. 5.14 – Microtexture comparison for creek gravel specimens with different emulsion rates at the end of 100,000 wheel applications in the SWTS test. (a) V_m value, (b) V_m loss percentage.

As shown in Fig. 5.15, for 100% rubberized chip seal specimens increasing the binder application rate from 0.25 gal/yd^2 to 0.50 gal/yd^2 increased the final V_m value for 1.0 mm^3/mm^2 which is corresponding to 7% reduction of the of V_m loss.

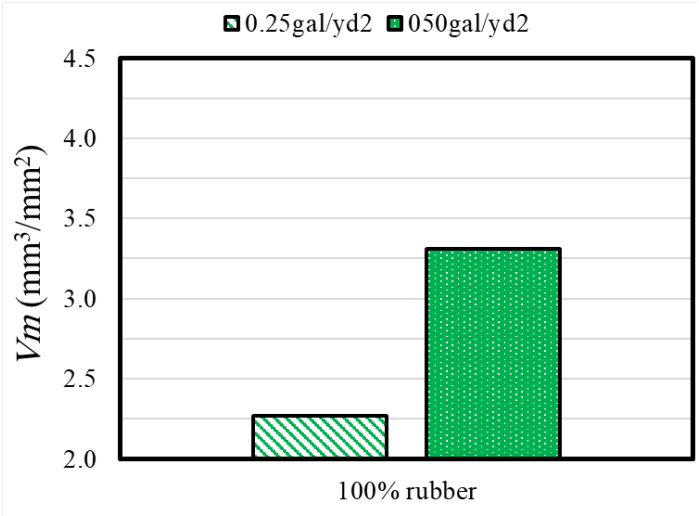

(a)

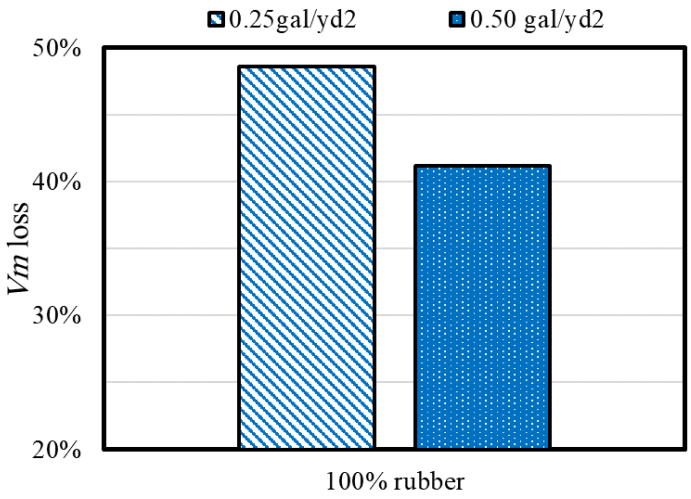

(b)

Fig. 5.15 – Microtexture comparison for crumb rubber specimens with different emulsion rates at the end of 100,000 wheel applications in the SWTS test. (a) V_m value, (b) V_m loss percentage.

In conclusion, increasing the binder rate from 0.25 to 0.50 gal/yd^2 considerably improved the raveling resistance of chip seal specimens made with trap rock, creek gravel, and crumb rubber. The V_m loss reduced up to 8% by increasing the binder rate from 0.25 to 0.50 gal/yd^2 for all three aggregate types. Since the higher binder application rate leads to a higher embedment depth of the particles which provides more surface area of the aggregate in contact with binder, leading to an improved bond. However, the risk of bleeding will increase with increasing the binder rate which should be considered. In this regards, visual inspection of the tested specimens indicated a moderate bleeding distress for 100% and 75% creek gravel specimen with 0.50 gal/yd^2 binder rate as shown in Fig. 5.16. However, for 75% creek gravel specimen the bleeding distress was lower than 100% creek gravel one. No other considerable bleeding distress observed for other test specimens.

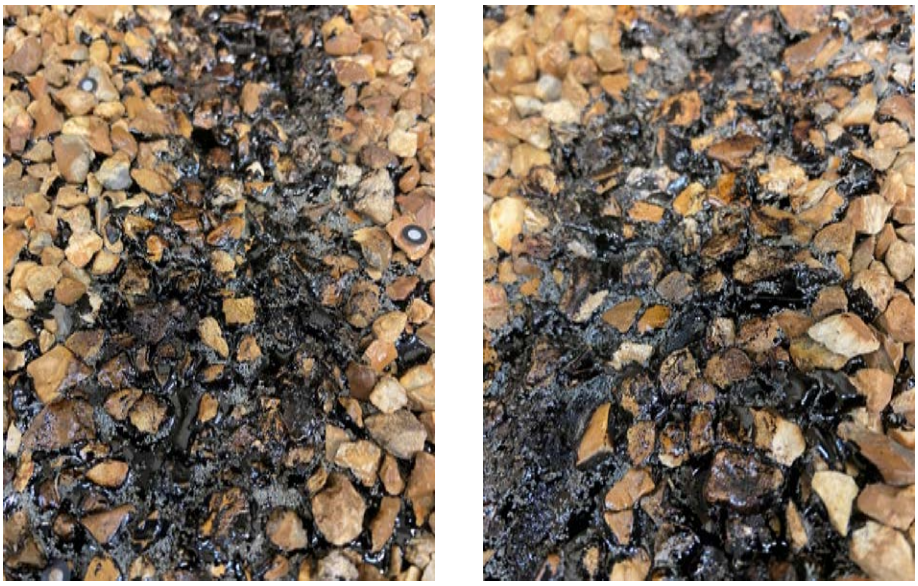

(a)

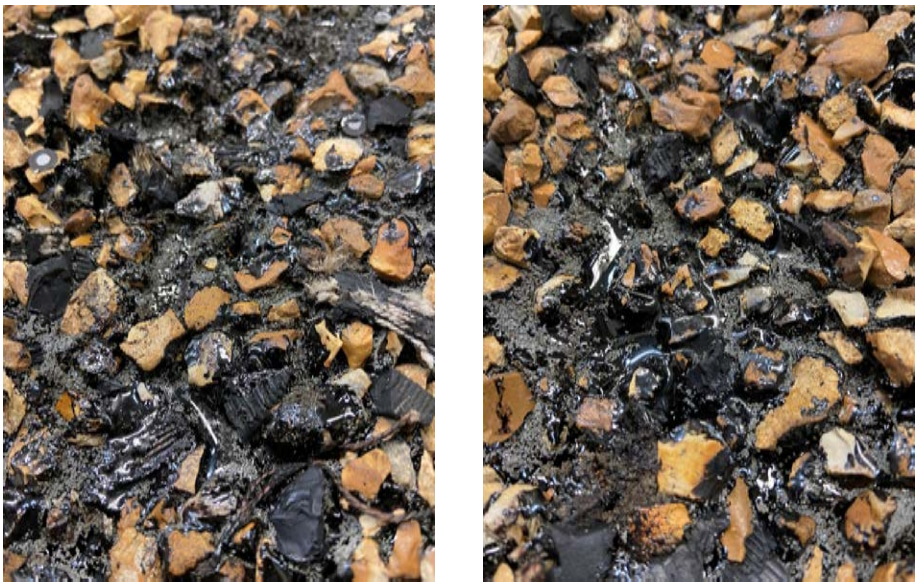

(b)

Fig. 5.16 – Bleeding distress observed in phase I tests for (a) 100C50E, (b) 75C50E specimens.

5.4.4. Effect of Aggregate Type

Fig. 5.17 and 5.18 provide a comparison of the V_m values at the end of the SWTS test for different natural aggregate used in this study, i.e., trap rock and creek gravel. Fig. 5.17a and 5.18a present the V_m value at the end of 100,000 wheel applications in the SWTS test for trap rock and

creek gravel specimens with binder rates of 0.25 gal/yd^2 and 0.50 gal/yd^2, respectively. Fig. 5.17b and 5.18b present the ratio of the V_m value at the end of 100,000 wheel applications to the initial V_m value of the same specimens for trap rock and creek gravel with binder rates of 0.25 gal/yd^2 and 0.50 gal/yd^2, respectively.

As shown in Fig. 5.17a at the binder application rate of 0.25 gal/yd^2, creek gravel specimens provided a higher final V_m value compared to trap rock specimens. The V_m value for creek gravel specimens with 0%, 25%, and 50% crumb rubber was 3.7, 3.5, and 3.2 mm^3/mm^2, respectively. While the V_m value for corresponding trap rock specimens with 0%, 25%, and 50% crumb rubber was 3.0, 2.8, and 3.0 mm^3/mm^2, respectively. The higher V_m value for creek gravel chip seal specimens can be attributed to the slightly higher D50 (median particle size) and D60 of the creek gravel aggregate used in this study compared to trap rock; the D50 and D60 of the creek gravel were 0.26 and 0.29, respectively, compared to 0.25 and 0.28 for the trap rock.

As shown in Fig. 5.17b at the binder application rate of 0.25 gal/yd^2, creek gravel specimens provided a lower V_m loss percentage compared to trap rock specimens in most cases. The V_m loss for creek gravel specimens with 0%, 25%, and 50% crumb rubber was 35, 35, and 41%, respectively. While the V_m loss for corresponding trap rock specimens with 0%, 25%, and 50% crumb rubber was 41, 38, and 37%, respectively. The lower V_m loss for creek gravel chip seal specimens can be attributed to the significantly lower flakiness index of the creek gravel aggregate used in this study compared to trap rock. Since the flakiness index of the creek gravel aggregate was 15 compared to 42 for the trap rock. Moreover, the creek gravel aggregate had a higher water absorption of 4.67% compared to 2.27% for trap rock. The higher water absorption would provide a higher bond between the creek gravel aggregate and the emulsified asphalt.

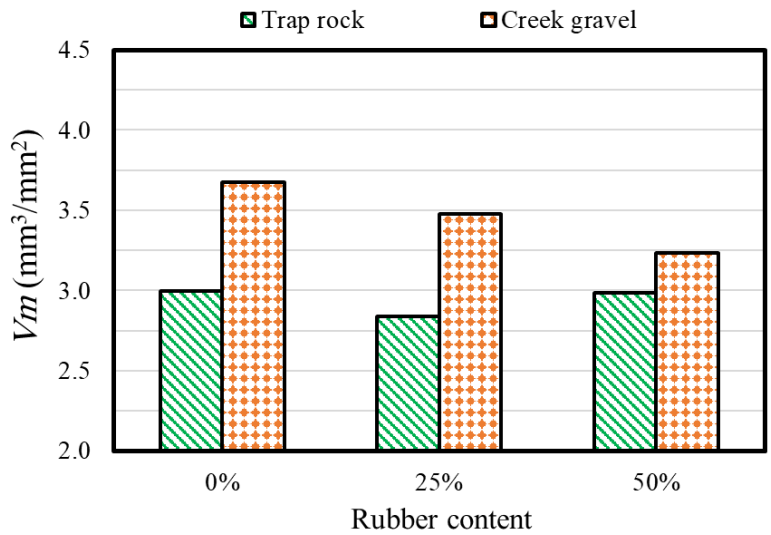

(a)

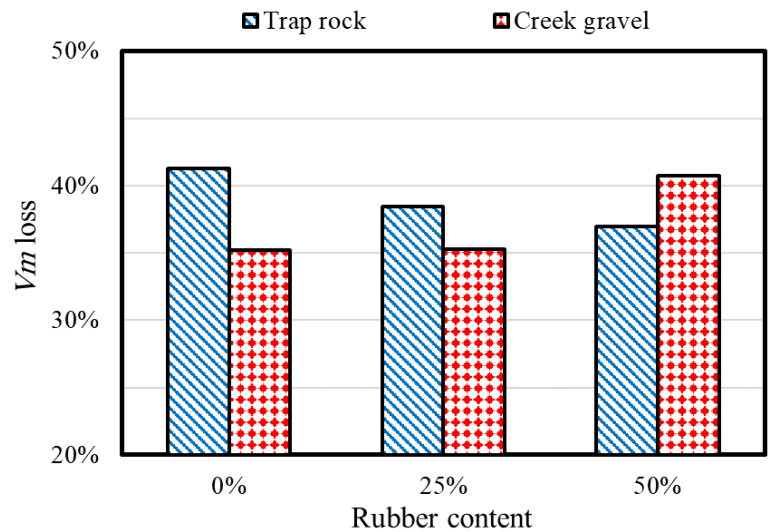

(b)

Fig. 5.17 – Microtexture comparison for chip seal specimens with 0.25 gal/yd^2 binder rate and different natural aggregate types at the end of 100,000 wheel applications in the SWTS test. (a) V_m value, (b) V_m loss percentage.

As shown in Fig. 5.18a, at the binder application rate of 0.50 gal/yd^2 creek gravel specimens also provided a higher final V_m value compared to trap rock specimens. The V_m value for creek gravel specimens with 0%, 25%, and 50% crumb rubber was 4.2, 4.3, and 4.0 mm^3/mm^2, respectively. While the V_m value for corresponding trap rock specimens with 0%, 25%, and 50%

crumb rubber was 3.9, 3.6, and 3.4 mm^3/mm^2, respectively. As mentioned earlier, the higher V_m value for creek gravel chip seal specimens can be attributed to the slightly higher D50 (median particle size) and D60 of the creek gravel aggregate used in this study compared to trap rock. The D50 and D60 of the creek gravel were 0.26 and 0.29, respectively, compared to 0.25 and 0.28 for the trap rock.

As shown in Fig. 5.18b, at the binder application rate of 0.50 gal/yd^2, creek gravel specimens also provided a lower V_m loss percentage compared to trap rock specimens for different rubber contents. The V_m loss for creek gravel specimens with 0%, 25%, and 50% crumb rubber was 28, 31, and 33%, respectively. While the V_m loss for corresponding trap rock specimens with 0%, 25% and 50% crumb rubber was 33, 34, and 36%, respectively. As mentioned earlier, the lower V_m loss for creek gravel chip seal specimens can be attributed to the significantly lower flakiness index of the creek gravel aggregate used in this study compared to trap rock, since the flakiness index of the creek gravel aggregate was 15, compared to 42 for the trap rock. Moreover, the creek gravel aggregate had a higher water absorption of 4.67% compared to 2.27% for trap rock. The higher water absorption would provide a higher bond between the creek gravel aggregate and the emulsified asphalt.

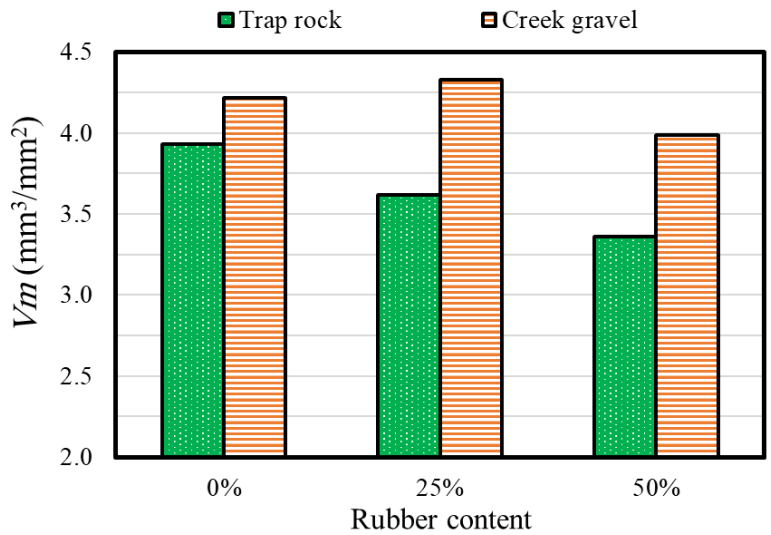

(a)

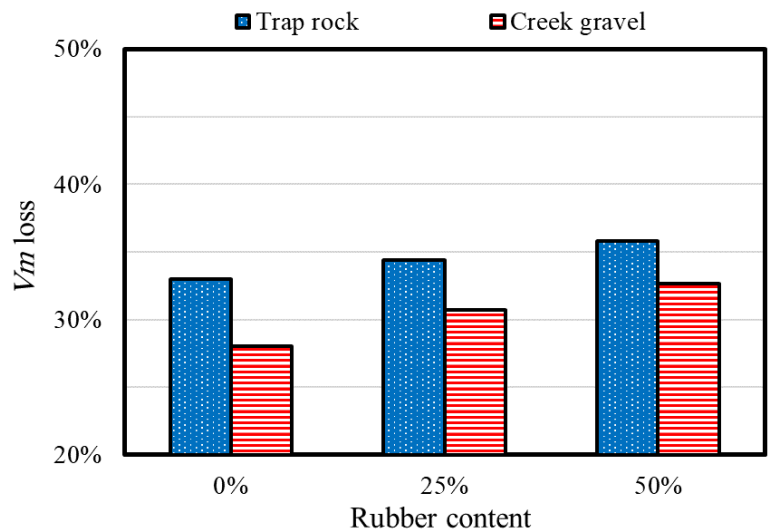

(b)

Fig. 5.18 – Microtexture comparison for chip seal specimens with 0.50 gal/yd^2 binder rate and different natural aggregate types at the end of 100,000 wheel applications in the SWTS test. (a) V_m value, (b) V_m loss percentage.

In conclusion, the creek gravel chip seal performed better in terms of raveling compared to trap rock chip seal. Creel gravel specimens experienced up to 6% V_m loss compared to trap rock specimens. Two reasons can be considered for these results. The first one is the considerably lower flakiness index of creek gravel particles compared to trap rock. The lower flakiness index indicates

more cubic shaped particles, which will provide a more stable chip seal surface under traffic load. The flakiness index of the creek gravel aggregate was 15 compared to 42 for the trap rock. Second, the creek gravel aggregate absorbs more water compared to trap rock, and the higher water absorption will provide a better bond between the aggregate and the emulsified asphalt. The water absorption of the creek gravel aggregate was 4.67% compared to 2.27% for trap rock.

5.4.5. Effect of Load Magnitude

Fig. 5.19 shows the final state of trap rock chip seal specimens with 0.50 gal/yd^2 emulsion rate and different volumetric crumb rubber content from 0% to 100% at the end of 100,000 wheel applications in the SWTS test. The specimens in Fig. 5.19a had been tested in Phase I of this study, and the specimens in Fig. 5.19b had been tested in Phase II. Phase II evaluates the effect of traffic load magnitude. The applied load magnitude in Phase II was 172.25 lb, which provided a surface contact stress of 27.87 psi compared to the load magnitude in Phase I that was 87.25 lb, which provided a surface contact stress of 14.12 psi under each wheel. Other specimens and loading parameters were identical for both series of specimens. Specimens that were compared in this section have been made with trap rock and crumb rubber with a binder application rate of 0.50 gal/yd^2 and tested under the loading speed of 120 wheel applications per minute (wpm).

Fig 5.19 also presents the topographic pseudo-color view for each chip seal specimen for better visualization of the surface which simply shows the difference in the texture of different spots. The dark blue color in the figures represents the points with the lowest elevation, and the red spots represent the points with the highest elevation on each surface. Also, the wheel path is outlined on the topographic surfaces in Fig. 5.19.

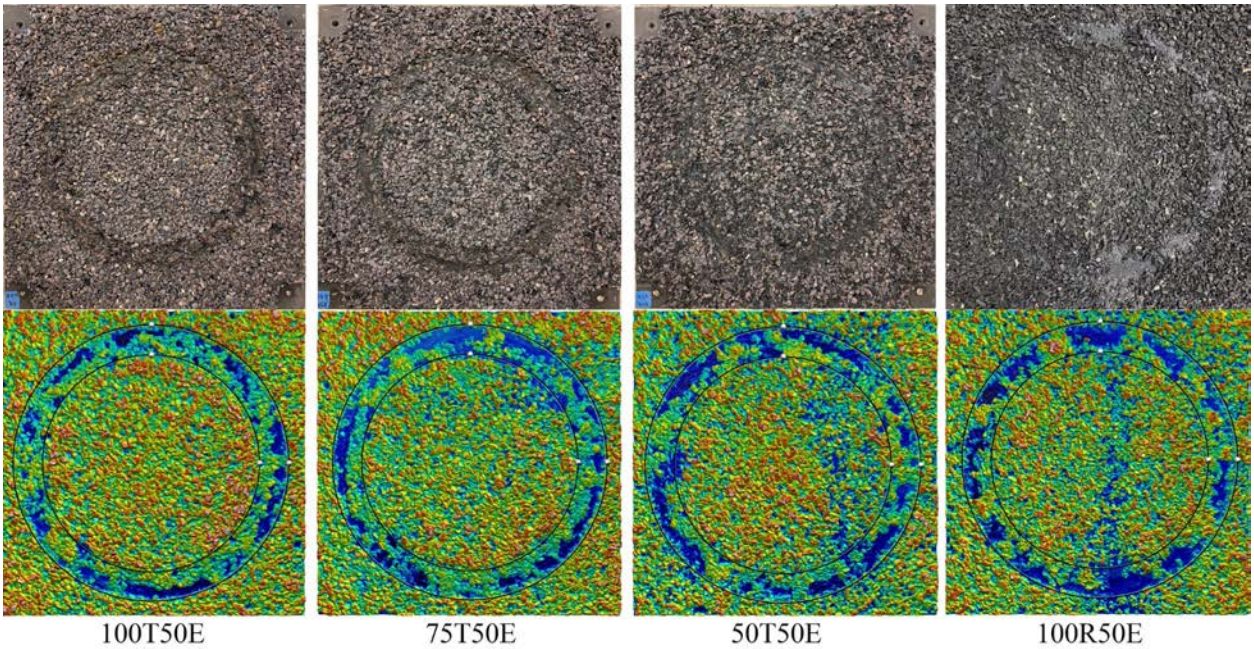

(a)

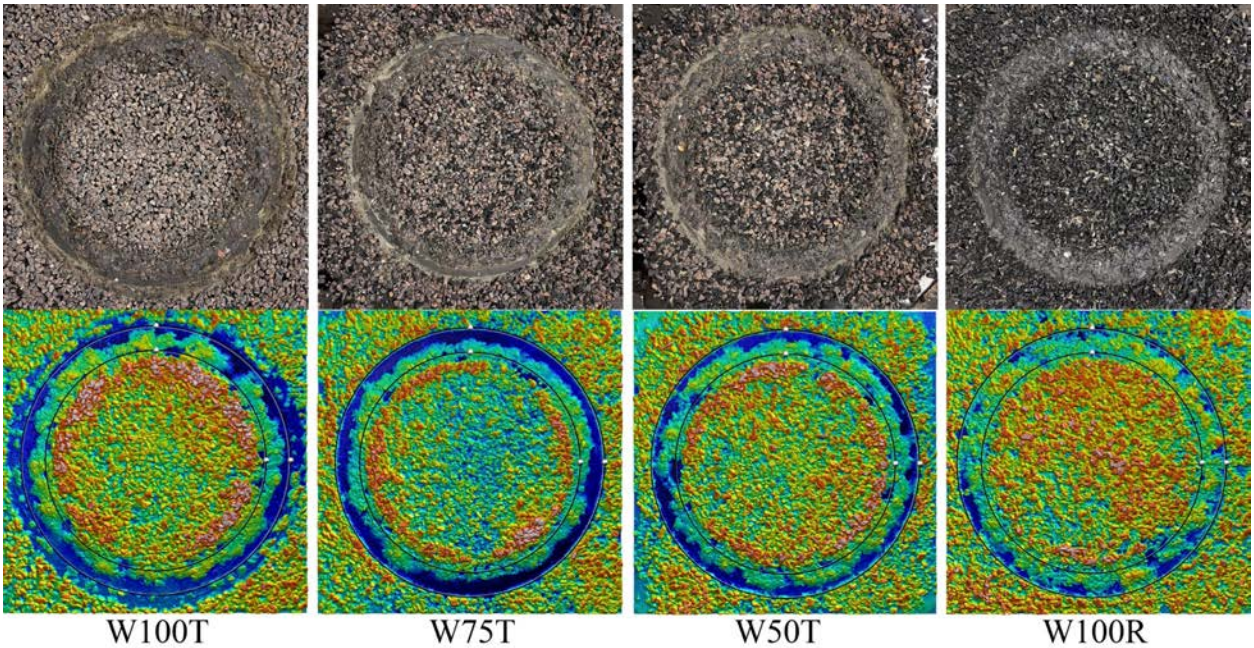

(b)

Fig. 5.19 – Real photo and topographic surface showing the final state of trap rock chip seal specimens tested for 100,000 wheel applications in the SWTS test under different load (a)14 psi and (b) 28 psi load pressure.

Fig. 5.20 shows the V_m vaues versus the number of wheel applications for trap rock specimens with 0.50 gal/yd^2 tested under 28 psi load pressure in Phase II of this study. Phase II specimens had different volumetric crumb rubber content from 0% to 100%. As shown in Fig. 5.20, different specimens have close initial V_m values. However, the initial V_m of the specimens were not identical because of the random orientation of the particles before experiencing any traffic load. Fig. 5.20 shows that with increasing the wheel applications on the chip seal surfaces, the specimens experienced more aggregate loss. However, different specimens experienced different amounts of aggregate loss.

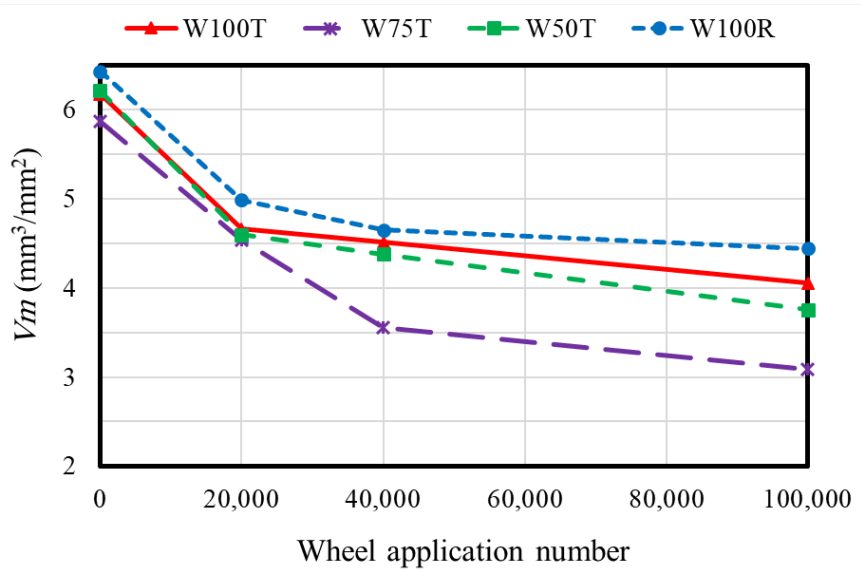

Fig. 5.20 – V_m versus wheel application number for Phase II specimens.

Fig. 5.21 provides a comparison of the V_m values at the end of the SWTS test between the different Phase II specimens and also with the Phase I corresponding specimens. Fig. 5.21a presents the V_m value at the end of 100,000 wheel applications in the SWTS test for both Phase I and Phase II specimens. Fig. 5.21b presents the ratio of the V_m value at the end of 100,000 wheel applications to the initial V_m value of the same specimens for Phase I and Phase II.

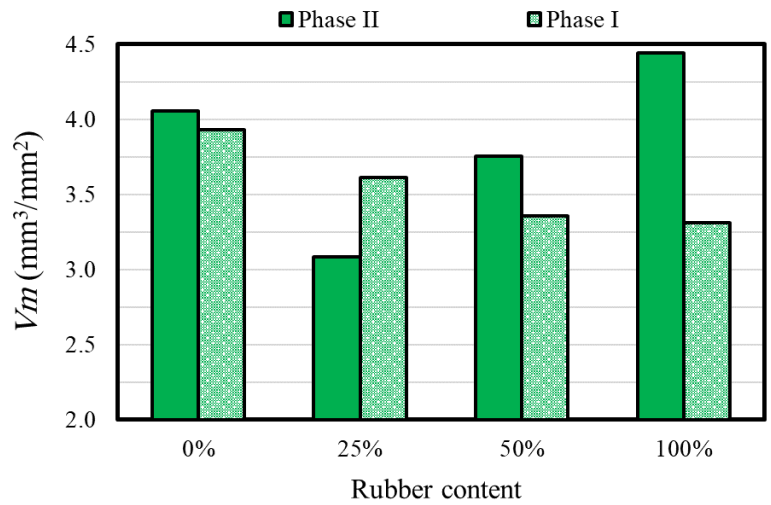

(a)

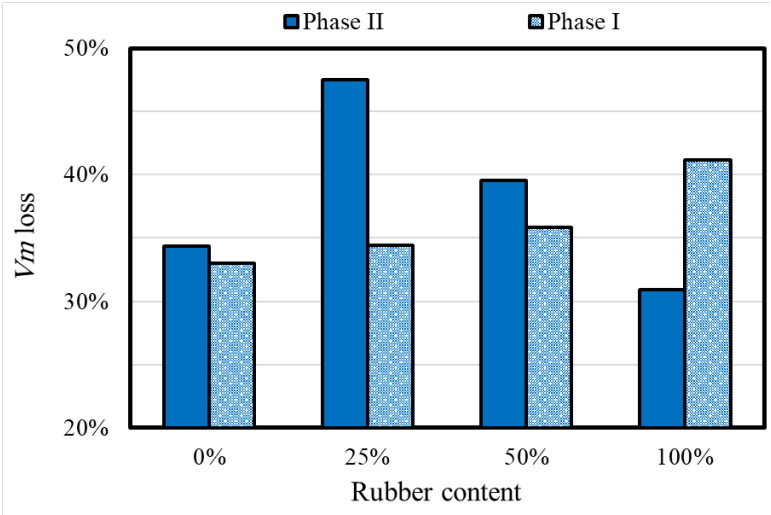

(b)

Fig. 5.21 – Microtexture comparison for chip seal specimens under different load magnitudes at the end of 100,000 wheel applications in the SWTS test. (a) V_m value, (b) V_m loss percentage.

As shown in Fig. 5.21a, for Phase II specimens with higher applied loads, with increasing the rubber content from 0 to 25%, the final V_m value reduced from 4.1 to 3.1 mm^3/mm^2, while with increasing the rubber content from 25 to 50 and then 100%, the final V_m value increased from 3.1 to 3.8 and 4.4 mm^3/mm^2, respectively. Also, the V_m loss percentage increased from 34 to 47% by increasing the rubber content from 0 to 25% as shown in Fig. 5.21b, while with increasing the

rubber content from 25 to 50 and then 100%, the V_m loss decreased from 47 to 40 and 31%, respectively. Based on the results of Phase II specimens, the 100% rubberized chip seal has performed a better raveling resistance than the other specimens.

Comparing the Phase II test results with Phase I, as shown in Fig. 5.21b, with an increase in the load magnitude on the chip seal specimens of 0% rubber to 50% rubber, the aggregate loss increased. However, the 50% rubberized chip seal still provides more macrotexture, i.e., V_m value under higher load compared to the corresponding specimens tested under lower load. In the case of the 100% rubberized chip seal, the aggregate loss decreased considerably, i.e., 10% reduction in the V_m loss under the higher load magnitude, compared to lower load magnitude.

In conclusion, the results showed that the raveling resistance of the trap rock natural aggregate will be impaired by increasing the applied traffic load magnitude. While for rubber aggregate, the behavior was the opposite and the raveling resistance was improved under a higher traffic load magnitude. The reason for this performance can be related to the natural characteristics of the crumb rubber particles. Although according to the Phase I test results, crumb rubber provided a weaker bond with the binder compared to the natural aggregate, it should be noted that rubber particles have different behavior under direct load compared to natural aggregate. This different behavior affected the rubberized chip seal performance under higher load magnitude. Rubber possesses the dual function of springing and damping. It has high hysteresis, i.e., energy loss or damping, and does not transmit completely the load imposed by the traffic to their bond with the binder, whereas hard materials like natural aggregates do not show hysteresis and will transmit the majority of the imposed traffic load to their bond with the binder. This behavior of the rubber particles may not be effective in regular loading conditions, while in high magnitudes of load, it was more pronounced and improved the raveling resistance. Therefore, replacing natural

aggregate with crumb rubber particles could be a solution for addressing the raveling distress under high magnitude traffic loads.

5.4.6. Effect of Traffic Speed

Fig. 5.22 shows the final state of trap rock chip seal specimens with a 0.50 gal/yd^2 emulsion rate and different volumetric crumb rubber content from 0% to 100% at the end of 100,000 wheel applications in the SWTS test. The specimens in Fig. 5.22a had been tested in Phase I of this study and the specimens in Fig. 5.22b had been tested in Phase III. Phase III evaluated the effect of traffic speed. The wheels' travel speed in Phase III was 160 wpm, which corresponds to a dynamic loading of 2.67 Hz on the chip seal surface. The wheels' travel speed in Phase I tests was 120 wpm, which corresponds to a dynamic loading of 2 Hz on the chip seal surface. Other specimens and loading parameters were identical for both series of specimens. Specimens that were compared in this section have been made with trap rock and crumb rubber aggregate with a binder application rate of 0.50 gal/yd^2 and tested under the load magnitude of 87.25 lb, which provided a surface contact stress of 14.12 psi under each wheel.

Fig 5.22 also presents the topographic pseudo-color view for each chip seal specimen for better visualization of the surface, which simply shows the difference in the texture of different spots. The dark blue color in the figures represents the points with the lowest elevation, and the red spots represent the points with the highest elevation on each surface. Also, the wheel path is outlined on the topographic surfaces in Fig. 5.22.

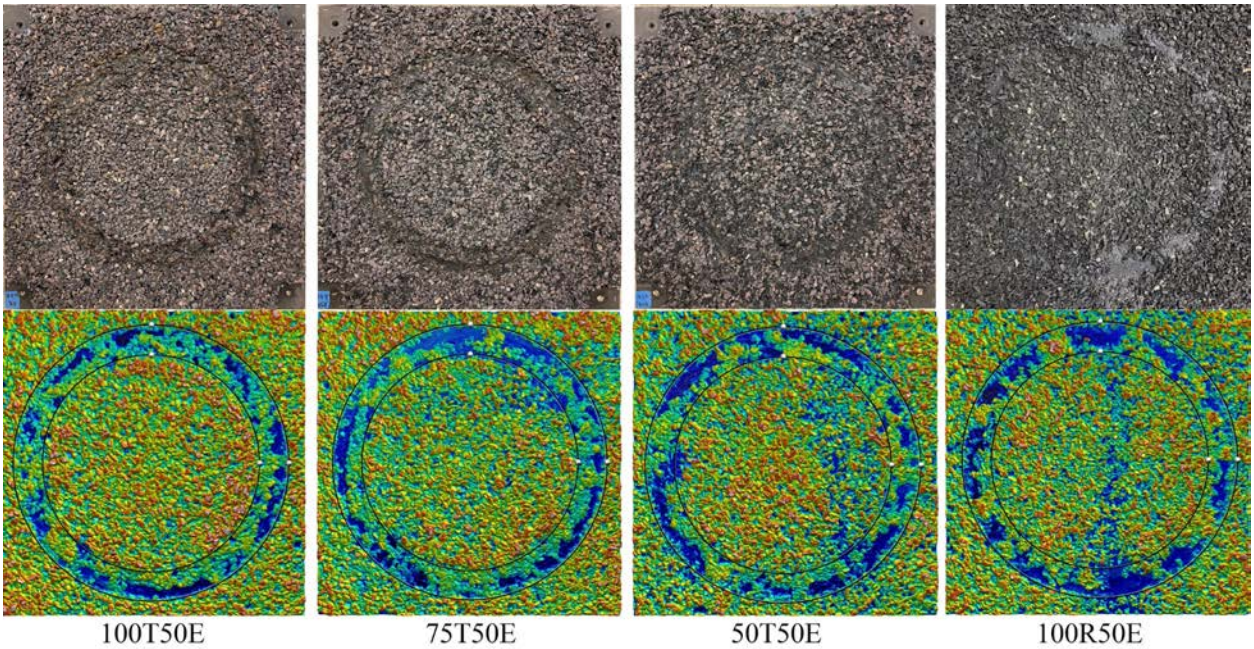

(a)

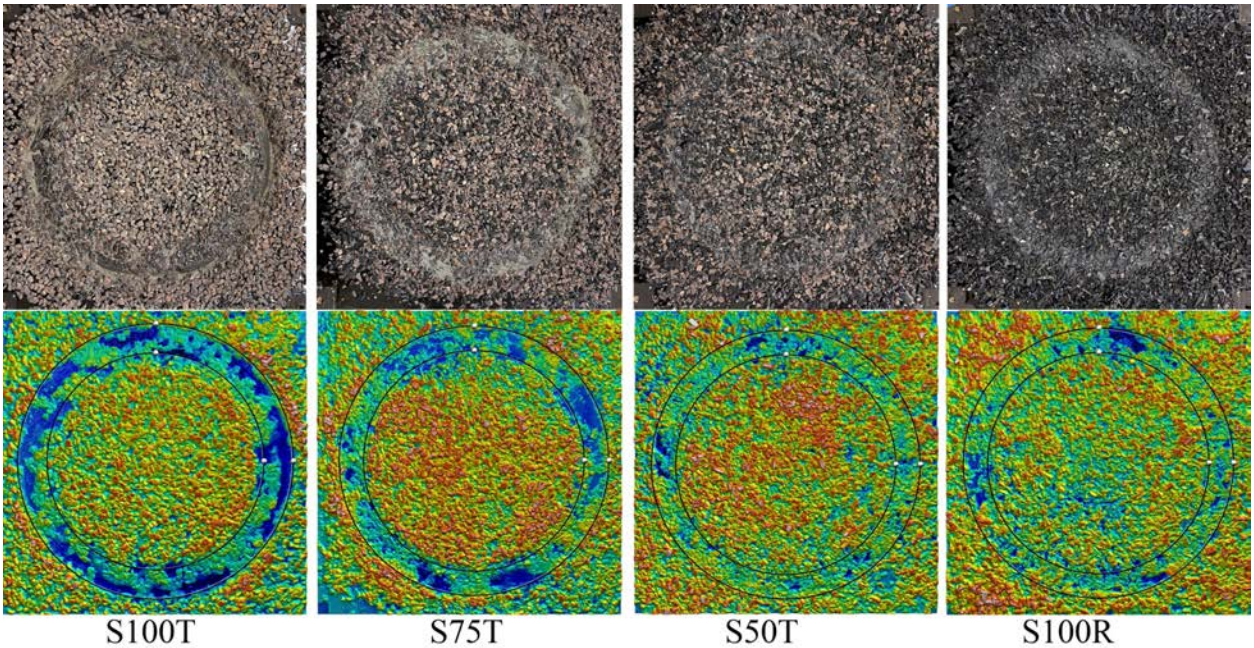

(b)

Fig. 5.22 – Real photo and topographic surface showing the final state of trap rock chip seal specimens tested for 100,000 wheel applications in the SWTS test under traffic speed of (a)120 wpm and (b) 160 wpm.

Fig. 5.23 shows the V_m values versus the number of wheel applications for trap rock specimens with 0.50 gal/yd^2 tested with 160 wpm loading speed in Phase III of this study. Phase III specimens shown in Fig. 5.23 had different volumetric crumb rubber content from 0% to 100%. As shown in Fig. 5.23, different specimens have close initial V_m values. However, the initial V_m of the specimens were not identical because of the random orientation of the particles before experiencing any traffic load. Fig. 5.23 shows that with increasing the wheel applications on the chip seal surfaces, the specimens experienced more aggregate loss. However, different specimens experienced different amounts of aggregate loss.

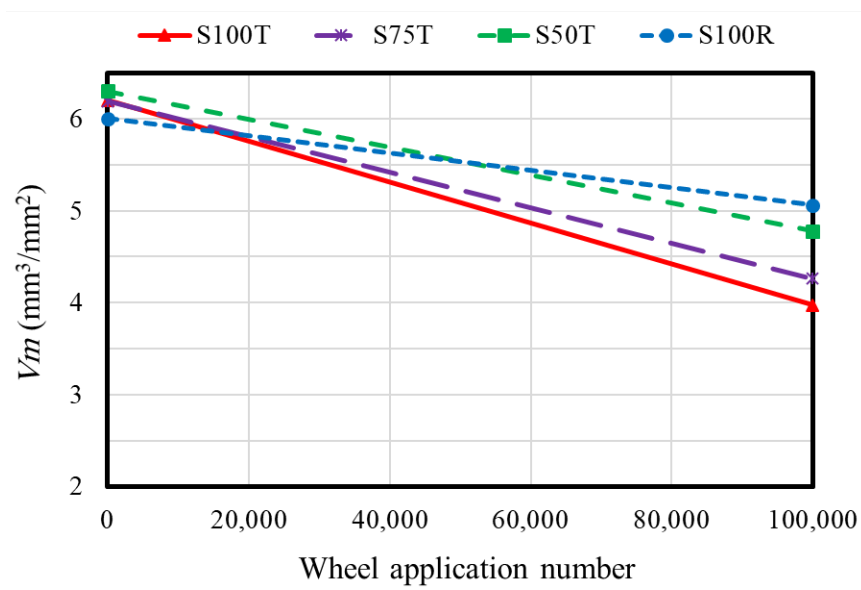

Fig. 5.23 – V_m versus wheel application number for Phase III specimens.

Fig. 5.24 shows the comparison of the V_m values at the end of the SWTS test between the different Phase III specimens and also with the Phase I corresponding specimens. Fig. 5.24a presents the V_m value at the end of 100,000 wheel applications in the SWTS test for both Phase I and Phase III specimens. Fig. 5.24b presents the ratio of the V_m value at the end of 100,000 wheel applications to the initial V_m value of the same specimens for Phase I and Phase III.

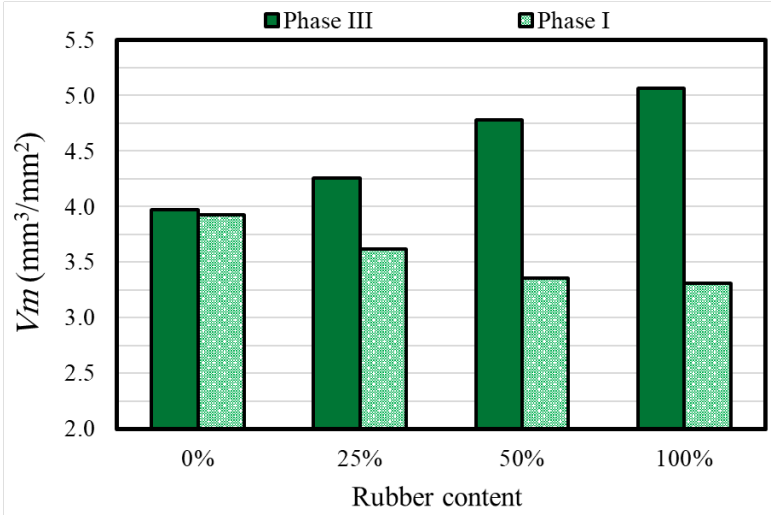

(a)

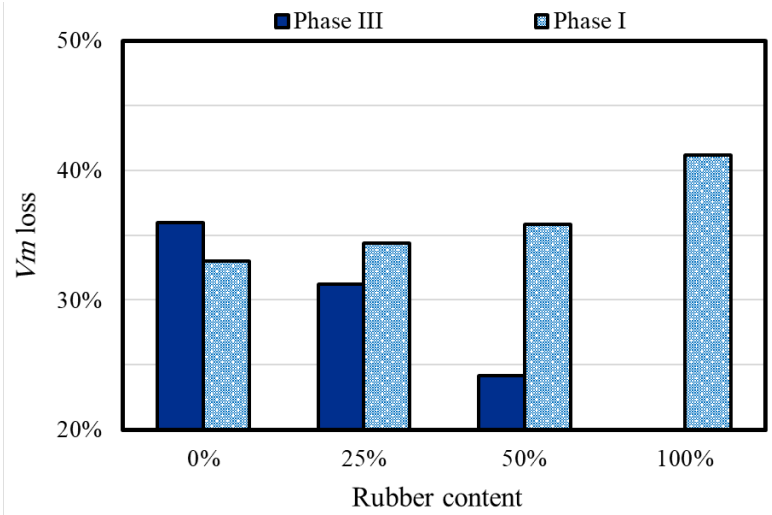

(b)

Fig. 5.24 – Microtexture comparison for chip seal specimens under different load speed at the end of 100,000 wheel applications in the SWTS test. (a) V_m value, (b) V_m loss percentage.

As shown in Fig. 5.24a, for Phase III specimens that were tested under higher loading speed, with increasing the rubber content from 0 to 100%, the final V_m value increased considerably from 4.0 to 5.1 mm^3/mm^2. Also, the V_m loss percentage reduced significantly from 36 to 16% by increasing the rubber content from 0 to 100% as shown in Fig. 5.24b. Comparing the results from the Phase III tests with Phase I tests shows 3% more V_m loss for the 100% trap rock specimen,

while increasing the rubber content reduced the aggregate loss in the higher loading speed of 160 wpm compared to the loading speed of 120 wpm. For example, the 100% crumb rubber chip seal, the final V_m value increased by 1.8 mm^3/mm^2 which corresponded to 25% less V_m loss by increasing the loading speed from 120 wpm to 160 wpm.

In conclusion, the results showed that the raveling resistance of trap rock chip seal under high traffic speeds will be considerably improved by increasing the crumb rubber content. The reason for this performance can be related to the natural characteristics of the crumb rubber particles, although according to the Phase I test results, crumb rubber provides a weaker bond with the binder compared to the natural aggregate. It should be noted that rubber particles have different behavior under direct load compared to natural aggregate. Rubber possesses a high elasticity along with a dual function of springing and damping. Therefore, under the high loading rate, i.e., high-speed cycles of loading and unloading, the rubber particles will perform a high hysteresis, which will damp and dissipate the imposed energy, whereas hard materials like natural aggregates with low elasticity do not show hysteresis and will transmit the majority of the imposed traffic load to their bond with the binder. This behavior of the rubber particles may not be effective in regular loading conditions, while in high traffic speed it was more pronounced and improved the raveling resistance. Therefore, replacing natural aggregate with crumb rubber particles could be a solution for addressing the raveling distress under high traffic speed.

5.4.2. Microtexture Evaluation

The microtexture of trap rock and crumb rubber aggregate at two different stages were observed under a scanning electron microscope (SEM) and compared with their initial stage and with each other. Fig. 5.25 shows the initial state of the surface of trap rock and crumb rubber particles side by side before experiencing any load at different magnification levels from 100X to

10,000X. As can be observed in Fig. 5.25, trap rock particle contains larger areas of the same elevation, i.e., flat areas, and fewer features over its surface. In contrast, crumb rubber particles have more surface variation which can be noticed from the topography contrast of the images. Also, more features can be observed on the crumb rubber surface, as can be noticed in Fig. 2.25c and 2.25d. Examination of Fig. 2.25 revealed that the crumb rubber particle has higher microtexture, i.e., a rougher surface, before applying any load.

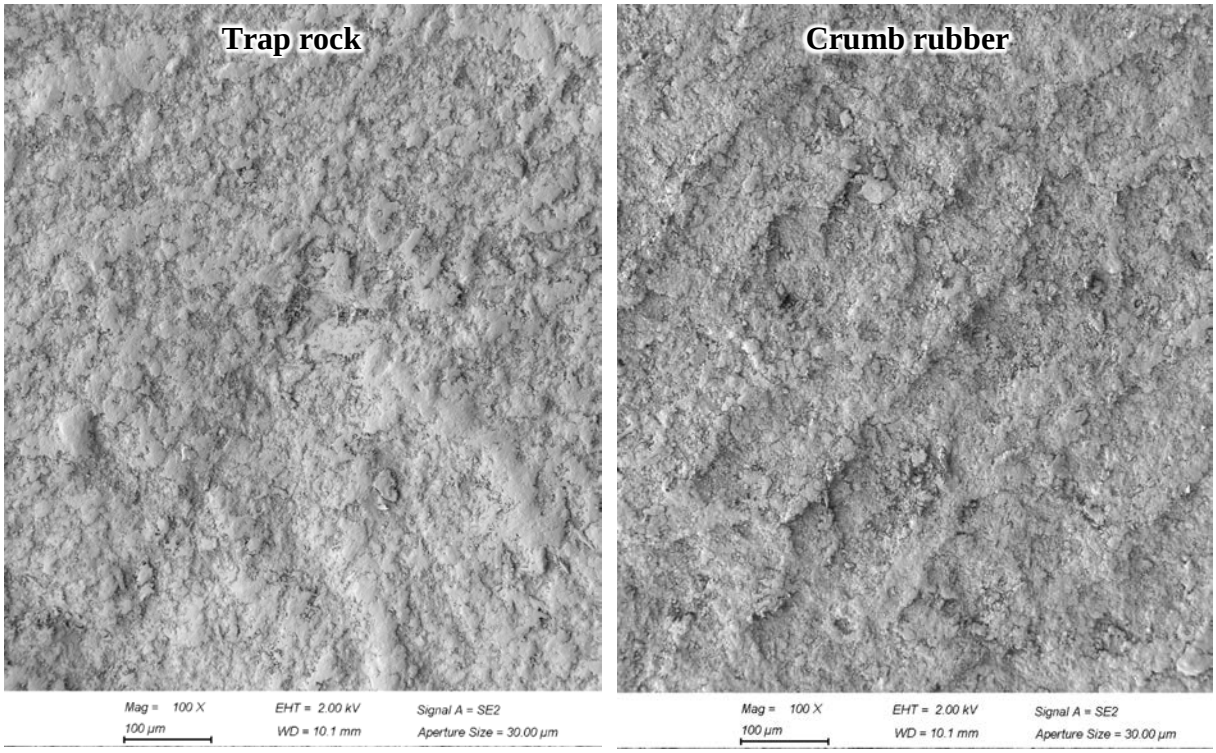

(a)

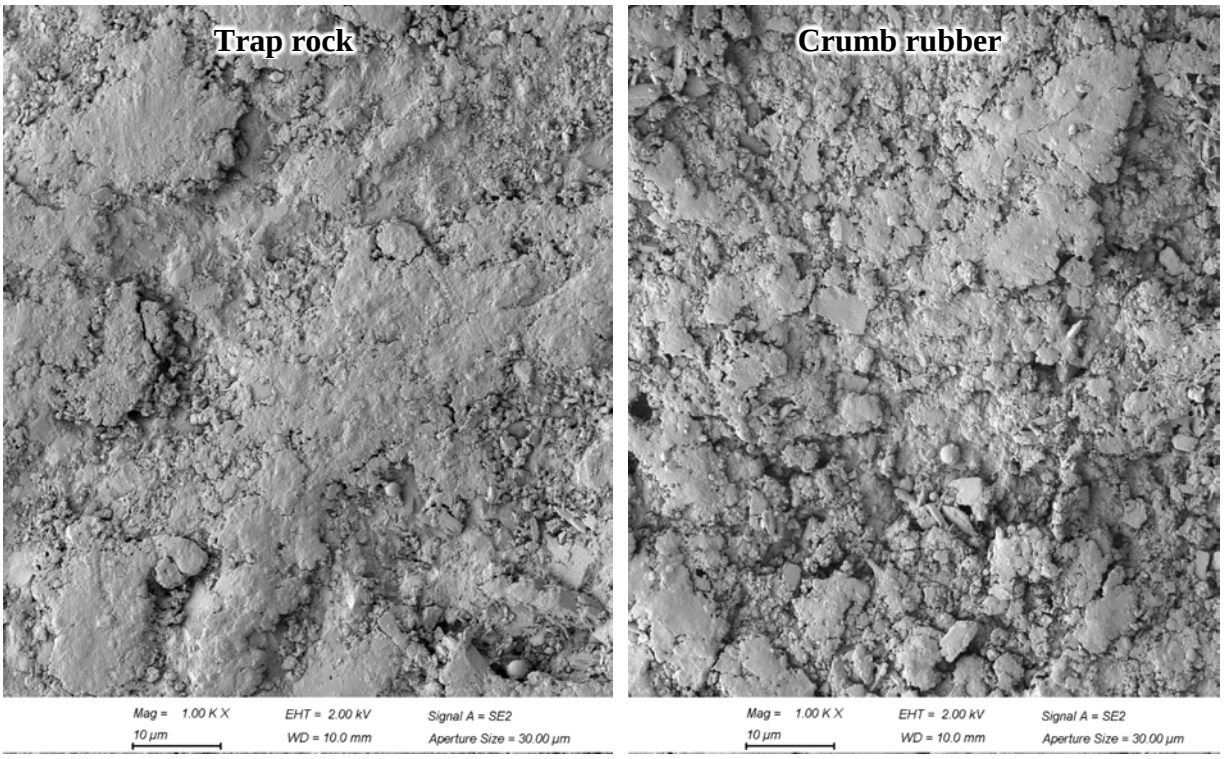
Trap rock
Crumb rubber
Mag = 1.00 K X
10 µm
EHT = 2.00 kV
WD = 10.0 mm
Signal A = SE2
Aperture Size = 30.00 µm
Mag = 1.00 K X
10 µm
EHT = 2.00 kV
WD = 10.0 mm
Signal A = SE2
Aperture Size = 30.00 µm

(b)

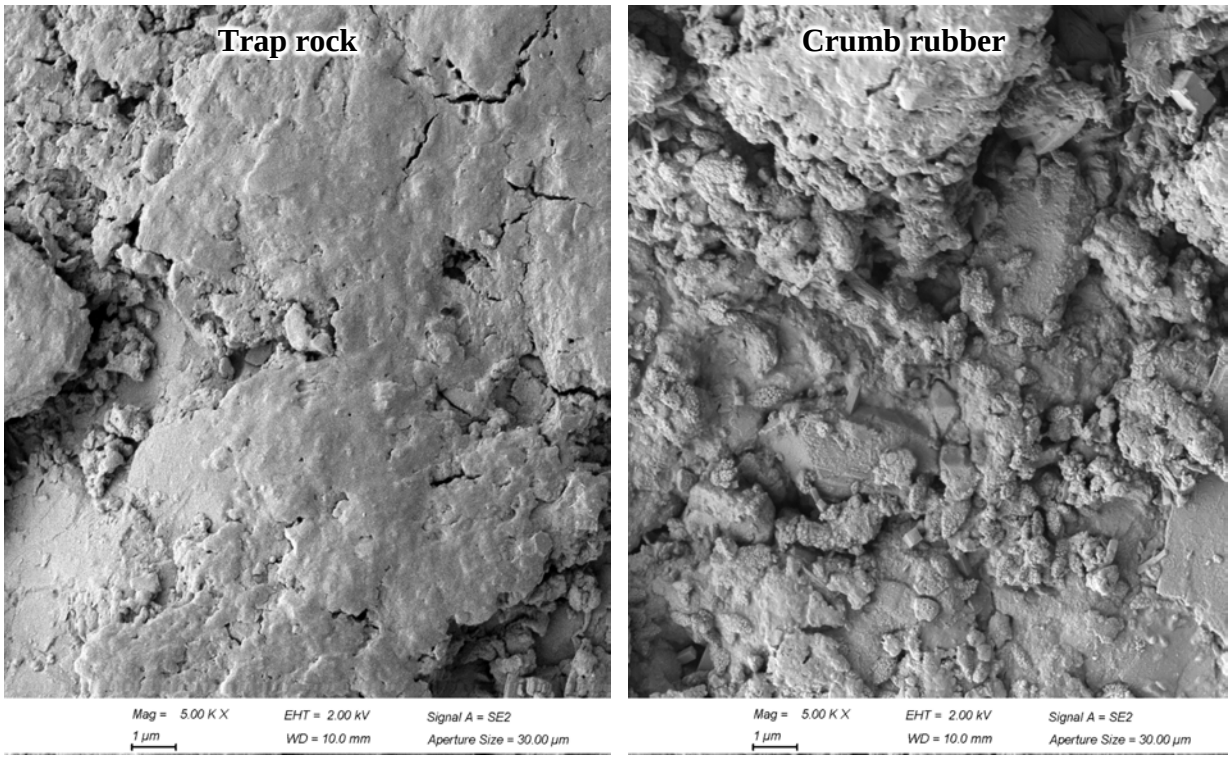
Trap rock
Crumb rubber
Mag = 5.00 K X
1 µm
EHT = 2.00 kV
WD = 10.0 mm
Signal A = SE2
Aperture Size = 30.00 µm
Mag = 5.00 K X
1 µm
EHT = 2.00 kV
WD = 10.0 mm
Signal A = SE2
Aperture Size = 30.00 µm

(c)

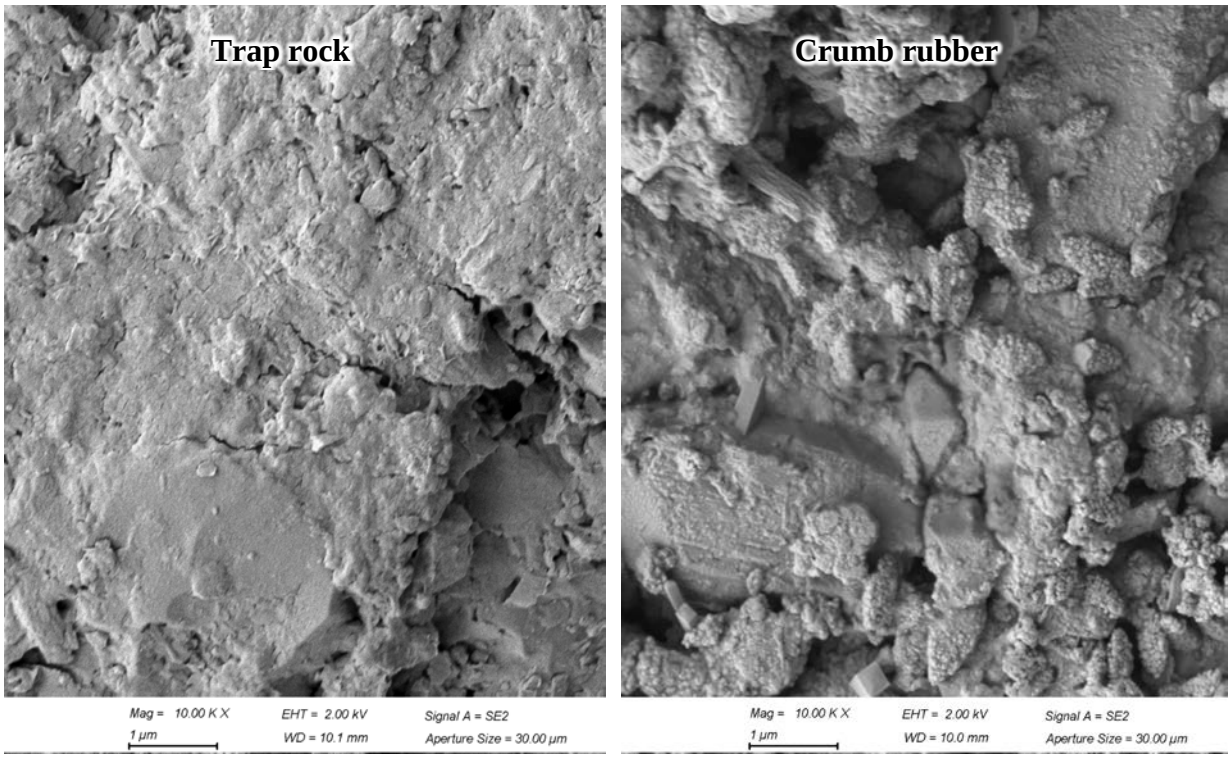

(d)

Fig. 5.25 – SEM images of trap rock and crumb rubber particles before experiencing any traffic load at different magnification levels of (a) 100X, (b) 1000X, (c) 5000X, and (d) 10000X.

Fig. 5.26 shows the trap rock and crumb rubber particles side by side after experiencing 100,000 wheel applications in the SWTS test at different magnification levels. As can be observed in Fig. 5.26, after being polished by traffic load, trap rock particle contains large flat areas and polished edges and less surface variation and features. In contrast, crumb rubber particles, after being polished by traffic load, have more surface variation, which can be noticed from topographic contrast of the images (Fig. 5.26a and 5.26b). Also, more features can be observed on the crumb rubber surface, as can be noticed in Fig. 2.26b and 2.26c. Examination of Fig. 2.26 revealed that the crumb rubber particle has higher microtexture, i.e., a rougher surface after applying simulated traffic load. Also, comparing Fig. 5.26 and 5.25 reveals that the crumb rubber particles have more resistance to polishing at the micro-level compared to trap rock aggregate.

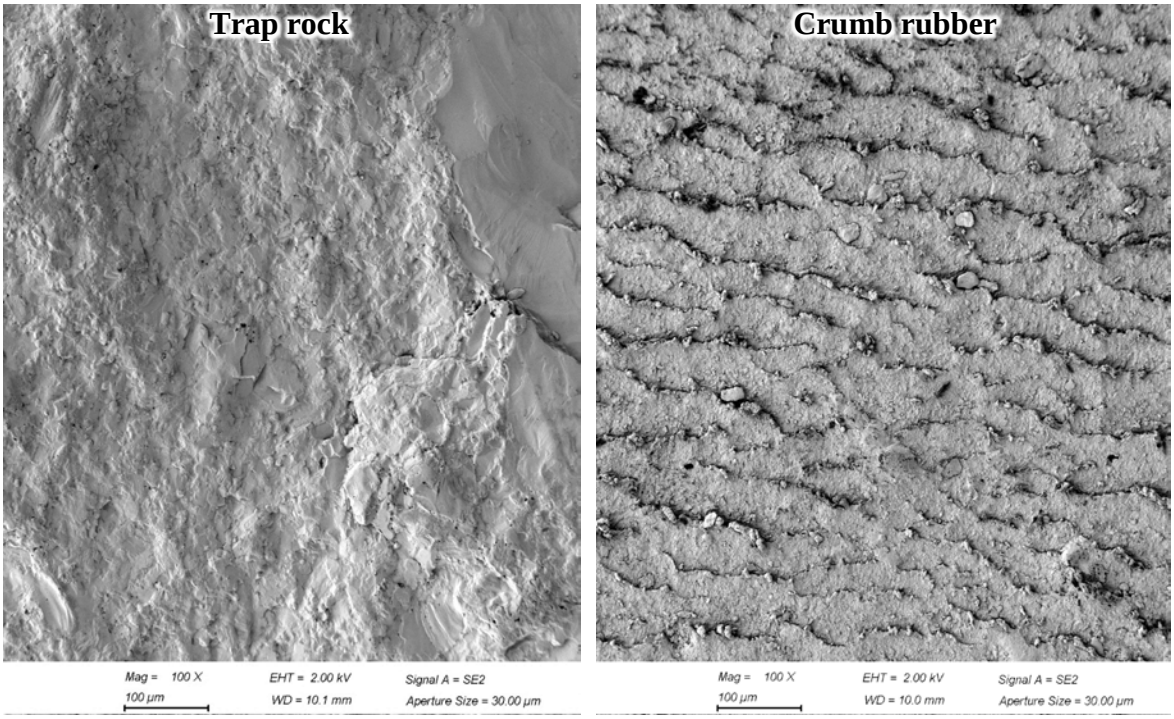
Trap rock
Crumb rubber
Mag = 100 X
100 µm
EHT = 2.00 kV
WD = 10.1 mm
Signal A = SE2
Aperture Size = 30.00 µm
Mag = 100 X
100 µm
EHT = 2.00 kV
WD = 10.0 mm
Signal A = SE2
Aperture Size = 30.00 µm

(a)

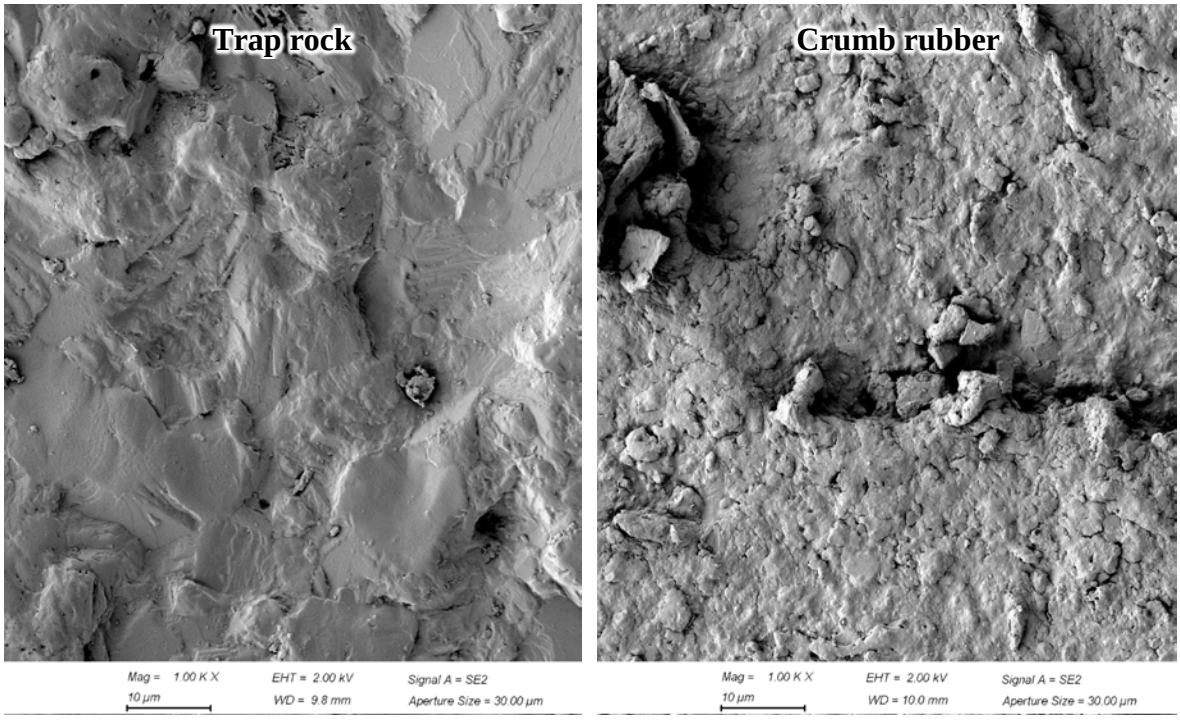
Trap rock
Crumb rubber
Mag = 1.00 K X
10 µm
EHT = 2.00 kV
WD = 9.8 mm
Signal A = SE2
Aperture Size = 30.00 µm
Mag = 1.00 K X
10 µm
EHT = 2.00 kV
WD = 10.0 mm
Signal A = SE2
Aperture Size = 30.00 µm

(b)

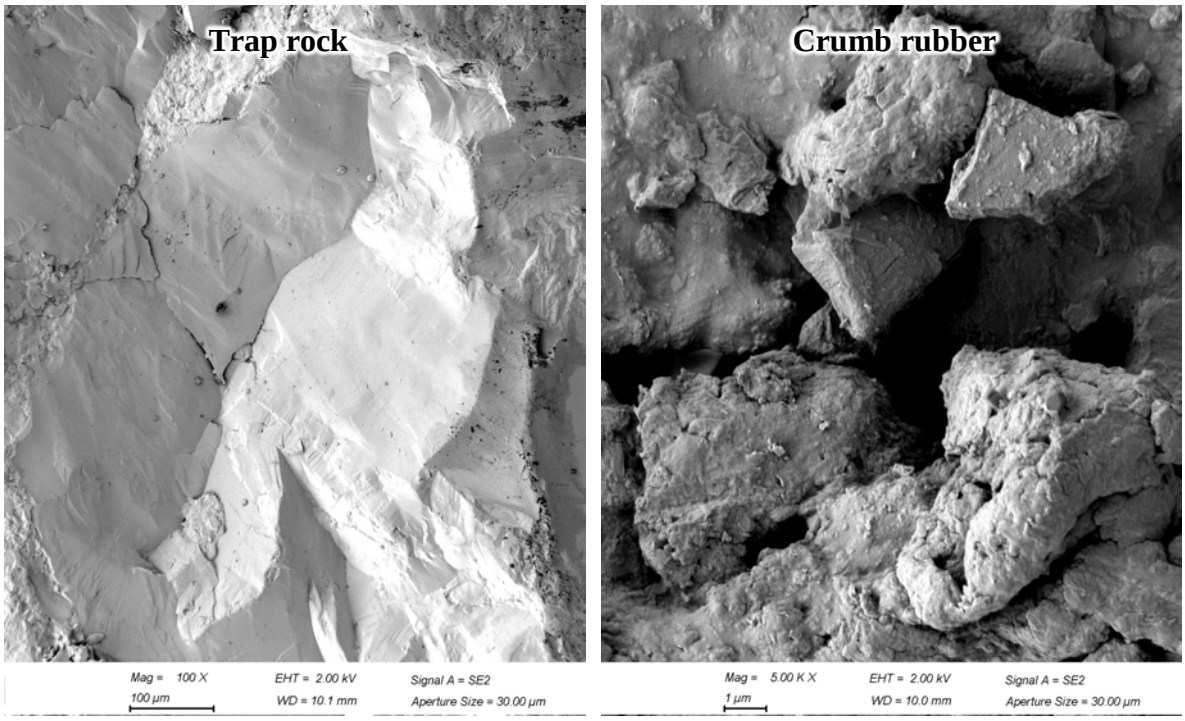

(c)

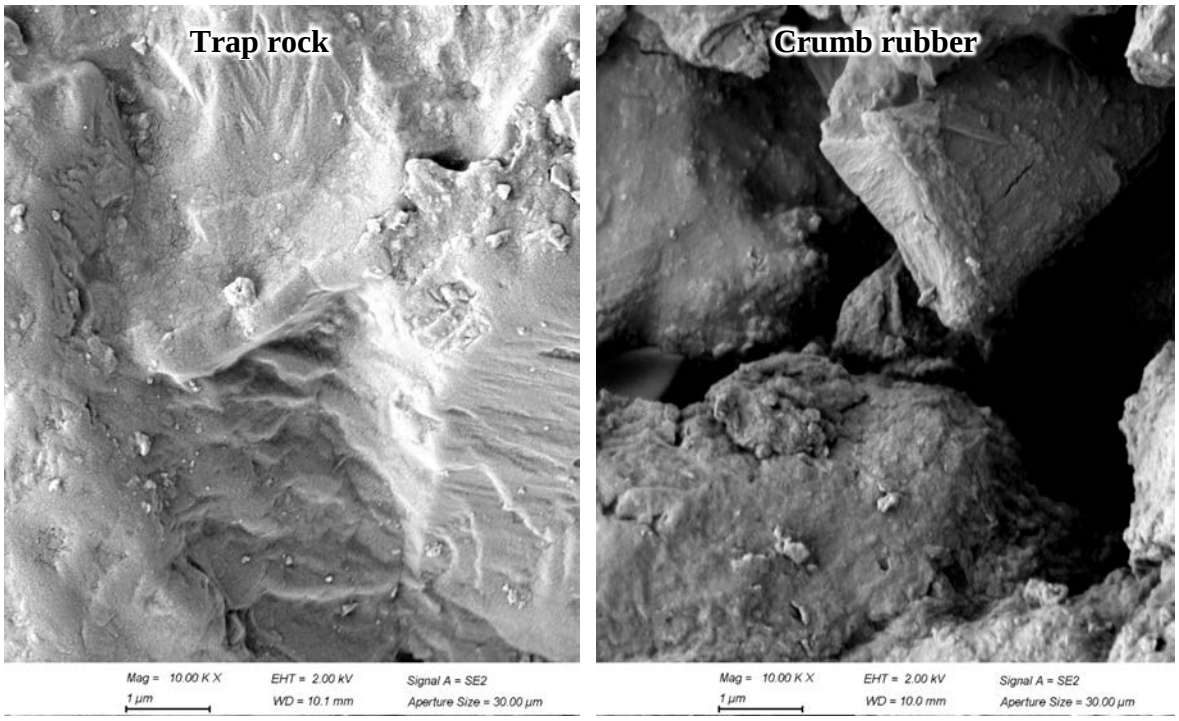

(d)

Fig. 5.26 – SEM images of trap rock and crumb rubber particles after experiencing 100,000 wheel applications in the SWTS test at different magnification levels of (a) 100X, (b) 1000X, (c) 5000X, and (d) 10000X.

Fig. 5.27 presents another crumb rubber particle that had been obtained from the wheel path of a chip seal specimen which had experienced very slight bleeding after 100,000 wheel applications in the SWTS test. This particle was covered with a thin layer of emulsified asphalt which could not be observed easily with bare eyes. As shown in Fig. 5.27, a very slight bleeding distress can cover the high microtexture of crumb rubber or any other particles. Comparing the images for crumb rubber particles in Fig. 5.27 with Fig. 5.26 indicates that a very slight bleeding action can cover the high microtexture of any particle and reduce the skid resistance of the surface considerably.

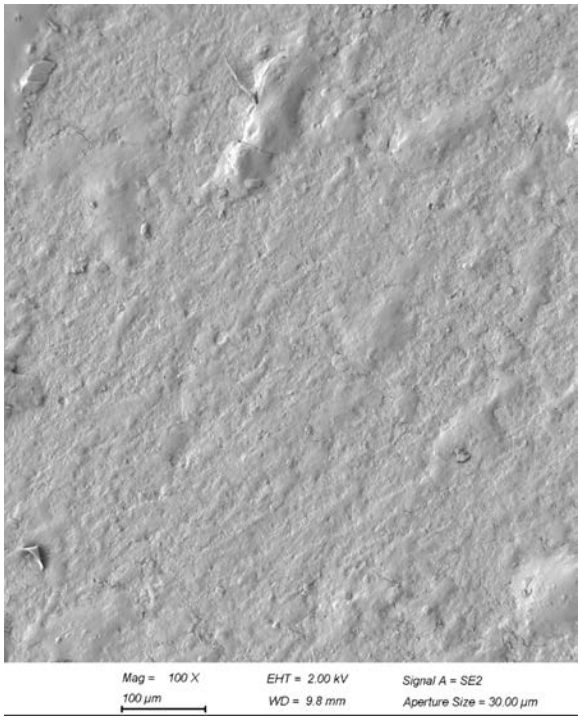

(a)

(b)

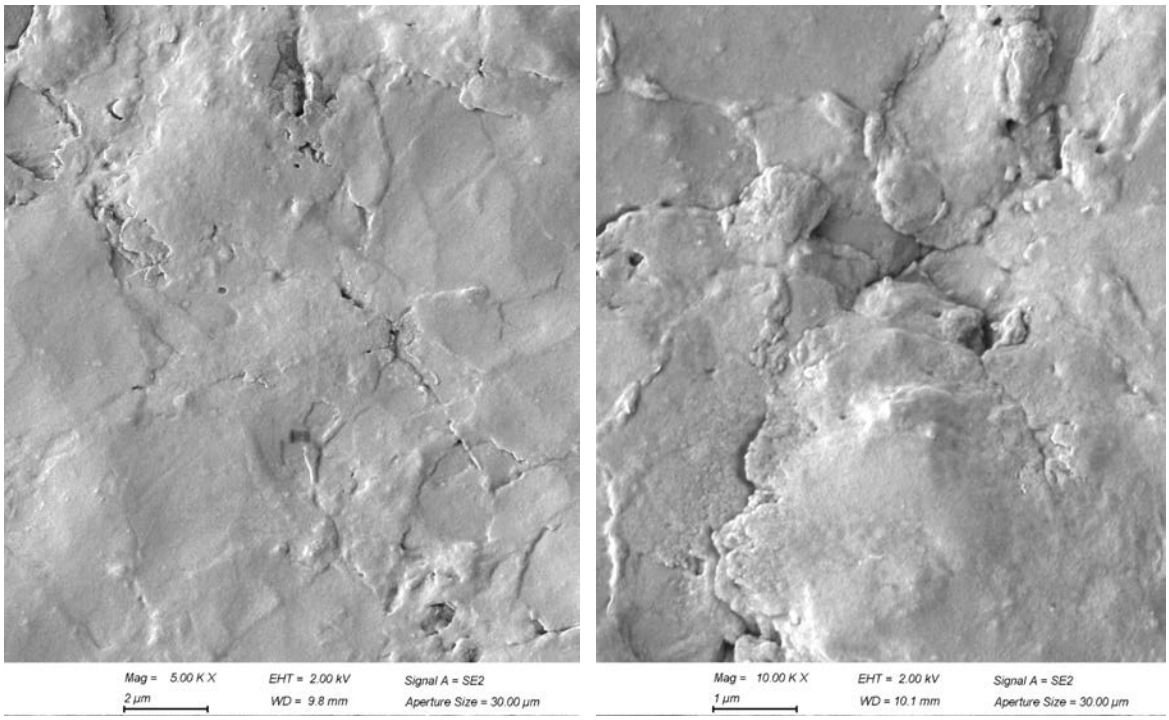

(c) (d)

Fig. 5.27 – SEM image of a crumb rubber particle from a chip seal surface with bleeding distress after experiencing 100,000 wheel applications in the SWTS test at different magnification levels of (a) 100X, (b) 1000X, (c) 5000X, and (d) 10000X.

5.5. Conclusions

This chapter evaluated the performance of conventional and rubberized chip seal in terms of raveling, i.e., aggregate loss, and aggregate polishing under simulated traffic load. The effect of different parameters such as aggregate type, binder rate, and crumb rubber content was evaluated. Also, the effect of applied load magnitude and speed, i.e., traffic load and rate, was investigated.

- For trap rock chip seal specimens, replacing up to 50% of the volume of trap rock aggregate with crumb rubber particles did not significantly affect the raveling resistance of the specimens for both 0.25 and 0.50 gal/yd^2 binder rates. Increasing the rubber content more than 50% for trap rock chip seal impaired the raveling resistance of the specimens.

- For creek gravel chip seal specimens, replacing up to 25% of the volume of creek gravel aggregate with crumb rubber particles did not significantly affect the raveling resistance of the specimens for both 0.25 and 0.50 gal/yd^2 binder rates. Increasing the rubber content more than 25% for creek gravel chip seal impaired the raveling resistance of the specimens.
- The chip seal specimens with 100% crumb rubber as aggregate performed poorly, especially with the lower binder application rate of 0.25 gal/yd^2 compared to trap rock and creek gravel chip seal. This can be attributed to the 0% water absorption ability of the crumb rubber.
- Increasing the binder rate from 0.25 to 0.50 gal/yd^2 considerably improved the raveling resistance of chip seal specimens made with trap rock, creek gravel, and crumb rubber. The V_m loss reduced up to about 8% by increasing the binder rate from 0.25 to 0.50 gal/yd^2 for all three aggregate types.
- The creek gravel chip seal performed better in terms of raveling compared to trap rock chip seal. Creek gravel specimens experienced up to 6% V_m loss compared to trap rock specimens. This can be attributed to the lower flakiness index and higher water absorption of the creek gravel aggregate compared to trap rock.
- The raveling resistance of the trap rock natural aggregate will be impaired by increasing the applied traffic load magnitude, while for rubber aggregate, the behavior was the opposite, and the raveling resistance was improved under a higher traffic load magnitude. This can be attributed to the natural high elasticity of the crumb rubber particles.

- The raveling resistance of trap rock chip seal under high traffic speeds will be considerably improved by increasing the crumb rubber content. This can be attributed to the natural load hysteresis characteristics of the crumb rubber particles.
- According to scanning electron microscopy (SEM) imaging observation, crumb rubber particles had a higher polishing resistance under traffic load compared to trap rock aggregate. Crumb rubber particles also had a higher microtexture compared to trap rock particles both before and after being polished by traffic load.

Chapter 6: Hybrid Traffic-Temperature Effects on Conventional and Rubberized Chip Seal Performance

6.1. Introduction

Traffic characteristics and environmental conditions are among the main factors that affect the performance of chip seal during its service life. Different traffic characteristics including the number of traffic load, traffic speed, and traffic load magnitude were simulated and evaluated in the previous chapter of this report. During this chapter, chip seal specimens similar to those in the previous chapter were tested using the small wheel traffic simulation machine (SWTS) while the specimens were subjected to different weather conditions while the SWTS test was going on.

This chapter evaluates the performance of conventional and rubberized chip seal in terms of raveling, i.e., aggregate loss, and bleeding in different temperatures representing the freezing winter and hot summer days in Missouri state under simulated traffic load. The compound effect of traffic application and the temperature was studied using different types of aggregate including natural, i.e., trap rock, and synthetic, i.e., crumb rubber, aggregates combined in different volumetric percentages.

6.2. Experimental Program

6.2.1. Test Specimens and Matrix

A total of 11 chip seal specimens of 2 ft by 2 ft were prepared and tested for the purpose of this chapter. Test specimens were prepared as per the procedure described in Chapter 4 of this

report. Two different aggregates with different inherent characteristics including crumb rubber and trap rock were used to study the effect of aggregate type. The used aggregates had a close gradation as presented in Fig. 4.2b. As per Chapter 4 of this report, aggregates of batch 2 were used for the test specimens included in this chapter. The characteristics of the aggregate are also reported in Table 4.1. Some specimens were prepared with combined aggregates consisting of 25% and 50% by volume of crumb rubber combined with trap rock. Test specimens used in this chapter are listed in Table 6.1.

According to the results from Chapter 5, chip seal specimens with 0.50 gal/yd^2 binder application rate presented a better performance compered to their counterpart specimens with binder application rate of 0.25 gal/yd^2. As a result, this binder application rate was selected to be used in this chapter. CRS-2P asphalt emulsion, which is a cationic rapid-setting and high-viscous type, was used during this study per the Missouri Department of Transportation (MoDOT) recommendation. The physical properties of CRS-2P are summarized in Table 4.2.

Table 6.1 – Traffic-Temperature SWTS Test Matrix

Test	Specimen ID	Emulsion rate (gal/yd^2)	Percentage of Aggregate		Chip seal surface temp. (°F)	Load (lbs)	Speed (wpm)
			Trap rock	Crumb rubber			
Low temperature SWTS	L100R	0.50	100	-	20±6	87	120
	L50T	0.50	50	50			
	L75T	0.50	75	25			
	L100T	0.50	100	-			
High temperature SWTS	H100R	0.50	100	-	100±5		
	H50T	0.50	50	50			
	H75T	0.50	75	25			
	H100T	0.50	100	-			

6.2.2. Traffic-Temperature SWTS Test

In order to achieve the objective of this report, a piece of laboratory equipment namely "SWTS" was developed as described in Chapter 3 (Fig. 6.1a). SWTS was used to apply controlled traffic in terms of number, load, and speed on chip seal specimens. Table 6.1 presents the SWTS test matrix of this study. An insulation layer was provided in all six sides of the test chamber to be able to apply a controlled temperature as shown in Fig. 6.1b.

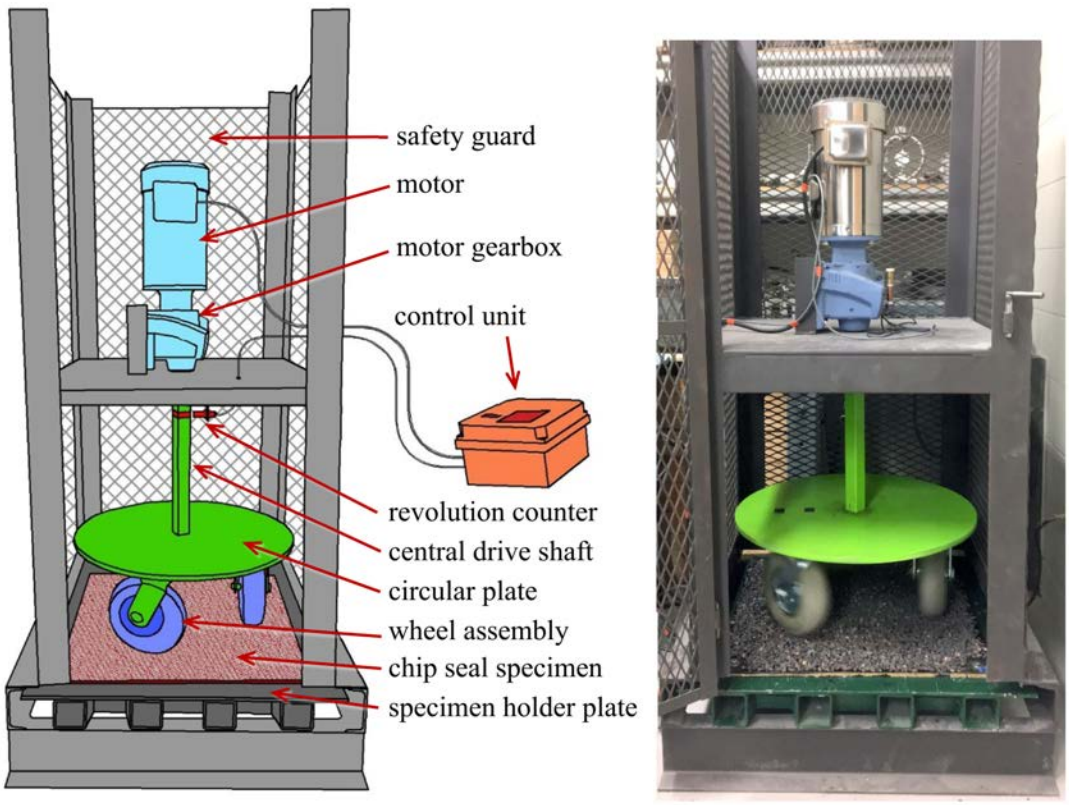

(a)

(b)

Fig. 6.1 – Small-wheel traffic simulation (SWTS) (a) test machine, and (b) insulated test chamber.

For low temperature assessment of the chip seal surfaces, the surface temperature of 20±6°F was provided. This was the measured temperature on the aggregates during the test and it was constant. The winter temperature in Missouri state varies and it records an extreme temperature of below -20° F during the night. However, this temperature is not the common day temperature during which the traffic is running on the pavement and also providing this temperature in the laboratory was not practical. Therefore, an average day time winter temperature was selected for the purpose of this test.

For high temperature assessment of the chip seal surfaces, the temperature of 100±5° F was provided. This was the measured temperature on the aggregates during the test and it was constant. The air temperature just above the chip seal surface was 95° F during this test. This temperature was selected since summers in Missouri state have an average high temperature in the 80° F to 90° F range, but it is common to observe many days together that remain above 100° F[96].

According to SWTS test results in Chapter 5, specimens did not experience a significant macrotexture loss after 40,000 wheel applications. Therefore, since providing a constant low temperature for a long time was not applicable and in order to keep the duration of experiment reasonable, chip seal specimens were tested up to 40,000 wheel applications. However, in order to make sure that the samples would not perform differently after 40,0000 wheel applications, two specimens with 100% trap rock and 100% crumb rubber were tested to 100,000 wheel applications. In the case of high temperature SWTS tests, since the specimens experienced a significant macrotexture loss by 3,000 wheel applications, the test was conducted up to 3,000 wheel applications for all specimens to be able to provide a comparison. As listed in Table 6.1, other SWTS test specifications were similar to Phase I tests in Chapter 5. Specimens were subjected to a load of 87.25 lb which provided a surface contact stress of 14.12 psi under each wheel, considering the contact area of 2.06 in^2 for each wheel. The wheels' travel speed was 120 wpm (wheel application per minute) which corresponds to a dynamic loading of 2 Hz on the chip seal surface.

The results from low temperature and high temperature SWTS tests were compared with the similar specimens of Phase I tests, as reported in Chapter 5. Phase I test specimens were tested using SWTS with the same loading parameters except for the temperature. The test temperature for Phase I tests was 78±4˚ F. It should be noted that specimens prepared in Phase I were made using aggregate from batch 1 as reported in Chapter 4. The aggregate properties which were different for the two aggregate batches are listed in Table 6.2.

Table 6.2 – Batch 1 and Batch 2 Aggregate Comparison

Property	crumb rubber		trap rock	
	batch 1	batch 2	batch 1	batch 2
Coefficient of uniformity	1.38	1.28	1.82	1.52
Median particle size (in)	0.24	0.32	0.25	0.30
Flakinees index (%)	31	46	42	31

6.2.3. Macrotexture Evaluation

A new non-contact measurement technique using a 3D scanner was used to examine the texture variation and aggregate loss during the SWTS test. The reason for using this technique is not being able to properly use the common method of sand patch [90] for macrotexture measurement due to the circular snowplow path with limited width. 3D surface scanning technique will also provide more accurate macrotexture measurements [42, 46, 91].

The scanner used in this project was a two-camera structured-light 3D scanner namely Thunk3D Fisher (Fig. 6.2a). The manufacturer declared accuracy of 0.04mm to 0.1mm having a scan speed of 1,200,00 points per second and a resolution of 0.2 mm with two 12mm/5mp lenses, two 1.31 mp CMOS sensors, and 1280x800 LED white light raster. The 3D scanner was consisting of a downward-looking projector and two cameras at a fixed orientation with respect to the projector. The projector projects a series of black and white patterns onto the scan surface. When light projects onto the object's surface, the patterns become distorted. Two cameras capture these images and calculate the distance from each point in the field of view using the triangulation system (Fig. 6.2b).

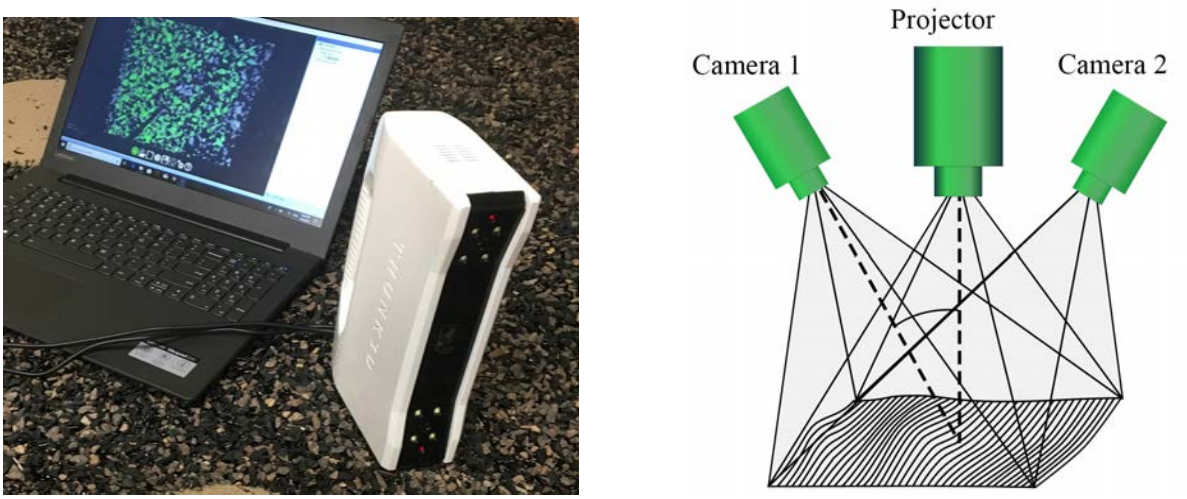

(a) (b)

Fig. 6.2 – (a) Handhold portable 3D scanner, and (b) basic setup of a structured-light triangular system.

Having the 3D surface of chip seal specimens, the macrotexture was assessed using Digital Surf MountainsMap Expert Version 8 surface analysis software [92]. Using MountainsMap, a special analysis was conducted in accordance with BS EN ISO 25178-2 [94]. Some post-processing operations such as rotating, leveling and extracting the area of interest, i.e., snowplowing path, were conducted on each surface. Fig. 6.3a shows an example of a chip seal 3D surface in MountainsMap software. The topographic pseudo-color view of the surface in Fig. 6.3a simply shows the difference in the texture of different spots.

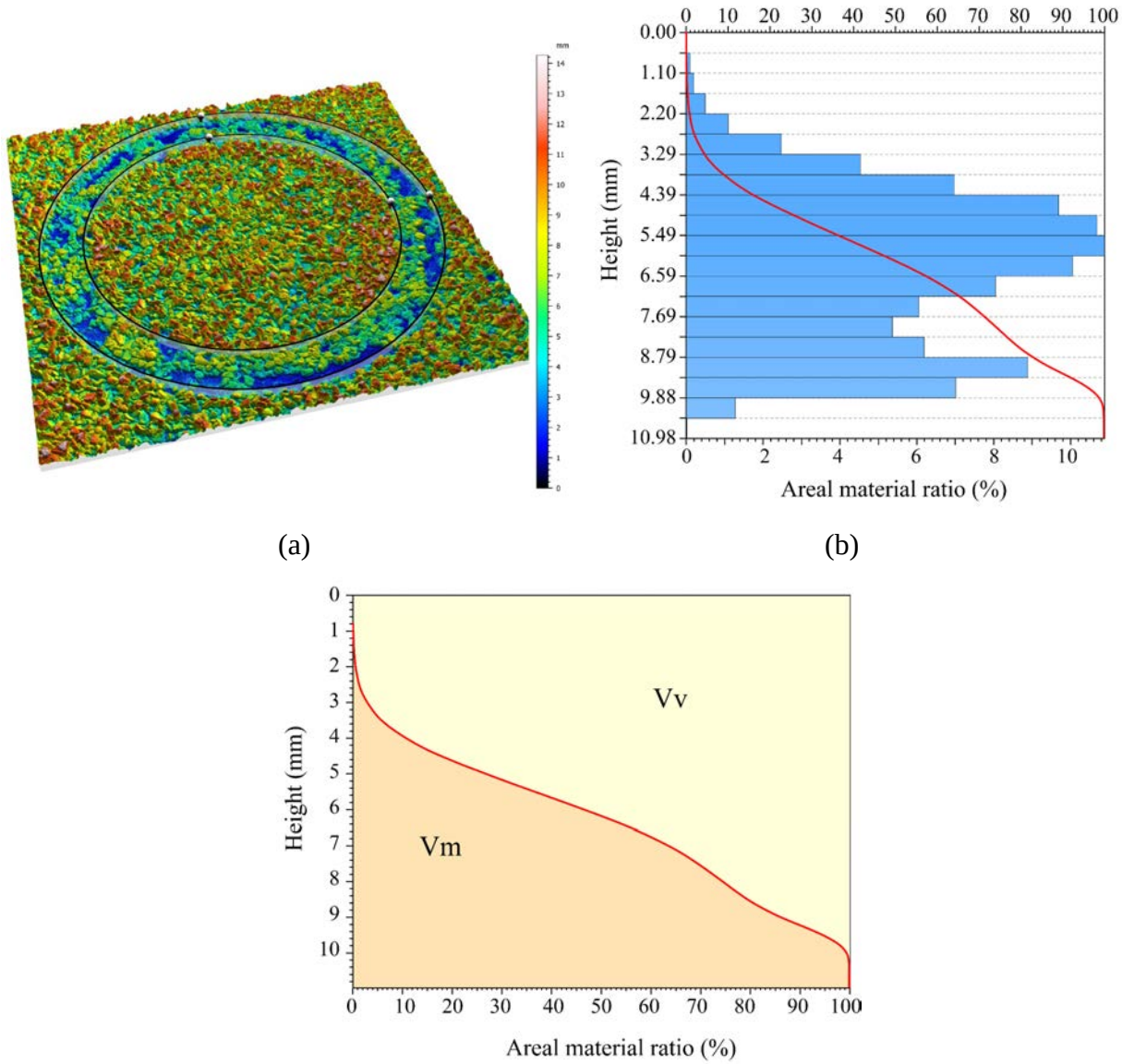

Fig. 6.3 – 3D surface data from MountainsMap software (a) example chip seal 3D surface, (b) height distribution and Abbott-Firestone curve, and (c) Abbott-Firestone curve and volumetric parameters.

Bearing area curve, also known as the Abbott-Firestone curve, which describes the surface texture was plotted for the surfaces. Abbott curve, introduced in ISO 13564-2 [95], mathematically represents the cumulative probability density function of the surface profile's height and can be calculated by integrating the profile trace. Fig. 6.3b shows the distribution of heights for the wheel

path area of the example chip seal surface shown in Fig. 6.3a. The bars indicate the percentage of surface area at heights within the range of bins (in this case bins of width 0.55 mm between 0 mm and 10.98 mm) and the superimposed line shows the cumulative height distribution. The curve is called the Abbott-Firestone curve which can be used to calculate two distinct parameters, as shown in Fig. 6.3c. V_m is defined as the area below the Abbott curve which indicates the volume of material on the surface at various heights from the highest peak to the lowest point on the selected area. V_v is defined as the area above the Abbot curve which indicates the volume of voids on the surface not occupied by the material on the given area. In other words, V_m represents the volume of material at areal material ratio [95]. The value of V_m in mm^3/mm^2 indicate that a layer of material with V_m mm thickness over the measured area would account for all the material in the given area. Therefore, V_m is actually representing the mean texture depth (MTD) of the material in the selected area. In this study, V_m of the wheel path and outside the wheel path was measured to compare the aggregate loss, i.e., texture loss, due to the simulated traffic loading in the SWTS test.

6.3. Traffic-Temperature SWTS Test Results

6.3.1. Low Temperature Performance

Fig. 6.4a to 6.4d shows the different stages of different chip seal specimens with volumetric crumb rubber content from 0% to 100% tested at 20±6°F temperature in SWTS. The topographic pseudo-color view of the surface is presented in Fig. 6.4 which provides better visualization of the surface by showing the difference in the texture of different spots. In these figures, the dark blue color represents the points with the lowest elevation and the red spots represent the points with the highest elevation on each surface. Also, the wheel path is outlined on the topographic surfaces.

Fig. 6.4 provides an overall perception of the low temperature SWTS test results. Texture measurements and evaluations are discussed in the following sections.

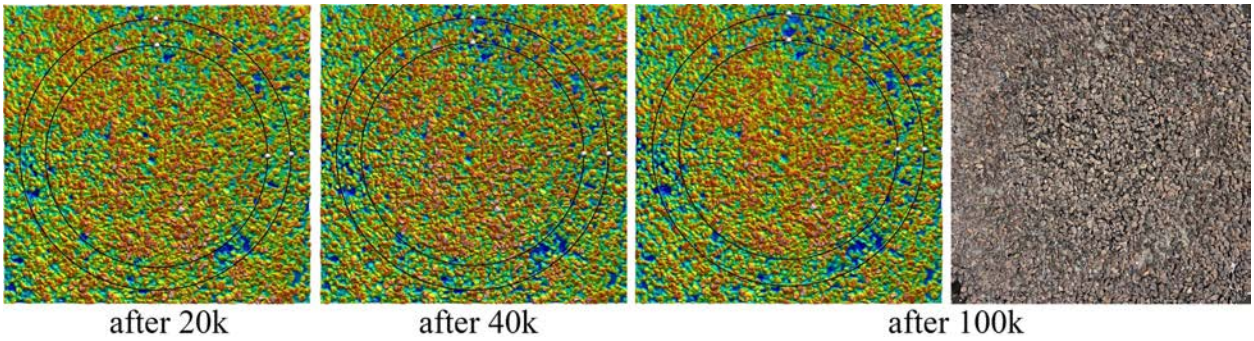

(a)

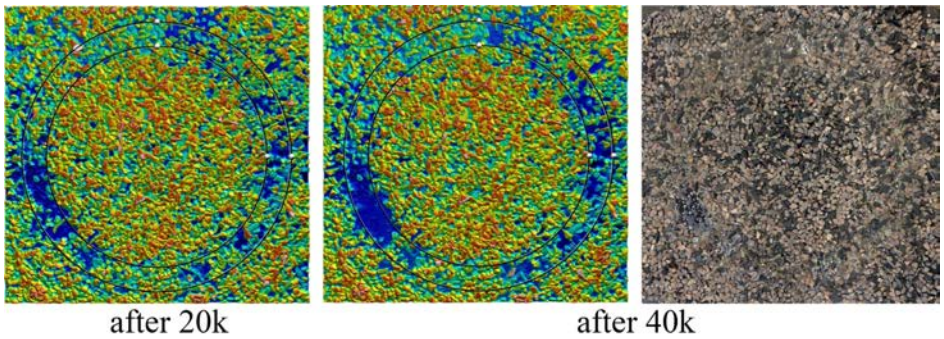

(b)

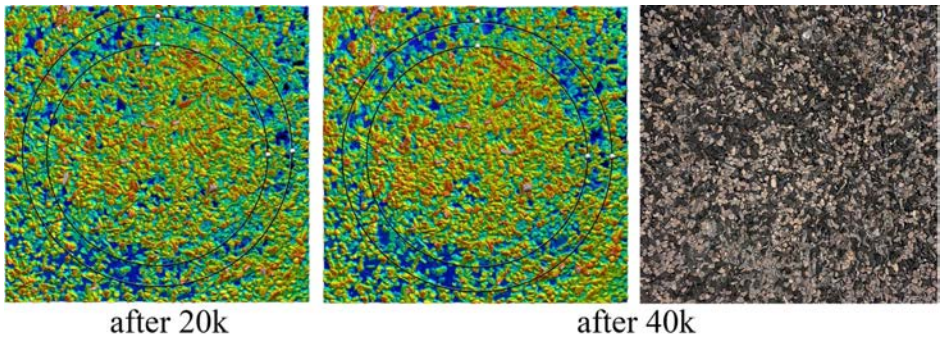

(c)

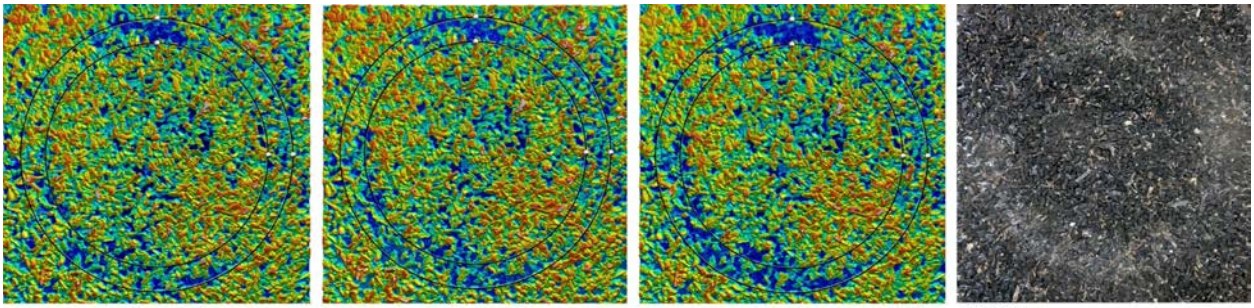

(d)

Fig. 6.4 – Low temperature SWTS test results after different wheel applications for (a) 0% rubber content, (b) 25% rubber content, (c) 50% rubber content, and (d) 100% rubber content.

Fig. 6.5 shows the V_m values on the wheel path versus the number of wheel applications for low temperature SWTS test specimens. Test specimens showed in Fig. 6.5 had different volumetric crumb rubber content from 0% to 100%. As explained earlier in this chapter, V_m was obtained from the analysis of the 3D scanned surface of chip seal specimens and represents the mean thickness of the macrotexture over the wheel path surface area. As shown in Fig. 6.5, different specimens had almost the same initial V_m and with increasing the wheel applications on the chip seal surfaces, the specimens experienced more aggregate loss. However, different specimens experienced different amounts of aggregate loss.

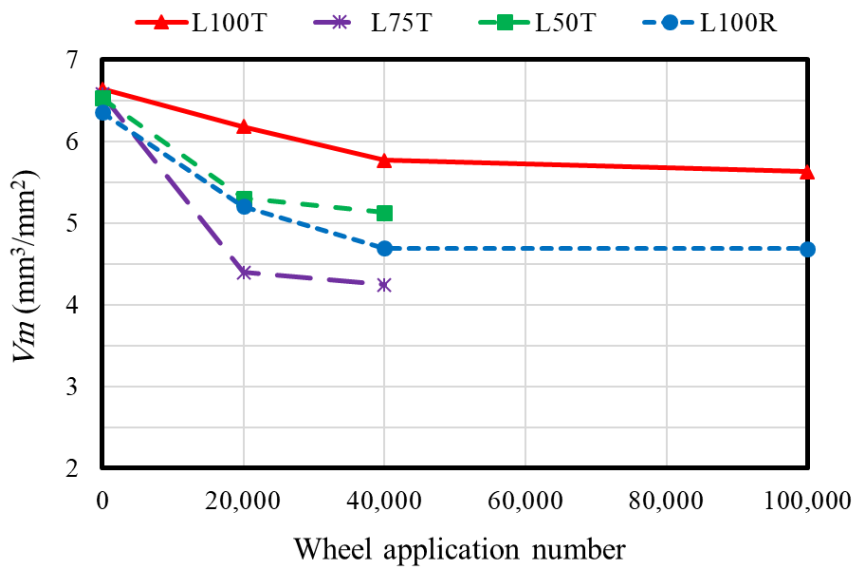

Fig. 6.5 – V_m versus wheel application number for low temperature SWTS test specimens with different rubber content.

All specimens were tested up to 40,000 wheel applications. Two specimens with 100% trap rock and 100% crumb rubber were tested to 100,000 wheel applications. As can be noticed in Fig. 6.4, not a significant macrotexture loss experienced after 40,000 wheel applications. Therefore, comparing the specimens at 40,000 wheel applications seems reasonable.

Fig. 6.6 provides a comparison for the V_m values on the wheel path versus the number of wheel applications for low temperature SWTS and Phase I SWTS test specimens. As mentioned earlier, Phase I SWTST specimens were tested under the same loading condition but in an ambient temperature of 78±4˚F compared to 20±6˚F for low temperature SWTS tests.

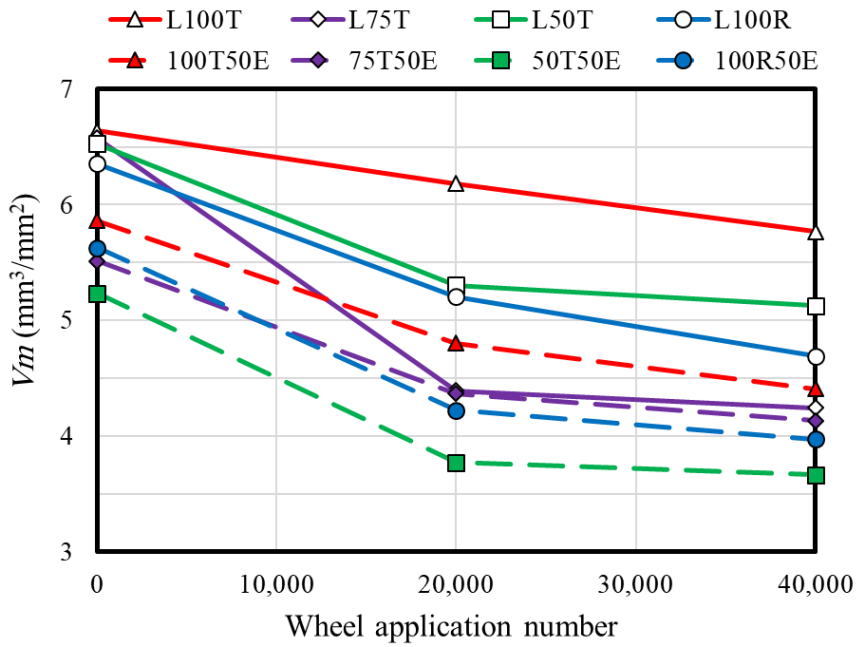

Fig. 6.6 – V_m versus wheel application number comparison between the low temperature SWTS and Phase I SWTS test specimens.

As shown in Fig. 6.6, low temperature SWTS specimens had a higher intimal V_m compared to the Phase I SWTS specimens. The reason is the larger aggregate size used for low temperature SWTS specimens as listed in Table 6.2. The almost same trend of the V_m reduction was observed in both series of specimens. Fig. 6.7 provide a clearer comparison of the V_m values for the low temperature SWTS and Phase I SWTS test specimens. Fig. 6.7a presents the V_m value at the end of 40,000 wheel applications in the SWTS test and Fig. 6.7b presents the ratio of the V_m value at the end of 40,000 wheel applications to the initial V_m value of the same specimens.

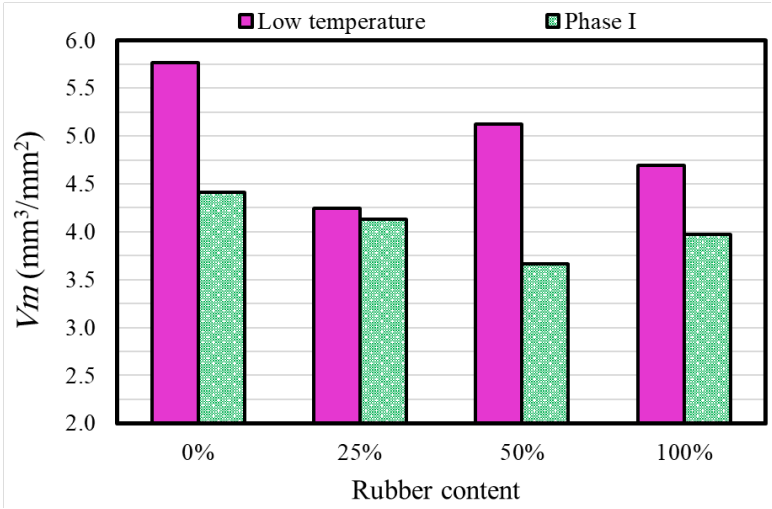

(a)

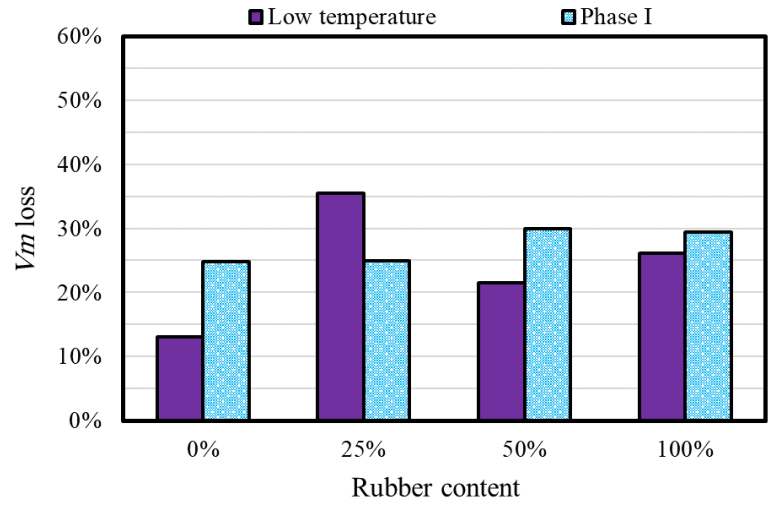

(b)

Fig. 6.7 –SWTS test results comparison for low temperature and Phase I specimens after 40,000 wheel applications. (a) final V_m value, and (b) V_m loss percentage.

As shown in Fig. 6.7, the same trend of final V_m values and V_m loss was observed for both series of specimens except the L75T, i.e., low temperature tested specimen with 25% rubber, which experienced more aggregate loss than other specimens in low temperature test which could be due to a defect related to specimens making or translocating. Fig. 6.7 shows that, for specimens tested in low temperature, with increasing the crumb rubber content from 0 to 100%, the final V_m reduced

from 5.8 mm^3/mm^2 to 4.7 mm^3/mm^2. Correspondingly, the V_m loss increased from 13 to 26%. Comparing the V_m loss in low temperature test specimens to Phase I test specimens indicates that in lower temperature, the raveling resistance of chip seal was better. This improve was more pronounced for trap rock specimens with 13% less V_m loss compared to room temperature testing. While the V_m loss for 50% and 100% rubberized chip seal was respectively 9% and 3% less in low temperature compared to room temperature.

The reason for more raveling resistance in the lower temperature is the thermo-plastic behavior of the asphalt material. The bituminous binder will get stiffer in lower temperatures; therefore, a more stable bond will be provided for the particles and they will be less susceptible to be sheared by the traffic load, and the particles will stay in their place. However, as concluded in Chapter 5, the bond between the binder and crumb rubber particles is weaker than with natural aggregate. Therefore, this behavior of the binder will be more pronounced with trap rock aggregate which has a better bond with it.

6.3.2. High Temperature Performance

Fig. 6.8a to 6.8d shows the final state of different chip seal specimens with volumetric crumb rubber content from 0% to 100% tested at 100±5°F temperature in SWTS for 3,000 wheel applications. High temperature SWTS test was only continued up to 3,000 wheel applications since most of the specimens experienced severe bleeding following with a severe raveling. Therefore, the test was stopped at 3,000 wheel applications.

The topographic pseudo-color view of the surface is presented in Fig. 6.8 which provides better visualization of the surface by showing the difference in the texture of different spots. In these figures, the dark blue color represents the points with the lowest elevation and the red spots represent the points with the highest elevation on each surface. Also, the wheel path is outlined on

the topographic surfaces. Fig. 6.8 provides an overall perception of the high temperature SWTS test results. Texture measurements and evaluations are discussed in the following sections.

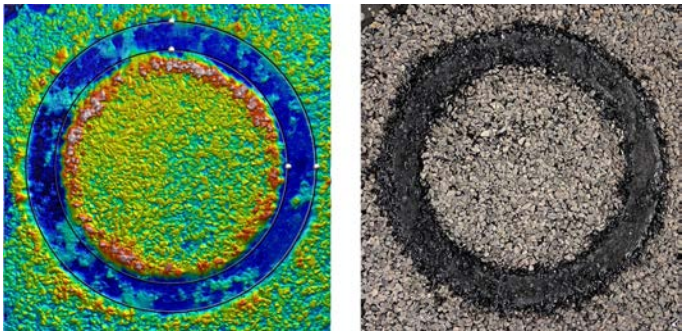

(a)

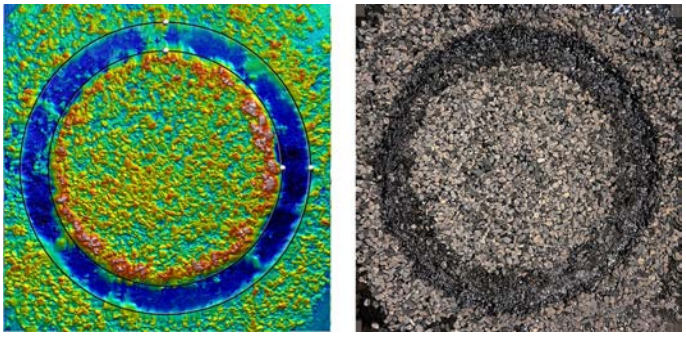

(b)

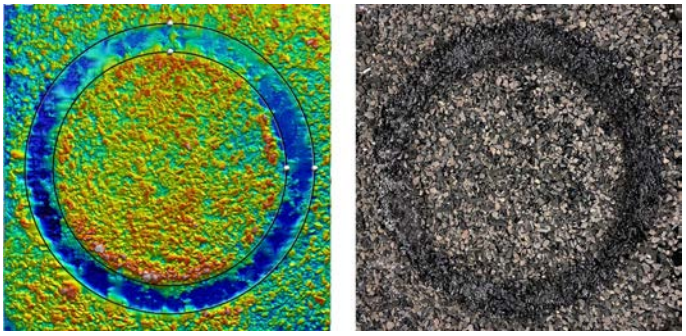

(c)

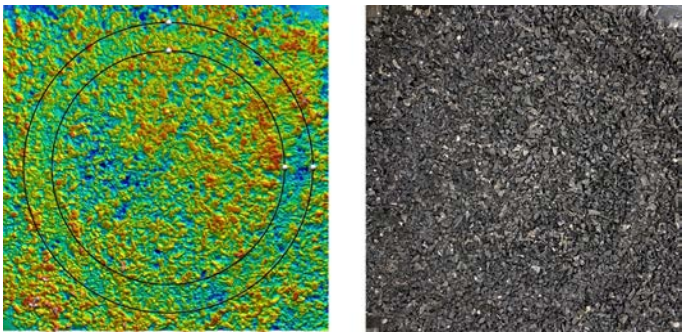

(d)

Fig. 6.8 – High temperature SWTS test results after 3,000 wheel applications for (a) 0% rubber content, (b) 25% rubber content, (c) 50% rubber content, and (d) 100% rubber content.

Fig. 6.9 shows the V_m values on the wheel path versus the number of wheel applications for high temperature SWTS test specimens. Test specimens showed in Fig. 6.9 had different volumetric crumb rubber content from 0% to 100%. As explained earlier in this chapter, V_m was obtained from the analysis of the 3D scanned surface of chip seal specimens and represents the mean thickness of the macrotexture over the wheel path surface area. As shown in Fig. 6.9, different specimens had almost close initial V_m and with increasing the wheel applications on the chip seal surfaces, the specimens experienced more aggregate loss. However, different specimens experienced different amounts of aggregate loss. It can also be observed in Fig. 6.9 that the specimen with 100% crumb rubber as aggregate performed significantly better in terms of raveling resistance compared to the other three specimens.

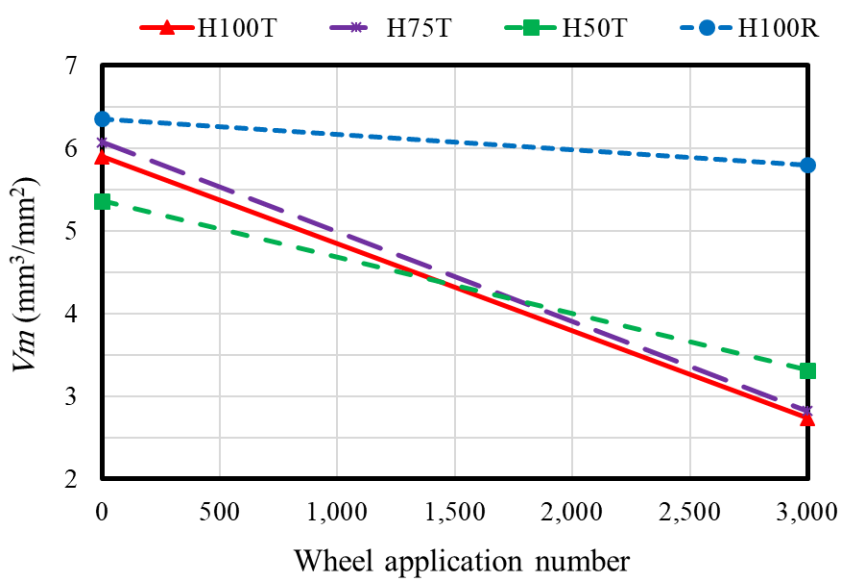

Fig. 6.9 – V_m versus wheel application number for high temperature SWTS test specimens with different rubber content.

Fig. 6.10 provides a comparison for the V_m values on the wheel path versus the number of wheel applications for high temperature SWTS and Phase I SWTS test specimens. As mentioned earlier, Phase I SWTST specimens were tested under the same loading condition but in an ambient temperature of 78±4˚F compared to 100±5˚F for high temperature SWTS tests.

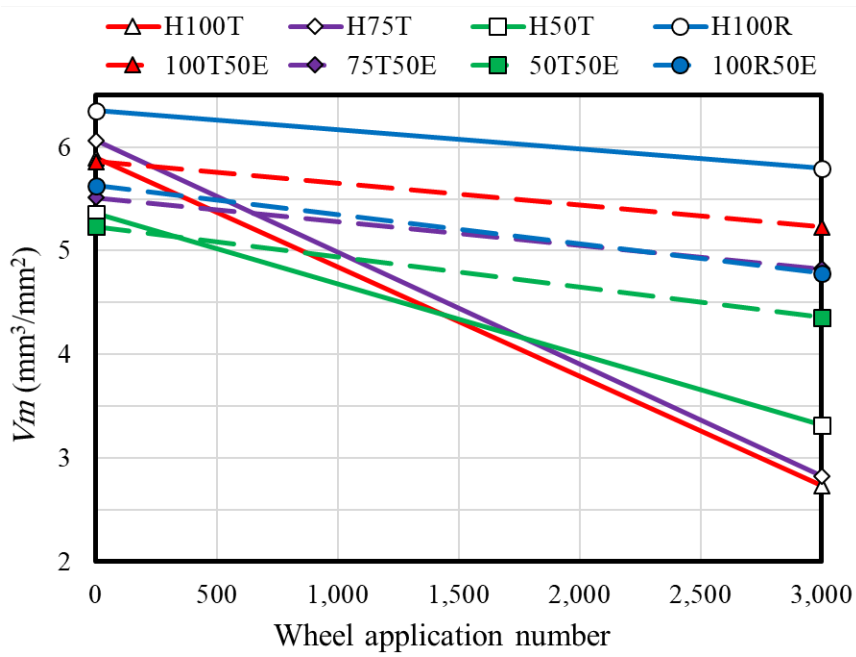

Fig. 6.10 – V_m versus wheel application number comparison between the high temperature SWTS and Phase I SWTS test specimens.

As shown in Fig. 6.10, high temperature SWTS specimens had a slightly higher intimal V_m compared to the Phase I SWTS specimens. The reason is the larger aggregate size used for high temperature SWTS specimens as listed in Table 6.2. Fig. 6.10 shows a higher rate of aggregate loss for the specimens tested in high temperature compared to room temperature tests except for 100% rubberized specimen. Fig. 6.11 provide a clearer comparison of the V_m values for the high temperature SWTS and Phase I SWTS test specimens. Fig. 6.11a presents the V_m value at the end

of 3,000 wheel applications in the SWTS test and Fig. 6.11b presents the ratio of the V_m value at the end of 3,000 wheel applications to the initial V_m value of the same specimens.

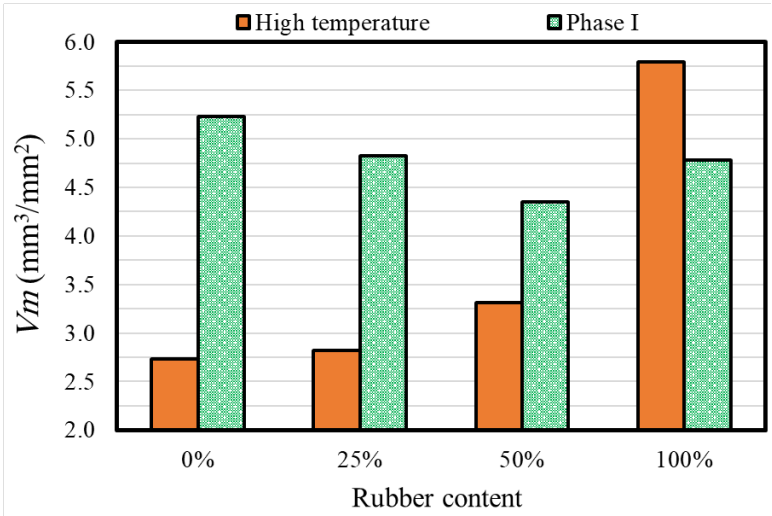

(a)

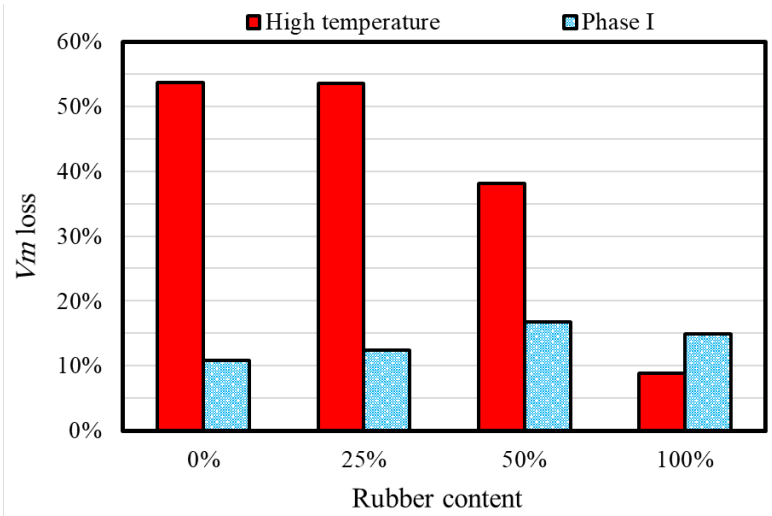

(b)

Fig. 6.11 –SWTS test results comparison for high temperature and Phase I specimens after 3,000 wheel applications. (a) final V_m value, and (b) V_m loss percentage.

As shown in Fig. 6.11, opposite trend of final V_m values and V_m loss was observed for the two different series of specimens. In the room temperature tests, with increasing the rubber content, the final V_m values reduced and more V_m loss was experienced. While in high temperature tests,

with increasing the rubber content, the final V_m values increased and less V_m loss was experienced. Fig. 6.11 shows that, for specimens tested in high temperature, with increasing the crumb rubber content from 0 to 25%, 50%, and 100%, the final V_m increased from 2.7 to 2.8, 3.3, and 5.8 mm^3/mm^2, respectively. Correspondingly, the V_m loss reduced from 54 to 53, 38, and 9%, respectively. Comparing the V_m loss for high temperature test specimens to Phase I test specimens indicates that in higher temperature, the raveling resistance of chip seal reduced significantly. However, at high temperature, the specimens with 100% crumb rubber performed even better than the one tested at room temperature. Increasing chip seal surface temperature increased the V_m loss from 11% to 54% for 0% crumb rubber specimen and from 17% to 38% for 50% crumb rubber specimen. While for 100% crumb rubber specimens the V_m loss reduced from 15% to 9% compared to room temperature testing. It is worth noting that, in order to make sure about the obtained results, another 100% rubber and 100% trap rock specimen were tested and the same results were obtained.

The reason for the excessive premature aggregate loss for trap rock specimens in high temperature tests was bleeding of the emulsified asphalt at that temperature. Since asphalt material is has a thermo-plastic chrematistic, in high temperatures the bituminous binder layer underneath the aggregates will get less stiff. Therefore, under the traffic load, the binder gets sheared and the aggregates slide away from their original place. This will make the aggregate being pushed together and the binder between them starts to bleed. Since the emulsion is hot and sticky, it stuck to the moving tires and spread over the wheel path which finally led to a premature excessive aggregate loss (Fig. 6.12). It can be noticed in Fig. 6.12a that the aggregates are pushed towards the center of the wheel path due to the viscous manner of the binder.

However, in the case of crumb rubber, due to the very low thermal conductivity of rubber particles compared to the aggregate, the binder underneath the rubber particles will not get that hot and soft, therefore the bleeding and consecutive aggregate loss did not happen. At the ambient temperature, the average thermal conductivity of mineral aggregate is between 1.83 and 2.90 (w/m.k) while the average thermal conductivity of rubber is 0.12 (w/m.k).

(a) (b)

Fig. 6.12 – Sevier bleeding and aggregate loss in high temperature SWTS test. (a) wheel path, and (b) tires covered with binder.

6.4. Conclusions

This chapter evaluated the performance of conventional and rubberized chip seal in terms of raveling and bleeding under simulated traffic load and different temperatures of 20º F, 78º F, and 100º F.

- In a low temperature of about 20º F, the raveling resistance of chip seal specimens presented a better raveling resistance compared to specimens tested at the temperature of about 78º F. This improvement was more pronounced for 100% trap rock specimens and had a reduced effect with increasing the rubber content.
- In a high temperature of about 100º F, the raveling resistance of chip seal specimens containing natural aggregate reduced significantly and severe bleeding and a subsequent severe aggregate loss happened due to the thermo-plastic behavior of the asphalt binder.
- In a high temperature of about 100º F, the chip seal specimens with 100% crumb rubber performed significantly better raveling and bleeding resistance than the chip seals containing natural aggregate.
- In a high temperature of about 100º F, the chip seal specimens with 100% crumb rubber performed a better raveling resistance than the 100% rubber chip seal specimen tested in about 78º F temperature due to the very low thermal conductivity of rubber particles compared to the natural aggregate.

Chapter 7: Effect of Crumb Rubber on Rainfall Water Drainage

7.1. Introduction

The drainage ability of the pavement surface is a significant factor in road safety. During rainy conditions, if rainwater cannot rapidly drain off the pavement surface, a water film will be formed. Water film acts as a lubricant and reduces the pavement friction, i.e., skid resistance. Tire-pavement friction decreases in an approximately exponential fashion when the water film depth (WFD) on the pavement surface increases. An uplift force from water film separates a portion of the vehicle's tires off the pavement surface. This uplift force increases with the increase of vehicle speed until the full separation of the tire from the pavement at a specific speed, called hydroplaning, also known as aquaplaning, speed. At hydroplaning speed, the tire is supported only by the water film, and since the water does not sustain shear forces, the friction between the tire and pavement drops significantly, which leads to an almost complete loss of vehicle braking and steering control [56, 97]. Vehicle hydroplaning is a major safety concern in wet-weather driving and is highly associated with the depth of the water film formed on the pavement surface. Excessive splash and spray is another phenomenon on flooded road surfaces, which causes a nuisance to motorists and decreases the safety on the road. Splash and spray is also related to stored water depth in or on the texture of the pavement. Therefore, calculating the WFD is the primary step in road safety evaluation.

The tendency for hydroplaning and splash and spray is reduced by reducing the WFD on the pavement which can be achieved by proper drainage of the surface [49, 55, 56, 97-100]. Among other approaches, grooving or using permeable pavements are the most common alternatives.

However, using a surface with higher macrotexture such as chip seal could be an efficient method to reduce the WFD on existing roads, since a higher surface texture will help drain water from the pavement surface to the pores or channels of the texture.

In this chapter, a comprehensive test was conducted to develop a relationship for predicting the WFD of highly textured surfaces like chip seal. Recently introduced eco-friendly rubberized chip seal [7-10, 101] was also tested in addition to conventional chip seal to evaluate the drainage capability of a chip seal surface made with crumb rubber particles. Chip seal specimens with different combinations of aggregates including mineral aggregate and crumb rubber particles and different embedment depths were tested for variable slopes, rainfall intensities, and drainage length using a piece of original laboratory equipment: advanced rainfall simulator (ARS). For this means, the ASTM standard method of sand patch was used to measure texture depth. Also, high rainfall intensities like flash flood conditions were imposed since chip seal is not susceptible to low rainfall intensities causing hydroplaning or splash and spray. Based on the data collected, highly accurate models were proposed for chip seal with different texture types and texture depths under different conditions.

7.2. WFD Contributing Factors

Pavement surface characteristics and rainfall intensity are the major contributing factors on pavement WFD [1-7,10-16]. Texture depth or mean texture depth (MTD) represents the pavement macrotexture. Macrotexture is defined as the texture with wavelengths of 0.02 to 2.0 in. MTD is one of the main intervening factors on WFD that was considered in this study. Highly textured surfaces can reduce the WFD by storing some surface water in the pavement texture (Fig. 7.1). At the same time, the pavement texture can provide flow paths to allow the water to be drained

out of the pavement into the provided drains. Rainfall intensity is another major factor that influences the WFD. Heavy rainfall with a long duration can provide a very high surface runoff [102]. However, the laboratory test was conducted in a relatively short time period. Therefore, high rainfall intensities were applied in this test to represent flash flooding conditions, considering the fact that low rainfall intensities will not provide a water film on highly textured surfaces like chip seal.

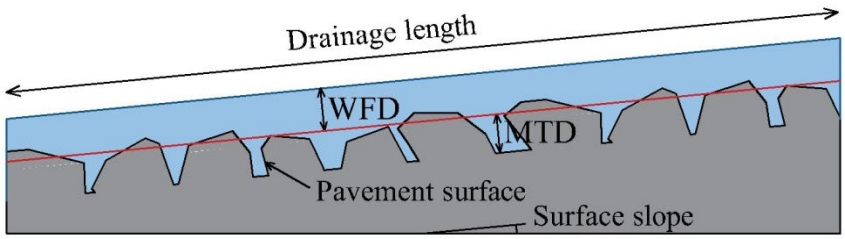

Fig. 7.1 – Pavement surface and WFD contributing factors.

Drainage path length and slope are other factors that were considered in this study (Fig. 7.1). Drainage path length or drainage length is defined as the maximum length that a rainfall droplet needs to flow between the point of contact with the surface and its point of exit from the pavement. The shorter drainage length leads to less rainfall accumulation, resulting in a lower WFD. The higher drainage path slope, i.e., pavement surface slope, also helps the water to drain faster, hence providing lower WFD. Since chip seal pavement is not a permeable surface, the effect of water penetration was not considered in this study.

7.3. Experimental Program

In order to fulfill the objective of this task, a comprehensive test was conducted to develop a relationship for predicting the WFD of highly textured surfaces like chip seal. The eco-friendly rubberized chip seal was tested in addition to the conventional chip seal to evaluate the drainage

capability of a chip seal surface made with crumb rubber particles. Chip seal specimens with different combinations of aggregates including mineral aggregate and crumb rubber particles and different embedment depths were tested for variable slopes, rainfall intensities, and drainage length using a piece of original laboratory equipment: advanced rainfall simulator (ARS). For this means, the ASTM standard method of sand patch was used to measure texture depth. Also, high rainfall intensities like flash flood conditions were imposed since chip seal is not susceptible to low rainfall intensities to cause hydroplaning or splash and spray.

7.3.1. Test Setup

An advanced rainfall simulator (ARS) was used in this study (Fig. 7.2). The ARS was composed of a rigid metallic frame of 8 ft by 4 ft, where the chip seal specimens were placed. The frame was adjustable to provide slope ranging from 0% to 20%. Within 2 ft above the frame, 8 storage tanks made of clear PVC were located. Each storage tank had 576 nozzles of 0.02 in diameter, making a total of 4,608 nozzles producing rainfall over the specimen. Different drainage lengths were provided during the tests by producing rainfall on the full length of specimens representing drainage lengths of 8, 6, and 4 ft from the funnel.

The ARS was capable of simulating rainfall with an intensity of 1 to 6 gallons per minute using a sump pump. The rainfall intensity was adjustable by the input valves and controlled by a digital flow meter which measures the input discharge. The rainfall was collected at the end of the specimen in an aluminum funnel attached to chip seal specimens, and the outlet discharge was measured by another digital flow meter on the outlet drain pipe. A data logger was programmed to record data from rainfall inlet and outlet each one-tenth of a second and data were transferred into a data management program and subsequently into a Microsoft Excel spreadsheet for processing.

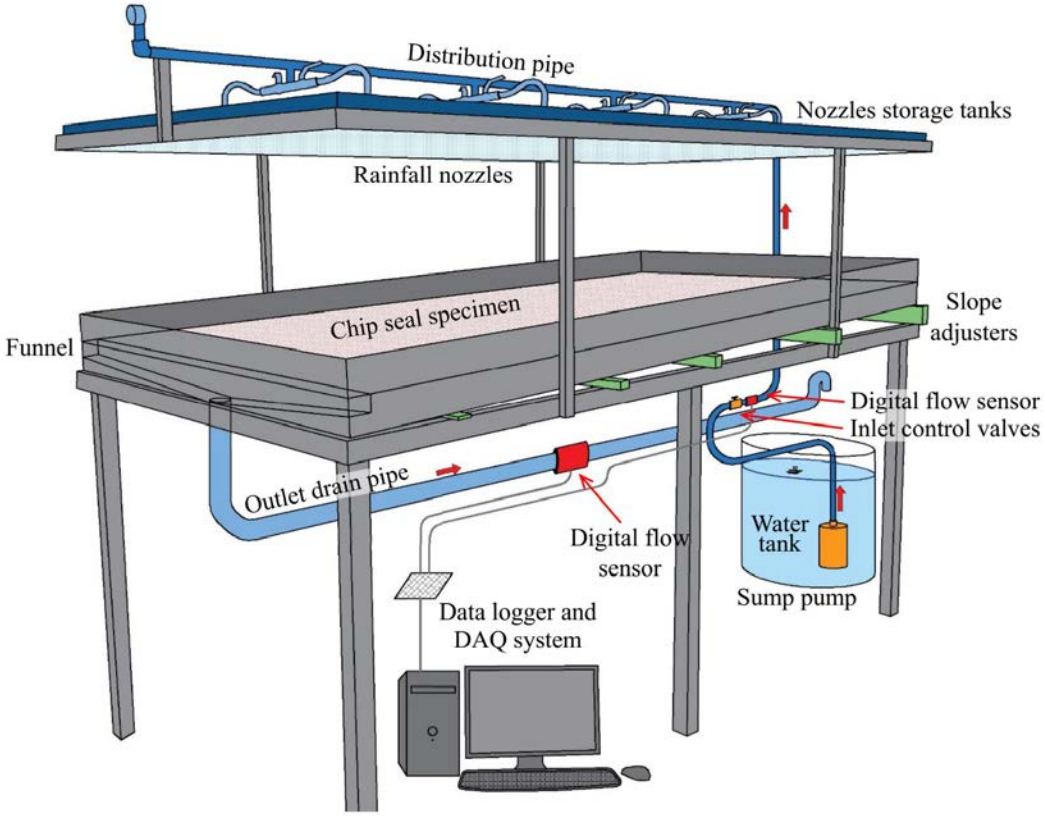

(a)

(b)

Fig. 7.2 – Advanced rainfall simulation (ARS) machine (a) schematic, (b) real view.

7.3.2. Test Matrix

Eight 8 ft x 4 ft chip seal specimens were constructed and tested in this study as shown in Fig. 7.3 and listed in Table 7.1. Different rubber contents of 0, 25, 50 and 100% were applied to investigate the effect of rubber content on drainage capability of the chip seal surface. Binder application rates of 0.25 and 0.50 gal/yd^2 were used in order to provide different MTD for samples with the same rubber content. Therefore, the effect of MTD could be considered independent of the rubber content. These binder application rates are selected based on the common practice range for chip seal. The specimens were subjected to different rainfall intensities of 1, 2, 3, 4, 5, and 6 gal/min equal to 3, 6, 9, 12, 15 and 18 in/hr, respectively. A wide range of rainfall intensities including high-intensity flows was selected to fill the existing gap in the literature. Also, lower intensities will not produce any WFD on chip seal surfaces due to the high MTD. Each specimen had three different slopes of 0.5, 1.5, and 2.5% for each rainfall intensity. The selected slops represented the longitudinal or transversal slopes of road surfaces. The drainage length was 8 ft for all specimens; then, lengths of 6 ft and 4 ft were also considered for some specimens (Table 7.1). Therefore, the effects of rainfall intensity, aggregate type, MTD, slope, and drainage length on the WFD formation were investigated. A total of 154 different tests were conducted, and each test was repeated at least two times to obtain reliable results. Therefore, more than 300 tests were conducted in this experimental study.

Fig. 7.3 – Rainfall simulation test specimens.

Table 7.1 – Test matrix

Specimen ID	Aggregate ratio (%) by volume		Binder ratio	Drainage length (ft)	Slope (%)	Rainfall intensity (in/hr)
	Rubber particle	Mineral aggregate	(Gal/yd2)			
0R0.50B	0	100	0.5	8	0.5	3, 6, 9, 12, 15, 18
					1.5	
					2.5	
				6	2.5	12
				4	0.5	6, 17
					1.5	6, 18
					2.5	6
0R0.25B	0	100	0.25	8	0.5	3, 6, 9, 12, 15, 18
					1.5	
					2.5	
				6	2.5	12
				4	0.5	6
					1.5	6, 17
					2.5	6, 18
25R0.50B	25	75	0.5	8	0.5	3, 6, 9, 12, 15, 18
					1.5	
					2.5	
				6	2.5	12
				4		6, 12
25R0.25B	25	75	0.25	8	0.5	3, 6, 9, 12, 15, 18
					1.5	
					2.5	
				4	0.5	6, 12
					1.5	
					2.5	
50R0.50B	50	50	0.5	8	0.5	3, 6, 9, 12, 15
					1.5	
					2.5	
50R0.25B	50	50	0.25	8	0.5	3, 6, 9, 12, 15
					1.5	
					2.5	
100R0.50B	100	0	0.5	8	0.5	3, 6, 9, 12, 15
					1.5	
					2.5	
100R0.25B	100	0	0.25	8	0.5	3, 6, 9, 12, 15
					1.5	
					2.5	

7.3.3. Test Procedure

After placing the chip seal specimen inside the ARS, a constant rainfall with the desired intensity was imposed, and the runoff discharge rate was recorded via a digital flow meter as schematically illustrated in Fig. 7.4. At the beginning of rainfall, a certain amount of water fills the voids of the surface texture before runoff occurs above the surface. The runoff rate increases to an equilibrium value equal to the rainfall intensity when the surface texture is saturated, since the chip seal surface is impermeable. By the time the runoff becomes constant, the WFD reaches its maximum value and remains constant. When the rainfall ceases, the runoff rate and the WFD both reduce back to zero.

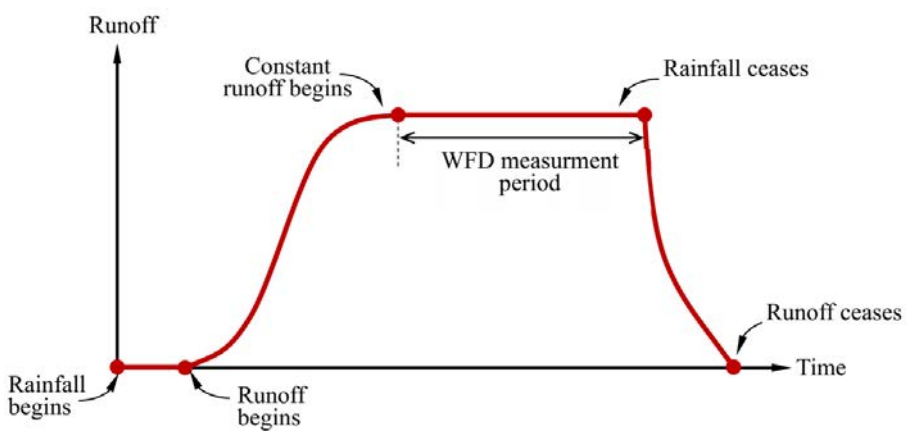

Fig 7.4 – Rainfall runoff hydrograph.

7.3.4. Water Film Depth Measurement

Fig. 7.5 defines the WFD as the water flow on the chip seal surface. WFD is the depth of water formed above the mean texture depth (MTD) of the surface, since the water below the MTD is trapped in the surface texture and does not contribute to hydroplaning. In this study, the WFD measurements were performed during the constant runoff period, since the WFD has its maximum value and remains constant (Fig. 7.4). In order to obtain a more accurate WFD measurement during

the test, the total water depth (TWD) based on a datum plane at the bottom of the texture, i.e., the top of the binder layer, was measured since the water depth above the texture may become zero or negative in some cases. Deducting the MTD from the measurements, i.e., TWD, leads to WFD. A narrow gauge was used for TWD measurement with an accuracy of 0.01 in. The measuring gauge, datum plane, TWD, WFD, MTD, and surface slope are illustrated in Fig. 7.5.

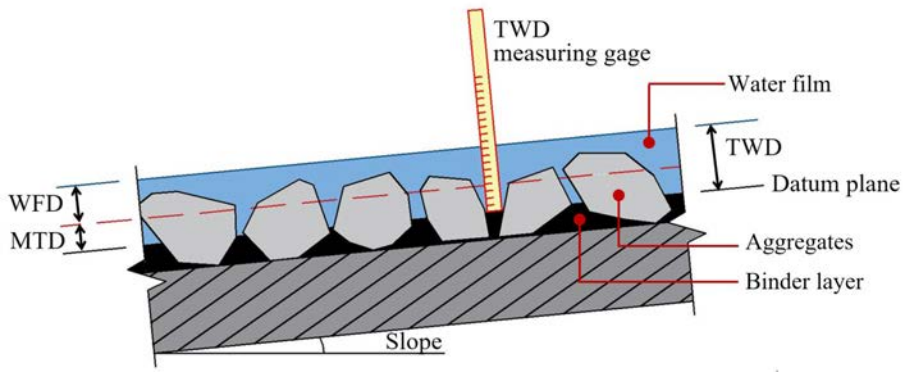

Fig. 7.5 – Chip seal surface and definition of parameters.

During each test, three WFD measurements across the width of the surface were taken at different locations along the length of the surface with about 2 ft equal distance from each other. For instance, in the case of tests with 8 ft drainage length, nine WFD measurements were conducted and the average of nine readings was considered as the WFD of that test. In total, 1,748 TWD readings were taken during this study leading to WFD ranging from -0.089 to 0.225 in as reported in Tables D.1 to D.3 of Appendix D.

7.3.5. Mean Texture Depth Measurement

ASTM E965 volumetric sand patch test [59] is the most common method to measure the macrotexture depth of the pavement surface. Therefore, the sand patch test was used to measure the mean texture depth (MTD) of the test specimens in this study. In this method, a known volume of fine sand was spread evenly over the surface of the specimen. The diameter of spread sand was

measured, and the MTD was calculated using the volume of sand and averaged diameter. A total of seven sand patch measurements was conducted on each specimen (Fig. 7.6), and the average was considered as the MTD of that specimen (Table 7.2). Detailed MTD measurements and results are presented in Table D.4 of Appendix D.

Table 7.2 – Mean texture depth values of the test specimens

Specimen ID	MTD (in)	Specimen ID	MTD (in)
0R0.50B	0.175	0R0.25B	0.154
25R0.50B	0.180	25R0.25B	0.160
50R0.50B	0.169	50R0.25B	0.154
100R0.50B	0.171	100R0.25B	0.196

Fig. 7.6 – Sand patch test on rainfall simulation test specimen.

7.4. Results and Discussion

7.4.1. Existing WFD Prediction Models

In this section, the results obtained from the experiments were compared with the results from the most common existing WFD models. Fig. 7(a) shows the WFD measured during the test versus the WFD calculated based on Gallaway et al.'s model [55]. As mentioned earlier, Gallaway et al.'s model [55] proposed a widely used empirical equation that relates drainage path length (L, ft), MTD (in), drainage path slope (S, ft/ft), and rainfall intensity (I, in/hr) to WFD (in).

$$WFD = 0.00338[MTD^{0.11}L^{0.43}I^{0.59}S^{-0.42}] - MTD \qquad \text{Eq. (7.1)}$$

As shown in Fig. 7.7(a), WFD values calculated by Gallaway's model were generally smaller than those measured experimentally. The coefficient of determination, i.e., R^2, between the measured and Gallaway's model WFD showed a low value of 0.23, indicating a very low correlation between the two values. It is worth noting that Gallaway et al.'s [103] experimental results showed a more pronounced effect of MTD on measured WFD when the MTD was higher than 0.05 in comparison to specimens having MTD less than 0.05 in. However, chip seal surfaces typically have an MTD of more than 0.10 in. This can explain the low correlation between the experimental and analytical WFD.

Another model, PAVDRN [56], was used to correlate the WFD to MTD per Eq. 7.2.

$$WFD = \left[\frac{n\ L\ I}{S^{0.5}}\right]^{0.6} - MTD \qquad \text{Eq. (7.2)}$$

where n is the Manning's roughness coefficient of the surface, which was considered 0.016 in this study [104]. As shown in Fig. 7.7(b), PAVDRN values present a better correlation with the measured WFD values compared to those predicted using Gallaway's model with an R^2 value of

0.72. Careful examination of Fig. 7.7(b) indicates that the PAVDRN model was able to predict quite well the WFD until approximately 0.05 in and corresponding to rainfall intensity of 9 in/hr with R^2 of 0.77. Beyond that, however, the model was less successful in predicting the WFD with R^2 of 0.34.

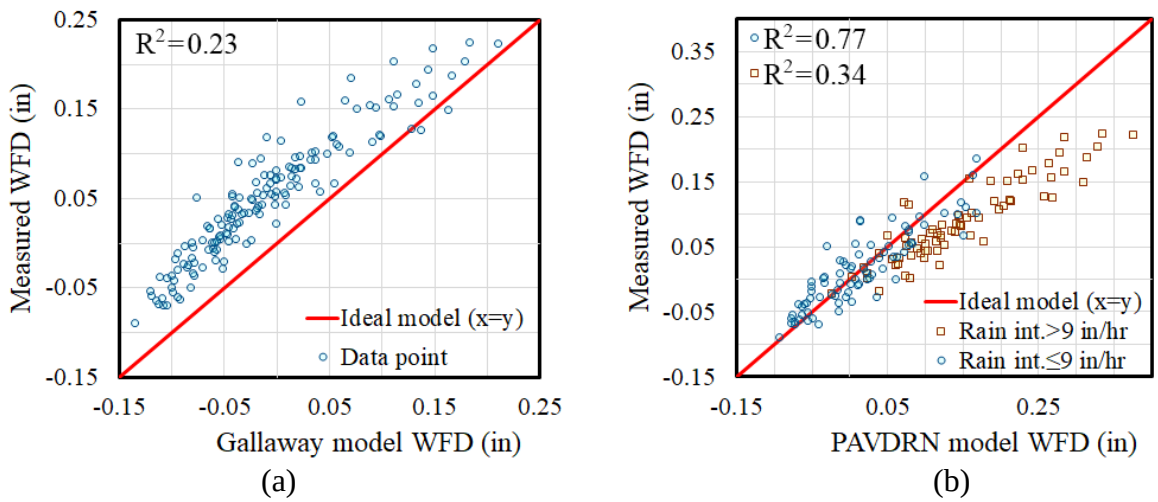

Fig. 7.7 – Evaluating of existing water film depth prediction models with experimental results for (a) Gallaway model, (b) PAVDRN model.

7.4.2. New WFD Prediction Model Development

To overcome the limitations of the available models, this study presented a new model to provide a more accurate prediction of the WFD of high macrotexture surfaces subjected to different rainfall intensities. For this means, first, individual factor analysis was conducted with the test results to evaluate the effect of different variables on the WFD. Fig. 7.8 shows the variation of different parameters including drainage slope, drainage length, MTD, rainfall intensity and rubber content, versus the measured WFD. The best fit line on each plot shows the general trend of the effect of each variable on WFD. The significance of effect, i.e., p-value, of each parameter on WFD was obtained using regression analysis as 1.2e-48, 1.2e-8, 2.3e-11, 7.3e-46, and 0.041 for drainage slope, drainage length, MTD, rainfall intensity, and rubber content, respectively.

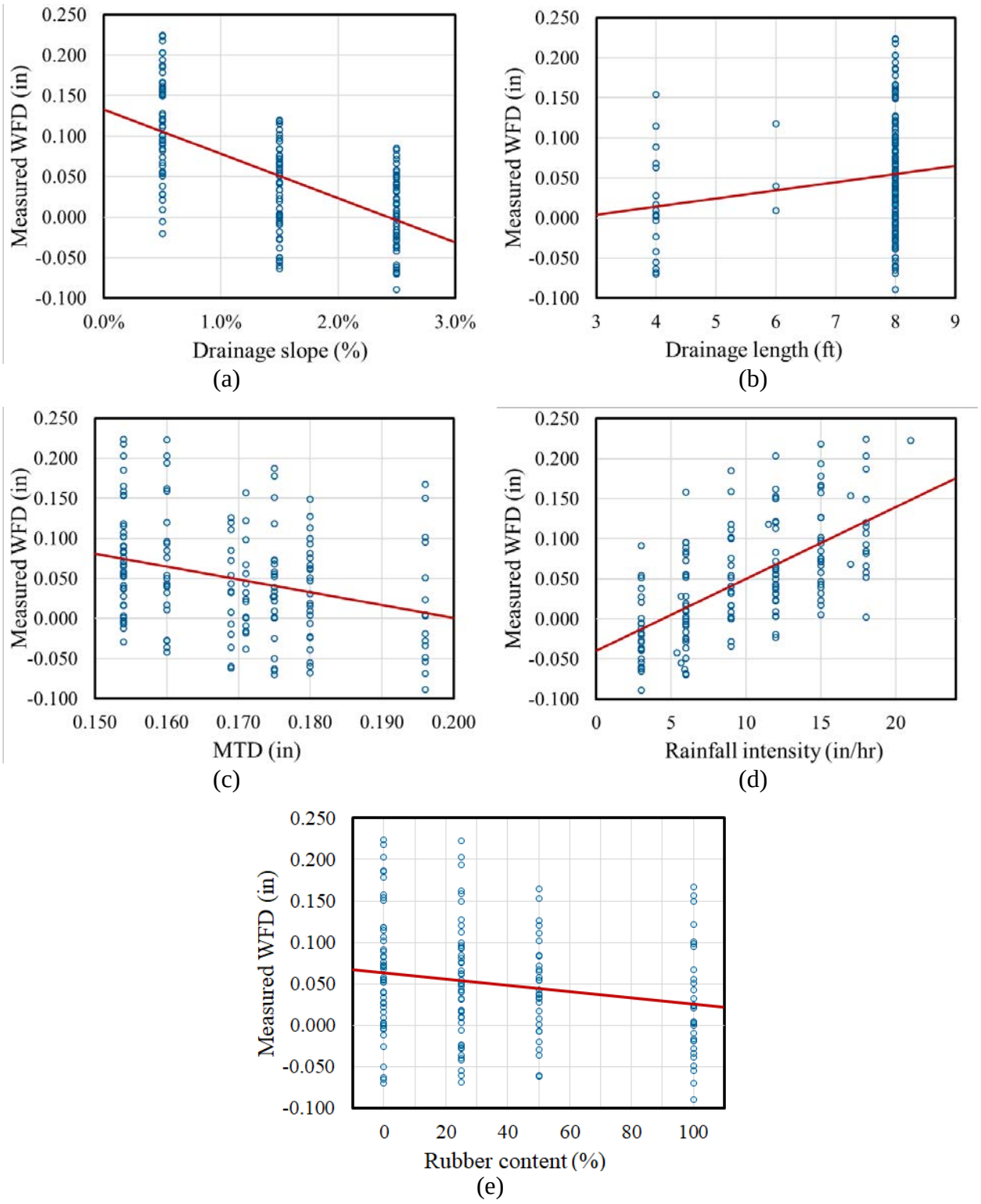

Fig. 7.8 – Variation range of test different test parameters and WFD.

Fig. 7.9 represents the effect of different variables on WFD more specifically. In this set of graphs, the effect of other variables was excluded by considering them constant with only two parameters varying in each plot. As shown in Fig. 7.9(a), with increasing the drainage slope, the WFD decreased. The effect of the slope was more pronounced at the lower slopes. For instance, for the sample with MTD of 0.196 in, increasing the slope for 1% from 0.5% to 1.5% decreased the WFD by 0.129 in, however, 1% more increase of the slope from 1.5% to 2.5% will only decrease the WFD by 0.006 in. Therefore, a 1.5% slope can be considered the maximum effective slope in case of a drainage length of 8 ft or less.

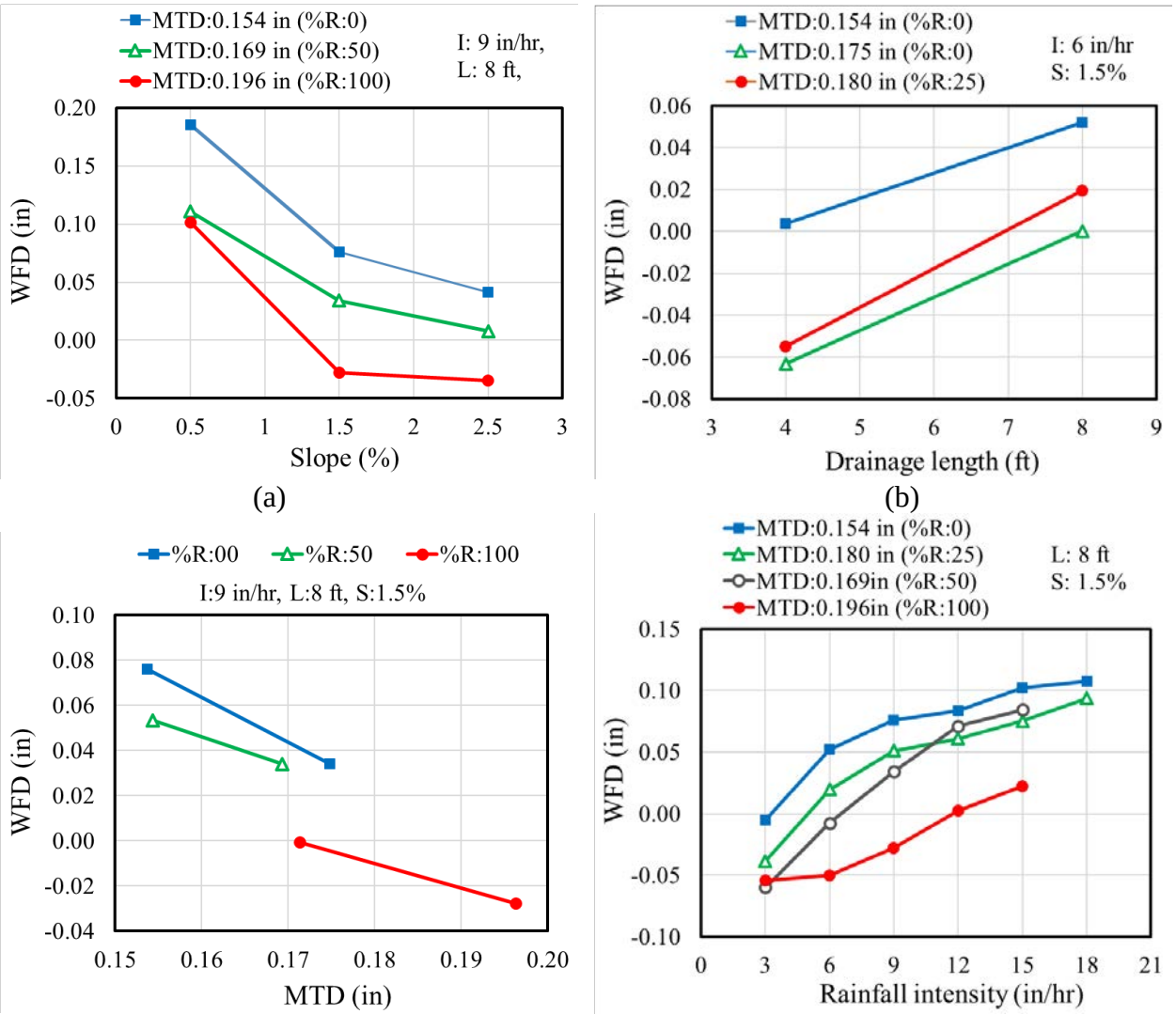

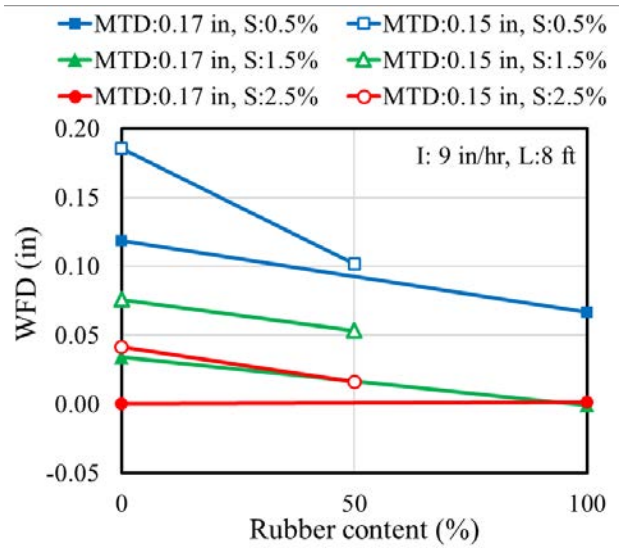

(e)

Fig. 7.9 – Effect of different parameters on WFD.

Fig. 7.9(b) shows that with increasing the drainage length, the WFD increased. The rate of increase was almost the same for samples with different MTD. As shown in Fig. 7.9(c), with increasing the MTD, the WFD decreased. The same result can be observed in Fig. 7.9(a) as well. The reason is that higher MTD will provide better drainage with higher asperities which can store the surface water and provide more inner texture channels for the water to be drained off the pavement. Fig. 7.9(c) also shows that higher rubber content created lower WFD. For instance, for MTD of around 0.17 in, the WFD was about 0.43 in, 0.32 in, and 0.02 in for samples with 0%, 50%, and 100% rubber content respectively.

As expected, increasing the rainfall intensity increased WFD as shown in Fig. 7.9(d). The effect of MTD on WFD can be observed in Fig. 7.9(d) as well. However, the sample with MTD of 0.180 in showed a higher WFD in most points compared to the sample with MTD of 0.169 in. This contradiction can be described by considering the rubber content of the samples. The sample with higher rubber content obtained lower WFD while its MTD was lower. Fig. 7.9(e) shows the effect of rubber content on WFD. It can be observed that with increasing the rubber content, the

WFD was decreased. The effect of rubber content was more pronounced at lower slopes. For instance, for the samples with MTD of 0.15 in, increasing the rubber content from 0% to 50% decreased the WFD by 0.183 in at a slope of 0.5%, however, the same increase in the rubber content decreased the WFD by only 0.025 in at a slope of 2.5%. The reason could be related to the lower flakiness of crumb rubber particles which provide more pores or channels for the water to be drained in lower slopes compared to more flaky mineral aggregate. However, at higher slopes the effect of the slope is more dominant with a p-value of 1.2e-48, therefore, the effect of rubber content would be less.

In order to develop a WFD prediction model, two different levels of significance of 0.01 and 0.05 was considered. According to the p-values obtained from the initial analysis, the effect of rubber content with a p-value of 0.041 was not considered in the first proposed model with the significance level of 0.01. Regression analyses were used to develop Eq. 7.3 and 7.4 based on the results of 154 sets of data collected through the experimental program. All parameters are defined earlier in this chapter (Fig. 7.5). As shown in Fig. 7.10(a), the regression analyses were quite accurate; Eq. 7.4 presents the measured data with an R^2 of 0.89.

$$TWD = 0.00639[MTD^{-0.46}L^{0.29}I^{0.37}S^{-0.29}] \quad \text{Eq. (7.3)}$$

$$WFD = 0.00639[MTD^{-0.46}L^{0.29}I^{0.37}S^{-0.29}] - MTD \quad \text{Eq. (7.4)}$$

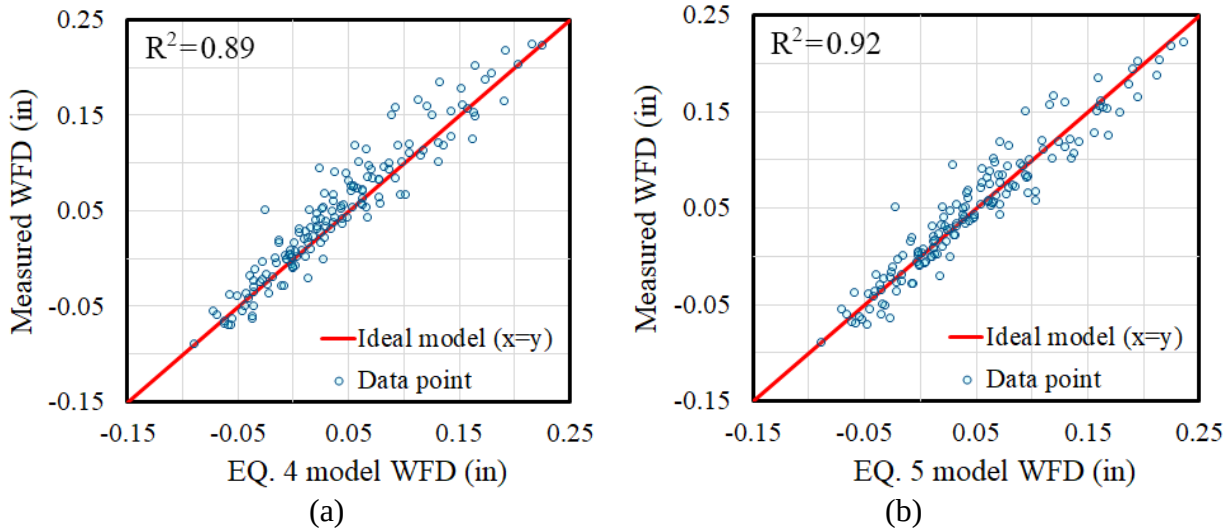

Fig. 7.10 – Evaluation of proposed water film depth prediction models with experimental results for (a) Eq. 7.4 model, and (b) Eq. 7.5 model.

Eq. 7.4 increases the weight of the MTD and decreases the weight of the drainage length compared to Eq. 7.1. Other researchers [105] also suggested that the MTD and drainage slope are more influential on the surface drainage capacity compared to the flow path length. Eq. 7.4 proposed an inverse relationship between WFD and MTD, indicating that with increasing the MTD, the WFD decreases as the macrotexture plays a significant role in the drainage of water from a pavement surface [106], and this was expected to be more pronounced since the water can be drained through the protuberances and depressions within the surface texture of a chip seal pavement.

Another WFD prediction model was proposed with a significance level of 0.05. This model was developed considering the effect of rubber particle content and is presented in Eq. 7.5.

$$WFD = 0.00751[MTD^{-0.36}L^{0.32}I^{0.37}S^{-0.30}R^{-0.02}] - MTD \qquad \text{Eq. (7.5)}$$

where R is the rubber content percentage. For conventional chip seal with 0% rubber, R is considered equal to 1, and it is equal to 25, 50, and 100 for 25, 50, and 100% rubberized chip seals,

respectively. Eq. 7.5 shows an inverse relationship between the rubber content and WFD which matches the trend of the measured experimental data shown in Fig. 7.8(e) and 7.9.

Fig. 7.10(b) shows that the model in Eq. 7.5 presented a very high correlation between the calculated and measured WFD for all the data sets of this study with R^2 equal to 0.92, which is greater than R^2 obtained from WFD predicted per the model in Eq. 7.4, which does not consider the effect of rubber particle content in chip seal (Fig. 7.10(a)). Fig. 7.11(a) and 7.11(b), respectively, show the predicted WFD values per Eq. 7.4 and Eq. 7.5 along with the measured values. As shown in Fig. 7.11(c, d), the WFD calculated based on Eq. 7.5 yielded a WFD comparable to those measured during the experiments.

Fig. 7.12(a) and 7.12(b), respectively, show the residual plots for calculated WFD per Eq. 7.4 and 7.5 for all 154 tests. Also, the best fit line and histogram of the residuals are shown in Fig. 7.12. The concentration of residuals on and around the zero line shows good accuracy of the WFD predicted by both models. However, Eq. 7.5 had proposed a comparatively higher accuracy with a greater number of residual points close to the zero line (Fig. 12(b)). Therefore, the model in Eq. 7.5 can be accepted as the best fitting model to predict WFD for chip seal surfaces made of mineral and/or rubber particles.

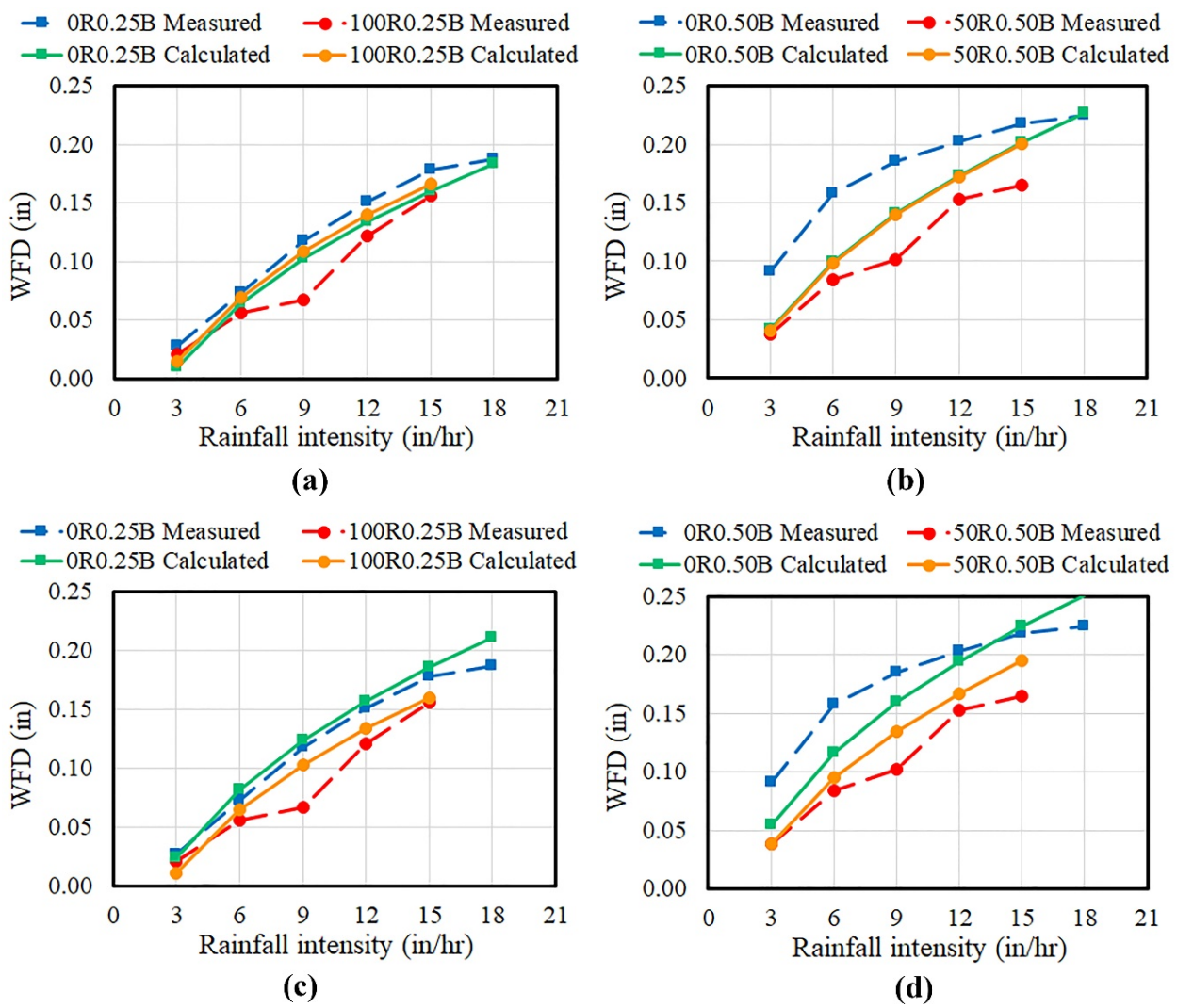

Fig. 7.11 – Evaluation of proposed models for considering the effect of rubber content according to (a, b) Eq. 7.4 model, and (c, d) Eq. 7.5 model with 0.05% slope.

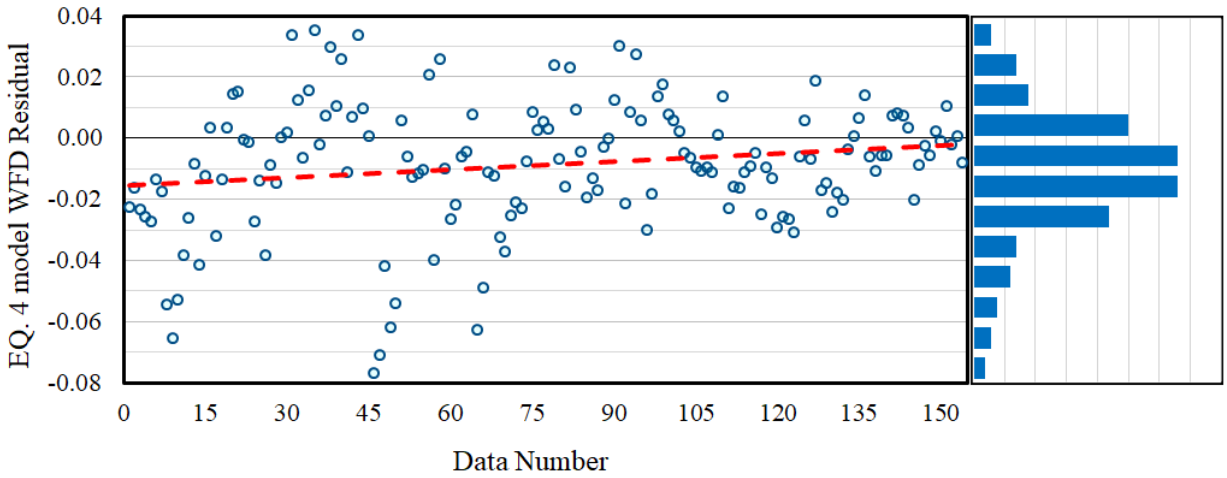

(a)

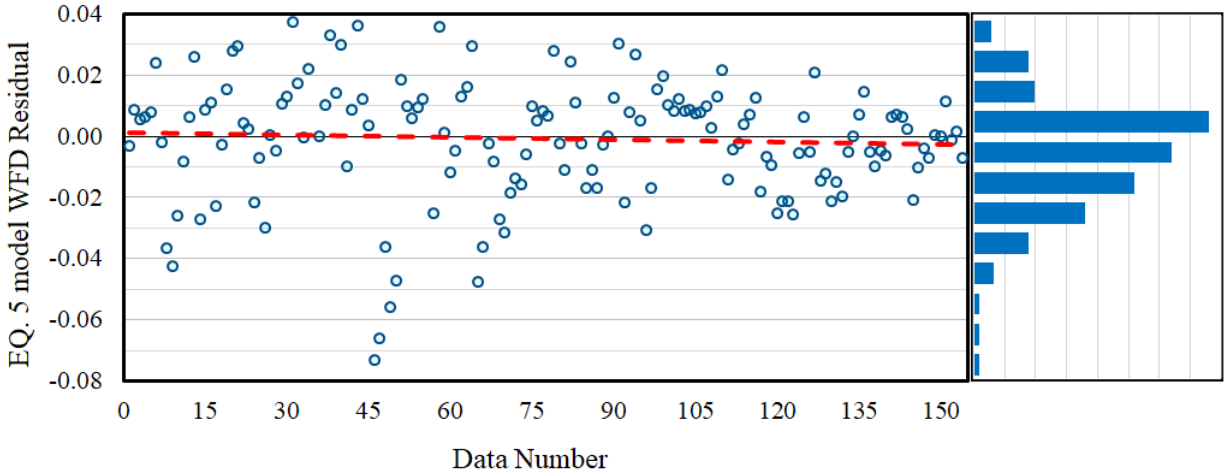

(b)

Fig 7.12 – Residual plots for WFD calculated per (a) Eq. 7.4 model, and (b) Eq. 7.5 model.

7.5. Conclusion

Water film depth (WFD) is an essential factor regarding the safety on the roads. Using highly textured pavement is one of the solutions to reduce WFD. Therefore, chip seal can be used as a viable option. However, the models presented for calculating WFD are not developed based on highly textured surfaces like chip seal. In addition, the rainfall intensity ranges used for developing most of these models do not raise safety issues on chip seal roads. In this study, an intensive experimental program was conducted in which 1,784 WFD readings were collected

through 154 different combinations of texture depth, texture type, slope, drainage length, and rainfall intensity. Based on the test results the following conclusions are derived:

- The Gallaway model does not provide accurate predictions for the WFD of chip seal surfaces. The correlation between Gallaway WFD and actual WFD measurements was very poor with small R^2=0.23.
- The PAVDRN model provides fair results for chip seal surface with rainfall intensities equal to or lower than 9 in/hr with R^2=0.77 between the predicted and actual WFD values. However, for higher rainfall intensities, the results were underestimated and not reliable with R^2=0.34 between the predicted and actual WFD values.
- The first model proposed in this study showed a very high correlation with actual WFD measurements with R^2=0.89. This model showed that WFD on the chip seal surface is highly related to mean texture depth, which is underestimated in the Gallaway model for highly textured surfaces.
- The second model proposed in this study incorporated a term to consider the effect of partially or fully rubberized chip seal surfaces, which can predict the WFD variation caused by only changing the aggregate type while other variables are identical. This model showed a very high correlation between the predicted and actual WFD values with R^2=0.92.
- Rubberized chip seal has enhanced drainage capabilities compared to conventional chip seal, especially in low slopes. For example, at the rainfall intensity of 3 in/hr and slope of 0.05%, replacing 50% of mineral aggregate with crumb rubber particles reduced the WFD by 58%.

Chapter 8: Effect of Mechanical Snow Removal

8.1. Introduction

Damage from mechanical snow removal, also known as mechanical snowplowing action, hereafter called snowplowing, is one of the major failure causes of chip seal. The destructive effect of snowplows has been observed in several cases including the field implementation conducted in this project as shown in Fig. 8.1a (see Chapter 10). Usually, in the area between the wheel paths and in other areas that do not experience a high traffic load, the aggregates will stand higher than the areas that experienced a higher traffic load. Also, aggregates in those places do not reorient to their lowest-dimension side, leaving a susceptible place to be damaged by a snowplow (Fig. 8.1b) [61].

In this chapter, laboratory simulation of snowplowing action is conducted on conventional and rubberized chip seal specimens. Evaluation of the effect of snowplowing on the different aggregate types and also the effect of snowplow angle with the pavement surface on snowplow damage were the objectives of this task.

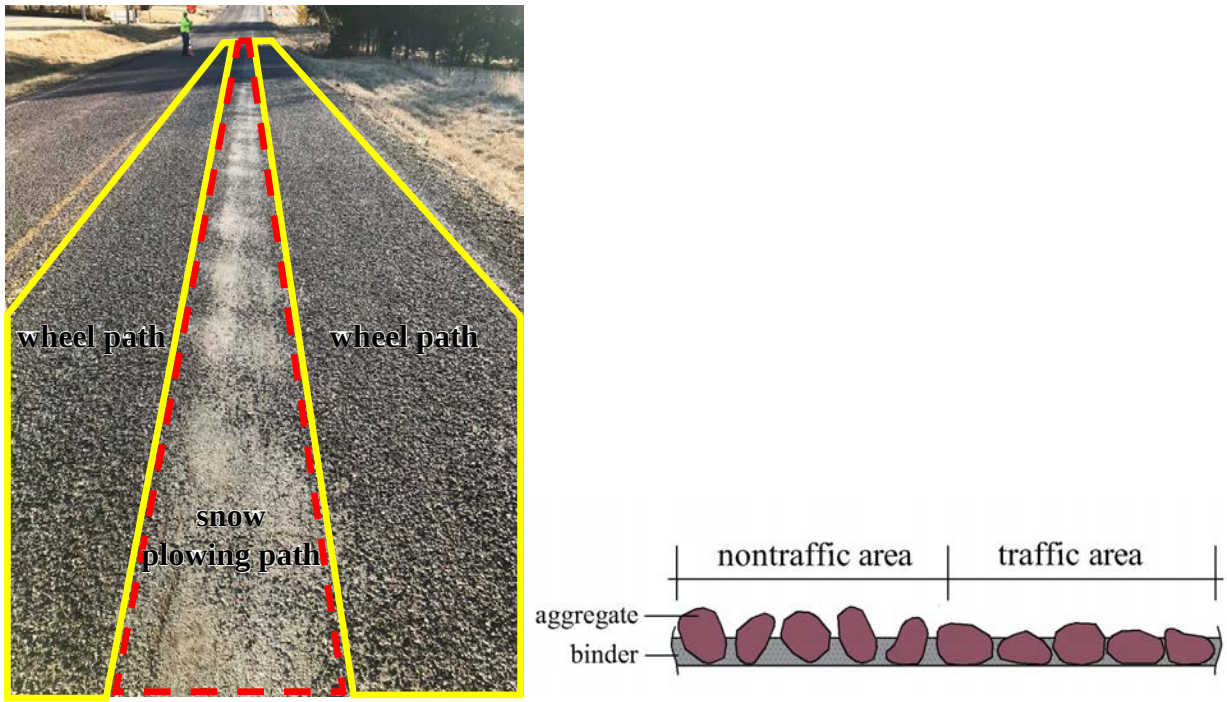

(a) (b)

Fig. 8.1 – (a) Snowplow damage between the wheel paths in the field implementation study of this project, (b) schematic view of chip seal surface in the wheel path and snowplow path.

8.2. Experimental Program

8.2.1. Test Specimens

Since the snowplow will mainly affect the area between the wheel paths and areas that do not experience any traffic, virgin specimens that did not undergo traffic loadings were used for this experiment. Four 2 ft by 2 ft chip seal specimens made with trap rock natural aggregate and 0%, 25%, 50%, and 100% crumb rubber content were tested. The specimens are labeled as per Table 8.1.

Since this is a comparison study for the effect of snowplowing on different aggregate types, binder rate was not considered as one of the variables. Therefore, the binder application rate for all four specimens was considered 0.50 gal/yd^2, since the results obtained in Chapter 5 of this study

indicated that specimens with a binder application rate of 0.50 gal/yd^2 performed better aggregate retention under traffic load compared to 0.25 gal/yd^2.

Crumb rubber and natural aggregate with flakiness indexes of 46 and 31, respectively, were used for specimens in this section. Other material specifications and sample preparation processes were as described in Chapter 4 of this report. It is worth noting that for specimen construction, the same gradation of aggregate size along with the same volumetric aggregate application rate was used for trap rock and crumb rubber to obtain the same macrotexture for different specimens.

Table 8.1 – Snowplowing Test Specimens

Specimen ID	Binder rare (gal/yd^2)	Percentage of Aggregate	
		Trap rock	Crumb rubber
00R	0.5	100	0
25R		75	25
50R		50	50
100R		0	100

8.2.2. Snowplowing Test

To evaluate the effect of snowplowing on conventional and rubberized chip seal, a comparative test was conducted using a snowplowing test setup (Fig, 8.2). The snowplowing test setup consisted of a 3/4 inch thick steel snowplow blade that was cut in 3 by 3 inches from a real scale blade obtained from the Missouri Department of Transportation (MODOT). The snowplow blade was aligned with the wheels in SWTS and was capable of providing different angles between the blade and chip seal surface, called the cutting angle, from 25 to 48 degrees. The cutting angle is shown as angle α in Fig. 8.2a. The total weight of 190 lbs was imposed on the chip seal surface through the three wheels and the snowplow blade. This weight was applied to keep the snowplow

blade in place and prevent it from raising the wheel assembly, since the snowplow blade would stop and raise the wheel assembly in the absence of the load, due to the interaction between the snowplow blade and surface texture. More detail about the snowplow assembly can be found in Chapter 3 of this report.

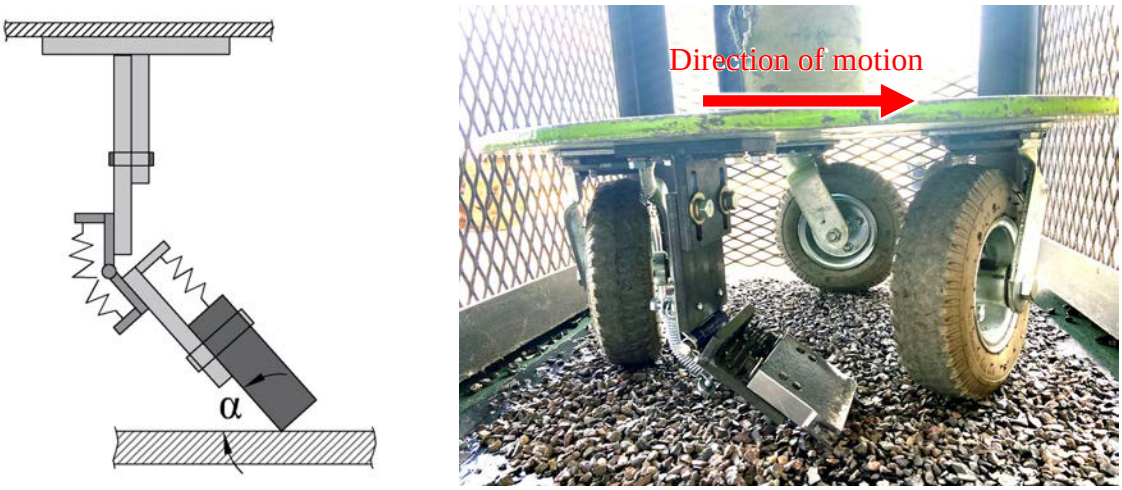

(a) (b)

Fig. 8.2 – Snowplowing assembly, (a) schematic view showing the snowplow cutting angle α, and (b) real view.

The snowplowing test was conducted on the specimens in the freezing condition to simulate the condition of the real field chip seal during the snowplowing action in winter. For this means the chip seal specimens were kept in a freezer for at least 2 hours prior to the test. The SWTS machine was also kept in the freezing temperature environment. Therefore, the surface temperature of the specimens was controlled to be 32±2˚F during the test.

The snowplowing test was conducted for a total of eight snowplow applications on the chip seal specimen in two steps. First, three snowplow applications were applied, and the texture loss of the specimens was assessed. However, since the aggregate loss was not severe, in order to obtain a better comparison, the test was continued for five more snowplow applications. The texture loss

after a total of eight snowplow applications was also assessed. The cutting angle is another key factor for a snowplowing mechanism, since different cutting angles will provide a different amount of energy imposed to the surface [107]. Therefore, different cutting angles were also tried on chip seal specimens in this test.

8.2.3. Macrotexture Evaluation

A new non-contact measurement technique using a 3D scanner was used to monitor the texture variation and aggregate loss during the snowplowing test. The reason for using this technique is first of all not being able to properly use the common method of sand patch [90] for macrotexture measurement due to the circular snowplow path with limited width. A 3D surface scanning technique will also provide more accurate macrotexture measurements [42, 46, 91].

The scanner used in this project was a two-camera structured-light 3D scanner namely Thunk3D Fisher (Fig. 8.3a). The manufacturer declared accuracy of 0.04mm to 0.1mm having a scan speed of 1,200,000 points per second and a resolution of 0.2 mm with two 12mm/5mp lenses, two 1.31 mp CMOS sensors, and 1280x800 LED white light raster. The 3D scanner consisted of a downward-looking projector and two cameras at a fixed orientation with respect to the projector. The projector projects a series of black and white patterns onto the scan surface. When light projects onto the object’s surface, the patterns become distorted. Two cameras capture these images and calculate the distance from each point in the field of view using the triangulation system (Fig. 8.4b).

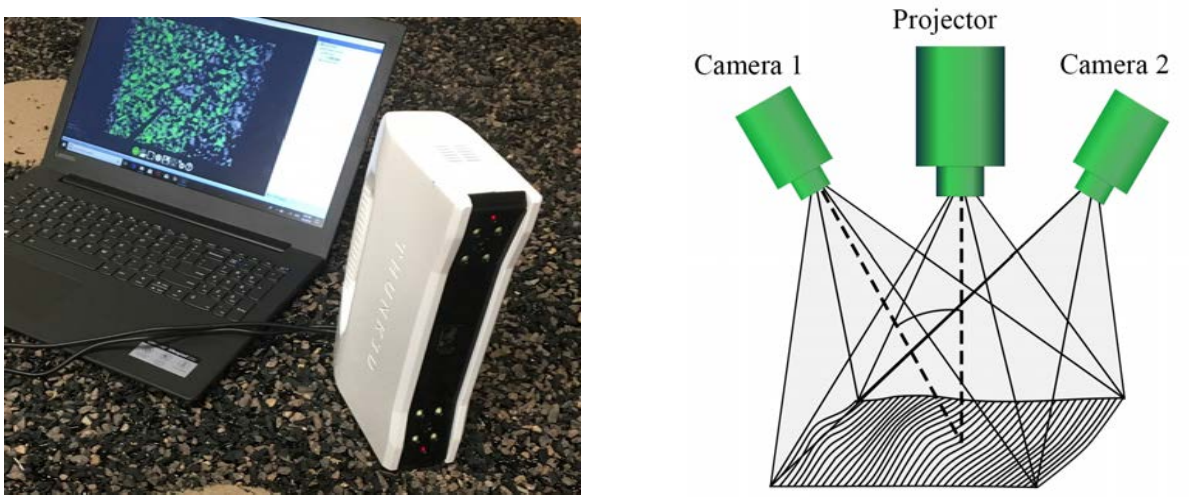

(a) (b)

Fig. 8.3 – (a) Handhold portable 3D scanner, and (b) basic setup of a structured light triangular system.

Having the 3D surface of chip seal specimens, the macrotexture was assessed using Digital Surf MountainsMap Expert Version 8 surface analysis software [92]. Using MountainsMap, a special analysis was conducted in accordance with BS EN ISO 25178-2 [94]. Some post-processing operations such as rotating, leveling, and extracting the area of interest, i.e., the snowplowing path, were conducted on each surface. Fig. 8.4a shows an example chip seal 3D surface in MountainsMap software. The topographic pseudo-color view of the surface in Fig. 8.4a simply shows the difference in the texture of different spots.

The bearing area curve, also known as the Abbott-Firestone curve, which describes the surface texture was plotted for the surfaces. The Abbott curve mathematically represents the cumulative probability density function of the surface profile's height and can be calculated by integrating the profile trace. Fig. 8.4b shows the distribution of heights for the wheel path area of the example chip seal surface shown in Fig. 8.4a. The bars indicate the percentage of surface area at heights within the range of bins (in this case bins of width 0.55 mm between 0 mm and 10.98

mm), and the superimposed line shows the cumulative height distribution. The curve is called the Abbott-Firestone curve, which can be used to calculate two distinct parameters, as shown in Fig. 8.4c. V_m indicates the volume of material on the surface at various heights the highest peak to the lowest point on the selected area. V_v is the volume of voids on the surface not occupied by the material on the given area. The value of V_m in mm^3/mm^2 would indicate that a layer of material with V_m mm thickness over the measured area would account for all the material from the highest peak to the lowest point in the given area. Therefore, V_m is actually representing the mean texture depth (MTD) of material in the selected area. In this study, V_m of the snowplow path was measured to evaluate the aggregate loss, i.e., texture loss, due to the snowplowing action.

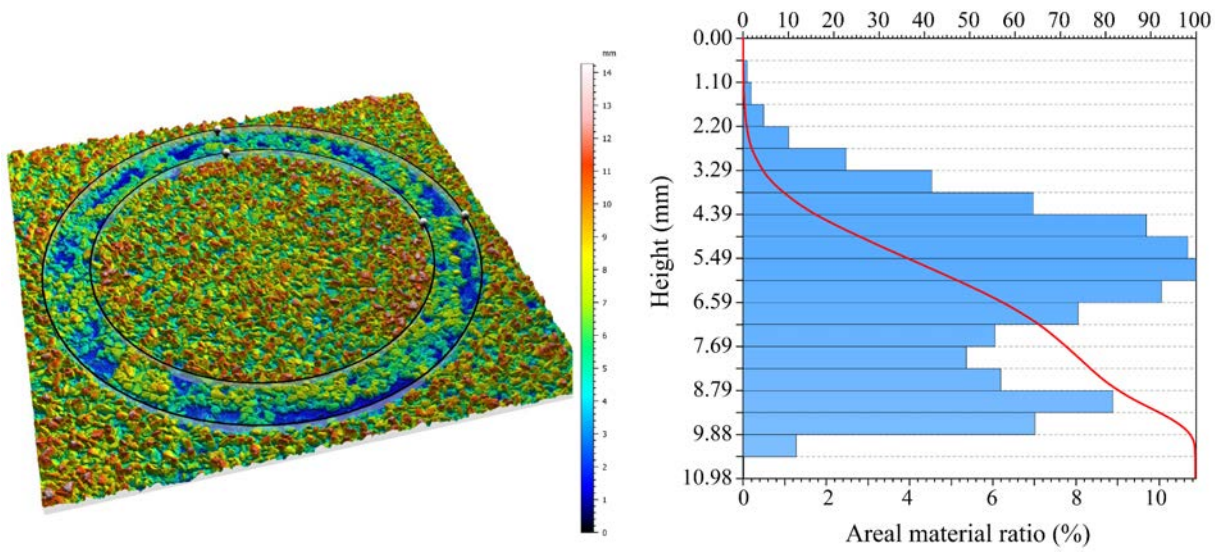

(a) (b)

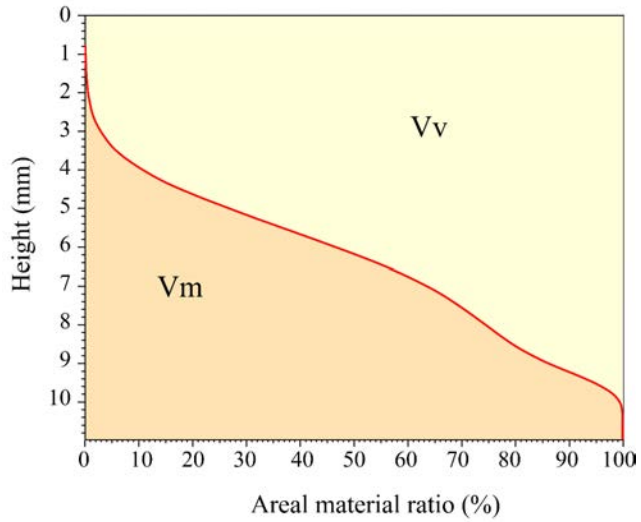

(c)

Fig. 8.4 – 3D surface data from MountainsMap software (a) example chip seal 3D surface, (b) height distribution and Abbott-Firestone curve, and (c) Abbott-Firestone curve and volumetric parameters.

8.3. Snowplowing Test Results

Fig. 8.5 shows the real view along with the 3D scanned surface of chip seal specimens after experiencing three and eight applications of the snowplow with a cutting angle of 25 degrees. Visional inspection after eight snowplow applications showed that the specimen with 100% crumb rubber aggregate experienced noticeably less aggregate loss due to snowplowing action compared to the other three specimens with 50%, 25%, and 0% crumb rubber.

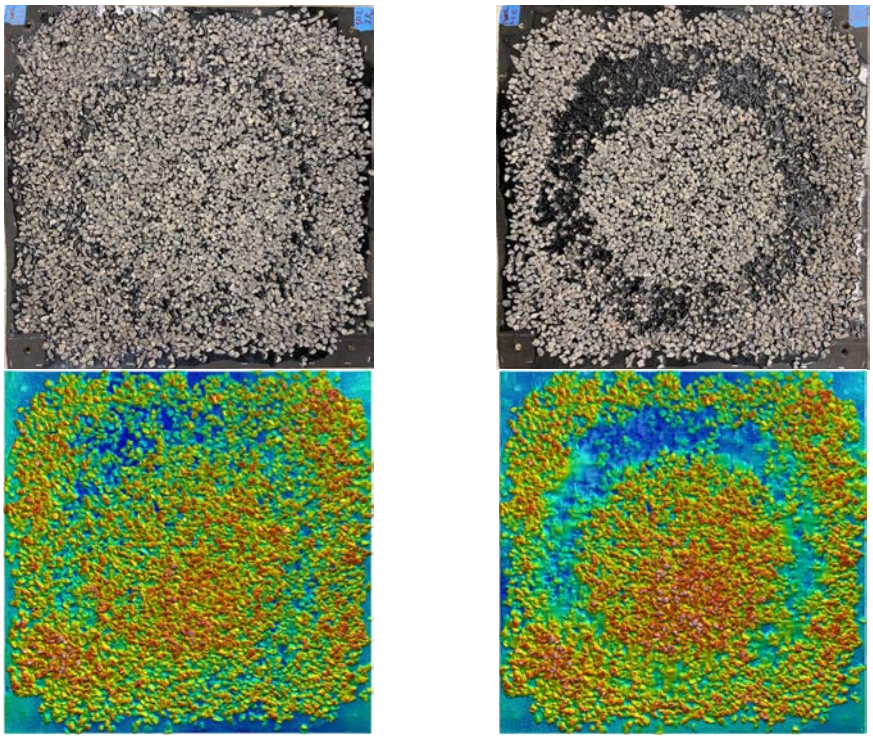

After 3 snowplow applications After 8 snowplow applications

(a) 00R specimen

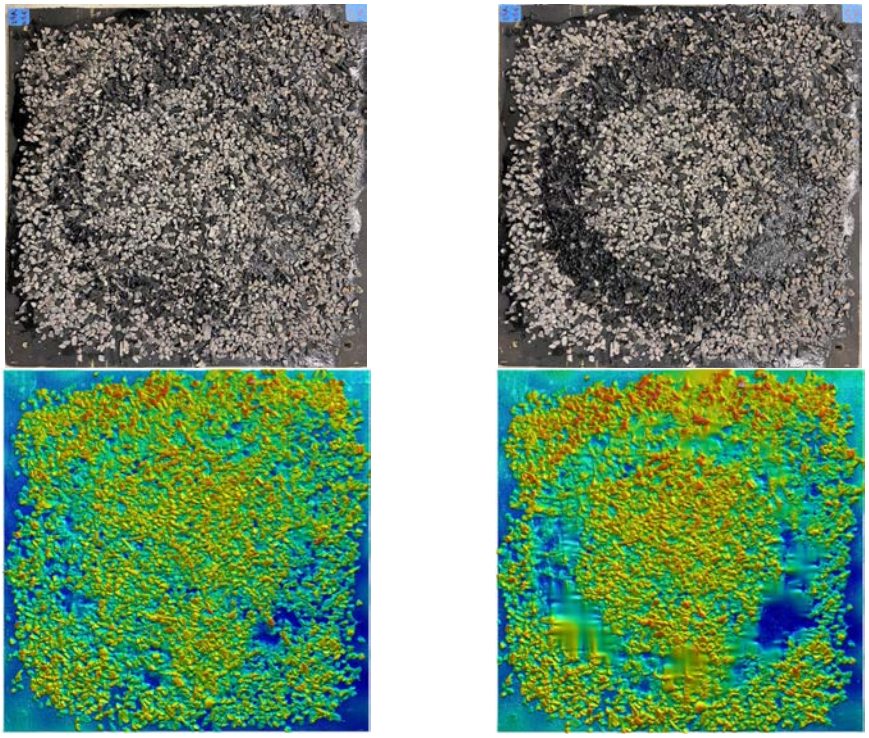

After 3 snowplow applications After 8 snowplow applications

(b) 25R specimen

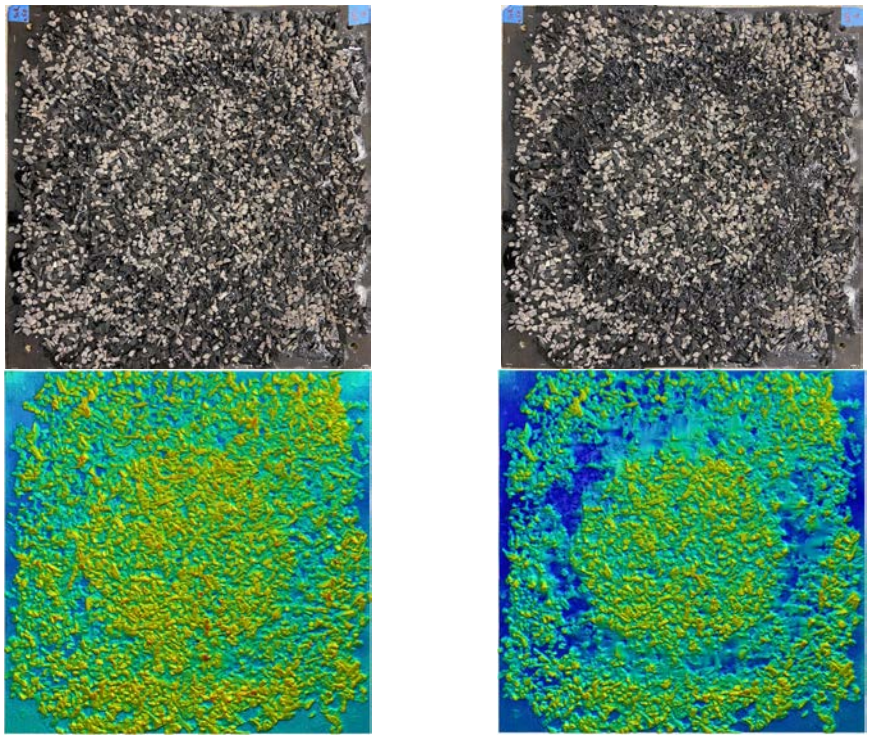

After 3 snowplow applications After 8 snowplow applications

(c) 50R specimen

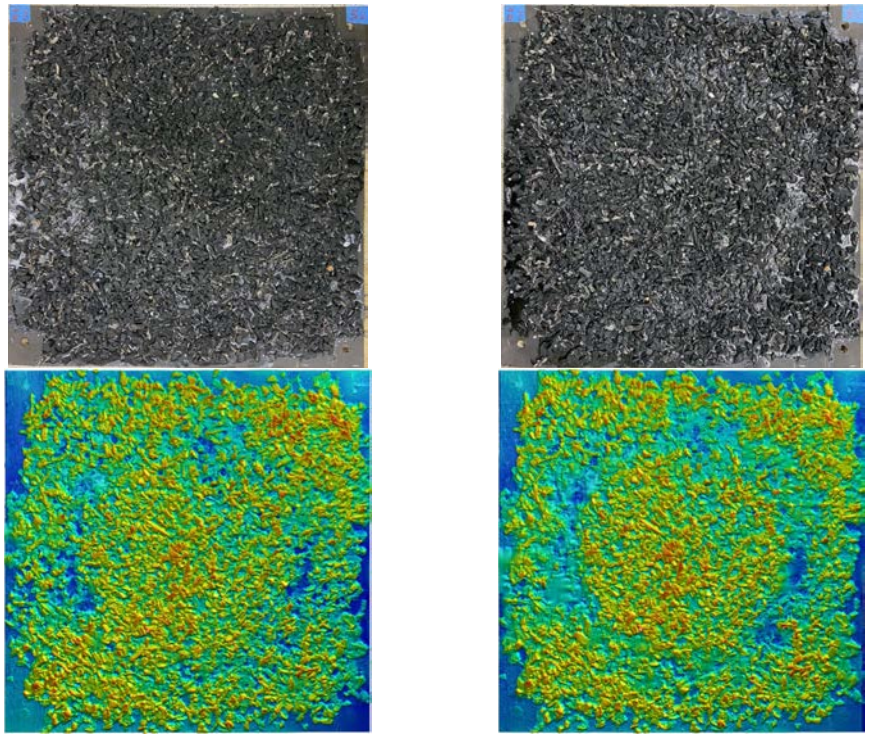

After 3 snowplow applications After 8 snowplow applications

(d) 100R specimen

Fig. 8.5 – Chip seal specimens after the snowplowing test.

Fig. 8.6 shows the Abbott curves for snowplow test specimens after eight snowplow applications. Abbott curves for other cases are provided in Appendix F. Using Abbott curves, the V_m value was calculated for each specimen and reported in Fig. 8.7. It should be noted that the initial V_m for specimens were calculated based on the central area of each specimen.

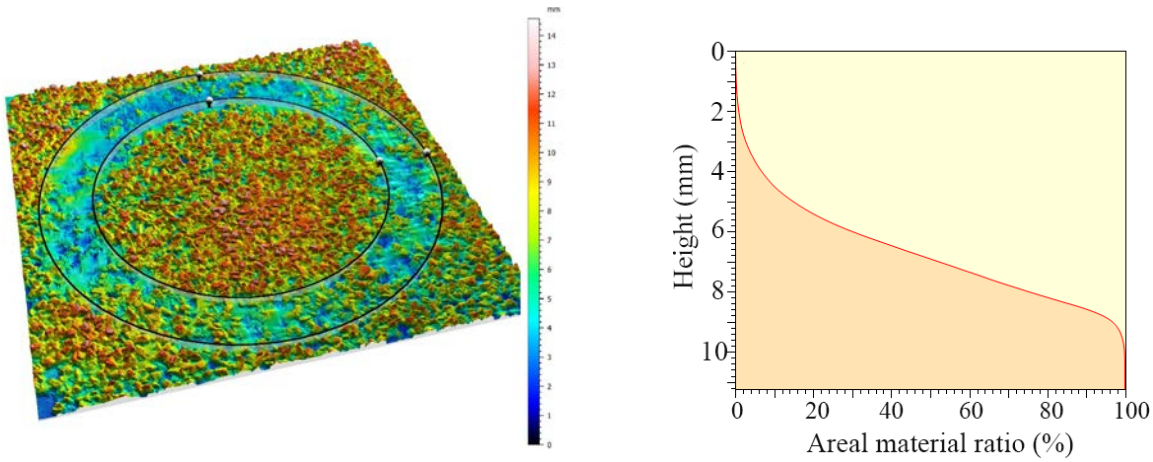

(a) 00R

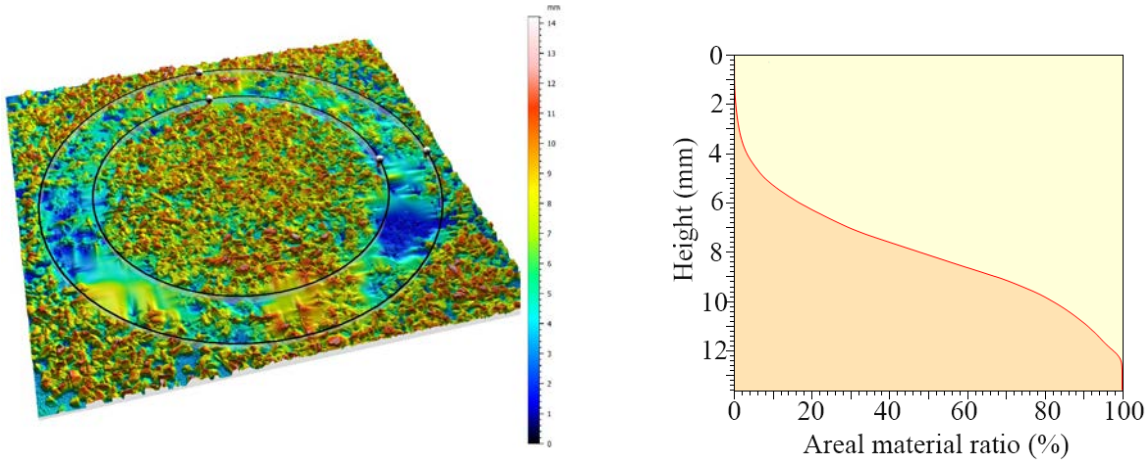

(b) 25R

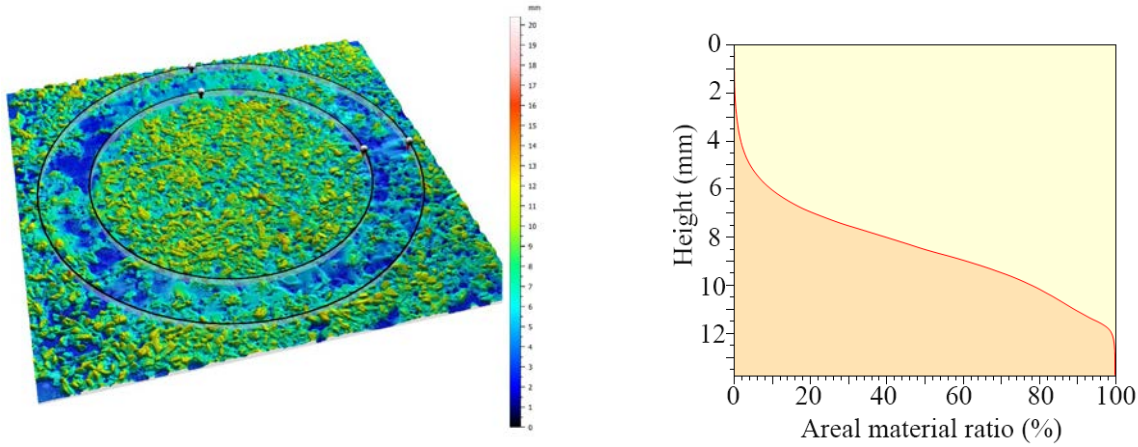

(c) 50R

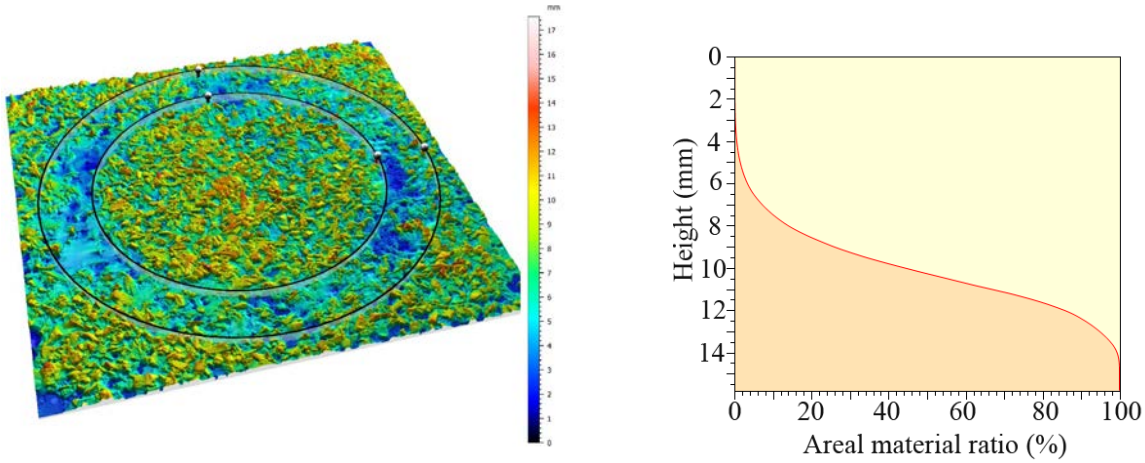

(d) 100R

Fig. 8.6 – 3D scanned surface and Abbott curve of the snowplow path for test specimens after eight snowplow applications.

Fig. 8.7 shows the V_m values versus the number of snowplow applications for different specimens. As shown in Fig. 8.7, initially, all the specimens had almost the same V_m of about 7.5 mm^3/mm^2. After that, when applying snowplowing action, the specimens experienced aggregate loss. This aggregate loss increased with increasing the number of snowplow applications. However, different specimens experienced different amounts of aggregate loss.

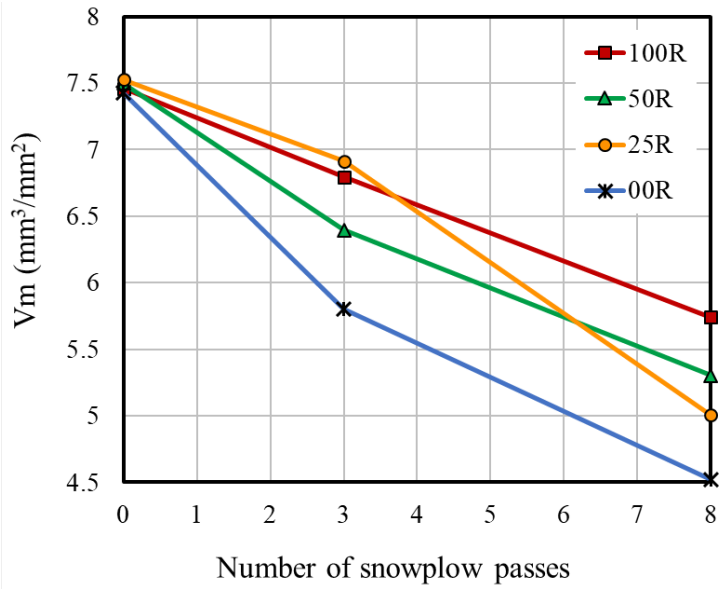

Fig. 8.7 – V_m of snowplow path versus the number of snowplow applications.

Fig. 8.8 presents the V_m loss percentage for different specimens after three and eight snowplow applications.

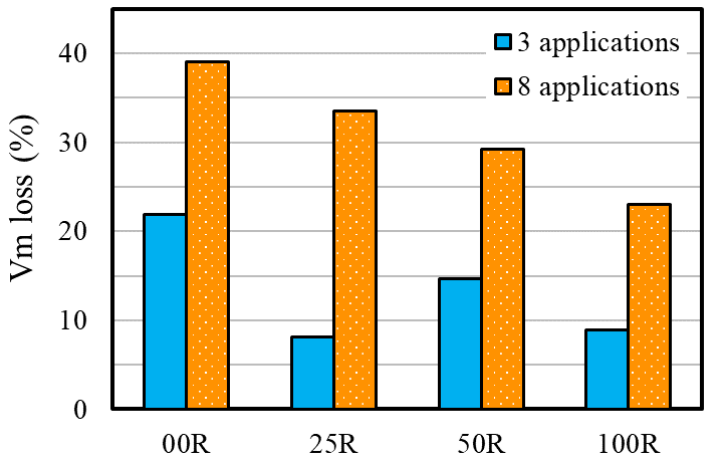

Fig. 8.8 – V_m loss percentage for different specimens after different snowplow applications.

From Fig. 8.7 and 8.8, it can be noticed that the 100R specimen with 100% crumb rubber aggregate experienced the least aggregate loss with 1.7 mm^3/mm^2 equal to 23% V_m loss, after eight snowplow applications. The 00R specimen with 100% trap rock and zero percent crumb rubber

experienced the most aggregate loss with 2.9 mm^3/mm^2 equal to 39% V_m loss, after eight snowplow applications. Specimens with 50% and 25% crumb rubber content were also matching this trend of aggregate loss with 2.2 and 2.5 mm^3/mm^2 equal to 29% and 33% V_m loss, respectively. Therefore, with increasing the crumb rubber content, the specimens experienced less texture loss under snowplowing action. Comparing the V_m loss, indicates that the 00R, 25R, and 50R specimens respectively experienced 1.7, 1.5, and 1.3 times more texture loss compared to the 100R specimens.

It is worth noting that the better performance of the crumb rubber particles is despite the fact that the crumb rubber particles used in this experimental program had a considerably higher flakiness index of 46 compering to trap rock aggregates with a flakiness index of 31. Higher flakiness will increase the risk of aggregate loss due to snowplowing action in non-traffic areas of chip seal (Fig.8.1b) [60, 61].

This performance can be related to the natural characteristics of the crumb rubber particles. Rubber has properties such as high elasticity, high damping, and large elongation capacity, which are in direct contrast with the properties of natural aggregate. Rubber possesses the dual function of springing and damping. Rubber particles have high hysteresis, i.e., energy loss or damping, and do not completely transmit the load imposed by the snowplow blade to their bond with the binder, whereas hard materials like natural aggregates do not show hysteresis and will transmit the impact load from the snowplow blade to their bond with the binder, leading to aggregate dislodging.

Snowplowing action with a higher cutting angle was also tried in this study. However, with higher cutting angles, the snowplow blade was stopped due to the interaction between the snowplow blade and surface texture, and the SWTS motor was not able to provide enough torque for the snowplow to move on the chip seal specimens. It can be concluded from this observation

that using a higher cutting angle will impose a higher load on the chip seal surface, which will lead to more aggregate loss and surface damage. As the previous research has also shown, the power required for plowing snow will increase with an increase in the snowplow cutting angle, as shown in Fig. 8.9 [107]. Therefore, using a low cutting angle is recommended on chip seal surfaces.

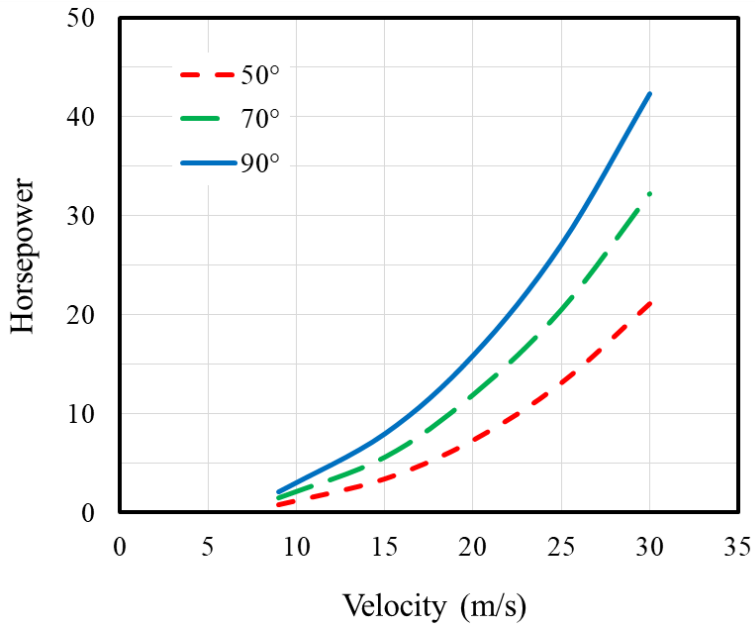

Fig. 8.9 – Horsepower consumed for snowplowing versus snowplow velocity for various cutting angles. Reproduced from [107].

8.4. Conclusions

In this chapter, the performance of the conventional and rubberized chip seal was evaluated under snowplowing action. Chip seal specimens with different crumb rubber content of 0%, 25%, 50%, and 100% were constructed and tested. The test results showed a better performance for the chip seal specimen with crumb rubber as aggregate. The amount of aggregate loss reduced considerably with increasing the rubber content in chip seal. Although crumb rubber particles used in this study had a higher flakiness index compared to natural aggregate, the specimens with 0%,

25%, and 50% crumb rubber content, respectively experienced 1.7, 1.5, and 1.3 times more texture loss compared to the specimen with 100% crumb rubber aggregate after eight snowplow applications.

Also, snowplowing with a higher cutting angle, i.e., the angle between the snowplow blade and pavement surface, required a higher power, which will lead to more damage to the surface. Therefore, using a low cutting angle was recommended for snowplowing the chip seal surfaces.

Chapter 9: Effect of Freezing and Thawing Cycles with Chemical Deicing on Conventional and Rubberized Chip Seal

9.1. Introduction

In cold regions, harsh temperature fluctuations cause freezing and thawing cycles that influence the performance of pavements. Surveys conducted in the US and Canada showed that the cold climate considerations, including freezing cycles, snowplowing, etc., are the major factors that determine the life span of the chip seal pavements [1]. In addition, in order to provide security and mobility of traffic with an ice-free surface, pavements are exposed to deicing salts such as calcium chloride during the winter season. This is also the case in coastal roads exposed to salty seawater due to tides and/or storms. Accumulated salt on the pavement surface may lead to erosion and crystal formation, which can damage the pavement material. Also, the existence of deicing agents has proven to intensify the freeze-thaw damage on asphalt concrete [81, 82], and it may also affect the chip seal surface. Therefore, freeze-thaw cycles and the use of deicing agents may have a significant effect on the performance of chip seal. This chapter studies the effect of freeze-thaw cycles and deicing salt on the performance of chip seal pavements composed of different types of mineral aggregate and crumb rubber particles.

9.2. Experimental Program

Chip seal specimens with different rubber content combined with two different mineral aggregate types i.e., trap rock and creek gravel were tested in two stages. At the first stage, chip seal specimens were tested for 50 consecutive freezing and thawing cycles in the presence of a

solution of calcium chloride and water as the most common deicing chemical used on the roads. This test was conducted following ACI C672 [108] entitled "Standard Test Method for Scaling Resistance of Concrete Surfaces Exposed to Deicing Chemicals." However, the surface evaluation according to the standard is by visual examination; for chip seal surfaces, the results were evaluated with the volumetric aggregate loss after each cycle. This test provides an indication for the durability of different chip seal specimens under freezing and thawing cycles only in the absence of any traffic load.

In the second stage, test specimens that had gone through 50 cycles of freezing and thawing were tested under simulated traffic load using the small-wheel traffic simulation machine (SWTS), and the aggregate retention performance of chip seal samples with different aggregate types was compared.

9.2.1. Test Specimens

A total of 7 chip seal specimens of 1 ft by 1 ft with an area of 144 in^2 were prepared for this study, as reported in Chapter 4. This size of specimens was selected due to two main reasons. First of all, according to ACI C672, the standard test for concrete surfaces exposed to deicing chemicals, the surface area of the test specimens should be at least 72 in^2. Second, a size should have been selected for specimens that could fit in the SWTS test machine for the second stage of this experimental program. The SWTS was designed to simulate traffic on 2 ft by 2 ft providing 576 in^2 area chip seal specimens. However, using such a large specimen for the first stage of this experimental program was not practical, since it would occupy a lot of space in the environmental chamber of freezing and thawing action. Also, controlled monitoring of the aggregate loss over a large area would be difficult. Moreover, a 576 in^2 area would need a huge amount of deicing solution, which would make the testing process inappropriate. Due to all these reasons, the authors

decided to make a 1 ft by 1 ft specimen for this test, which could be tested properly in the first stage and also in SWTS as a group of four.

Different aggregate types and contents were used for test specimens as shown in Fig. 9.1. Crumb rubber, trap rock, and creek gravel were the three aggregate types that were used in this study. Aggregate properties and gradation are reported in Chapter 4 of this report. The same volume of aggregate was used for all specimens with the same amount of binder. The binder used for this study was CRS2P asphalt emulsion with properties reported in Chapter 4 of this report. A 0.25 gal/yd^2 binder application rate was used for test specimens. Since this is a comparative study to evaluate the performance of different aggregate types, the binder application rate was identical for all specimens. Specimens used in this study are shown in Table 9.1 and Fig. 9.2. All the test specimens were made at the same time and kept at room temperature for curing for more than 10 days to make sure that the curing time will not affect the test results. The specimens were swept before testing to remove the loose particles.

Fig 9.1 – Different aggregate combinations used.

Table 9.1 – Deicing Test Specimens

Specimen ID	Binder rate (gal/yd^2)	Percentage of Aggregate		
		Trap rock	Creek gravel	Crumb rubber
R100	0.25	-	-	100
T100		100	-	-
T50		50	-	50
T25		25	-	75
C100		-	100	-
C50		-	50	50
C25		-	25	75

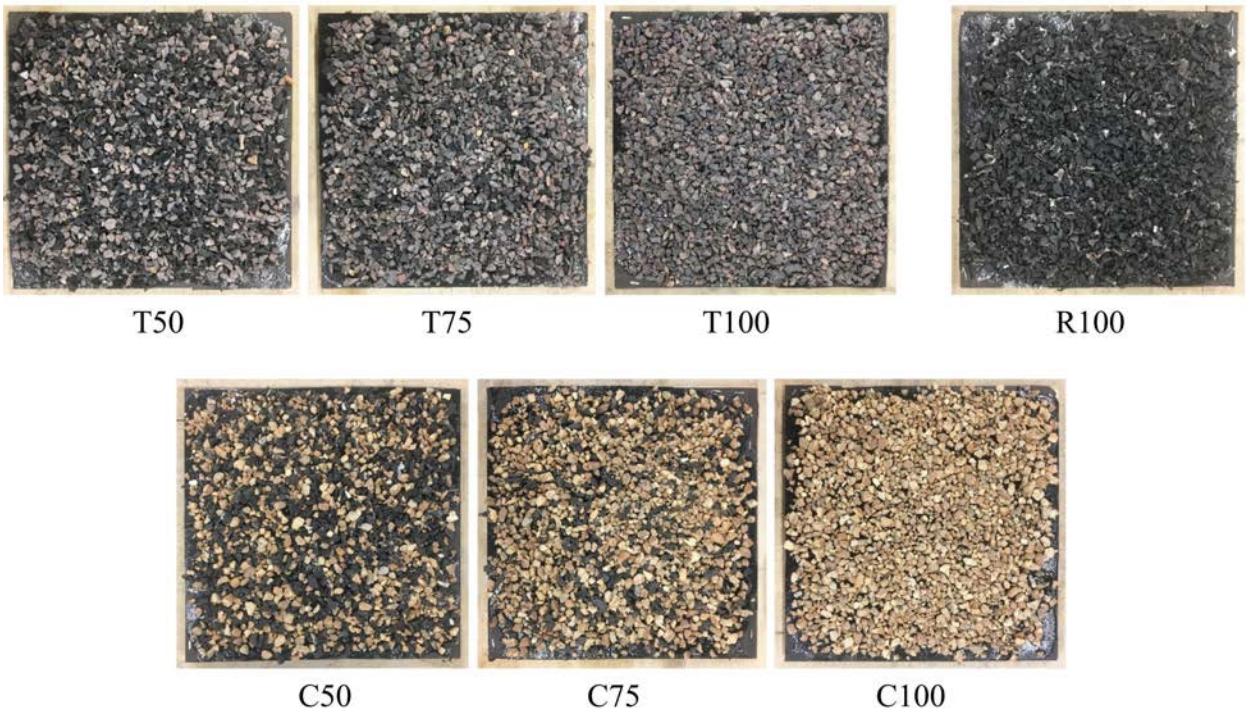

Fig. 9.2 – Freezing and thawing test specimens.

9.2.2. Freeze-Thaw Test

Since there is no standard test to be used for chip seal specimens under freezing and thawing cycles in the presence of deicing chemicals, the specifications and test method of ASTM

C672 [108] was adopted and used for this task. ASTM C672 is a standard test method for scaling resistance of concrete surfaces exposed to deicing chemicals. A total of seven chip seal test specimens, as described in the previous section, was used for this test. A dike was placed on the sides of each test specimen in order to keep the solution of deicing and water over the specimens during the freeze-thaw cycles (Fig. 9.3). According to ASTM C672, a solution of calcium chloride and water with a concentration of 4% (5.34 oz/gal) was used with an average thickness of 1/4 in. over the surface of specimens. Freezing and thawing cycles were applied in accordance with ASTM C672. Specimens were placed in an environmental chamber simulating 17 hours of freezing temperature followed by 7 hours of 75° F and relative humidity of 50% (Fig. 9.4).

Fig. 9.3 – Dike made around the specimens for ponding the deicing solution.

At the end of every 5 cycles of freezing-and-thawing, the specimens were taken out of the chamber, the surface was flushed off thoroughly, and the solution was replaced. However, ASTM C672 has proposed a visual examination of the concrete surface for the surface resistance evaluation after 5, 10, 15, 25, and 50 cycles. However, in this study of chip seal specimens, the

volumetric aggregate loss was measured at the end of every 5 cycles. Loose aggregate was collected after flushing off the surface on a sieve. The specimens were examined with a hand passing over the surface to make sure no loose aggregate remained. Collected aggregates were weighed according to the type, i.e., trap rock, creek gravel, or crumb rubber (Fig. 9.4). Since the specific gravity of used aggregates was different, the weight of each aggregate type was then converted to volume so the results of aggregate loss could be compared (Table 4.1). The test was continued for 50 cycles.

(a)

(b)

(c) (d) (e)

Fig. 9.4 – Freeze-thaw test procedure (a) test specimens inside the environmental chamber, (b) surface covered with 1/4 inch of the deicing solution, (c) flushing off the surface, (d) hand examination for loose aggregate, and (e) weighing the aggregate according to the type.

9.2.3. Small-Wheel Traffic Simulation (SWTS) Test

A piece of laboratory equipment, namely the small-wheel traffic simulation machine (SWTS) was developed as described in Chapter 3 of this report (Fig. 9.5). SWTS was used to apply controlled traffic in terms of number, load, and speed on chip seal specimens. SWTS consisted of three main parts of driving system, wheel assembly, and specimen holder. The driving system was capable of providing variable speeds. The wheel assembly consisted of three pneumatic tires with 8 inches diameter and 2-1/2 inches width providing a wheel tracking diameter of 15-3/4 inches center to center. It was also possible to provide different pressures on the chip seal surface through the tires by adding weights on the wheel assembly. The specimen holder was designed to hold a 2ft by 2 ft specimen. In this study, SWTS was used to assess the aggregate retention behavior of chip seal samples after experiencing cycles of freezing and thawing under traffic load.

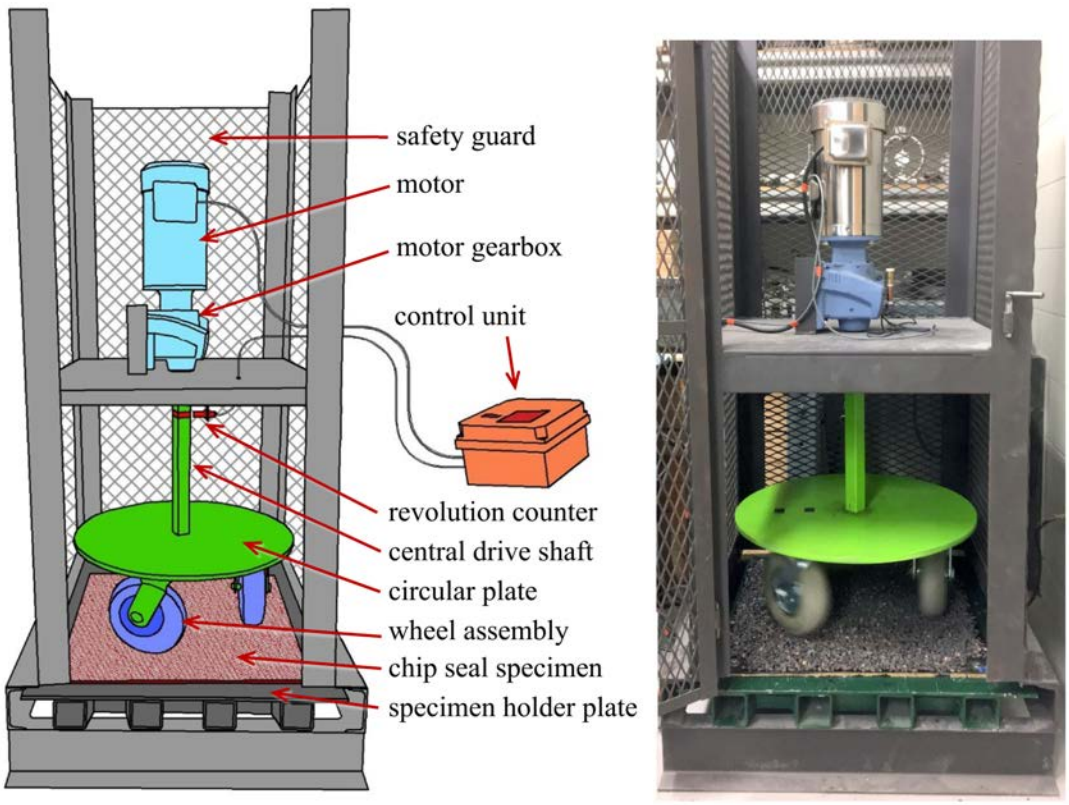

Fig. 9.5 – SWTS test machine.

Chip seal specimens that have experienced 50 cycles of freezing and thawing were flushed off thoroughly and placed at room temperature for 15 days. Afterward, the specimens were tested using SWTS for 5,000 wheel passes at traffic speed of 120 wheel applications per minute (wpm), which corresponds to dynamic loading of 2.00 Hz with 87.25 lbs applied load, correspondsing to 14.12 psi under each tire at the ambient temperature of 80±2˚ F.

In order to test the 1 ft by 1 ft specimens in SWTS, the specimens were put in sets of four as shown in Fig. 9.6, since the standard specimen size for SWTS was 2 ft by 2 ft. The texture variation of the specimens due to the SWTS test was assessed using a 3D scanning technique discussed in the next section. The results were compared for specimens with different aggregate types.

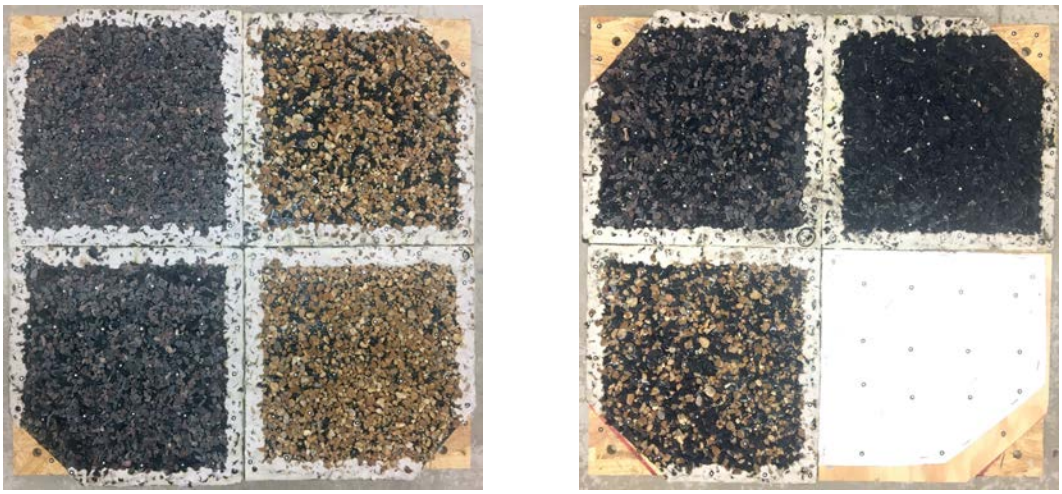

Fig. 9.6 – SWTS test specimens made up of specimens subjected to 50 cycles of freezing and thawing with deicing chemicals before the SWTS test.

9.2.4. Macrotexture Evaluation

A new non-contact measurement technique using a 3D scanner was used to monitor the texture variation and aggregate loss during the snowplowing test. The reason for using this technique is first of all not being able to properly use the common method of sand patch [90] for macrotexture measurement due to the circular snowplow path with limited width. The 3D surface scanning technique will also provide more accurate macrotexture measurements [42, 46, 91].

The scanner used in this project was a two-camera structured-light 3D scanner, namely Thunk3D Fisher (Fig. 9.7a). The manufacturer declared accuracy of 0.04mm to 0.1mm having a scan speed of 1,200,00 points per second and a resolution of 0.2 mm with two 12mm/5mp lenses, two 1.31 mp CMOS sensors, and a 1280x800 LED white light raster. The 3D scanner consisted of a downward-looking projector and two cameras at a fixed orientation with respect to the projector. The projector projects a series of black and white patterns onto the scan surface. When light projects onto the object's surface, the patterns become distorted. Two cameras capture these

images and calculate the distance from each point in the field of view using the triangulation system (Fig. 9.7b).

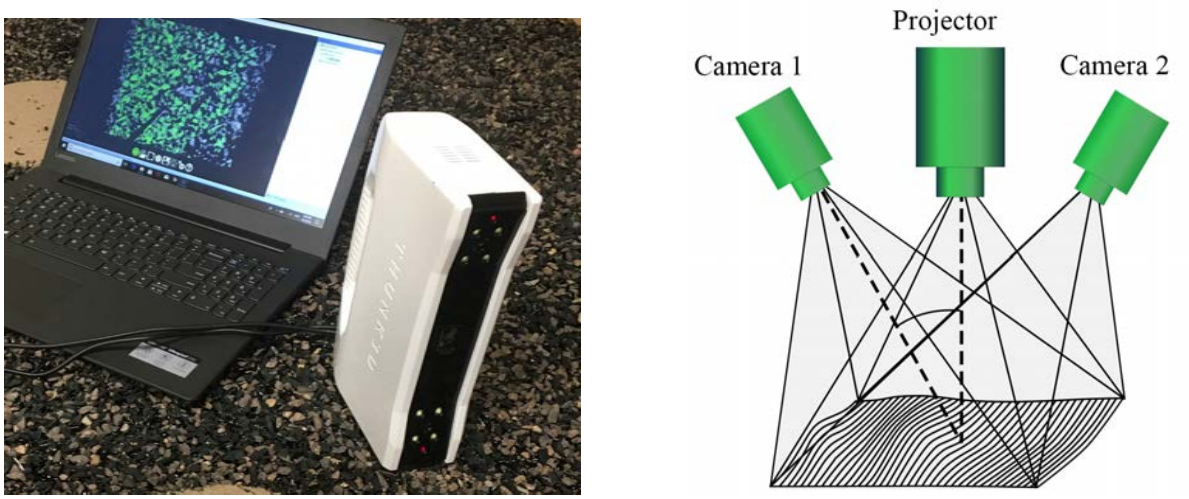

(a) (b)

Fig. 9.7 – (a) Handhold portable 3D scanner, (b) basic setup of a structured light triangular system.

Having the 3D surface of chip seal specimens, the macrotexture was assessed using Digital Surf MountainsMap Expert Version 8 surface analysis software [92]. Using MountainsMap, a special analysis was conducted in accordance with BS EN ISO 25178-2 [94]. Some post-processing operations such as rotating, leveling and extracting the area of interest, i.e., snowplowing path, were conducted on each surface. Fig. 9.8a shows an example of a chip seal 3D surface in MountainsMap software. The topographic pseudo-color view of the surface in Fig. 9.8a simply shows the difference in the texture of different spots.

The bearing area curve, also known as the Abbott-Firestone curve, which describes the surface texture, was plotted for the surfaces. The Abbott curve mathematically represents the cumulative probability density function of the surface profile's height and can be calculated by integrating the profile trace. Fig. 9.8b shows the distribution of heights for the wheel path area of

the example chip seal surface shown in Fig. 9.8a. The bars indicate the percentage of surface area at heights within the range of bins (in this case bins of width 0.55 mm between 0 mm and 10.98 mm), and the superimposed line shows the cumulative height distribution. The curve can be used to calculate two distinct parameters, as shown in Fig. 9.8c. V_m indicates the volume of material on the surface at various heights, the highest peak to the lowest point on the selected area. V_v is the volume of voids on the surface not occupied by the material on the given area. The value of V_m in mm^3/mm^2 would indicate that a layer of material with V_m mm thickness over the measured area would account for all the material from the highest peak to the lowest point in the given area. Therefore, V_m actually represents the mean texture depth (MTD) of material in the selected area. In this study, V_m of the wheel path and outside the wheel path was measured to compare the aggregate loss, i.e., texture loss, due to the simulated traffic loading in the SWTS test.

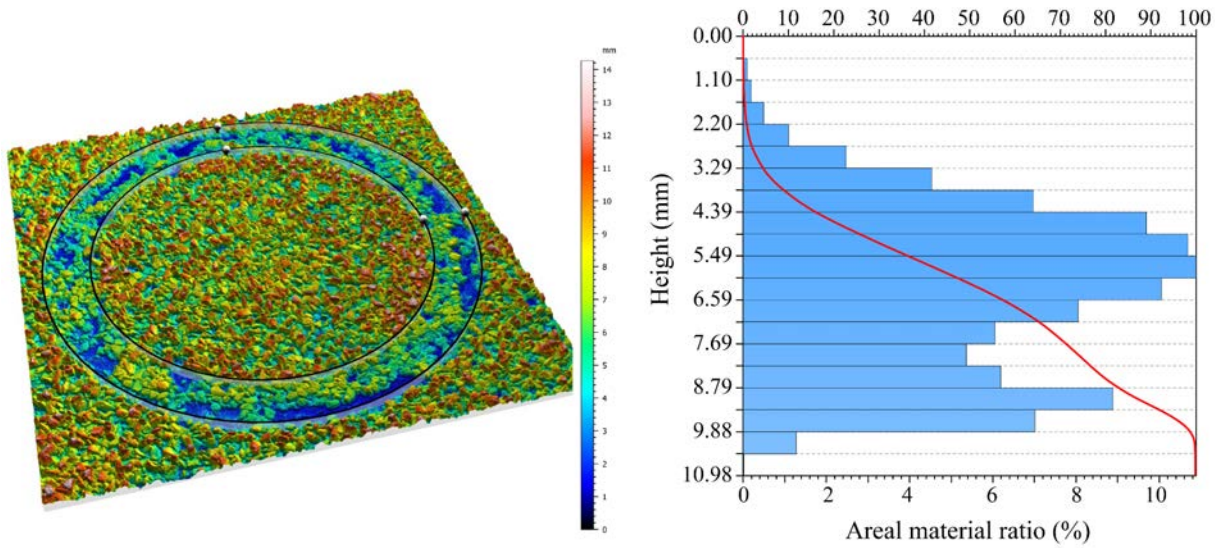

(a) (b)

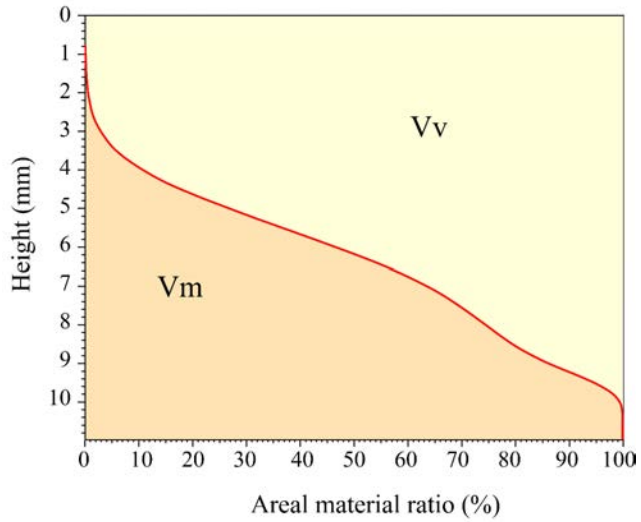

(c)

Fig. 9.8 – 3D surface data from MountainsMap software (a) example chip seal 3D surface, (b) height distribution and Abbott-Firestone curve, and (c) Abbott-Firestone curve and volumetric parameters.

9.3. Test Results

9.3.1. Freeze-Thaw Test

Fig. 9.9 shows the cumulative volume of total aggregate loss versus the number of freezing and thawing cycles for different test specimens. Results indicated that freezing and thawing cycles affected different aggregate types and combinations differently. The T100 specimen with 100% trap rock aggregate showed the best resistance to freezing and thawing cycles with only 0.53 in^3 aggregate loss at the end of 50 cycles, while C100 specimens with 100% creek gravel had 1.77 in^3 aggregate loss at the end of 50 cycles, which was 3.4 times greater than that of T100. The higher aggregate loss for creek gravel specimens compared to trap rock can be related to the creek gravel aggregate's susceptibility to freeze-thaw cycles, since the lost particles from creek gravel specimens during the freeze-thaw test were mainly the result of aggregate crush (Fig. 9.10). Also, the soundness test results, which indicate the resistance of the aggregates to disintegration by

freezing and thawing cycles, comply with this performance. According to the soundness test results presented in Chapter 2 of this report, creek gravel aggregate had about two times more weight loss compared to trap rock (Fig. 2.3).

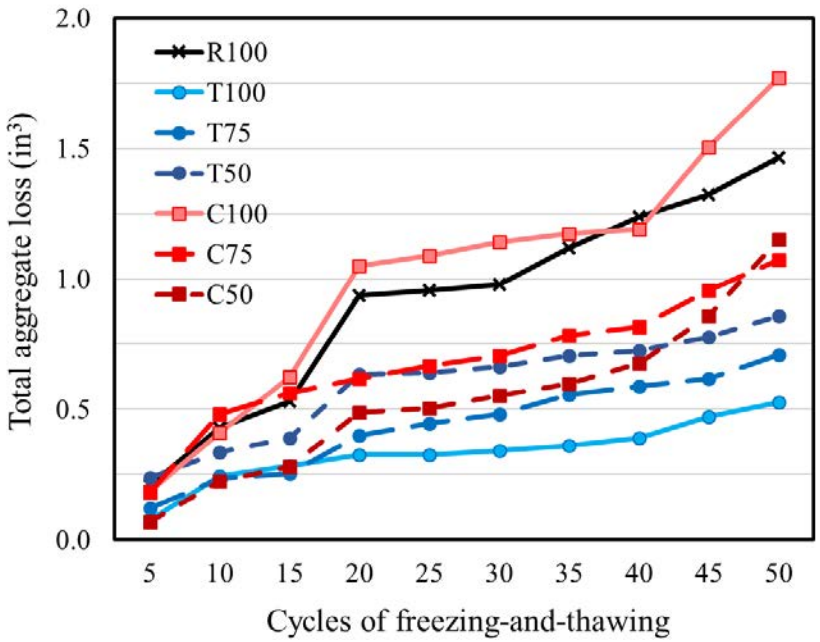

Fig. 9.9 – Freeze-thaw test results

(a)

(b)

Fig. 9.10 – Crushed aggregates (circled) after the freeze-thaw test. (a) creek gravel, and (b) trap rock.

Fig. 9.11 shows the cumulative volume of total aggregate loss at the end of 50 cycles of freezing and thawing for different test specimens. Results showed an improvement of the resistance to freezing and thawing for creek gravel chip seal by adding rubber particles, since the total aggregate loss decreased in creek gravel specimens by 35% by increasing the rubber content from 0 to 50%. However, the total aggregate loss increased in trap rock specimens by about 60% by increasing the rubber content from 0 to 50%. Yet, the aggregate loss for T50 is still 20% less than the best performance of creek gravel specimens observed for C75.

In the case of the R100 specimen with 100% crumb rubber particles, the aggregate loss was 1.47 in^3, which was 2.8 times the aggregate loss for T100. Crumb rubber particles did not experience any crushing in the freeze-thaw test. Soundness test results reported in Chapter 2 of this report also indicated 0% weight loss for crumb rubber. Therefore, the aggregate loss in the freeze-thaw test should be due to the weakened bond between the emulsion and crumb rubber particles during freezing and thawing.

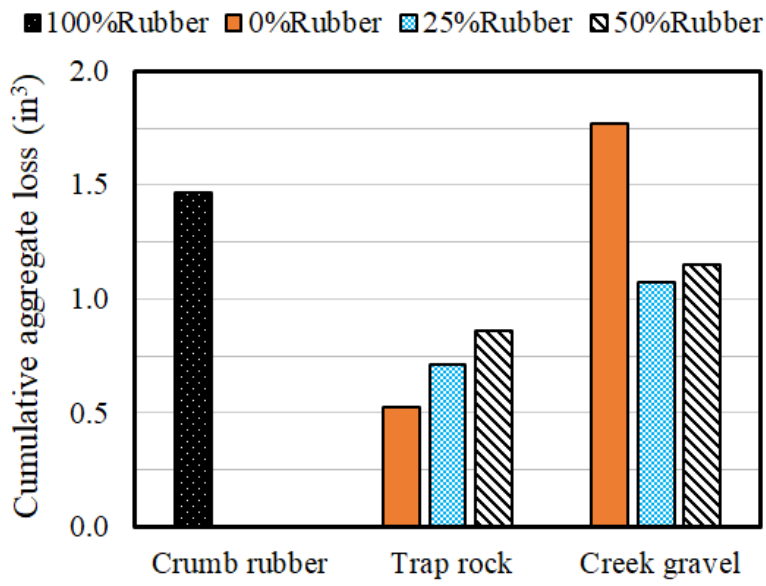

Fig. 9.11 – Cumulative aggregate loss after 50 cycles of freezing and thawing.

Fig. 9.12 shows the normalized cumulative volume of rubber and natural aggregate loss for each specimen. The normalized volume is obtained by dividing the loss volume by the original volumetric percentage of the aggregate used to make the specimen. For instance, for the T75 specimen with 25% crumb rubber and 75% trap rock, the volume of lost crumb rubber was divided by 0.25 and the volume of lost trap rock was divided by 0.75. Therefore, Fig. 9.12 presents a comparable indication of the loss for each type of aggregate used in specimens with mixed aggregates, i.e., T50, T75, C50, and C75. Results showed relatively more crumb rubber loss rather than trap rock in trap rock specimens, i.e., T50 and T75. However, the loss of crumb rubber and trap rock was very close in the T50 specimen with 50% rubber content (Fig. 9.8b). In contrast, for creek gravel specimens relatively more creek gravel loss was experienced rather than crumb rubber. For instance, at the end of 50 cycles of freezing and thawing, T75 had 1.66 times more rubber loss than trap rock, while C75 had 2.52 times more creek gravel loss than crumb rubber. Also for T50, rubber loss was 1.32 times more than trap rock, while for C50, creek gravel loss was 2.06 times more than crumb rubber.

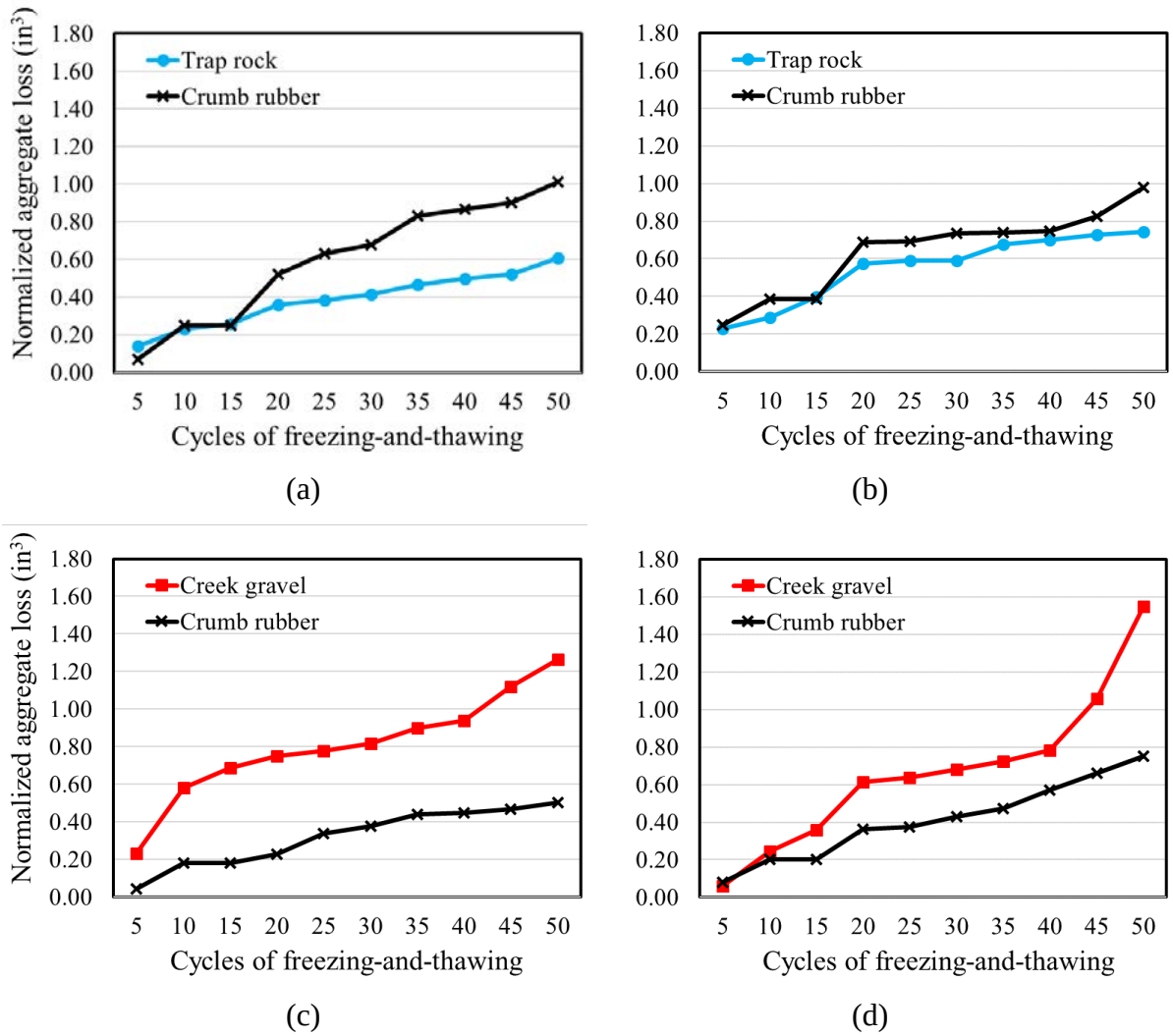

Fig. 9.12 – Normalized aggregate loss for (a) T75, (b) T50, (c) C75, and (d) C50 specimens.

9.3.2. SWTS Test

Fig. 9.13 shows the surface of the different chip seal samples after the SWTS test for 5,000 wheel applications. As mentioned earlier, the specimens were tested in SWTS after experiencing 50 cycles of freezing and thawing with deicing chemicals. As shown in Fig. 9.13(b), the specimens were 3D scanned and the volume of material (V_m) on the surface within the wheel path and outside the wheel path were measured for different specimens and reported in Table 9.2. 3D scanning

method and definitions of V_m was presented earlier in this chapter. It is worth reminding that V_m represents the mean texture depth (MTD) of the surface.

(a)

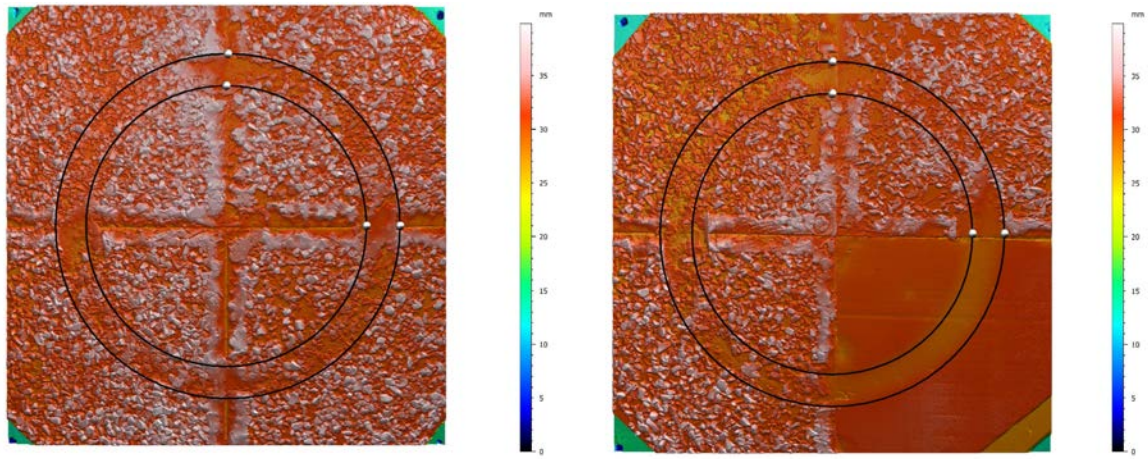

(b)

Fig. 9.13 – Specimens experienced 50 cycles of freezing and thawing with deicing chemicals after 5,000 wheel applications in the SWTS test (a) real view, and (b) 3D scanned surface.

Table 9.2 – SWTS Test Results from 3D Scanned Surface

Specimen	Vm (mm3/mm2)		Vm degradation (%)
	outside wheel path	on wheel path	
R100	4.31	3.69	14%
T100	4.54	4.13	9%
T75	5.55	4.21	24%
T50	5.35	4.46	17%
C100	4.66	3.60	23%
C75	5.55	4.81	13%
C50	4.88	4.05	17%

Fig. 9.14 compares the V_m degradation for different specimens in the SWTS test for 5,000 wheel applications. The results obtained for chip seal specimens under traffic load were similar to what the specimens experienced in the freeze-thaw test (Fig. 9.11). T100 experienced the least, and C100 experience a high amount of V_m degradation, i.e., texture loss. The texture loss increased by increasing the rubber content for trap rock specimens, while the texture loss decreased with increasing the rubber content for creek gravel specimens. The V_m degradation for R100, T100, and C100 specimens were 14%, 9%, and 23%. For trap rock specimens, with increasing the rubber content from 0 to 25%, the V_m degradation increased by 14%. Increasing the rubber content from 0 to 50% increased the V_m degradation by 8%. For creek gravel specimens, the opposite happened. With increasing the rubber content from 0 to 25%, the V_m degradation decreased by 10%. Increasing the rubber content from 0 to 50% decreased the V_m degradation by 6%.

Both freeze-thaw and SWTS test results showed that trap rock aggregates were less affected by freezing and thawing cycles and creek gravel aggregates were highly susceptible to freezing and thawing. The susceptibility of natural aggregates was mainly due to the crushing action that happened due to freezing and thawing. While crumb rubber did not experience any

crushing during the freeze-thaw test, the behavior should be due to the weakened bond between the emulsion and crumb rubber particles. Therefore, according to the results from both the freeze-thaw and SWTS tests, it can be concluded that crumb rubber is more susceptible to freezing and thawing than trap rock and creek gravel is more susceptible to freezing and thawing than crumb rubber. That's why by replacing creek gravel particles with crumb rubber, the performance was improved, and by replacing trap rock particles with crumb rubber, the performance was aggravated.

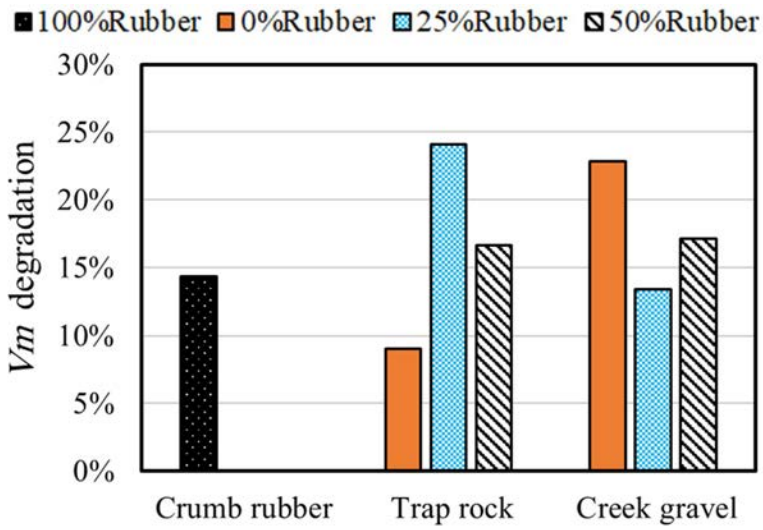

Fig. 9.14 – V_m degradation after 5,000 wheel applications in SWTS for different aggregate types and rubber content.

9.4. Conclusions

This task first studied the effect of 50 consecutive freezing and thawing cycles in the presence of deicing salt on the chip seal specimens composed of two different types of natural aggregate, i.e., trap rock and creek gravel, along with crumb rubber particles as synthetic aggregate. Afterward, a simulated traffic load was applied on the same chip seal specimens using a small-wheel traffic simulation machine (SWTS) to evaluate the durability of chip seal specimens which

have experienced 50 cycles of freezing and thawing. Based on the test results the following conclusions were derived:

- Trap rock aggregate performed significantly better than creek gravel and crumb rubber aggregate by about 3.4 and 2.8 times less volumetric aggregate loss, respectively, after 50 cycles of freezing and thawing.
- Replacing creek gravel by crumb rubber particles up to 50% improved the freeze-thaw resistance of chip seal specimens by 35%.
- After 50 cycles of freezing and thawing, the specimen with 100% rubber experienced the least macrotexture loss under simulated traffic loading with almost half of the texture loss experienced by trap rock and creek gravel specimens.
- After 50 cycles of freezing and thawing, due to simulated traffic load, macrotexture loss increased 8% by adding 50% crumb rubber to trap rock specimens and decreased 6% by adding 50% crumb rubber to creek gravel.
- It can be concluded from both the freeze-thaw test and SWTS test that adding crumb rubber to trap rock chip seal will aggravate the performance in terms of aggregate retention under freezing and thawing actions.
- It can be concluded from both the freeze-thaw test and SWTS test that adding crumb rubber to creek gravel chip seal will improve the performance in terms of aggregate retention under freezing and thawing actions.

Chapter 10: Field Implementation of Rubberized Chip Seal

10.1. Introduction

It was necessary to investigate the applicability and feasibility of the implementation and performance of rubberized chip seal in the field. In the beginning, this task evaluated the feasibility of implementing the rubberized chip seal in the field using conventional machinery and equipment. For this means two field sections in Rolla, Missouri, and Boonville, Missouri were surfaced with chip seal. In the second stage, the performance of rubberized chip seal with different percentages of rubber will be evaluated by comparing them with the conventional chip seal under the same volume of traffic during the same periods. The Rolla section was used for the means of the long-term performance evaluation, since it was implemented using various crumb rubber content from 0% to 100% in different parts on the same road, which makes it possible to compare the performance. The Boonville section was implemented using only 20% rubber content. The objective of the Boonville section implementation was to address the issues faced in the Rolla section in terms of the construction process only.

10.2. Road Location and Traffic Information

The field construction of two sections is reported in this study. The first is a 2000 ft two-lane test section constructed on Route CC, Rolla, Missouri (Fig. 10.1). The Rolla section was divided into five segments constructed using 0%, 25%, 50%, 75%, and 100% crumb rubber replacing trap rock aggregate by volume. Another 1000 ft two-lane road was paved with rubberized

chip seal on 2nd Street and Vine Street, Boonville, Missouri (Fig. 10.2). The Boonville section was constructed using 20% by volume crumb rubber and 80% by volume trap rock aggregate.

Fig. 10.1 – Location of the Rolla construction site.

Fig. 10.2 – Location of the Boonville construction site.

The average daily traffic on the Rolla section road according to the last MoDOT three-year cycle traffic volume map was 958 vehicle/day (Fig. 10.3). The effect of traffic was not taken into consideration when comparing the chip seal test segments since all the test segments would have the same traffic loads. The Boonville section selected roads are considered very low traffic roads with annual average traffic of fewer than 200 vehicles daily.

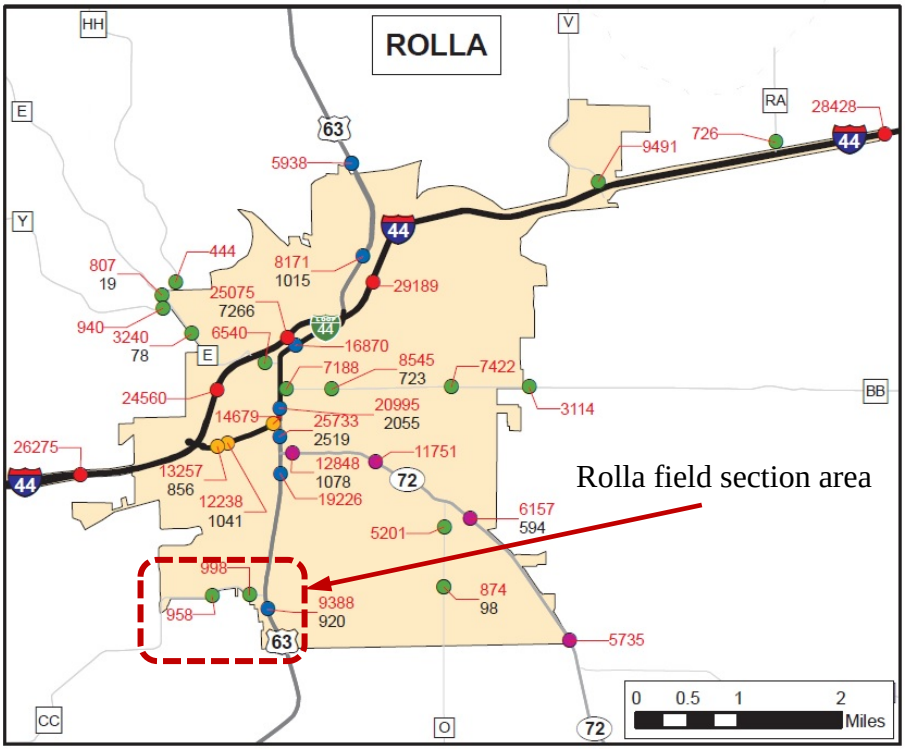

Fig. 10.3 – MoDOT three-year cycle traffic volume count map (2016) for the Rolla section.

10.3. Field Implementation of Rolla Section

10.3.1. Material Properties

Sieve analysis and properties of the aggregate used in the Rolla section are presented in Fig. 10.4 and Table 10.1. An ambient processed crumb rubber with a median particle size of 0.31 inches and a maximum aggregate size of 0.50 inches was used. The median size and maximum

aggregate size of the used natural aggregate, i.e., trap rock, in this project were 0.27 and 0.37 inches, respectively. Therefore, the median size of the crumb rubber was 15% larger than that of the natural aggregate used in the blend. CRS2P cationic rapid-setting, high-viscous asphalt emulsion was used as the binder. The properties of the binder were as reported in Table 4.2 of this report.

Table 10.1 – The Rolla Section Aggregate Properties

Property	Crumbed Rubber	Trap Rock
Coefficient of uniformity	1.57	1.67
Median particle size (in)	0.31	0.27
Materials passing sieve No. 200 (%)	0.20	0.52
Bulk specific gravity	0.87	2.56
Water absorption (%)	0.00	2.27
Loose dry unit weight (lb/ft^3)	26	78
Voids in loose aggregates (%)	79.5	43.9
Particles with no fractured faces (%)	0.0	0.0
Particles with one or more fractured faces (%)	100	100
Particles with two or more fractured faces (%)	100	100
Los Angeles loss by abrasion and impact (%)	0.37	22.2
Micro Deval weight loss (%)	0.40	4.1
Flakiness index (%)	31.3	42.0

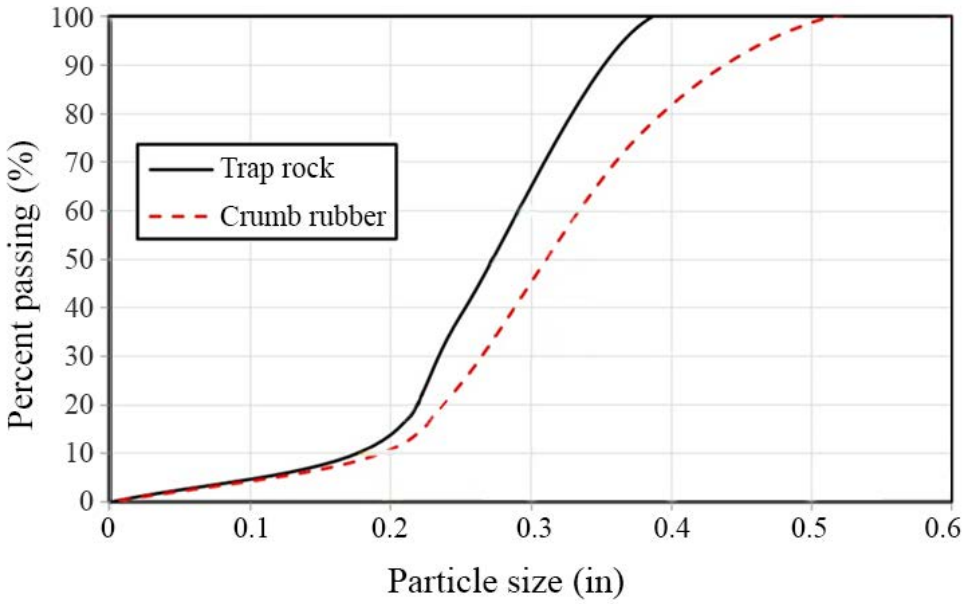

Fig. 10.4 – Sieve analysis of used aggregate in the Rolla section.

10.3.2. Construction Procedure

For the Rolla section, CRS2P emulsion with a temperature at the application time of 130° F was used. The air temperature during construction was 78° F. Traditional chip seal procedures were used to apply the rubberized chip seal (Fig. 10.5) with the conventional emulsion application rate of 0.25 to 0.40 gal/yd^2. The emulsion rate was varied during the construction to find a proper rate in terms of matching the construction equipment such as pavers and compactors, as will be discussed later. The road was swept using a sweeping truck and opened for traffic within one hour from the application of emulsion. This was not enough to evaporate the water in the used emulsion (Fig. 4.3). As shown in Fig. 4.3, it required six hours of curing time to evaporate 83% of the water at 95° F and longer curing times at lower temperatures.

Fig. 10.5 – Construction of rubberized chip seal using conventional equipment in the Rolla section. (a) spraying the binder, (b) uniform layer of binder sprayed on the surface, (c) spreading the aggregates, and (d) compaction using a steel roller.

During the aggregate spreading and compaction process, it was noticed that rubber aggregate particles adhered to the tires of the compactors and spreader. The reason was the

flexibility of the rubber particles, which led the tires to penetrate and squeeze the crumb rubber layer in the absence of natural aggregate and reach the emulsion film. Also, the excessive amount of binder was another reason. As a result, the binder application rate was reduced, and the rubber tire compactors were replaced by steel roller compactors. These actions made it possible to compact the material appropriately.

Chip seal application and compaction went smoothly and normalyl up to 50% crumb rubber replacement ratios. In the cases of 75% and 100% crumb rubber replacement ratios, there was a problem with spreading the mixture of trap rock and crumb rubber because of the low unit weight of crumb rubber which made it hard to spread the crumb rubber by gravity. Besides, the low unit weight of crumb rubber made it easy to push the rubber particles in front of the spreader's tires before the full curing of emulsion occurred. However, with 25% and 50% crumb rubber replacement ratios, the presence of trap rock, which has high unit weight, helped in pushing the crumb rubber particles through the spreader. For future applications and with gaining more application experience, the research team believes that replacing 100% of trap rock with crumb rubber is feasible.

Samples were taken from the test section and were tested in the Material Testing Laboratory at Missouri S&T. The test specimens needed to be undisturbed and be representative of the construction procedure and material. The test specimens were collected across the longitudinal direction of the road to avoid high sample-to-sample variability observed when transverse samples were collected [109]. The samples were collected by placing six pieces of asphalt felt (Fig. 10.7). To reduce the disturbance of the test specimens, the specimens were left to cure for 60 minutes which allowed the binder to have a good cohesion with the aggregate particles;

then, the samples were removed from their locations and were placed on rigid plates to provide rigid support.

Fig. 10.6 – Collecting chip seal samples from the construction site.

10.4. Field Implementation of The Boonville Section

10.4.1. Material Properties

Sieve analysis and properties of the aggregate used in the Boonville section is presented in Fig. 10.7 and Table 10.2. An ambient processed crumb rubber with a median particle size of 0.33 inches and a maximum aggregate size of 0.50 inches was used. The median size and maximum aggregate size of used natural aggregate, i.e., trap rock, in this project were 0.28 and 0.38 inches, respectively. Therefore, the median size of the crumb rubber was 18% larger than that of the natural aggregate used in the blend. CRS2P cationic rapid-setting, high-viscous asphalt emulsion was used as the binder. The properties of the binder were as reported in Table 4.2 of this report.

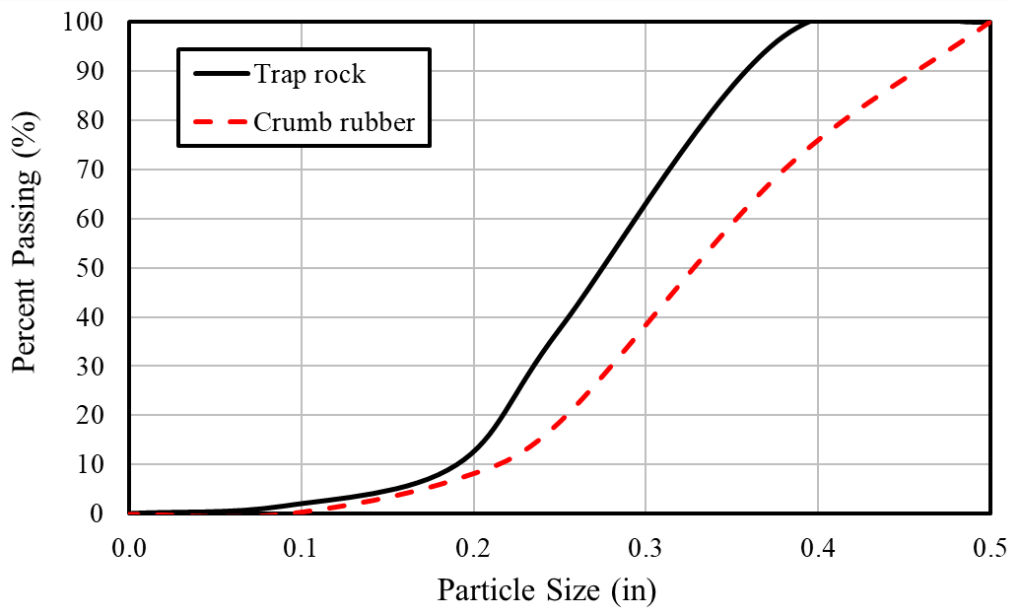

Fig. 10.7 – Sieve analysis of used aggregate in the Boonville section.

Table 10.2 – The Boonville Section Aggregate Properties

Property	Crumbed Rubber	Trap Rock
Coefficient of uniformity	1.73	1.57
Median particle size (in)	0.33	0.28
Materials passing sieve No. 200 (%)	0.30	0.66
Bulk specific gravity	0.87	2.56
Water absorption (%)	0.00	2.27
Loose dry unit weight (lb/ft^3)	26	78
Voids in loose aggregates (%)	79.5	43.9
Particles with no fractured faces (%)	0.0	0.0
Particles with one or more fractured faces (%)	100	100
Particles with two or more fractured faces (%)	100	100
Los Angeles loss by abrasion and impact (%)	0.37	22.2
Micro Deval weight loss (%)	0.40	4.1
Flakiness index (%)	31.3	42.0

10.4.2. Construction Procedure

For the Boonville section, CRS2P emulsion with a temperature at the application time of 130° F was used. The air and pavement temperature during construction was 72° F and 75° F, respectively. Similar to the Rolla section, traditional chip seal procedure and equipment were used to apply the rubberized chip seal, as shown in Fig. 10.8. Based on the field experience obtained in the Rolla section, the binder application rate of 0.34 gal/yd^2 was applied. The goal was to use 25% by volume crumb rubber and 75% trap rock as aggregate, however, after mixing the material in the field, the final mixture contained 20% by volume crumb rubber and 80% trap rock . The mixed aggregates were spread at a rate of 19.5 lb/yd^2.

Fig. 10.8 – Construction of rubberized chip seal using conventional equipment including rubber tire compactor in the Boonville section. (a) spraying the binder, (b) spreading the aggregates, (c) compaction using a steel roller, and (d) companion using a rubber tire roller.

Aggregate spreading and compaction went smoothly and normally. Even using the rubber tire compactor was successful, as shown in Fig. 10.8d. The rubber-tired roller was used with no rubber particles sticking to the rubber tires due to the selection of the correct binder and aggregate rates, which left neither extra aggregate to accumulate in front of the tires nor road spots uncovered with aggregate, making them exposed and in direct contact with the tires. Overall, no obstacle or difficulty was observed by the research team or contractors' staff in the field during the implementation of rubberized chip seal compared to the conventional chip seal.

10.5. Field Investigation of Rolla Section

The research team visited the Rolla chip seal section in six separate times during the first 12 months of service life. The first visit occurred one day after the road was open to traffic. Table 10.3 summarizes the dates and special weather events that occurred before the visits. The test sections were visually evaluated during each visit where both the right and left lanes were investigated; of particular interest was the wheel path, which is at the left and right side of each lane, and the snowplowing path, which is in between the wheel paths at the middle crest of each lane as shown in Fig. 10.9. In addition to the visual inspection, sand patch measurements were carried out during each visit to determine the MTD, which is an indication of the aggregate embedment depth. Also, a British pendulum tester (BPT) was carried out at the beginning and end of the project.

Table 10.3 – Summary of Field Investigation Visits

Visit No.	Date	Weather	Tests
0	09/20/2017	Sunny day, an average temp of 75˚ F	Field implementation
1	09/22/2017	Sunny day, an average temp of 75˚ F	Visual inspection, Sand patch and skid test
2	12/18/2017	Partly cloudy, an average temp of 48˚ F	Visual inspection, Sand patch
3	01/25/2018	Clear day, an average temp of 46˚ F, this visit was after a snowstorm with a snowplowing of the road.	Visual inspection, Sand patch
4	05/09/2018	Cloudy day, an average temp of 75˚ F, this visit was after a heavy rainstorm.	Visual inspection, Sand patch
5	06/28/2018	Sunny day, an average temp of 86˚ F, this visit was after a rainstorm.	Visual inspection, Sand patch
6	10/15/2018	Mostly cloudy day, an average temp of 43˚ F	Visual inspection, Sand patch and skid test

10.5.1. Visual Inspection

In terms of visual inspection, the major loss of the chip seal was in the middle of each traffic lane, i.e., not in the wheel paths, which is the area with the highest elevation (Fig. 10.9). This raveling type of distress was due to the snowplowing after the snowstorms on December 23rd, 2017 and January 15th, 2018.

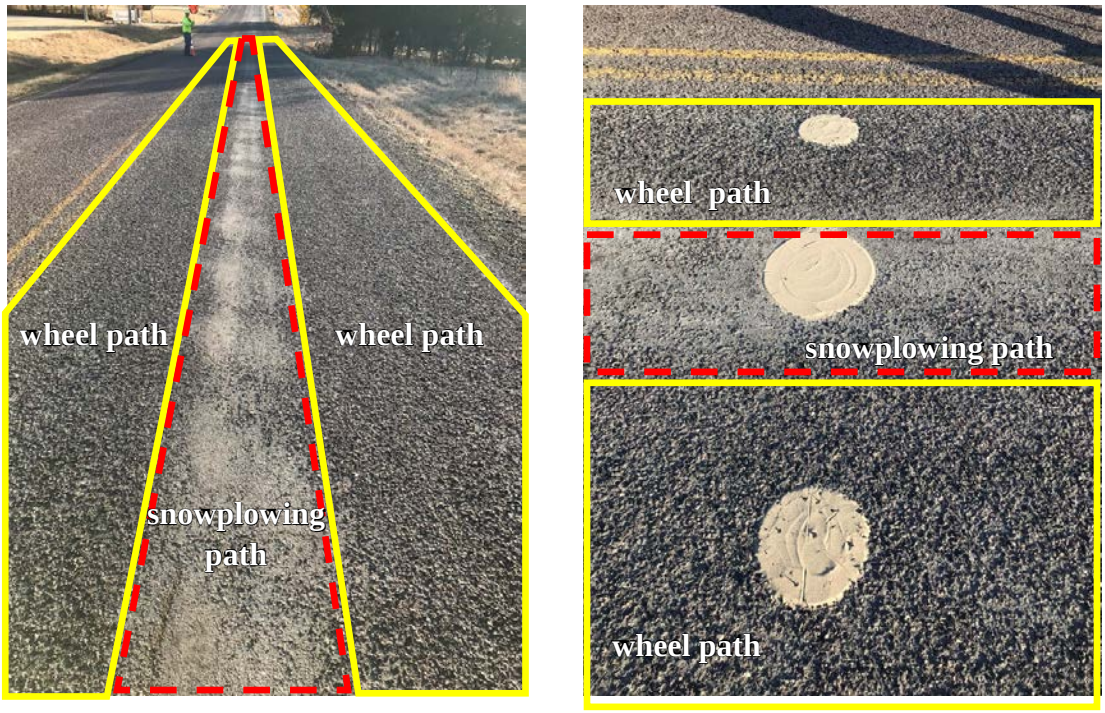

Fig. 10.9 – Raveling distress due to the snowplowing.

10.5.2. Macrotexture Measurement Using Sand Patch Test

The standard ASTM E965 sand patch test [90] was used to determine the MTD of the in-situ chip seal coating. Two volumes of sand, namely 125 ml and 60 ml, passing a No. 60 sieve and retained on a No. 80 sieve, were prepared in containers. Then, each volume of sand was independently spread uniformly on the surface of each of the investigated spots using an ice hockey puck with its bottom surface covered with a hard rubber material. Hence, for each spot, two readings were obtained at each visit. Sand patch measurements were carried out at a total of 24 spots distributed on both lanes. In each lane, a tested transverse section was selected where the sand patch was performed on two spots in the wheel paths and one spot in the snowplow path at the center of the lane (Fig. 10.10). The diameter of the spreading sand on each investigated spot was measured at least four times in four different orientations. The average diameter, D, at each spot was determined using the measurements from the two sand volumes and four diameter

measurements which was then implemented in Eq. 10.1, repeated here for convenience, to determine MTD.

$$MTD = \frac{4\,V}{\pi\,D^2} \qquad \text{Eq. (10.1)}$$

where V is the sand volume.

(a)

(b)

Fig. 10.10 – Field sand patch test on (a) visit #2 and (b) visit #5.

Detailed results of the MTD at the different spots are summarized in Appendix G. The results of the sand patch test during each visit at different locations and spots are shown in Fig. 10.11a and 10.12a for the wheel path and snowplowing path, respectively. The MTD versus service life age is also shown in Fig. 10.11b and 10.12b for the wheel path and snowplowing path, respectively. As shown in the figures, the MTD significantly increased with an increase in rubber content. At the wheel path, the MTD increased from 0.098 inches for 0% rubber to 0.118 inches and 0.130 inches for 25% and 50%, respectively, representing 20.5% and 22.5% increases over that of the trap rock for the 25% and 50% crumb rubber replacements, respectively. Expectedly, the MTD of the chip seal decreased with an increase in its service life. However, this reduction was more pronounced for trap rock compared to crumb rubber segments. The MTD decreased to 0.028 inches, 0.049 inches, and 0.050 inches after 388 days of service life for sections with 0%, 25%, and 50% crumb rubber replacement, respectively. Therefore, the MTD of the rubberized chip seal represents 72% and 75% increases over that of the trap rock after more than one year of service life. It is worth noting that the authors believe that the significant reduction in the MTD observed during the visit on December 18, 2017, for all types of aggregate was related to the early opening of the road for traffic with a curing time of less than one hour.

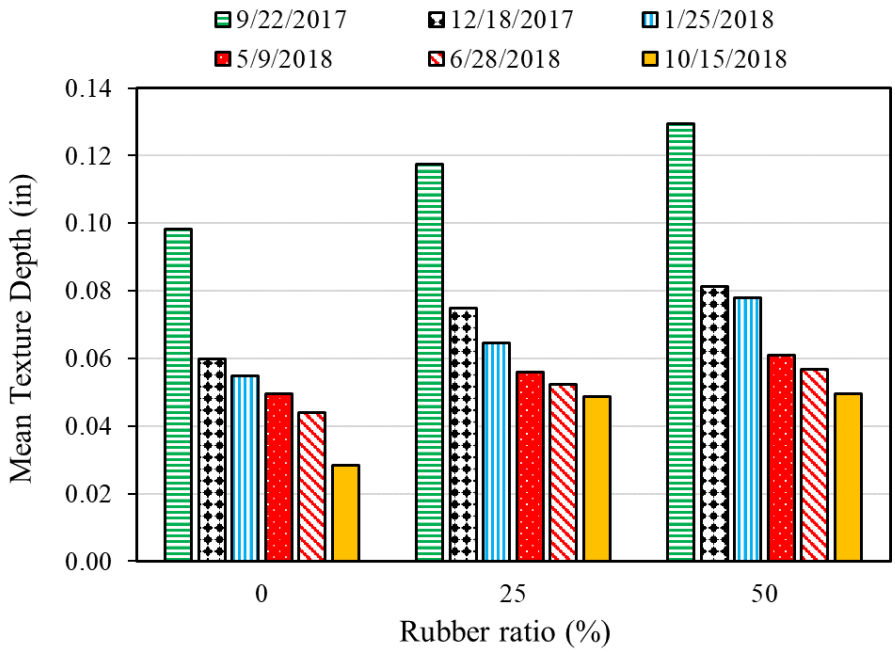

(a)

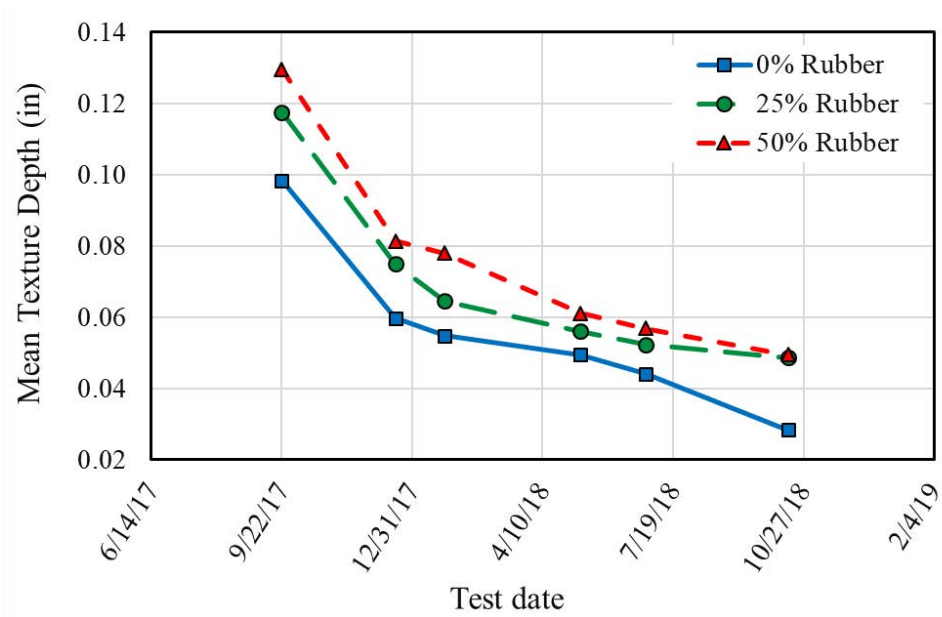

(b)

Fig 10.11 – Variation of wheel path MTD versus (a) percentage of crumb rubber, and (b) time, from the sand patch test.

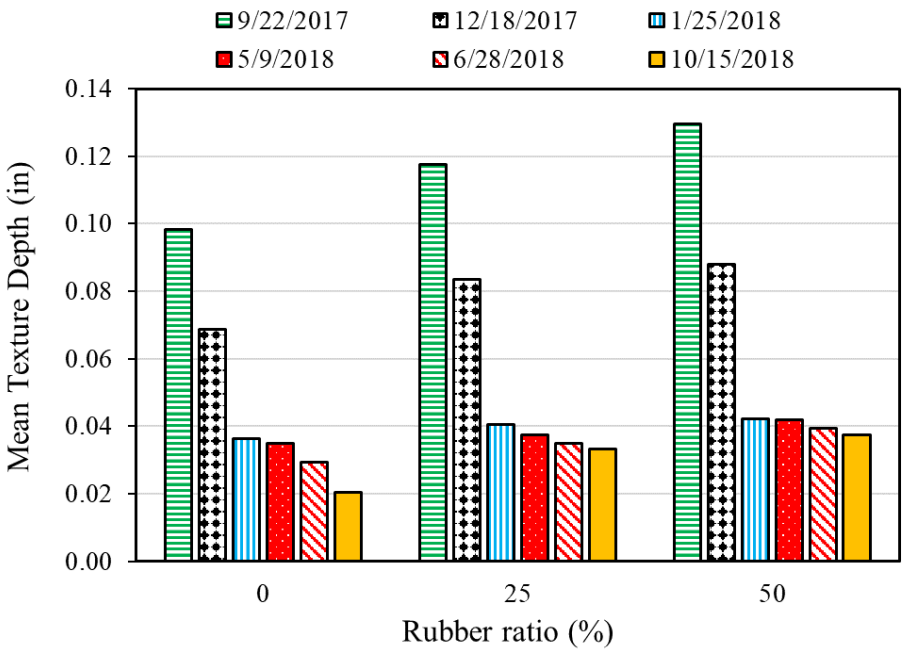

(a)

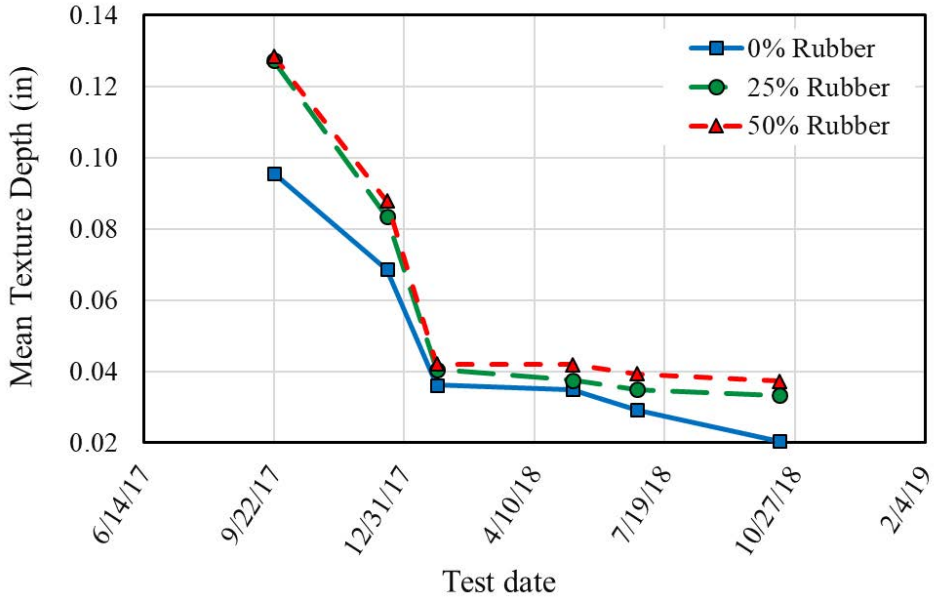

(b)

Fig. 10.12 – Variation of snowplowing path MTD versus (a) percentage of crumb rubber, and (b) time, from the sand patch test.

It is worth noting that the chip seal constructed using trap rock or rubber suffered from a significant loss in the MTD at the snowplowing path after two snow days on December 23rd, 2017

and January 15th, 2018. As shown in Figure 10.12b, the reductions in the MTD values were 47%, 51%, and 52% for 0%, 25%, and 50% crumb rubber, respectively. Figure 10.13 shows the temporal development of the ratio between the MTD at the wheel path to that at the snowplowing path. As shown in this figure, the MTD values of both lanes immediately after construction were approximately the same. Beyond that, the MTD at the wheel path was smaller than that at the snowplowing path due to the daily traffic on the wheel path. However, after the snowplowing on December 23rd, 2017 and January 15th, 2018, the MTD at the wheel path was much higher than that of the snowplowing path due to the raveling distress at the middle of each lane as a result of snowplowing action.

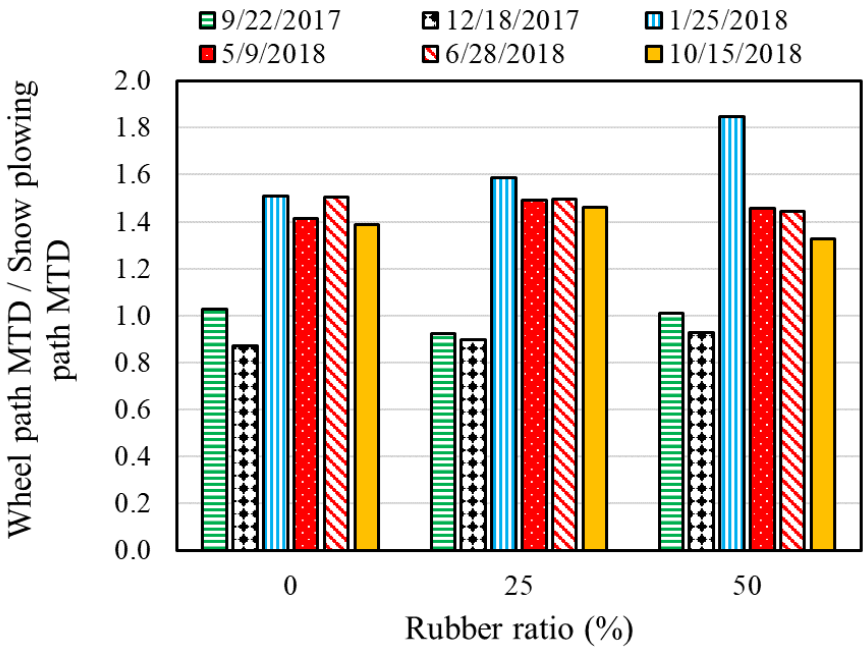

Fig. 10.13 – Effect of snowplowing on the ratio of the MTD on the wheel path to that on the snowplowing path.

10.5.3. Skid Measurement Following ASTM E303

In addition to the sand patch, the British pendulum tester (BPN) [89] was also measured. The BPT was vertically adjusted in order to achieve a slider contact path on the chip seal surface of 5 ± 1/16 inch. The distance between the center of gravity of the pendulum and the center of oscillation was 16.2 ± 0.2 inches. Water was sprinkled on the tested surface before running the test per ASTM E-303 [89]. After releasing the pendulum, the BPN was recorded and used to present the friction resistance of the surface. The test was repeated four times after one trial test to get the average BPN for each area (Fig. 10.14).

Fig. 10.14 – Field British pendulum skid resistance test.

As shown in Figure 10.15, right after applying the chip seal, the BPN slightly decreased by increasing the rubber content. The BPN was 88, 83, and 77 for the trap rock, 25% crumb rubber, and 50% crumb rubber replacement, which represents a 5.70% and 12.5% reduction in the BPN values, respectively. This is similar to the measured data in the laboratory; however, after more than a year of service life, the crumb rubber significantly outperformed the trap rock and the

rubberized chip seal segments displaying higher BPN values of 67 and 65 with 25% and 50% crumb rubber replacement ratios, respectively, compared to 42 for the trap rock chip seal segment representing 60% and 55% increases in the BPN values, respectively.

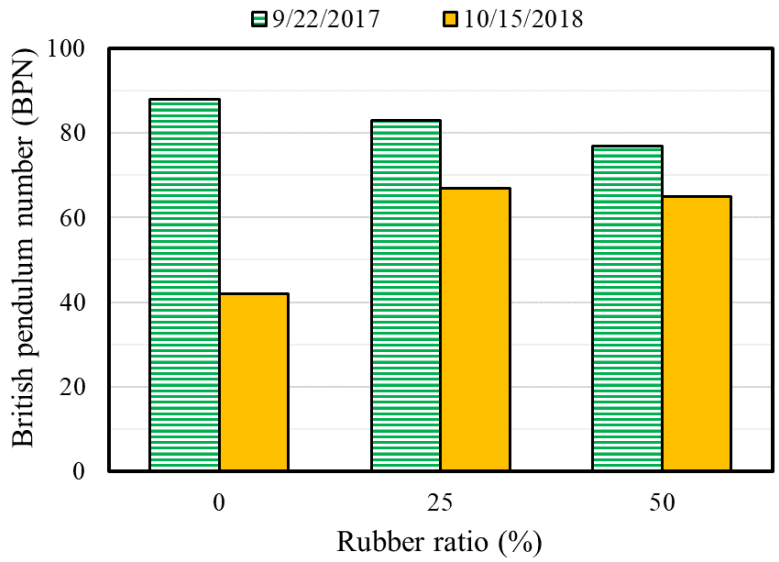

Fig. 10.15 – BPN versus percentage of rubber.

10.5.4. Skid Measurement Following ASTM E274

In this task, the effects of speed on friction and skid resistance of rubberized chip seal were determined following ASTM E274 [110]. MoDOT engineers utilized the locked wheel skid trailer (LWST) to determine the pavement friction in the eastbound (EB) and westbound (WB) lanes (Fig. 10.16). Note that ASTM E274 uses 40 mph as the standard testing speed. As shown in Fig. 10.17, using a chip seal with trap rock or rubber increased the skid number (SN) by an average of 46% compared to segments where a chip seal was not used. Furthermore, similar to BPN, using rubber reduced the SN. Using 25%, and 50% rubber reduced the SN by 14%, and 12%, respectively.

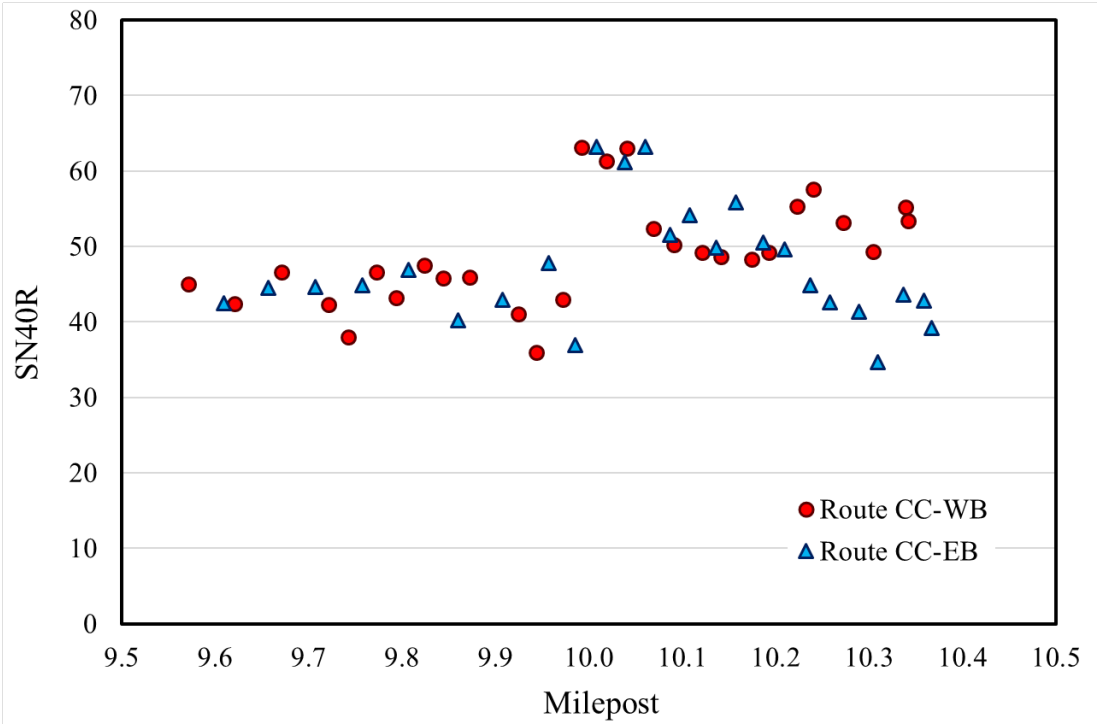

Fig. 10.16 – Locked wheel skid trailer test (LWST) results.

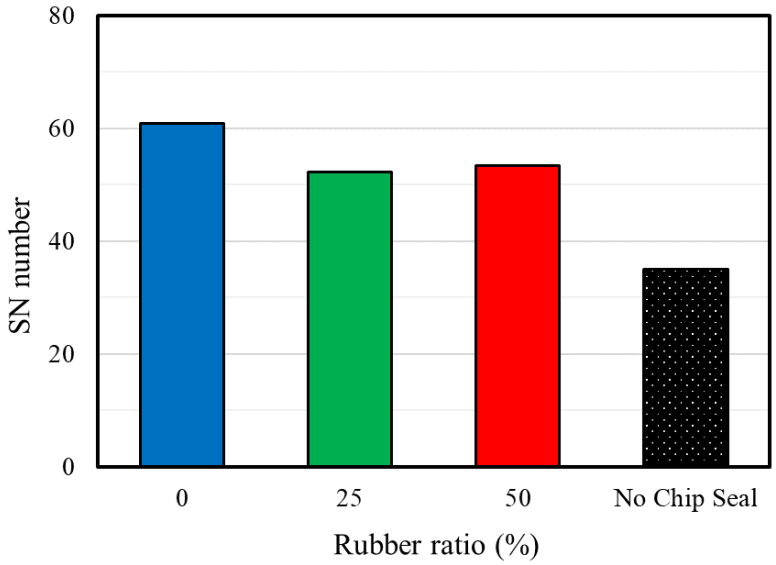

Fig. 10.17 – Comparing LWST results for different percentages of rubber and no chip seal surface.

10.6. Conclusions

This task studied the field implementation feasibility and long-term performance of the rubberized chip seal on two different sections in Rolla, Missouri and Boonville, Missouri. Based on the field experience and evaluations, the following conclusions are derived:

- Using up to 50% crumb rubber as a partial replacement for trap rock was successfully implemented in the field using the procedures and equipment traditionally used for the construction of chip seal pavement. However, using the rubber tire compactor was not feasible in the Rolla section, and a steel roller was successfully used instead. However, in the Boonville section, rubberized chip seal with 20% crumb rubber was compacted successfully using a rubber tire compactor. This is due to the selecting of binder and aggregate rates which did not leave extra aggregate to accumulate in front of the rubber tires of the spreader or compactor and also did not leave any road spots uncovered with aggregate and exposed to direct contact with the rubber tires of the spreader and compactor.

- The macro-texture, measured in the form of MTD, of the crumb rubber in the field significantly outperformed the trap rock chip seal segment. Moreover, during its service life, the degradations in the crumb rubber chip seal segments were much slower than that of the trap rock chip seal segment. For example, the initial MTD increased significantly at higher rubber contents where the trap rock chip seal segment had an MTD of 0.0983 inches while the 50% crumb rubber rubberized chip seal segment had an MTD of 0.1296 inches representing an increase of 32%. Furthermore, after 13 months of service life, including snowplowing, the MTD of the trap rock chip seal decreased to 0.0283 inches compared with 0.0495 inches for

the 50% crumb rubber chip seal representing a 75% improvement in the case of rubberized chip seal over the trap rock chip seal.

- Measurements of the British Pendulum Number (BPN) immediately after the construction of the field implementation section showed that the 50% crumb rubber chip seal segment displayed a reduction of approximately 12.5% in the BPN compared to that of the segment having 100% trap rock. However, after a service life of more than a year, chip seal road segments with 25% and 50% crumb rubber replacement ratios had BPN numbers of 67 and 65, respectively, compared to 42 for the trap rock chip seal segment.
- Concerning the overall performance of the chip seal in the field, the major distress in the chip seal occurred in the middle of each lane, which is the area with the highest transverse elevation. This raveling type of distress was due to the snowplowing action rather than the traffic conditions.

Chapter 11: Findings and Recommendations

Chip seals are one of the most cost and performance effective pavement preservation treatments commonly used in the United States. An eco-friendly chip seal pavement, in which the natural aggregate was replaced by crumb rubber obtained from scrap tires, was investigated in this project.

Two pieces of laboratory equipment were manufactured for the means of this project. A small wheel traffic simulator (SWTS) machine which was a chip seal testing device capable of providing a loading mechanism similar to the traffic loading condition through rotating pneumatic tires. Since it would be costly and time-consuming to prepare multiple filed sections and it was impractical to apply controlled traffic load on the field sections. SWTS was capable of providing simulated traffic load with different wheel application numbers, wheel application speeds, and load magnitudes within a controlled temperature. The other original piece of equipment was an advanced rainfall simulator (ASR) machine which was capable of simulating rainfall with different intensities on different chip seal surfaces. The machine was adjustable to provide different drainage length and slopes on the specimens.

During this project, 55 laboratory chip seal specimens with different sizes from 8 ft by 4 ft to 1 ft by 1 ft were prepared using CRS-2P emulsified asphalt and two different natural aggregates, i.e. trap rock and creek gravel, along with crumb rubber. Different tests including aggregate soundness test, Simulated traffic load test with different aggregate, emulsion rate, and loading parameters, as well as different temperatures of Missouri summer and winter. Drainage capability of different chip seal samples, mechanical snowplowing test, and freeze-thaw resistance test in the

presence of deicing chemicals. The macrotexture of the chip seal specimens was measured using a 3D surface scanning during this study. Also, the feasibility of the implementation and performance of rubberized chip seal in the field was investigated in two different field sections. The following findings and conclusions were drawn from the current project:

1. The soundness test results showed that crumb rubber particles are significantly resistant to freezing and thawing action since they do not absorb any water. Trap rock aggregate also performed better than creek gravel aggregate with more than two times smaller weight loss. It was observed that the weight loss by the soundness test results was proportionate with water absorption of the aggregates and was following the same trend of the Micro Deval abrasion test results.

2. The SWTS test results indicated that for trap rock chip seal specimens, replacing up to 50% of the volume of trap rock aggregate with crumb rubber did not significantly affect the raveling resistance of the specimens at both 0.25 and 0.50 gal/yd^2 binder rates. Increasing the rubber content more than 50% for trap rock chip seal impaired the raveling resistance of the specimens.

3. The SWTS test results indicated that for creek gravel chip seal specimens, replacing up to 25% of the volume of creek gravel aggregate with crumb rubber did not significantly affect the raveling resistance of the specimens for both 0.25 and 0.50 gal/yd^2 binder rates. Increasing the rubber content more than 25% for creek gravel chip seal impaired the raveling resistance of the specimens.

4. The SWTS test results indicated that the chip seal specimens with 100% crumb rubber performed poorly, especially with the lower binder application rate of 0.25 gal/yd^2

compared to trap rock and creek gravel chip seal. This can be attributed to the 0% water absorption ability of the crumb rubber.

5. The SWTS test results indicated that increasing the binder rate from 0.25 to 0.50 gal/yd^2 considerably improved the raveling resistance of chip seal specimens made with trap rock, creek gravel, and crumb rubber. The V_m loss reduced up to about 8% by increasing the binder rate from 0.25 to 0.50 gal/yd^2 for all three aggregate types.

6. The SWTS test results indicated that the creek gravel chip seal performed better in terms of raveling compared to trap rock chip seal. Creek gravel specimens experienced up to 6% V_m loss compared to trap rock specimens. This can be attributed to the lower flakiness index and higher water absorption of the creek gravel aggregate compared to trap rock.

7. The SWTS test results indicated that the raveling resistance of the trap rock natural aggregate will be impaired by increasing the applied traffic load magnitude, while for rubber aggregate, the behavior was the opposite, and the raveling resistance was improved under a higher traffic load magnitude. This can be attributed to the natural high elasticity of the crumb rubber particles.

8. The SWTS test results indicated that the raveling resistance of trap rock chip seal under high traffic speeds will be considerably improved by increasing the crumb rubber content. This can be attributed to the natural load hysteresis characteristics of the crumb rubber particles.

9. According to scanning electron microscopy (SEM) imaging observation, crumb rubber particles had a higher polishing resistance under traffic load compared to trap rock

aggregate. Crumb rubber particles also had a higher microtexture compared to trap rock particles both before and after being polished by traffic load.

10. The SWTS test of chip seal specimens at a low temperature of about 20º F indicated a better raveling resistance comparing to specimens tested at the temperature of about 78º F. This improvement was more pronounced for 100% trap rock specimens and had a reduced effect with increasing the rubber content.

11. The SWTS test at a high temperature of about 100º F indicated that the raveling resistance of chip seal specimens containing natural aggregate reduced significantly and severe bleeding and a subsequent severe aggregate loss happened due to the low stiffness of the behavior at high temperature.

12. The SWTS test at a high temperature of about 100º F indicated that the chip seal specimens with 100% crumb rubber performed significantly better raveling and bleeding resistance than the chip seals containing natural aggregate.

13. The SWTS test at a high temperature of about 100º F indicated that the chip seal specimens with 100% crumb rubber performed better raveling resistance than the 100% rubber chip seal specimen tested in about 78º F temperature due to the very low thermal conductivity of rubber particles compared to the natural aggregate.

14. The Gallaway water film depth (WFD) prediction model does not provide accurate predictions for the WFD of chip seal surfaces. The correlation between Gallaway WFD and actual WFD measurements was very poor with small R^2=0.23.

15. The PAVDRN water film depth (WFD) model provides fair results for chip seal surface with rainfall intensities equal to or lower than 9 in/hr with R^2=0.77 between the predicted

and actual WFD values. However, for higher rainfall intensities, the results were underestimated and not reliable with R^2=0.34 between the predicted and actual WFD values.

16. The first water film depth (WFD) model proposed in this study showed a very high correlation with actual WFD measurements with R^2=0.89. This model showed that WFD on the chip seal surface is highly related to mean texture depth, which is underestimated in the Gallaway model for highly textured surfaces.

17. The second water film depth (WFD) model proposed in this study incorporated a term to consider the effect of partially or fully rubberized chip seal surfaces, which can predict the WFD variation caused by only changing the aggregate type while other variables are identical. This model showed a very high correlation between the predicted and actual WFD values with R^2=0.92.

18. Rubberized chip seal has enhanced drainage capabilities compared to conventional chip seal, especially in low slopes. For example, at the rainfall intensity of 3 in/hr and slope of 0.05%, replacing 50% of mineral aggregate with crumb rubber particles reduced the WFD by 58%.

19. The snowplowing test results showed a better performance for the chip seal specimen with crumb rubber as aggregate. The amount of aggregate loss reduced considerably with increasing the rubber content in chip seal. Although crumb rubber particles used in that test had a higher flakiness index compared to natural aggregate, the specimens with 0%, 25%, and 50% crumb rubber content, respectively experienced 1.7, 1.5, and 1.3 times more texture loss compared to the specimen with 100% crumb rubber aggregate after eight snowplow applications.

20. Snowplowing with a higher cutting angle, i.e., the angle between the snowplow blade and pavement surface, required a higher power, which will lead to more damage to the surface. Therefore, using a low cutting angle was recommended for snowplowing the chip seal surfaces.

21. Freeze-thaw test results indicated that trap rock aggregate performed significantly better than creek gravel and crumb rubber aggregate by about 3.4 and 2.8 times less volumetric aggregate loss, respectively, after 50 cycles of freezing and thawing.

22. Freeze-thaw test results indicated that replacing creek gravel by crumb rubber particles up to 50% improved the freeze-thaw resistance of chip seal specimens by 35%.

23. Freeze-thaw test results indicated that after 50 cycles of freezing and thawing, the specimen with 100% rubber experienced the least macrotexture loss under simulated traffic loading with almost half of the texture loss experienced by trap rock and creek gravel specimens.

24. Freeze-thaw test results indicated that after 50 cycles of freezing and thawing, due to simulated traffic load, macrotexture loss increased 8% by adding 50% crumb rubber to trap rock specimens and decreased 6% by adding 50% crumb rubber to creek gravel.

25. It can be concluded from both the freeze-thaw test and the SWTS test that adding crumb rubber to trap rock chip seal will aggravate the performance in terms of aggregate retention under freezing and thawing actions.

26. It can be concluded from both the freeze-thaw test and the SWTS test that adding crumb rubber to creek gravel chip seal will improve the performance in terms of aggregate retention under freezing and thawing actions.

27. Using up to 50% crumb rubber as a partial replacement for trap rock was successfully implemented in the field using the procedures and equipment traditionally used for the construction of chip seal pavement. However, using the rubber tire compactor was not feasible in the Rolla section, and a steel roller was successfully used instead. However, in the Boonville section, rubberized chip seal with 20% crumb rubber was compacted successfully using a rubber tire compactor. This is due to the selecting of binder and aggregate rates which did not leave extra aggregate to accumulate in front of the rubber tires of the spreader or compactor and also did not leave any road spots uncovered with aggregate and exposed to direct contact with the rubber tires of the spreader and compactor.

28. The macrotexture, measured in the form of MTD, of the crumb rubber in the field significantly outperformed the trap rock chip seal segment. Moreover, during its service life, the degradations in the crumb rubber chip seal segments were much slower than that of the trap rock chip seal segment. For example, the initial MTD increased significantly at higher rubber contents where the trap rock chip seal segment had an MTD of 0.0983 inches while the 50% crumb rubber rubberized chip seal segment had an MTD of 0.1296 inches representing an increase of 32%. Furthermore, after 13 months of service life, including snowplowing, the MTD of the trap rock chip seal decreased to 0.0283 inches compared with 0.0495 inches for the 50% crumb rubber chip seal representing a 75% improvement in the case of rubberized chip seal over the trap rock chip seal.

29. Measurements of the British Pendulum Number (BPN) immediately after the construction of the field implementation section showed that the 50% crumb rubber chip seal segment displayed a reduction of approximately 12.5% in the BPN compared to that of the segment having 100% trap rock. However, after a service life of more than a year, chip seal road

segments with 25% and 50% crumb rubber replacement ratios had BPN numbers of 67 and 65, respectively, compared to 42 for the trap rock chip seal segment.

30. Concerning the overall performance of the chip seal in the field, the major distress in the chip seal occurred in the middle of each lane, which is the area with the highest transverse elevation. This raveling type of distress was due to the snowplowing action rather than the traffic conditions.

11.1. Recommendations

1. Using flaky aggregate whether crumb rubber or natural aggregate is not recommended since lower fakeness was proved to provide better stability and retention under traffic. Also, flaky aggregate will be more exposed to snowplow blade in nontraffic areas leading to more aggregate loss.

2. Using a binder application rate of more than 0.25 gal/yd^2 and less than 0.50 gal/yd^2 is recommended for emulsified asphalt since binder rate less than 0.25 gal/yd^2 will not provide enough raveling resistance for the conventional nor rubberized hip seal. Binder rate more than 0.50 gal/yd^2 will increase the risk of bleeding.

3. For low traffic roads, a crumb rubber replacement ratio less than 50% is recommended. Since using more rubber will reduce the raveling and freeze-thaw resistance under low traffics.

4. For high-speed roads, a crumb rubber replacement ratio of 100% is recommended. Since rubber particles proved to perform better under higher loading rates. Also, the potential dislodged flying rubber particles will not cause a risk for vehicles in high-speed traffic because of the low density of crumb rubber.

5. For areas with high temperatures, a crumb rubber replacement ratio of 100% is recommended. Since rubber particles will reduce the risk of bleeding in high temperatures by acting as insulation and preventing the binder from heating up.

6. More studies are required to study the bond force between the rubber or natural aggregates with the binder in different temperatures. Since the bond force and relative deformations of the aggregates and binder will help to better understand the performance.

7. More studies are required to investigate the chip seal interaction with the asphalt layer underneath it under the traffic load and different environmental conditions. Since the raveling and bleeding performance of the chip seal may be affected by the elasticity or temperature susceptibility of the asphalt layer underneath it.

References

1. Gransberg, D.D. and James, D.M., *Chip seal best practices*. Vol. 342. 2005: Transportation Research Board.
2. Jackson, D.C., Jackson, N.C., and Mahoney, J.P., *Washington state chip seal study.* Transportation Research Record, 1990(1259).
3. Langer, W.H., Drew, L.J., and Sachs, J.S., *Aggregate and the Environment*. Vol. 8. 2004.
4. Mehta, K.P., *Reducing the environmental impact of concrete.* Concrete International, 2001. **23**(10): p. 61-66.
5. Bribián, I.Z., Capilla, A.V., and Usón, A.A., *Life cycle assessment of building materials: Comparative analysis of energy and environmental impacts and evaluation of the eco-efficiency improvement potential.* Building and Environment, 2011. **46**(5): p. 1133-1140.
6. USTMA, *2017 U.S. Scrap Tire Management Summary*. 2018, U.S. Tire Manufacturers Association: Washington, DC.
7. Gheni, A.A., et al., *Texture and design of green chip seal using recycled crumb rubber aggregate.* Journal of Cleaner Production, 2017. **166**: p. 1084-1101.
8. Gheni, A.A., Lusher, S.M., and ElGawady, M.A., *Retention behavior of crumb rubber as an aggregate in innovative chip seal surfacing.* Journal of Cleaner Production, 2018. **197**: p. 1124-1136.
9. Pourhassan, A., Gheni, A., and ElGawady, M.A., *Effect of Aggregate Size on the Retention of Conventional and Rubberized Chip Seal*, in *IABSE Congress*. 2019: New York City.
10. Gheni, A., et al., *Leaching assessment of eco-friendly rubberized chip seal pavement.* Transportation Research Record: Journal of the Transportation Research Board, 2018. **2672**(52): p. 67-77.
11. Wu, Y., Parker, F., and Kandhal, K., *AGGREGATE TOUGHNESS/ABRASION RESISTANCE AND DURABILITY/SOUNDNESS TESTS RELATED TO ASPHALT CONCRETE PERFORMANCE IN PAVEMENTS.* 1998.
12. Saeed, A., Hall Jr, J., and Barker, W., *Performance-related tests of aggregates for use in unbound pavement layers*. 2001.
13. Kandhal, P.S. and Parker, F., *Aggregate tests related to asphalt concrete performance in pavements*. Vol. 405. 1998: Transportation Research Board.
14. Rogers, C., Bailey, M., and Price, B., *Micro-Deval test for evaluating the quality of fine aggregate for concrete and asphalt*. 1991.
15. Hasan, S., Meyer, A.H., and Fowler, D.W., *ESTABLISHMENT OF ACCEPTANCE LIMITS FOR 5-CYCLE MSS AND MODIFIED WET BALL MILL TESTS FOR AGGREGATES USED IN SEAL COATS AND HMAC SURFACES. FINAL REPORT*. 1991.
16. Harman Jr, J.W., Cady, P.D., and Bolling, N.B., *Slow-Cooling Tests for Frost Susceptibility of Pennsylvania Aggregates.* Highway Research Record, 1970(328).
17. Garrity, L.V., et al. *Studies of the accelerated soundness tests*. in Highway Research Board Proceedings. 1936.

18. Wu, Y., Parker, F., and Kandhal, P.S., *Aggregate toughness/abrasion resistance and durability/soundness tests related to asphalt concrete performance in pavements.* Transportation Research Record, 1998. **1638**(1): p. 85-93.
19. Paul, I. *Magnesium Sulphate Accelerated Soundness Test on Concrete Aggregates*. in Highway Research Board Proceedings. 1933.
20. Shuler, S., *Performance of Chip Seals Using Local and Minimally Processed Aggregates for Preservation of Low Traffic Volume Roadways*. 2013.
21. Gürer, C., et al., *Effects of construction-related factors on chip seal performance.* Construction and Building Materials, 2012. **35**: p. 605-613.
22. Roque, R., Anderson, D., and Thompson, M., *Effect of material, design, and construction variables on seal-coat performance.* Transportation Research Record, 1991. **1300**: p. 108-115.
23. Karasahin, M., et al., *Laboratory and In Situ Investigation of Chip Seal Surface Condition Improvement.* 2015. **29**(2): p. 04014047.
24. Liu, L., Hossain, M., and Miller, R. *Life of chip seal on Kansas highways*. in Compendium of Papers from First International Conference on Pavement Preservation. 2010.
25. Lukanen, E.O., *An Evaluation of Aggregate and Chip Seal Surfaced Roads at Mn/Road*. 1997.
26. Zhu, J., *Surface Wear Test Research and Analysis of Asphalt Rubber Chip Seal*, in *ICTE 2013: Safety, Speediness, Intelligence, Low-Carbon, Innovation*. 2013, ASCE. p. 1184-1194.
27. Lee, J., Kim, Y.R., and McGraw, E.O., *Performance evaluation of bituminous surface treatment using third-scale model mobile loading simulator.* Transportation Research Record, 2006. **1958**(1): p. 59-70.
28. Adams, J.M. and Richard Kim, Y., *Mean profile depth analysis of field and laboratory traffic-loaded chip seal surface treatments.* International Journal of Pavement Engineering, 2014. **15**(7): p. 645-656.
29. Aktaş, B., et al., *Effect of aggregate surface properties on chip seal retention performance.* Construction and Building Materials, 2013. **44**: p. 639-644.
30. ASTM, *ASTM D6372, Standard Practice for Design, Testing, and Construction of Microsurfacing*. 2015, ASTM International: West Conshohocken, PA.
31. Chaturabong, P., Hanz, A.J., and Bahia, H.U., *Development of Loaded Wheel Test for Evaluating Bleeding in Chip Seals.* Transportation Research Record, 2015. **2481**(1): p. 48-55.
32. Boz, I., et al., *Establishing Percent Embedment Limits to Improve Chip Seal Performance*. 2018, Michigan State University. p. 109.
33. Vollor, T.W. and Hanson, D.I., *Development of Laboratory Procedure for Measuring Friction of HMA Mixtures–Phase I.* Final Report of NCAT, 2006(06-06).
34. Wilson, D. and Dunn, R., *Polishing aggregates to equilibrium skid resistance.* Transport Research Journal, 2005. **14**(2): p. 55-71.
35. Lee, J., et al., *A Comparison Study of Friction Measurements for Chip Seal.* Journal of Testing and Evaluation, 2012. **40**(4): p. 603-611.
36. Uz, V.E. and Gökalp, İ., *The effect of aggregate type, size and polishing levels to skid resistance of chip seals.* Materials and Structures, 2017. **50**(2): p. 126.
37. El Gendy, A., et al., *Stereo-vision applications to reconstruct the 3D texture of pavement surface.* International Journal of Pavement Engineering, 2011. **12**(03): p. 263-273.

38. Yaacob, H., et al., *Comparison of sand patch test and multi laser profiler in pavement surface measurement.* Jurnal Teknologi, 2014. **70**(4).
39. Vaiana, R., et al., *Pavement surface performances evolution: an experimental application.* Procedia-Social and Behavioral Sciences, 2012. **53**: p. 1149-1160.
40. KIM, H.B., et al., *Measurement of texture depth of pavement using potable laser profiler.* Journal of the Eastern Asia Society for Transportation Studies, 2013. **10**: p. 1576-1589.
41. Wang, W., et al., *Design and verification of a laser based device for pavement macrotexture measurement.* Transportation Research Part C: Emerging Technologies, 2011. **19**(4): p. 682-694.
42. Fisco, N. and Sezen, H., *Comparison of surface macrotexture measurement methods.* Journal of Civil Engineering Management, 2013. **19**(sup1): p. S153-S160.
43. Flintsch, G.W., et al., *Pavement surface macrotexture measurement and applications.* Transportation Research Record, 2003. **1860**(1): p. 168-177.
44. Praticò, F. and Vaiana, R., *A study on the relationship between mean texture depth and mean profile depth of asphalt pavements.* Construction and Building Materials, 2015. **101**: p. 72-79.
45. Sengoz, B., Topal, A., and Tanyel, S., *Comparison of pavement surface texture determination by sand patch test and 3D laser scanning.* Periodica Polytechnica Civil Engineering, 2012. **56**(1): p. 73-78.
46. Čelko, J., Kováč, M., and Kotek, P., *Analysis of the pavement surface texture by 3D scanner.* Transportation Research Procedia, 2016. **14**: p. 2994-3003.
47. Bitelli, G., et al., *Laser scanning on road pavements: A new approach for characterizing surface texture.* 2012. **12**(7): p. 9110-9128.
48. Dondi, G., et al. *Characterization of pavement surface texture using 3D Laser scanner technique*. in Proceedings of the 11th International Conference on Asphalt Pavement. August. 2010.
49. Ong, G.P. and Fwa, T.F. *Hydroplaning risk management for grooved pavements*. in 7th International Conference on Managing Pavement Assets. 2008.
50. Ross, N. and Russam, K., *The depth of rain water on road surfaces.* 1968.
51. Marek, M., *Hydraulic Design Manual, Texas Department of Transportation (TxDOT).* 2011, Design Division (DES): Texas, USA.
52. NAASRA, *Drainage of wide flat pavements*. 1974: National Association of Australian State Road Authorities.
53. Luo, W., et al., *Surface drainage evaluation of asphalt pavement using a new analytical water film depth model.* Road Materials Pavement Design, 2019: p. 1-20.
54. Kane, M. and Do, M.T., *Kinematic wave approach to model water depth on road surfaces during and after rainfall events.* International Journal of Pavement Engineering, 2012. **13**(5): p. 385-394.
55. Gallaway, B., et al., *Pavement and geometric design criteria for minimizing hydroplaning*. 1979.
56. Horne, W.B. and Dreher, R.C., *PHENOMENA OF PNEUMATIC TIRE HYDROPLANING.* 1963.
57. Luo, W., Wang, K.C., and Li, L., *Field test validation of water film depth (WFD) prediction models for pavement surface drainage.* International Journal of Pavement Engineering, 2017: p. 1-12.

58. Chesterton, J., Nancekivell, N., and Tunnicliffe, N., *The use of the Gallaway formula for aquaplaning evaluation in New Zealand*, in *Transportation and the Pursuit of Excellence - NZIHT & Transit NZ 8th Annual Conference*. 2006: New Zealand
59. ASTM, *ASTM E965-15, Standard test method for measuring pavement macrotexture depth using a volumetric technique*. 2015, ASTM International: West Conshohocken PA.
60. Janisch, D.W. and Gaillard, F.S., *Minnesota seal coat handbook*. 1998, Minnesota Department of Transportation, Office of Research Services.
61. Wood, T.J. and Olson, R.C., *Rebirth of chip sealing in Minnesota.* Transportation Research Record, 2007. **1989**(1): p. 260-264.
62. Wood, T.J. and Olson, R.C., *Nine steps to constructing high-quality chip seals.* Transportation Research Record, 2011. **2204**(1): p. 54-57.
63. Jahren, C.T. and Behling, K.R., *Thin maintenance surface treatments: Comparative study.* Transportation Research Record, 2004. **1866**(1): p. 20-27.
64. Pan, P., et al., *Effect of freezing-thawing and ageing on thermal characteristics and mechanical properties of conductive asphalt concrete.* Construction and Building Materials, 2017. **140**: p. 239-247.
65. Badeli, S., et al., *Evaluation of the durability and the performance of an asphalt mix involving Aramid Pulp Fiber (APF): Complex modulus before and after freeze-thaw cycles, fatigue, and TSRST tests.* Construction and Building Materials, 2018. **174**: p. 60-71.
66. Goh, S.W. and You, Z. *Evaluation of hot-mix asphalt distress under rapid freeze-thaw cycles using image processing technique*. in Twelfth COTA International Conference of Transportation ProfessionalsAmerican Society of Civil EngineersTransportation Research Board. 2012.
67. Özgan, E. and Serin, S., *Investigation of certain engineering characteristics of asphalt concrete exposed to freeze–thaw cycles.* Cold Regions Science Technology, 2013. **85**: p. 131-136.
68. Kennedy, T.W., Roberts, F.L., and Lee, K.W., *Evaluation of moisture effects on asphalt concrete mixtures*. 1983.
69. Stroup-Gardiner, M. and Epps, J., *Four variables that affect the Performance of Lime in Asphalt-Aggregate Mixtures.* Transportation Research Record, 1987. **1115**: p. 12-22.
70. Janoo, V.C. and Berg, R.L., *Thaw weakening of pavement structures in seasonal frost areas.* Transportation Research Record, 1990(1286).
71. Simonsen, E. and Isacsson, U., *Thaw weakening of pavement structures in cold regions.* Cold Regions Science Technology, 1999. **29**(2): p. 135-151.
72. Williams, T.M. and Miknis, F.P., *Use of environmental SEM to study asphalt-water interactions.* Journal of Materials in Civil Engineering, 1998. **10**(2): p. 121-124.
73. Wood, T.J., Janisch, D.W., and Gaillard, F.S., *Minnesota seal coat handbook 2006*. 2006.
74. Höbeda, P., *Water sensitivity of asphalt pavements.* Swedish National Road Transport Research Institute VTI note, 1998. **35**.
75. Kettil, P., Engström, G., and Wiberg, N.-E., *Coupled hydro-mechanical wave propagation in road structures.* Computers Structures, 2005. **83**(21-22): p. 1719-1729.
76. Feng, D., et al., *Impact of salt and freeze–thaw cycles on performance of asphalt mixtures in coastal frozen region of China.* Cold Regions Science Technology, 2010. **62**(1): p. 34-41.
77. Yazgan, B., *A new testing protocol for seal coat (chip seal) aggregate-binder compatibility*. 2003, Texas Tech University.

78. Wasiuddin, N.M., et al., *Field and laboratory evaluation of environmental effects on chip seal performance: Freeze-thaw and asphalt aging.* Journal of Testing Evaluation, 2014. **43**(4): p. 820-832.
79. You, L., et al., *Investigation of adhesion and interface bond strength for pavements underlying chip-seal: Effect of asphalt-aggregate combinations and freeze-thaw cycles on chip-seal.* Construction and Building Materials, 2019. **203**: p. 322-330.
80. Xiao-Bin, H., *Seawater salt spray on harm and preventive measures of asphalt pavement.* Fujian Traffic Science and Technology, 2009. **2**: p. 33-35.
81. Hassan, H.F., Al-Oraimi, S., and Taha, R., *Evaluation of open-graded friction course mixtures containing cellulose fibers and styrene butadiene rubber polymer.* Journal of Materials in Civil Engineering, 2005. **17**(4): p. 416-422.
82. Hassan, Y., et al., *Effects of runway deicers on pavement materials and mixes: comparison with road salt.* Journal of Transportation Engineering, 2002. **128**(4): p. 385-391.
83. Yu, X., et al., *The Effects of Salt on Rheological Properties of Asphalt after Long-Term Aging %J The Scientific World Journal.* 2013. **2013**: p. 10.
84. Yi-Sha, Y., *Research of the influence about the performance of asphalt and asphalt mixture by sulfate.* Chang'an University, 2007.
85. McCutchon, J., Joseph, A., and Valkenberg, J. *Assessment of the effect of urea deicing solution on asphaltic concrete pavements*. in PROCEEDINGS OF THE ANNUAL CONFERENCE-CANADIAN TECHNICAL ASPHALT ASSOCIATION. 1998. POLYSCIENCE PUBLICATIONS INC.
86. Dahir, S. and Meyer, W., *The Polishing Characteristics of Common Rock Types Used as Aggregate in Bituminous Pavement Surfaces.* Journal of Testing Evaluation, 1978. **6**(1): p. 52-59.
87. Salt, G.F., *Research on Skid-resistance at the Transport and Road Research Laboratory (1927-1977).* Transportation Research Record, 1977. **622**: p. 26-38.
88. Hyyppa, J., *The Polishing of Mineral Aggregate in Road Surfacings/In English and Finnish.* 1969.
89. ASTM, *ASTM C88-18, Standard Test Method for Soundness of Aggregates by Use of Sodium Sulfate or Magnesium Sulfate*. 2018, ASTM International: West Conshohocken, PA.
90. ASTM, *ASTM E965-15 Standard Test Method for Measuring Pavement Macrotexture Depth Using a Volumetric Technique*. 2015, ASTM International: West Conshohocken, PA.
91. Pourhassan, A., Gheni, A., and ElGawady, M., *Rubberized chip seal implementation in Mid-Missouri*. 2019, Missouri University of Science and Technology, A. Dept. of Civil, and Environmental Engineering.
92. Surfe, D., *MountainsMap*. 2019: Besançon, France.
93. *Missouri standard specifications for highway construction*. 2019: Missouri Highway and Transportation Commission.
94. Institute, B.S., *ISO 25178-2 Geometric product specifications (GPS) - Surface texture: Areal terms, definitions and surface texture parameters*, in *Areal terms, definitions and surface texture parameters*. 2012: London.
95. Institute, B.S., *ISO 13565-2: Geometrical Product Specifications (GPS) - Surface texture: Profile method; Surfaces having stratified functional properties*, in *Part 2: Height characterization using the linear material ratio curve*. 1996: London.

96. *National weather service*. National oceanic and atmospheric administration; Available from: www.weather.gov.
97. Kulakowski, B.T. and Harwood, D.W., *Effect of water-film thickness on tire-pavement friction*, in *Surface characteristics of roadways: international research and technologies*. 1990, ASTM International.
98. Horne, W.B., *Tire hydroplaning and its effects on tire traction.* Highway Research Record, 1968(214).
99. Okano, T. and Koishi, M. *Hydroplaning simulation using MSC. dytran*. in Proceedings of the 3rd European LS-DYNA Users Conference. 2001.
100. Christopher, B.R. and McGuffey, V.C., *Pavement subsurface drainage systems*. Vol. 239. 1997: Transportation Research Board.
101. Liu, X., et al., *Reduced zinc leaching from scrap tire during pavement applications.* Waste Management, 2018. **81**: p. 53-60.
102. Lanza, L., Vuerich, E., and Gnecco, I., *Analysis of highly accurate rain intensity measurements from a field test site.* Advances in Geosciences, 2010. **25**: p. 37-44.
103. Gallaway, B.M., Schiller, R.E., and Rose, J.G., *The effects of rainfall intensity, pavement cross slope, surface texture, and drainage length on pavement water depths*. 1971, Study No 138.
104. ODOT, *Hydraulics Manual: Hydrology–Appendix A.* 2014, Orefon Department of Transportation.
105. Luo, W., et al., *Surface drainage evaluation for rigid pavements using an inertial measurement unit and 1-mm three-dimensional texture data.* Transportation Research Record, 2014. **2457**(1): p. 121-128.
106. Dunford, A., *Friction and the texture of aggregate particles used in the road surface course*. 2013, University of Nottingham.
107. Hansen, A.C., *Analysis of Energy Dissipation Caused by Snow Compaction During Displacement Plowing.* Transportation Research Record, 1991(1304).
108. ASTM, *ASTM C672/C672M-12 Standard Test Method for Scaling Resistance of Concrete Surfaces Exposed to Deicing Chemicals*. 2012, ASTM International: West Conshohocken, PA.
109. Lee, J., *Quantifying the Benefits of Improved Rolling of Chip Seals.* 2009.
110. ASTM, *ASTM E274/E274M-15, Standard Test Method for Skid Resistance of Paved Surfaces Using a Full-Scale Tire*. 2015, ASTM International: West Conshohocken, PA.

Appendix A: Chip Seal Specimens Construction

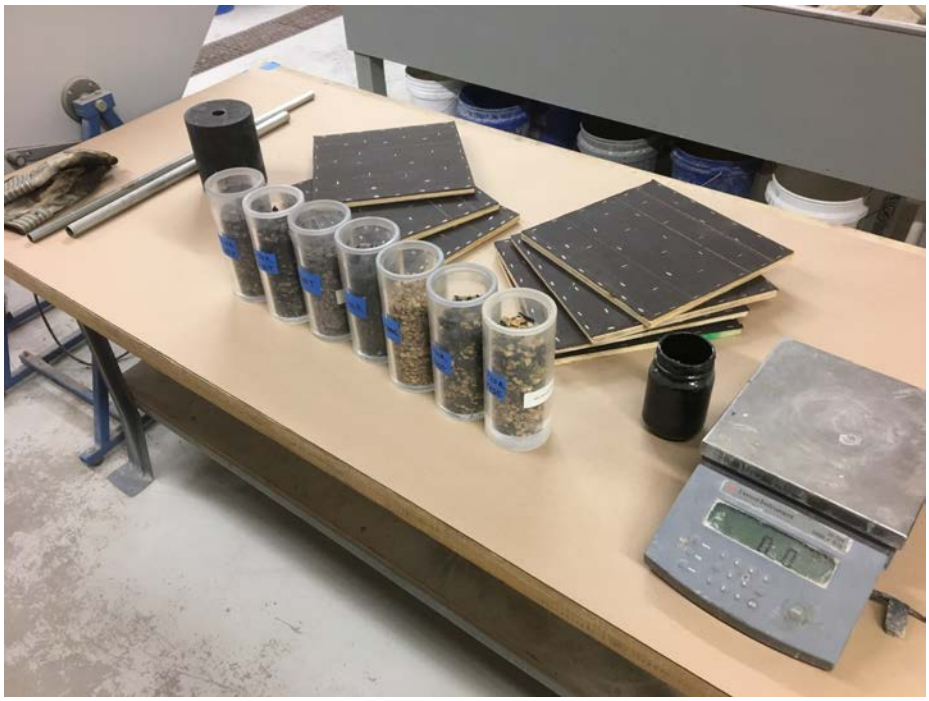

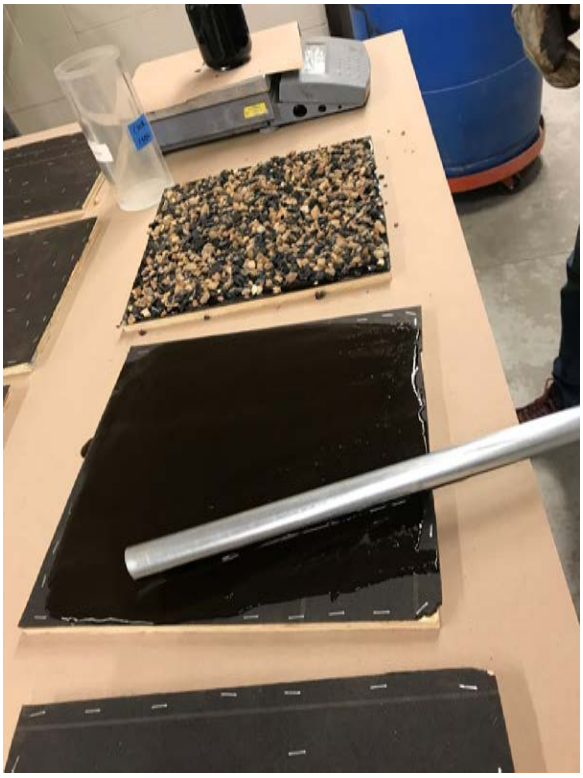

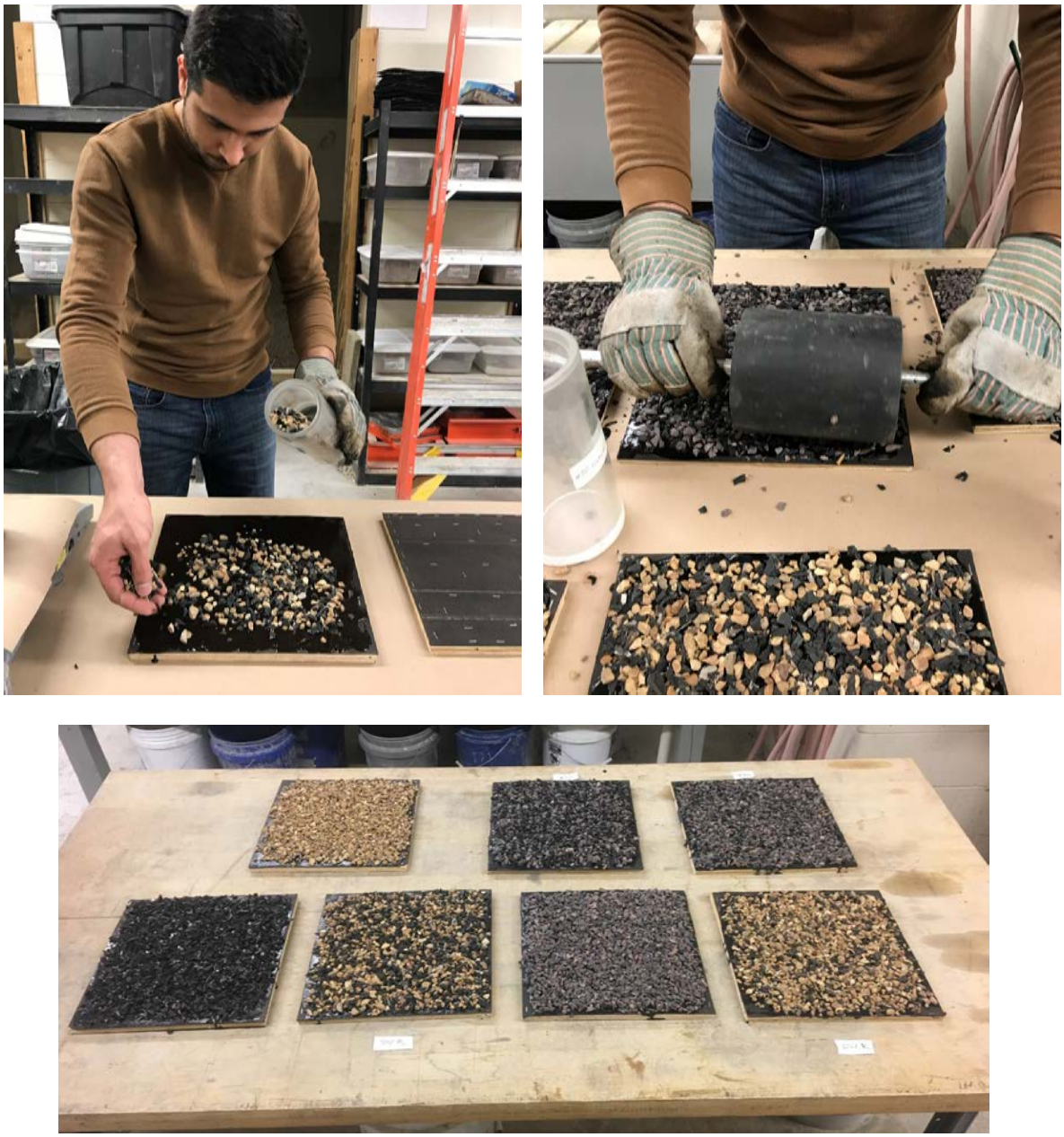

Fig. A.1 – 1 ft by 1 ft chip seal specimens' preparation.

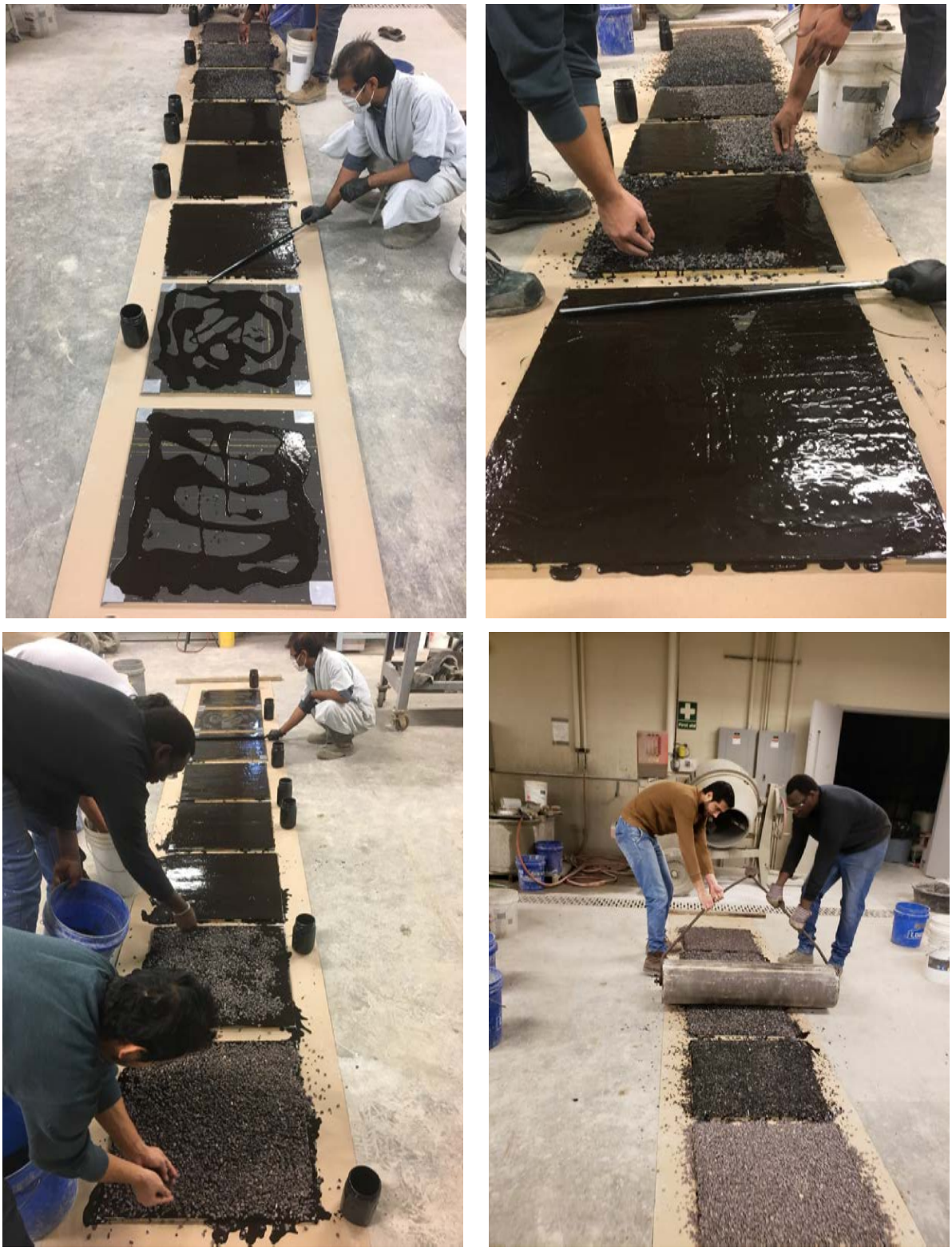

Fig. A.2 – 2 ft by 2 ft chip seal specimens' preparation.

Fig. A.3 – 2 ft by 2 ft chip seal specimens.

Fig. A.4 – 8 ft by 4 ft chip seal specimens' preparation.

Appendix B: SWTS Test Results for Phase I, II, and III

B.1. Phase I SWTS Test Results

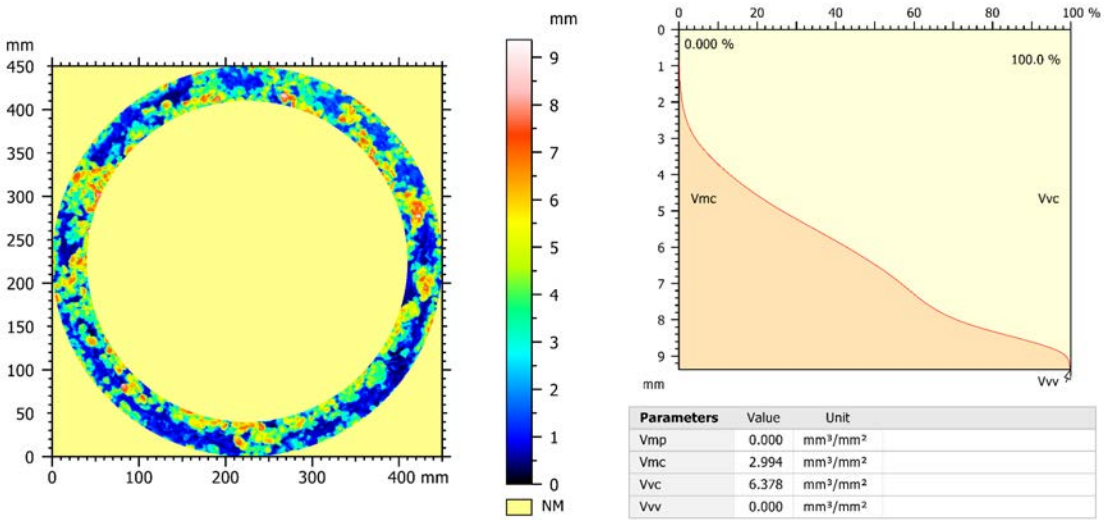

Parameters	Value	Unit
Vmp	0.000	mm³/mm²
Vmc	2.994	mm³/mm²
Vvc	6.378	mm³/mm²
Vvv	0.000	mm³/mm²

(a)

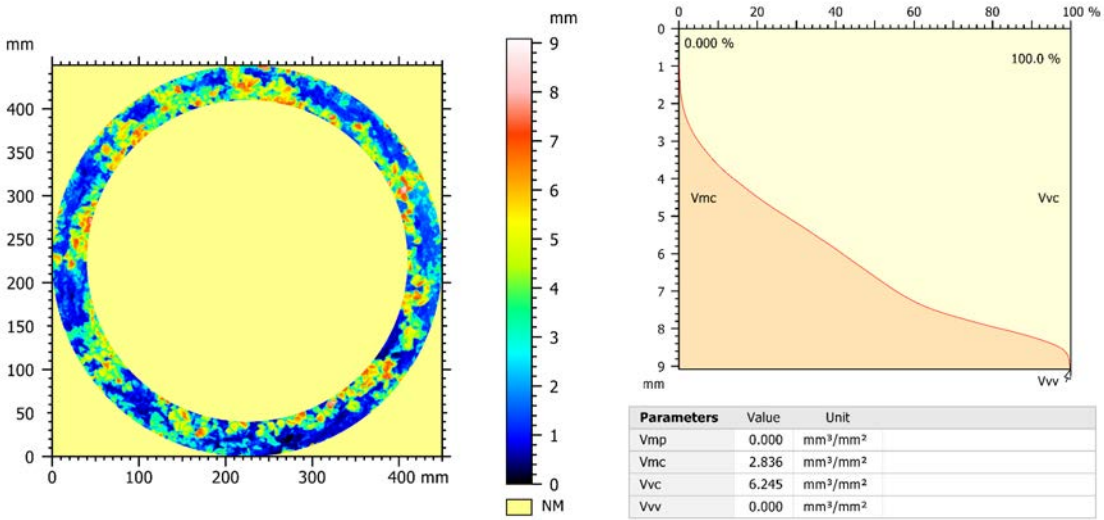

Parameters	Value	Unit
Vmp	0.000	mm³/mm²
Vmc	2.836	mm³/mm²
Vvc	6.245	mm³/mm²
Vvv	0.000	mm³/mm²

(b)

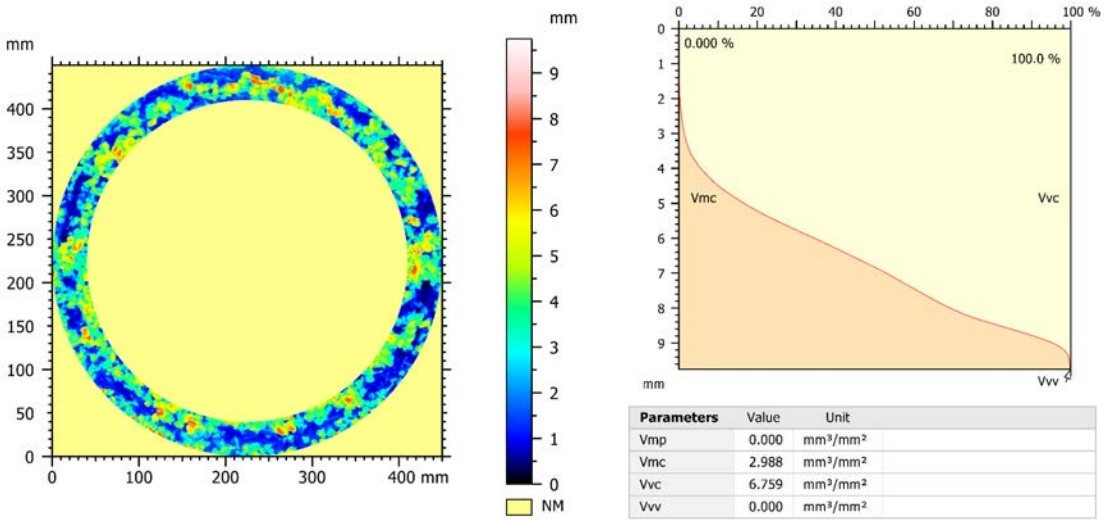

(c)

Fig. B.1 – Phase I SWTS test results for trap rock chip seal specimens with 0.25 gal/yd^2 binder rate (a)100T25E, (b) 75T25E, and (c) 50T25E.

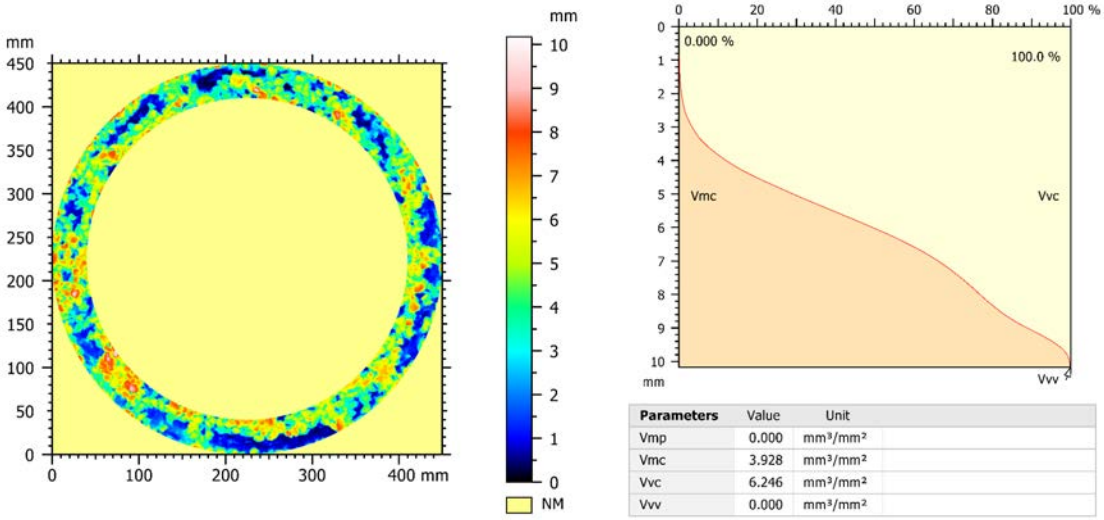

(a)

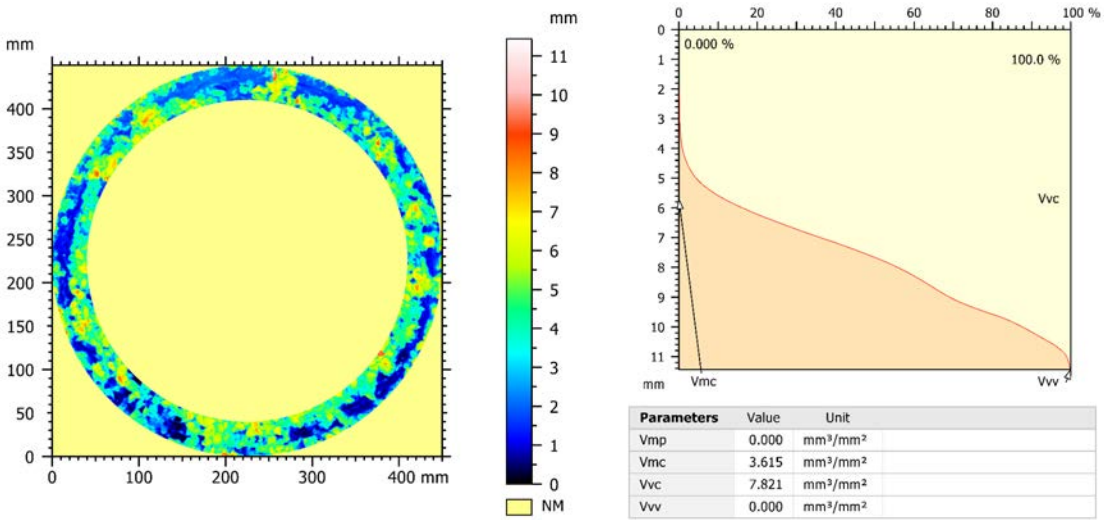

(b)

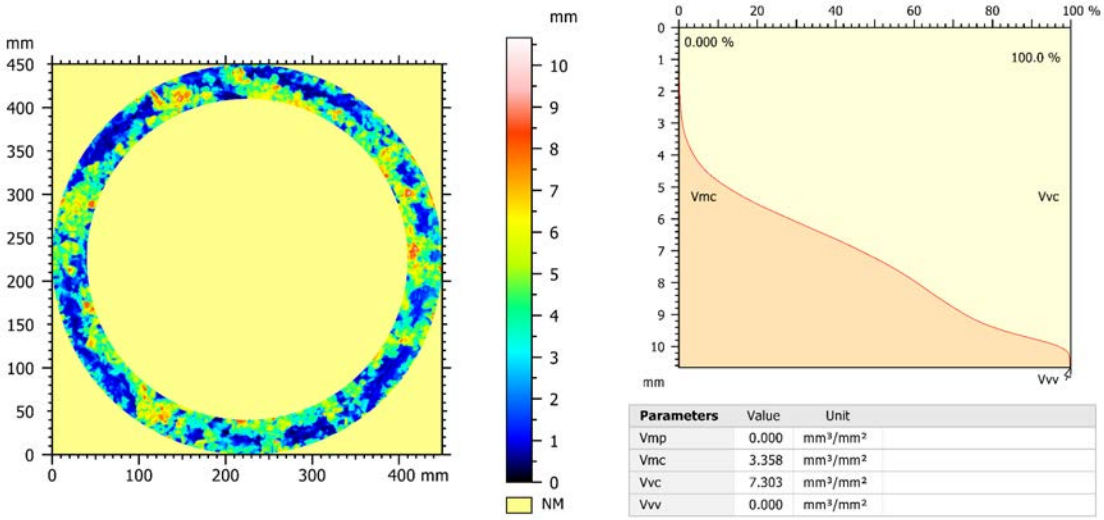

(c)

Fig. B.2 – Phase I SWTS test results for trap rock chip seal specimens with 0.50 gal/yd^2 binder rate (a)100T50E, (b) 75T50E, and (c) 50T50E.

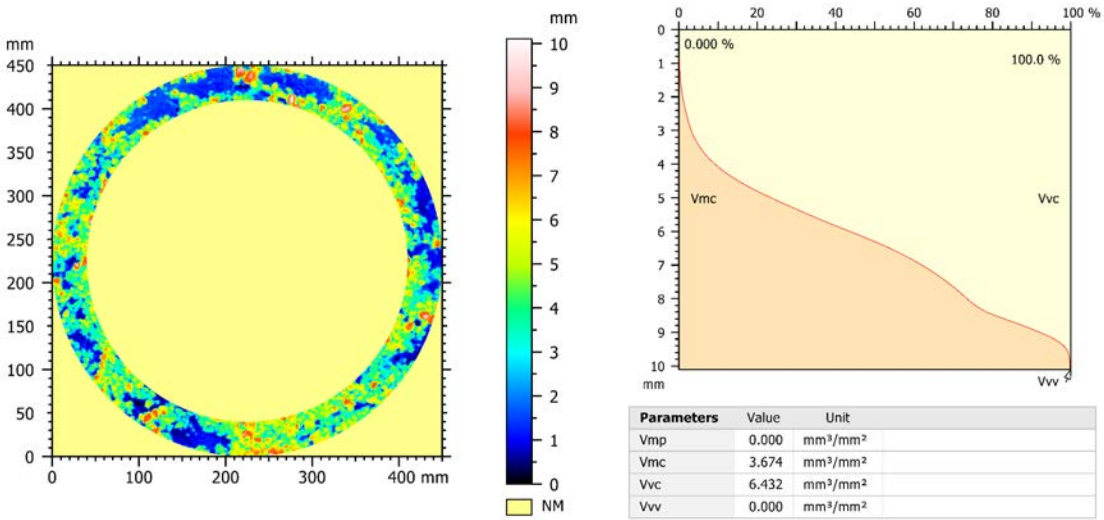

Parameters	Value	Unit
Vmp	0.000	mm³/mm²
Vmc	3.674	mm³/mm²
Vvc	6.432	mm³/mm²
Vvv	0.000	mm³/mm²

(a)

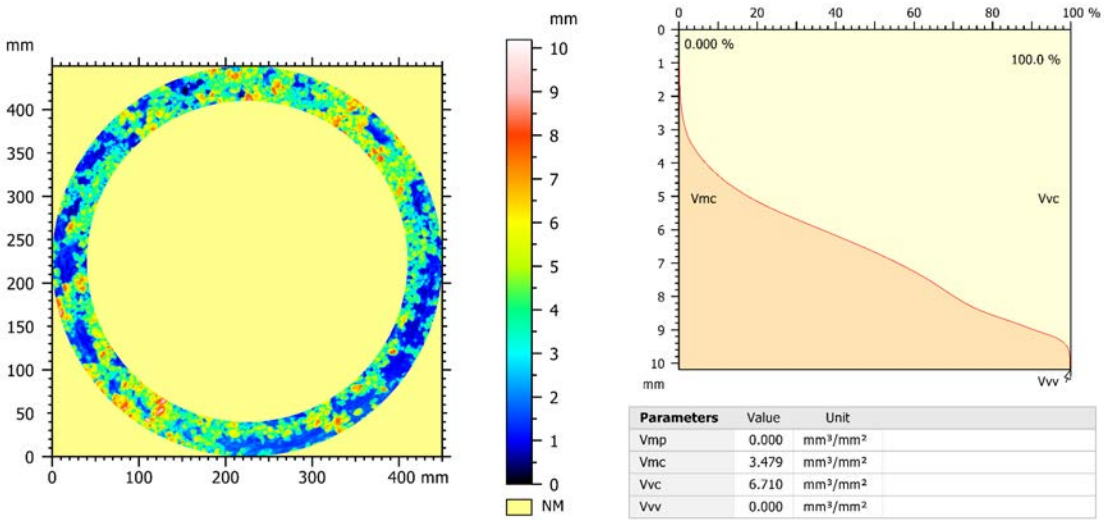

Parameters	Value	Unit
Vmp	0.000	mm³/mm²
Vmc	3.479	mm³/mm²
Vvc	6.710	mm³/mm²
Vvv	0.000	mm³/mm²

(b)

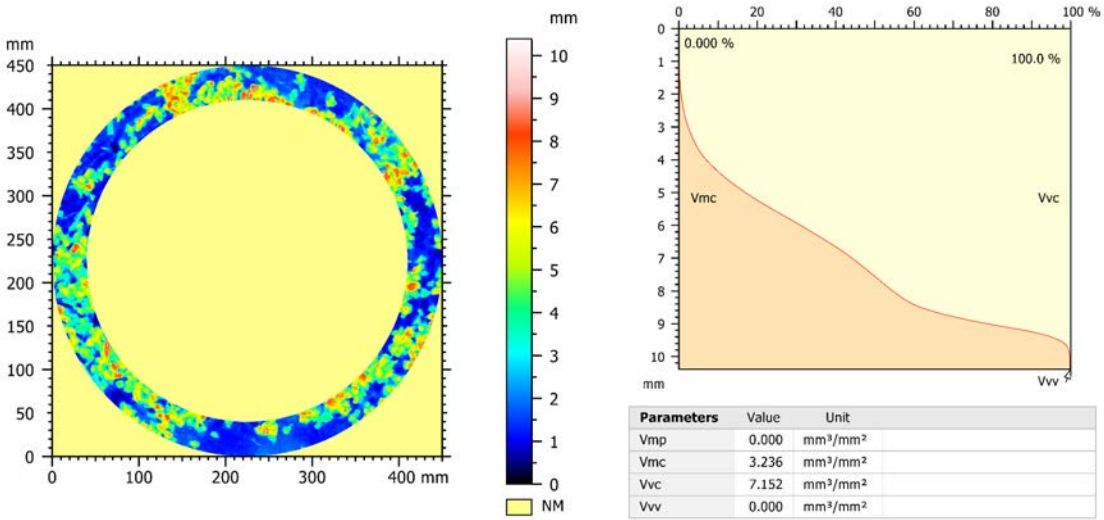

(c)

Fig. B.3 – Phase I SWTS test results for creek gravel chip seal specimens with 0.25 gal/yd^2 binder rate (a)100C25E, (b) 75C25E, and (c) 50C25E.

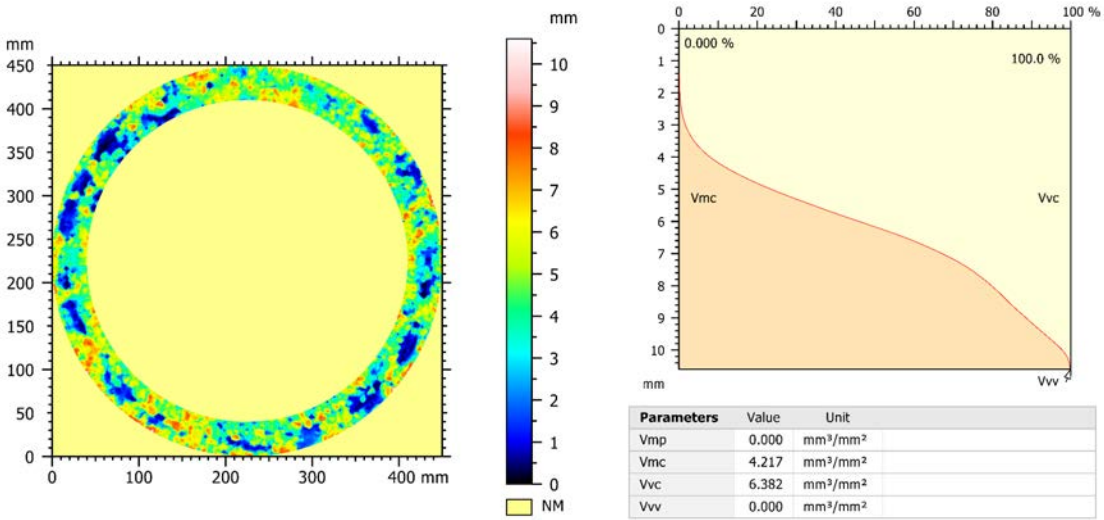

(a)

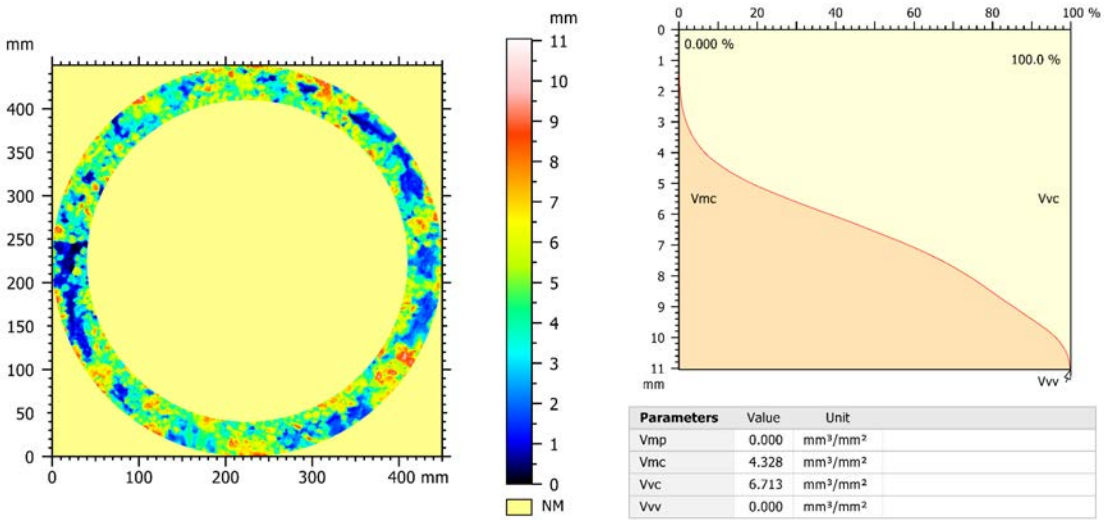

(b)

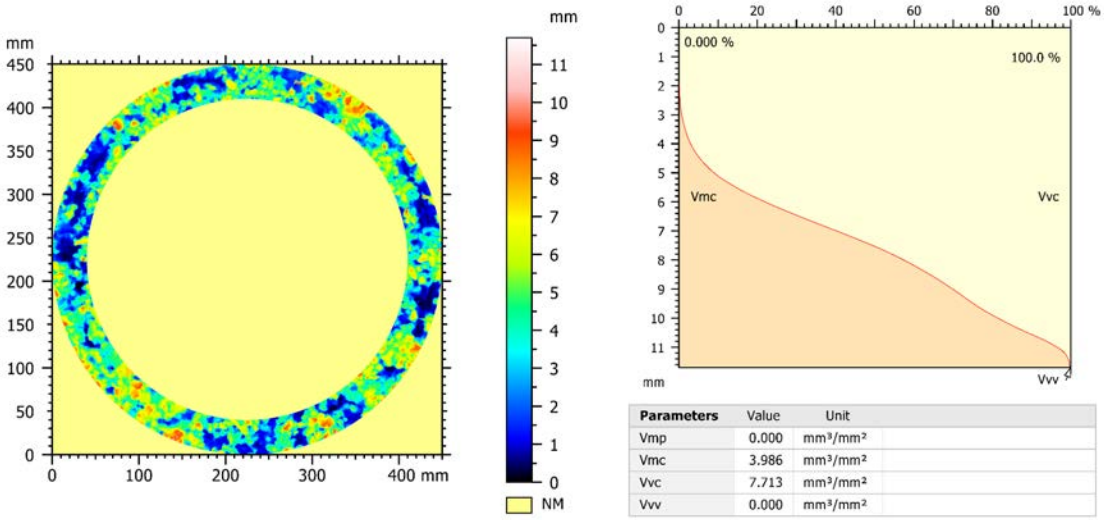

(c)

Fig. B.4 – Phase I SWTS test results for creek gravel chip seal specimens with 0.50 gal/yd^2 binder rate (a)100C50E, (b) 75C50E, and (c) 50C50E.

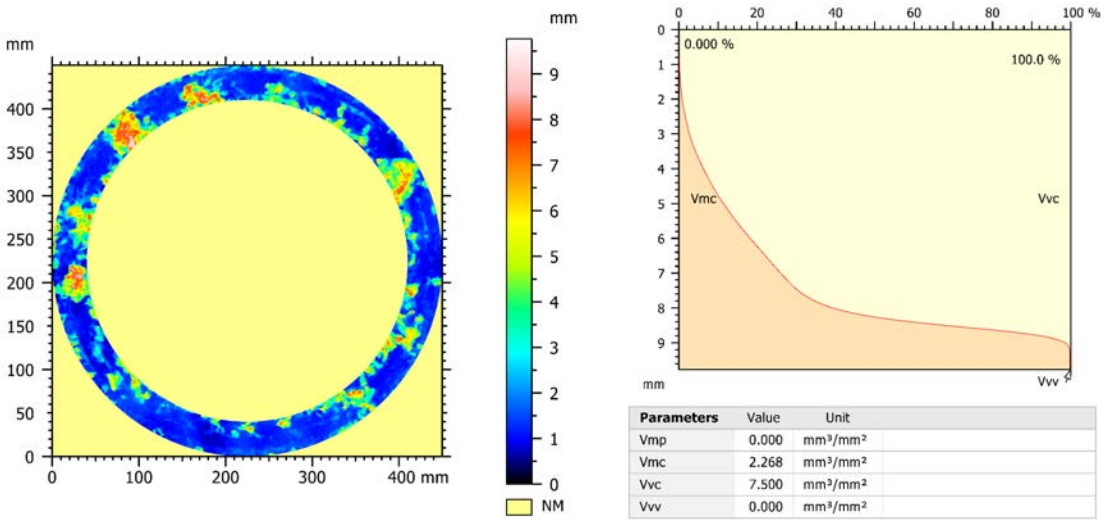

(a)

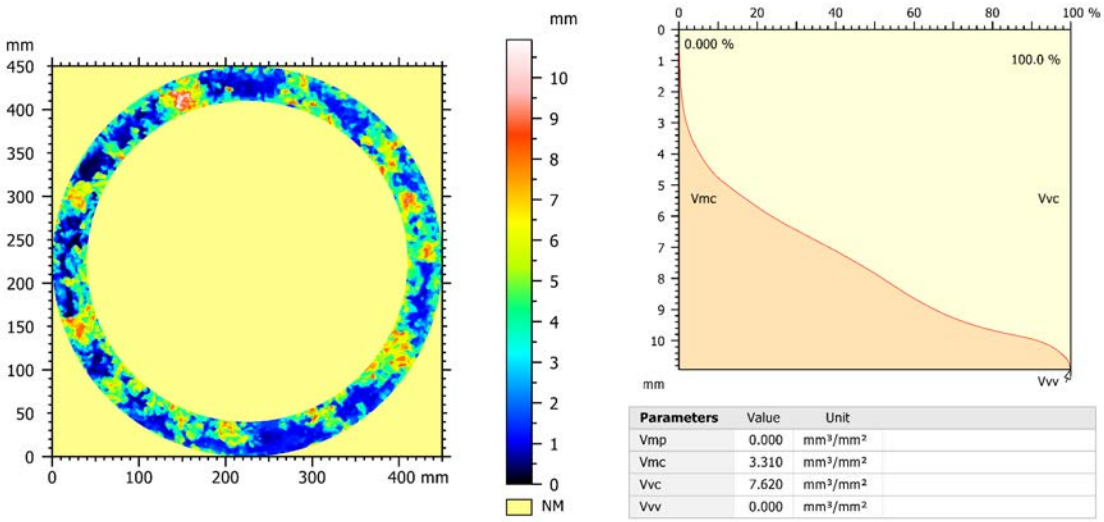

(b)

Fig. B.5 – Phase I SWTS test results for crumb rubber chip seal specimens with (a) 0.25 gal/yd^2, and (b) 0.50 gal/yd^2 binder rate.

B.2. Phase II SWTS Test Results

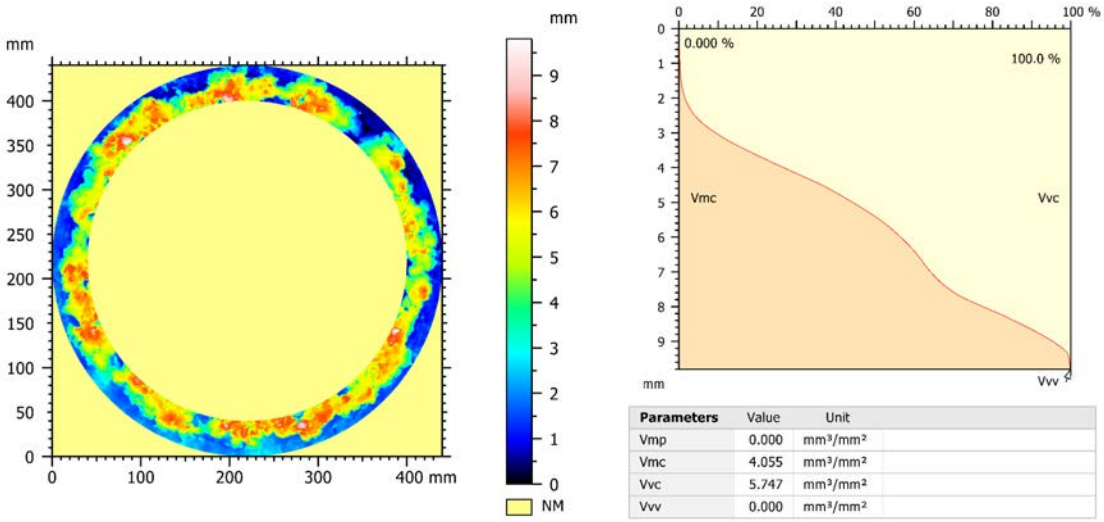

Parameters	Value	Unit
Vmp	0.000	mm³/mm²
Vmc	4.055	mm³/mm²
Vvc	5.747	mm³/mm²
Vvv	0.000	mm³/mm²

(a)

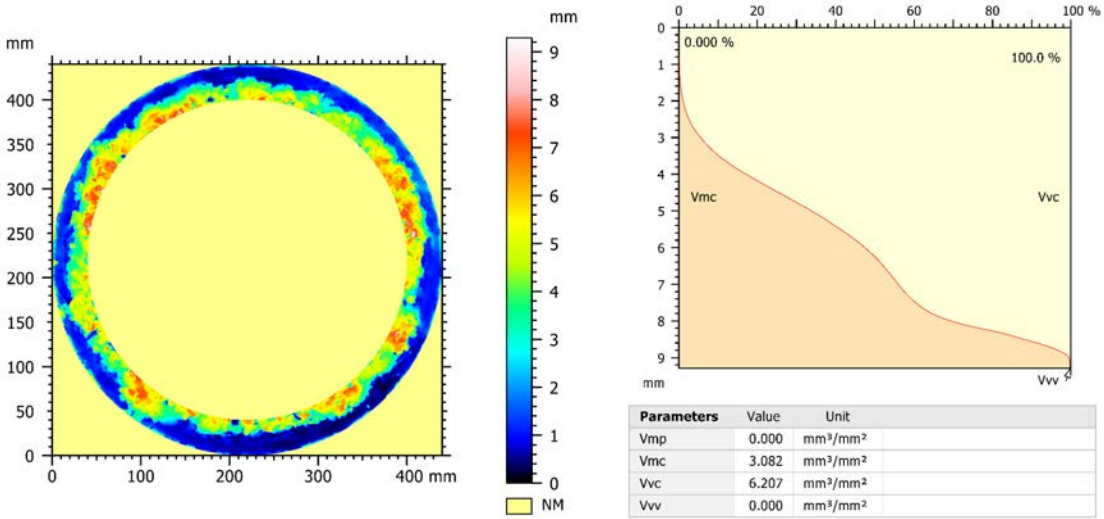

Parameters	Value	Unit
Vmp	0.000	mm³/mm²
Vmc	3.082	mm³/mm²
Vvc	6.207	mm³/mm²
Vvv	0.000	mm³/mm²

(b)

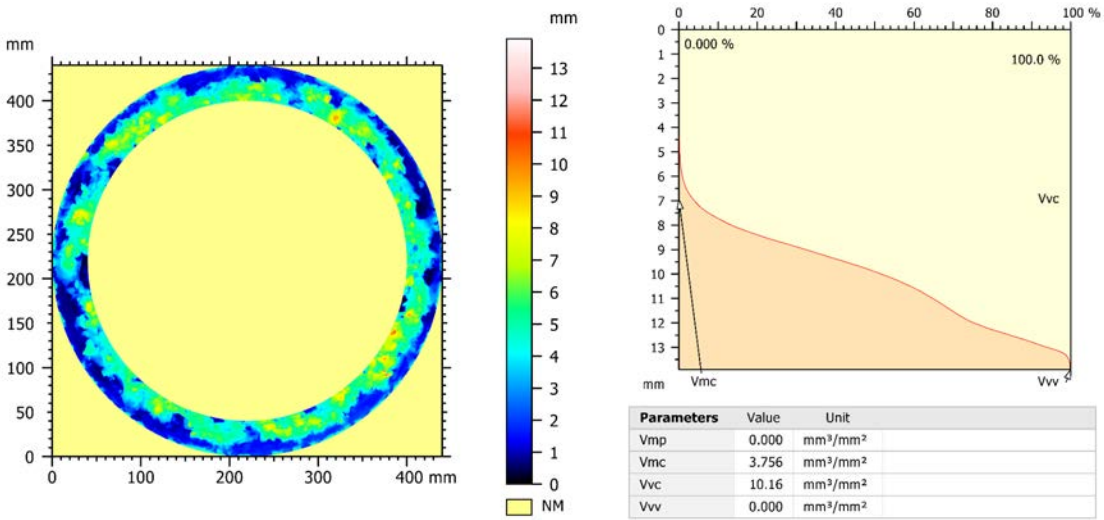

(c)

Fig. B.6 – Phase II SWTS test results for trap rock specimens with 0.50 gal/yd^2. (a) W100T, (b) W75T, (c) W50T, and (d) W100R.

B.2. Phase II SWTS Test Results

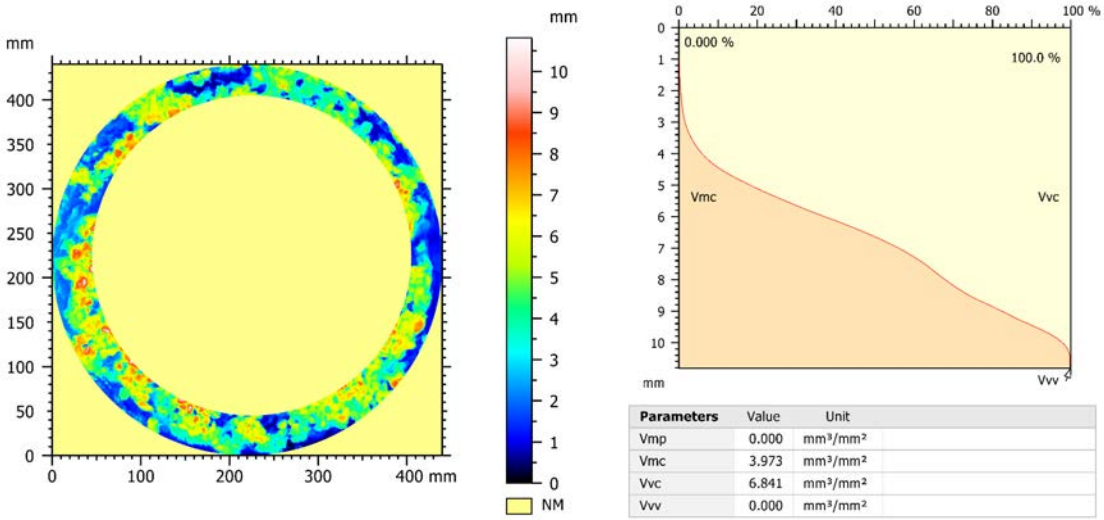

Parameters	Value	Unit
Vmp	0.000	mm³/mm²
Vmc	3.973	mm³/mm²
Vvc	6.841	mm³/mm²
Vvv	0.000	mm³/mm²

(a)

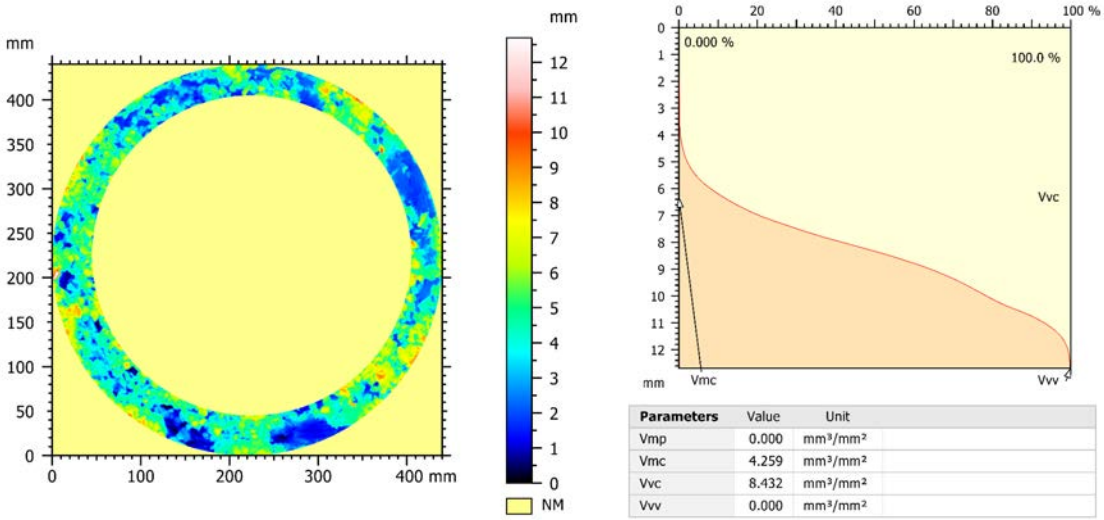

Parameters	Value	Unit
Vmp	0.000	mm³/mm²
Vmc	4.259	mm³/mm²
Vvc	8.432	mm³/mm²
Vvv	0.000	mm³/mm²

(b)

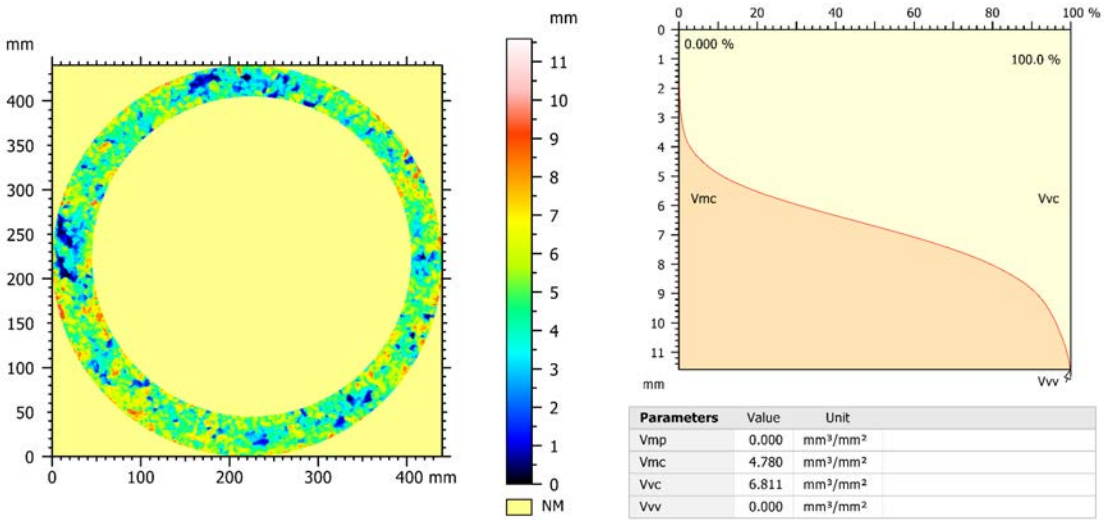

(c)

Fig. B.7 – Phase III SWTS test results for trap rock specimens with 0.50 gal/yd^2. (a) S100T, (b) S75T, (c) S50T, and (d) S100R.

Appendix C: Hybrid Traffic-Temperature effect SWTS test results

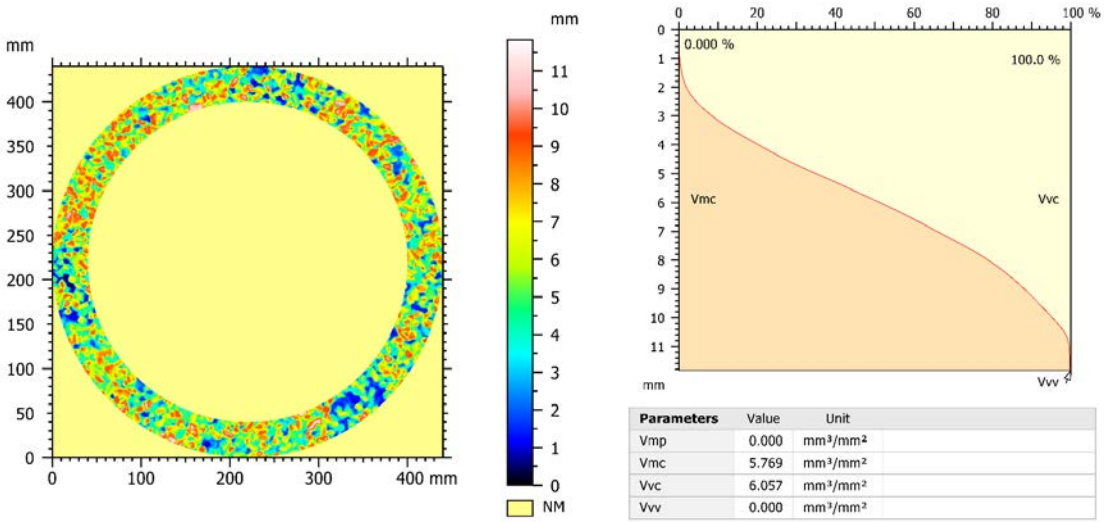

Parameters	Value	Unit
Vmp	0.000	mm³/mm²
Vmc	5.769	mm³/mm²
Vvc	6.057	mm³/mm²
Vvv	0.000	mm³/mm²

(a)

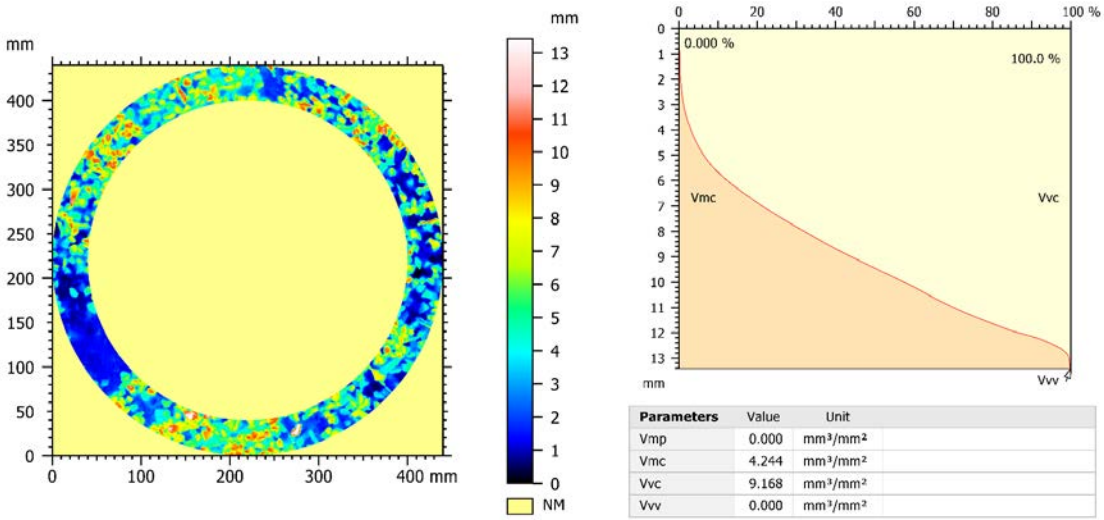

Parameters	Value	Unit
Vmp	0.000	mm³/mm²
Vmc	4.244	mm³/mm²
Vvc	9.168	mm³/mm²
Vvv	0.000	mm³/mm²

(b)

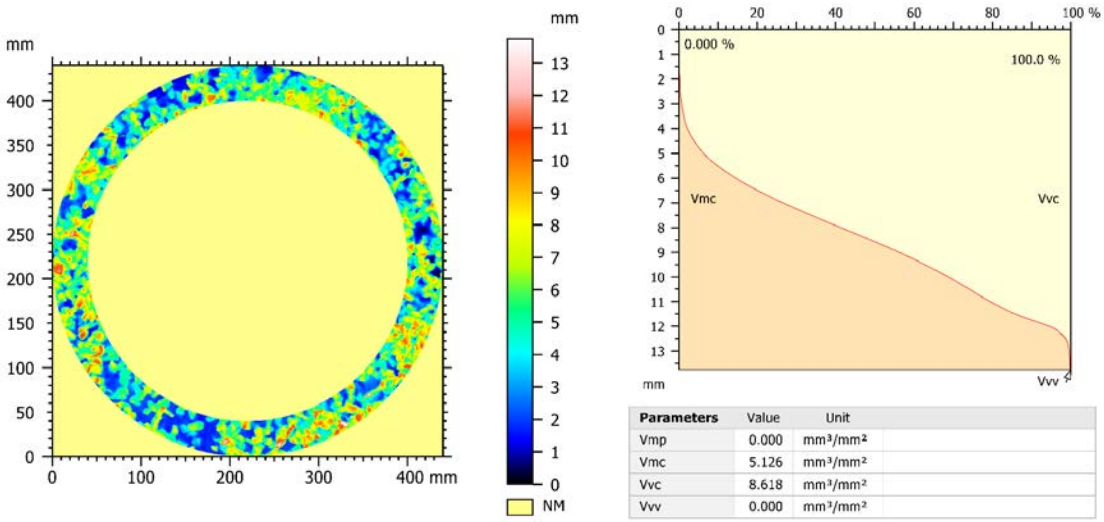

(c)

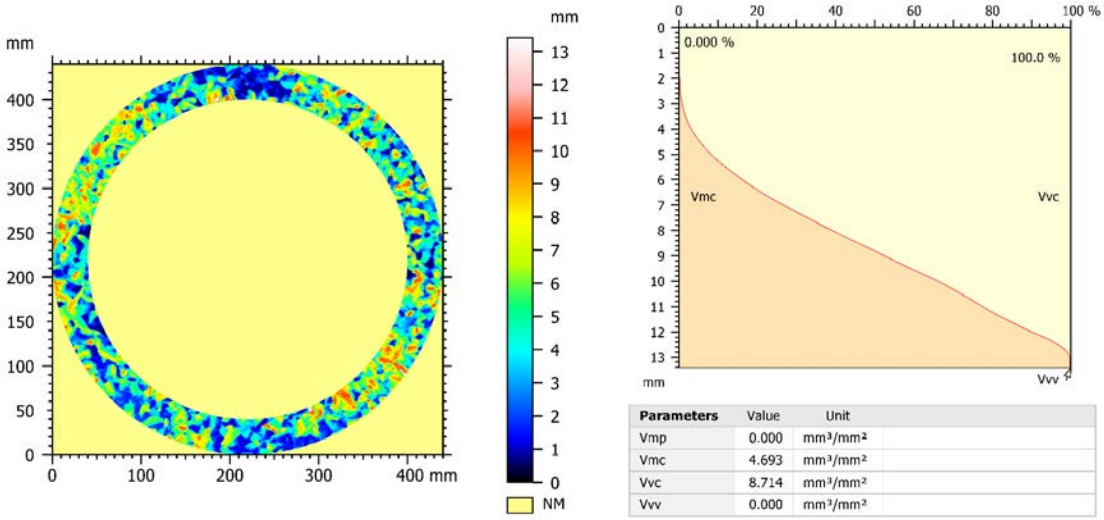

(d)

Fig. C1 – Low temperature SWTS test results after 40,000 wheel applications for (a) L100T, (b) L75T, (c) L50T, and (d) L100R.

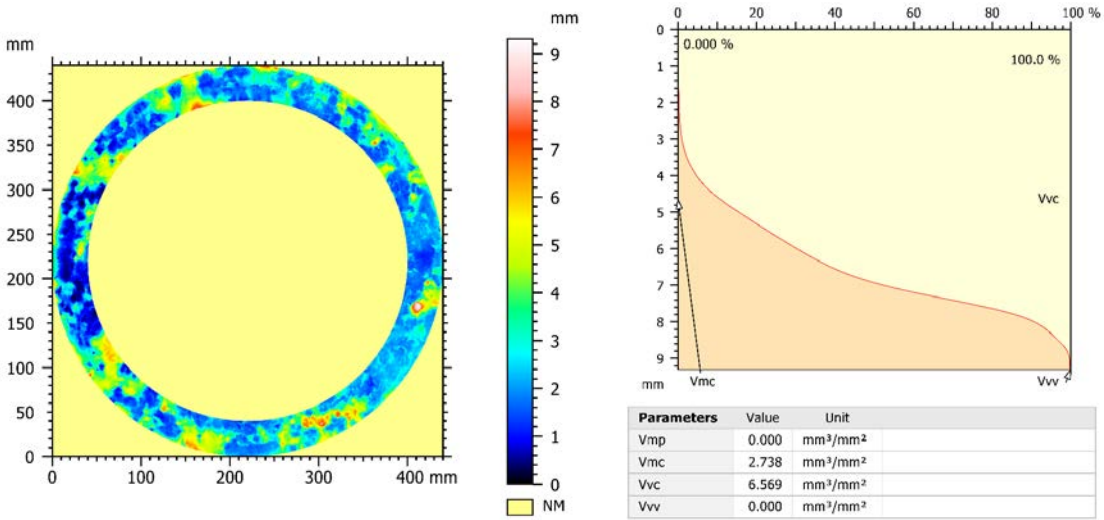
mm
400
350
300
250
200
150
100
50
0
0
100
200
300
400 mm
mm
9
8
7
6
5
4
3
2
1
0
NM
0
20
40
60
80
100 %
0.000 %
100.0 %
Vvc
Vmc
Vvv
mm
Parameters Value Unit
Vmp 0.000 mm³/mm²
Vmc 2.738 mm³/mm²
Vvc 6.569 mm³/mm²
Vvv 0.000 mm³/mm²

(a)

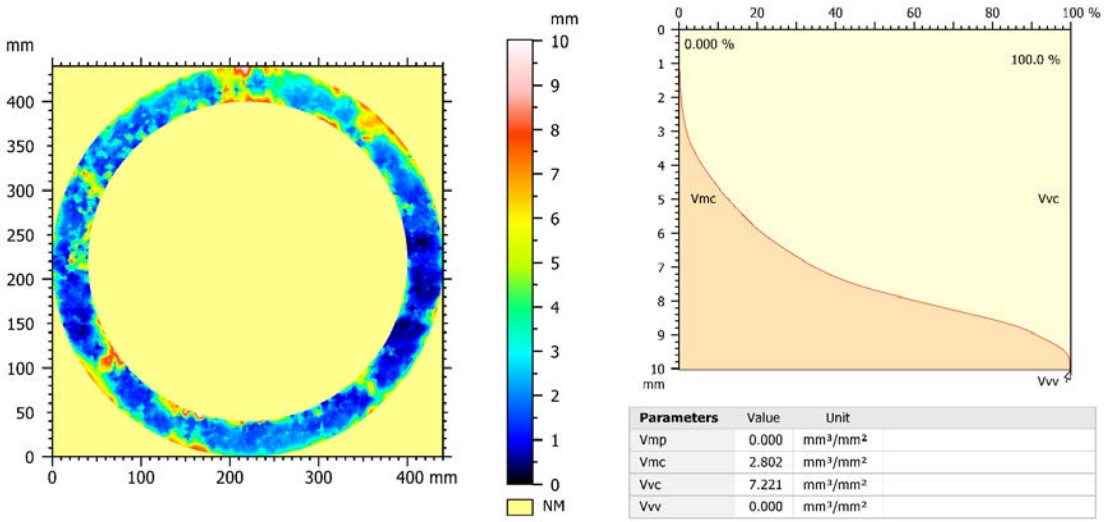
mm
400
350
300
250
200
150
100
50
0
0
100
200
300
400 mm
mm
10
9
8
7
6
5
4
3
2
1
0
NM
0
20
40
60
80
100 %
0.000 %
100.0 %
Vmc
Vvc
Vvv
mm
Parameters Value Unit
Vmp 0.000 mm³/mm²
Vmc 2.802 mm³/mm²
Vvc 7.221 mm³/mm²
Vvv 0.000 mm³/mm²

(b)

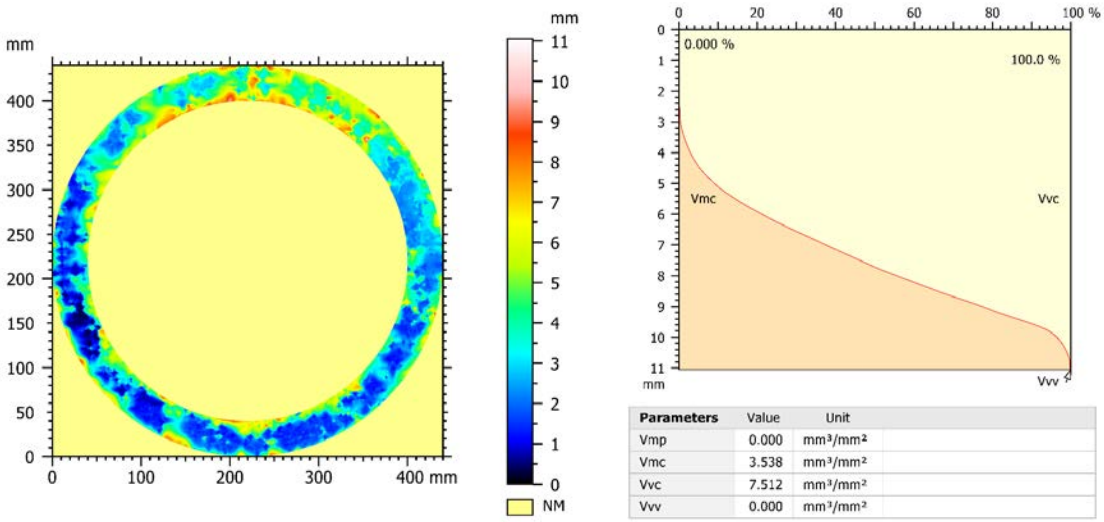

(c)

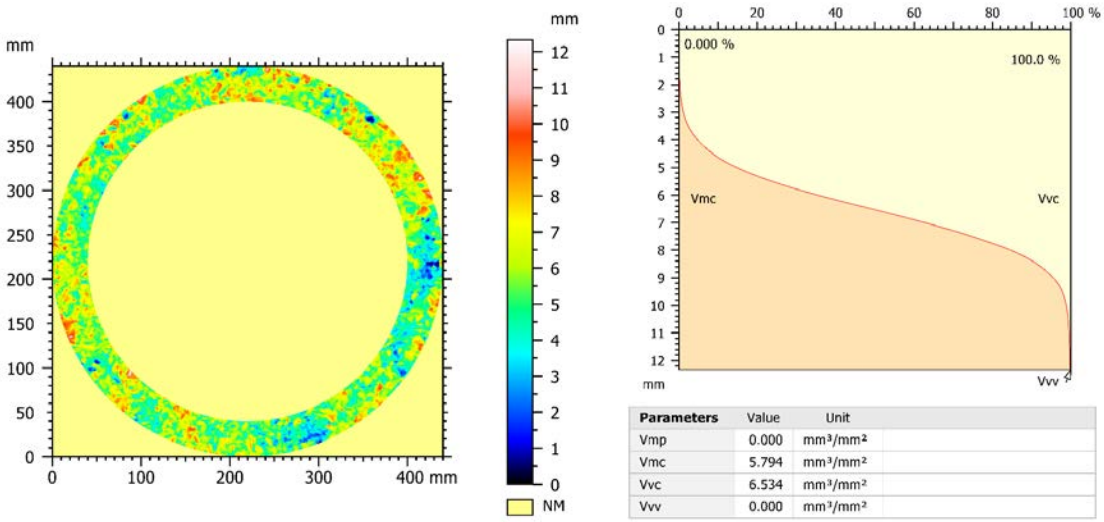

(d)

Fig. C2 – High temperature SWTS test results after 3,000 wheel applications for (a) H100T, (b) H75T, (c) H50T, and (d) R100T.

Appendix D: Rainfall Simulation Test Results

Table D.1 – Total Water Depth Readings for Rainfall Simulation Test with 0.5% Slope

Specimen ID	Intensity (in/hr)	TWD Readings (mm)									TWD Average (in)
0R0.25B	3	6.0	6.0	4.0	4.0	5.0	3.5	6.0	4.5	3.5	0.20
		6	6	4	7.5	7.5	5.5	6	4.5	3	
	6	7	6.5	5	6	8.5	4	6.5	6	4.5	0.25
		8	7	4.5	7	8.5	6.5	7	7	4	
	9	7.5	8	6.5	8	8	7.5	8	7	6	0.29
		8.5	8	7	8.5	7.5	5.5	8.5	7.5	6.5	
	12	8.5	8.5	8	9.5	8	7	8.5	7	7	0.33
		9	8	7	9.5	10	7	10	9.5	7	
	15	9	10	9	8.5	7	9.5	10	8	8	0.35
		10	9.5	8.5	9.5	10.5	8.5	10	8.5	7.5	
	18	9.5	9.5	8	10.5	9.5	8.5	9.5	8	8	0.36
		11	10	8	10.5	9.5	8	10.5	9.5	7.5	
0R0.50B	3	6.5	5	7	6	7	5	4	5.5	6.5	0.24
		6.5	5.5	9	6.5	6	8	6	7	5	
	6	9	8	9	6	8	8.5	7	8.5	7.5	0.31
		8.5	7	10.5	6.5	7	9	7.5	7.5	7.5	
	9	10	8	10.5	9	8	11	6.5	8	8.5	0.34
		8.5	8	9	8	8	10.5	7	8	8.5	
	12	10	8.5	8	8.5	8	9.5	7.5	8.5	10	0.36
		9	10.5	8.5	10	9	10.5	9.5	8	9.5	
	15	9	9	9	10	10.5	11	10.5	10	10.5	0.37
		9.5	9	9.5	8.5	9	10	10	9.5	10	
	18	10	10.5	9	10	8.5	11	9.5	8	10	0.38

Table D.1 (continued) – Total Water Depth Readings for Rainfall Simulation Test with 0.5% Slope

Specimen ID	Intensity (in/hr)	TWD Readings (mm)									TWD Average (in)
25R0.25B	3	5.5	4	4	5	4	3.5	4.5	4.5	5.5	0.17
		4.5	4	4	4.5	4	4	5	4	5	
	6	7.5	6	6.5	6.5	6	7	7	6.5	7	0.26
		7.5	6	7	6.5	5	7	7.5	6	7	
	9	6	7	6.5	7	6.5	7	7.5	7	7.5	0.28
		8	7	7	7	6	6.5	9	7	8.5	
	12	6.5	7.5	7.5	7.5	6.5	7	8	7.5	9.5	0.29
		7.5	7.5	7.5	7.5	6.5	6.5	8	7.5	8	
	15	8.5	8	6.5	7	7	6.5	8.5	8	8.5	0.31
		8	8	8	8	7	7.5	8.5	8	9	
	18	8	8	8.5	9	7	9	9.5	8	8.5	0.33
		8.5	8	8	8.5	7	8.5	9	8	9.5	
25R0.50B	3	4.5	6	6	5	5	6.5	5	5	6	0.21
		4	8	5.5	6	6	6	5	4.5	4	
	6	6	9	6	6.5	7	7.5	5	5	6.5	0.26
	9	8	9	9	9	8	7	8	8	7	0.32
		9.5	9	9.5	9	7	7.5	8	7	6.5	
	12	7	10	7.5	8	8	9	8	9	7	0.32
	15	9	10	8.5	10	9	8.5	9	8.5	8.5	0.35
	18	10.5	8	10	10.5	8	10	10	9	7	0.36
	21	9	10	9.5	12.5	9	8.5	11	8	10	0.38
50R0.25B	3	5	4	5	5	4	3	3	3	2	0.15
	6	6	5	4	7	5	7	5	6	6	0.22
	9	6	8	9	9	8	8	6	6	5	0.28
		6	8	9.5	6	7.5	8	5	6	7	
	12	9	6	10	7	8	7	7	7	5	0.29
	15	8	8	11	9	8	8	6	4	5.5	0.30
50R0.50B	3	2.5	5	8	3.5	4	5	6.5	5	4.5	0.19
	6	3.5	4	9	5	5.5	8.5	8	4.5	6.5	0.24
	9	1.5	6	8.5	6	6	9.5	8.5	6	6.5	0.26
	12	6	9	9	6.5	8	9.5	9	7	8	0.31
	15	6	8	8.5	7	8	10	8	9	8.5	0.32

Table D.1 (continued) – Total Water Depth Readings for Rainfall Simulation Test with 0.5% Slope

Specimen ID	Intensity (in/hr)	TWD Readings (mm)									TWD Average (in)
100R0.25B	3	6	6	3	6.5	4	4	7	3.5	4	0.19
	6	6	4	4	8	6	7	7	3.5	6.5	0.23
	9	8	4	4	7	6	7	7.5	5	6	0.24
	12	10	7	5	8	6.5	8	8	7.5	7	0.29
	15	11	8.5	6	10	8	7.5	9.5	8	6.5	0.33
100R0.50B	3	7	7.5	6	6.5	6.5	8	6	4	5	0.25
	6	8	10	6.5	8.5	8	8.5	8	4.5	5	0.29
	9	8.5	8.5	7	8.5	7.5	6.5	8	6	7.5	0.30
	12	9.5	9	9.5	9.5	9.5	9.5	9	6	9.5	0.35
	15	9.5	10	9	10.5	9	10	9.5	7	8.5	0.36

Table D.2 – Total Water Depth Readings for Rainfall Simulation Test with 1.5% Slope

Specimen ID	Intensity (in/hr)	TWD Readings (mm)									TWD Average (in)
0R0.25B	3	4	2	2	4	5	3	3.5	3.5	2	0.12
		4	2.5	1.5	4	4.5	2.5	3.5	3.5	2	
	6	4.5	4	4	6	6	3	6.5	5	3.5	0.17
		3	3	2.5	4	7	4	5.5	4.5	4	
	9	5	5	4	6	6.5	5.5	6	5.5	5	0.21
		5	5	4	5	7	4.5	6	6	4.5	
	12	6	5	4.5	8	6	6	5.5	6	5.5	0.23
	15	6	6	5.5	5.5	8	6	7	7	5.5	0.25
	18	5	5	5	6	9	5	5.5	6	5	0.23
		5	6	6	5	7	5	8.5	7	5.5	
0R0.50B	3	2.5	1.5	4.5	5.5	2.5	4.5	2	5.5	3.5	0.15
		4	2	4	4.5	2.5	5	4.5	4.5	5	
	6	6	2	6	6	4	6.5	4.5	5.5	6.5	0.21
		5	3.5	5.5	6	3.5	5	6	6	6.5	
	9	5.5	3	4.5	5.5	5	7	7.5	8	6	0.23
		6	3.5	5	6.5	4.5	7	6.5	6.5	7.5	
	12	6	4	6	7	6.5	7.5	6	6.5	6	0.24
		5.5	4	6	7	4.5	7.5	5	7.5	6	
	15	6	4	6	7	7.5	8	6	8	8	0.26
		6	3	6	7.5	5.5	8	8.5	6.5	5.5	
	18	6.5	3.5	5	7	5.5	8	6	9	7.5	0.26
		6	4	6	7.5	8	8.5	5	9.5	7	
25R0.25B	3	4	2	3	3.5	3	4	5	2	4.5	0.14
		4	2.5	2.5	4.5	3	4	6.5	2.5	4	
	6	5.5	4	5	5.5	4	5	7	5	5.5	0.20
		5.5	4	5	6.5	3.5	5	6	4	5	
	9	6	5	5.5	7	5	6.5	6.5	5	5	0.23
		7	5	5	6.5	5	6.5	7.5	5	6.5	
	12	6.5	5	4.5	6.5	5	6	7.5	5	8	0.24
		6.5	6	5.5	7	5	7	6.5	6	6.5	
	15	6.5	6	6	8.5	6	7	7.5	6.5	6.5	0.25
		5.5	6	5	7	6	6.5	7.5	6	6.5	
	18	8	6	5.5	7	6	7	9.5	6	6.5	0.27
		7.5	6	6.5	7.5	6.5	7	7.5	7	8	

Table D.2 (continued) – Total Water Depth Readings for Rainfall Simulation Test with 1.5% Slope

Specimen ID	Intensity (in/hr)	TWD Readings (mm)									TWD Average (in)
25R0.50B	3	1.5	4	1	3.5	4.5	4	3	4	5	0.13
	6	3	4	1.5	4	6	6	4	5	4.5	0.17
		3	4	2.5	4	3.5	6	4.5	6	6.5	
	9	3.5	5.5	4.5	4	7	5	4	6.5	6	0.20
	12	3.5	5	6	4.5	5.5	6.5	4.5	5	6	0.20
	15	4.5	8	5	6	6	6.5	7	8	7	0.25
	18	5.5	6.5	6	6	7.5	8	7	9	8.5	0.28
50R0.25B	3	2	3	2	2	4	3	4	3	2	0.11
	6	3	5	4	3	6	4	4	4	4	0.16
	9	5	7	7	6	5	4	4	3	3	0.20
		5	7	8	6	6	6	3	5	3	
	12	8	7	7	6	6	5	5	6	5	0.24
	15	8	7	6	7	6	6	6	5	7	0.25
50R0.50B	3	1	3.5	4.5	5	4	4.5	4.5	4	4.5	0.16
	6	3	5	3	4.5	4.5	5	6	5.5	5	0.18
	9	3.5	5	5.5	6	5	5	6.5	6	5	0.21
	12	4	5	6	5	5	5.5	5.5	7	7	0.22
	15	5	6.5	4.5	4.5	6	7	3.5	5.5	8	0.22
100R0.25B	3	3.5	4	1.5	5.5	5.5	2.5	4.5	3	5	0.15
	6	3.5	5	0	5.5	5.5	3.5	4.5	4	5.5	0.16
	9	4	5	3	6	3	5	5	3	5	0.17
	12	3	4.5	5	7.5	5	6	7.5	4.5	6	0.21
	15	4	7.5	6	8	8	7	7.5	6.5	7	0.27
100R0.50B	3	5	4.5	1	5	4	5	3	3.5	1.5	0.14
	6	4	4	1	5.5	4	4.5	5.5	3.5	1.5	0.15
	9	5	4.5	1	5.5	5	4.5	5.5	3.5	4	0.17
	12	4	4	3	5.5	7	6	5.5	5	5.5	0.20
	15	5	5	5.5	4.5	6	6	5.5	6	6.5	0.22

Table D.3 – Total Water Depth Readings for Rainfall Simulation Test with 2.5% Slope.

Specimen ID	Intensity (in/hr)	TWD Readings (mm)									TWD Average (in)
0R0.25B	3	2.5	1.5	1.5	3	3.5	2.5	3	3.5	2.5	0.11
		2	2.5	2.5	2.5	3.5	3	3	3.5	3	
	6	3	3.5	3	4.5	4.5	4	4	4.5	4	0.15
	9	5	3.5	2.5	4	6.5	4.5	6.5	5.5	3	0.18
	12	4	4	4	4	7	5.5	5.5	6.5	6	0.20
		3.5	5	3.5	6	5.5	6	6	5	6.5	
	15	4.5	4.5	4	4	6	5.5	7	7	6.5	0.21
	18	4	4.5	5	4	6	6	6.5	7.5	8.5	0.23
0R0.50B	3	3	1	3.5	3	3	4.5	4	5.5	5	0.14
	6	6	3	5	4.5	5	4	5	4	4.5	0.17
		5	3	3	5	4	5	5	5	4	
	9	6.5	3	5	5.5	4	5	6.5	6	5.5	0.20
		5.5	3	5.5	4.5	5	5	6	6	6	
	12	6.5	3	5	5.5	4	6.5	6	6	6.5	0.21
		6	3.5	5	6	5	6	5.5	6	6	
	15	6.5	2.5	5	6.5	6	6.5	7.5	7.5	6.5	0.23
		5	3	6	6	6.5	6.5	4.5	7.5	6.5	
	18	5	3.5	4	6.5	4.5	6.5	7	7	7.5	0.24
		6	3	5.5	6.5	4.5	7	8	6	7.5	
25R0.25B	3	3.5	2	2.5	3.5	2.5	3.5	5	2.5	4	0.12
		2.5	2	3	2.5	2.5	3	3	3	4.5	
		4	2.5	3	3.5	3.5	3.5	3.5	3	4	
	6	4	3.5	3	4.5	3	5	4	4	4	0.16
		4	3	3.5	4.5	3.5	4	5	4	5	
	9	6	3.5	4	5	4.5	5.5	8	4	5	0.20
		4.5	4	4.5	5	4.5	5	6.5	4.5	5.5	
	12	5.5	5	4	6	5	5.5	8	5	5	0.21
		5.5	4	5	6	5	5	6.5	5	5.5	
	15	5.5	5	5	5	6.5	5.5	7.5	5	7.5	0.23
		6	5	5	6	5	6.5	8	5	5	
	18	6	5	6	6.5	6	5.5	8.5	6.5	6.5	0.25
		6	5	5	7	5.5	6	8.5	6	7	

Table D.3 (continued) – Total Water Depth Readings for Rainfall Simulation Test with 2.5% Slope

Specimen ID	Intensity (in/hr)	TWD Readings (mm)									TWD Average (in)
25R0.50B	3	3	4	2.5	2.5	4.5	3.5	2.5	4	3.5	0.12
		1.5	3.5	2	2	2.5	4	3.5	4	3.5	
	6	1	3.5	1	3.5	4	5	4	4	4	0.13
		3	3.5	1	2.5	4	4	3	5	4.5	
	9	3	4.5	3.5	3	6	7	5	6	6	0.19
	12	3.5	5	4	3.5	6.5	8	5	7	5.5	0.21
	15	4	6	5	4	7	9	5	8	6	0.24
	18	4	6	4	4	8	8	6	8	8	0.24
50R0.25B	3	3	2.5	3	2	4.5	4	2.5	3	0	0.11
	6	5	4	4	2	4	5	1.5	3	2	0.13
	9	5	5	6	3.5	4.5	6	3	3.5	4	0.18
	12	5	6	8	4	6	7	3	4	3	0.20
	18	5	6	9	3	5	8	4	4	6	0.21
		6	7	6	5	5	7	3	4	4	
50R0.50B	3	0	4.5	2	0.5	5	4.5	4	4	4	0.12
	6	0.5	1	2	5	6	5	6	4	4	0.15
	9	0	3.5	5	4.5	6	4	6	6	4	0.17
	12	2.5	3.5	3.5	4.5	5	4.5	6.5	6	6.5	0.19
	15	4	4.5	4	7	6.5	6	5.5	6	5	0.21
100R0.25B	3	4	4	1	4.5	4	2	4	2.5	4.5	0.13
	6	3	4	1	4	4	5	5	3.5	6	0.16
	9	3.5	4	1	4.5	4	5.5	6.5	4	6.5	0.17
	12	2.5	5	4	5	6	5.5	6.5	4	6	0.19
	15	2.5	5	5	4.5	6	6.5	6.5	4.5	6	0.20
100R0.50B	3	3	3.5	0.5	3	3	3	4	2	2.5	0.11
	6	3	5	1	4.5	2	4	3	3.5	3	0.13
	9	3	4	4	5	3.5	4	5	3.5	5	0.16
	12	4	5	4.5	5	4	5	4	5	4	0.18
	18	5	5	5	5	5	5	6	4.5	5.5	0.20

Table D.4 – Mean Texture Depth Readings for Rainfall Simulation Test Specimens

Specimen ID	Spot #	Sand Patch Diameter (in)				Average Diameter (in)	Sand Volume (in3)	MTD (in)
0R0.25B	1	9.50	9.50	9.25	9.50	9.27	11.80	0.17
	2	9.38	9.25	9.25	9.00			
	3	9.25	9.00	9.25	9.00			
	4	9.50	9.25	9.38	9.50			
	5	9.50	9.00	9.38	8.88			
	6	8.88	9.25	9.50	9.25			
	7	9.50	9.00	9.25	9.50			
0R0.50B	1	9.75	9.38	9.50	9.75	9.89	11.80	0.15
	2	10.75	10.00	10.50	10.00			
	3	10.25	10.13	10.00	10.38			
	4	9.50	10.13	10.00	10.00			
	5	9.50	9.13	9.25	9.75			
	6	10.00	10.00	10.13	9.75			
	7	9.75	9.75	10.00	9.88			
25R0.25B	1	9.00	9.25	8.38	9.75	9.15	11.80	0.18
	2	9.75	9.25	9.00	9.50			
	3	9.25	8.75	9.25	8.88			
	4	9.25	9.13	9.25	9.00			
	5	9.00	9.00	9.00	9.25			
	6	8.88	9.25	9.25	9.00			
	7	9.25	9.13	9.00	9.50			
25R0.50B	1	9.75	10.25	9.88	9.75	9.70	11.80	0.16
	2	9.88	9.50	9.25	9.50			
	3	8.75	9.38	8.75	9.13			
	4	9.63	9.13	9.75	9.50			
	5	9.38	9.38	10.00	9.50			
	6	11.00	10.25	10.13	10.25			
	7	10.00	9.88	10.13	10.50			
	8	10.13	10.13	10.00	7.88			
50R0.25B	1	9.75	9.75	8.88	9.63	9.42	11.80	0.17
	2	9.13	9.75	9.13	9.00			
	3	9.75	9.00	9.00	9.75			
	4	9.50	9.00	9.75	9.00			
	5	9.75	9.25	9.13	9.63			
	6	9.38	9.50	9.50	9.25			
	7	9.50	10.00	9.75	9.50			

Table D.4 (continued) – Mean Texture Depth Readings for Rainfall Simulation Test Specimens

Specimen ID	Spot #	Sand Patch Diameter (in)				Average Diameter (in)	Sand Volume (in3)	MTD (in)
50R0.50B	1	9.13	10.00	9.75	9.75	9.87	11.80	0.15
	2	10.00	9.75	10.13	9.63			
	3	10.13	8.50	9.75	9.63			
	4	10.00	10.00	10.38	10.00			
	5	9.88	10.00	10.38	10.00			
	6	9.50	9.75	9.75	10.13			
	7	10.00	10.25	10.25	10.00			
100R0.25B	1	8.75	9.13	8.75	8.75	9.37	11.80	0.17
	2	9.00	8.88	9.00	9.00			
	3	9.25	10.00	9.75	9.38			
	4	9.13	9.50	9.75	8.88			
	5	9.75	9.63	9.75	9.00			
	6	9.50	9.88	9.50	9.63			
	7	10.13	9.25	9.63	9.75			
100R0.50B	1	8.75	9.50	8.50	9.50	8.75	11.80	0.20
	2	9.25	8.50	8.75	9.25			
	3	8.75	9.25	9.50	8.50			
	4	8.50	9.00	8.25	8.75			
	5	8.75	9.00	8.50	9.00			
	6	8.00	9.50	8.50	8.13			
	7	7.88	8.25	8.75	8.25			

Appendix E: Snowplowing Test Results

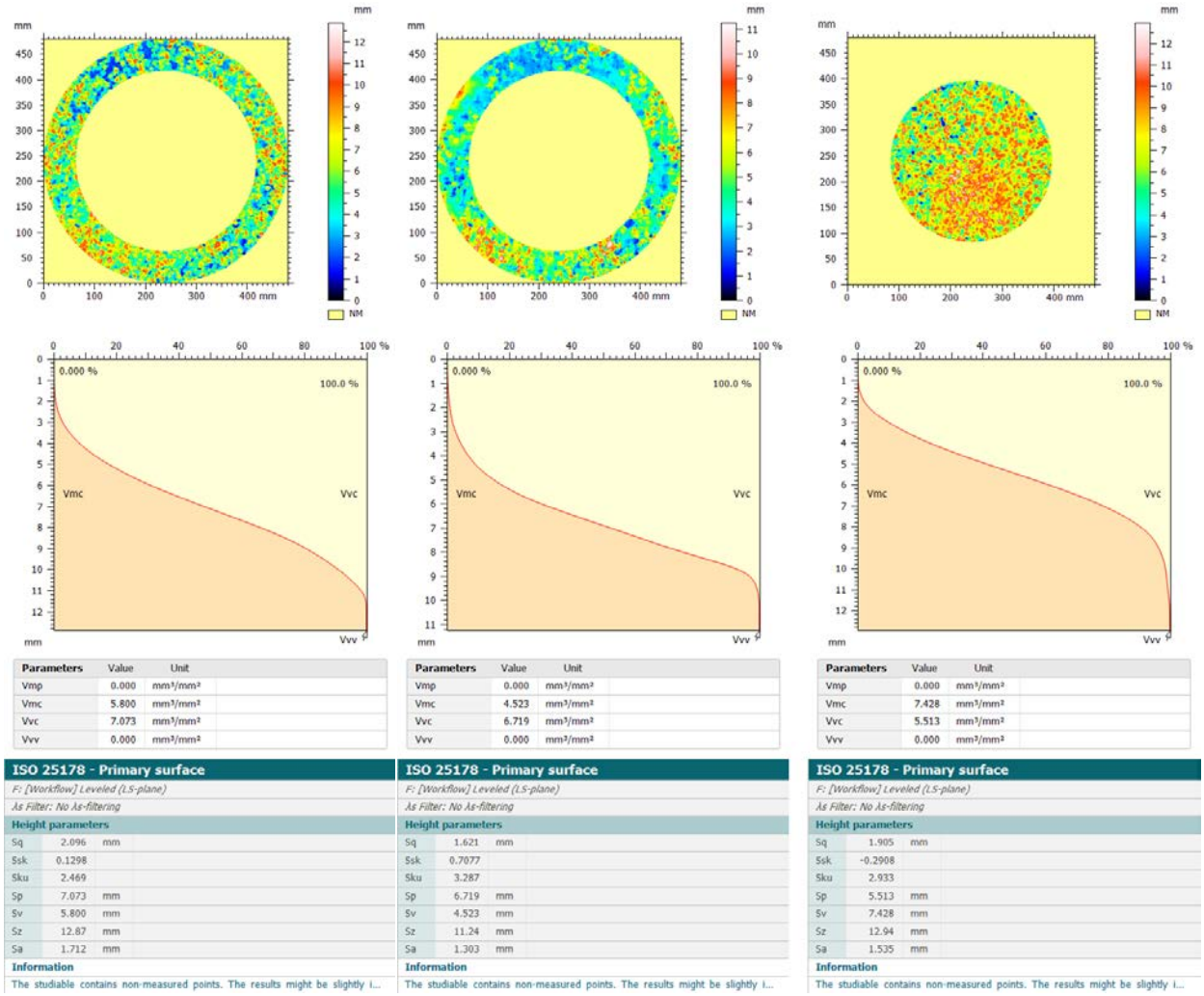

(a) (b) (c)

Fig. E.1 – 00R specimens surface analysis (a) after three snowplow applications, (b) after eight snowplow applications, and (c) outside the snowplow path.

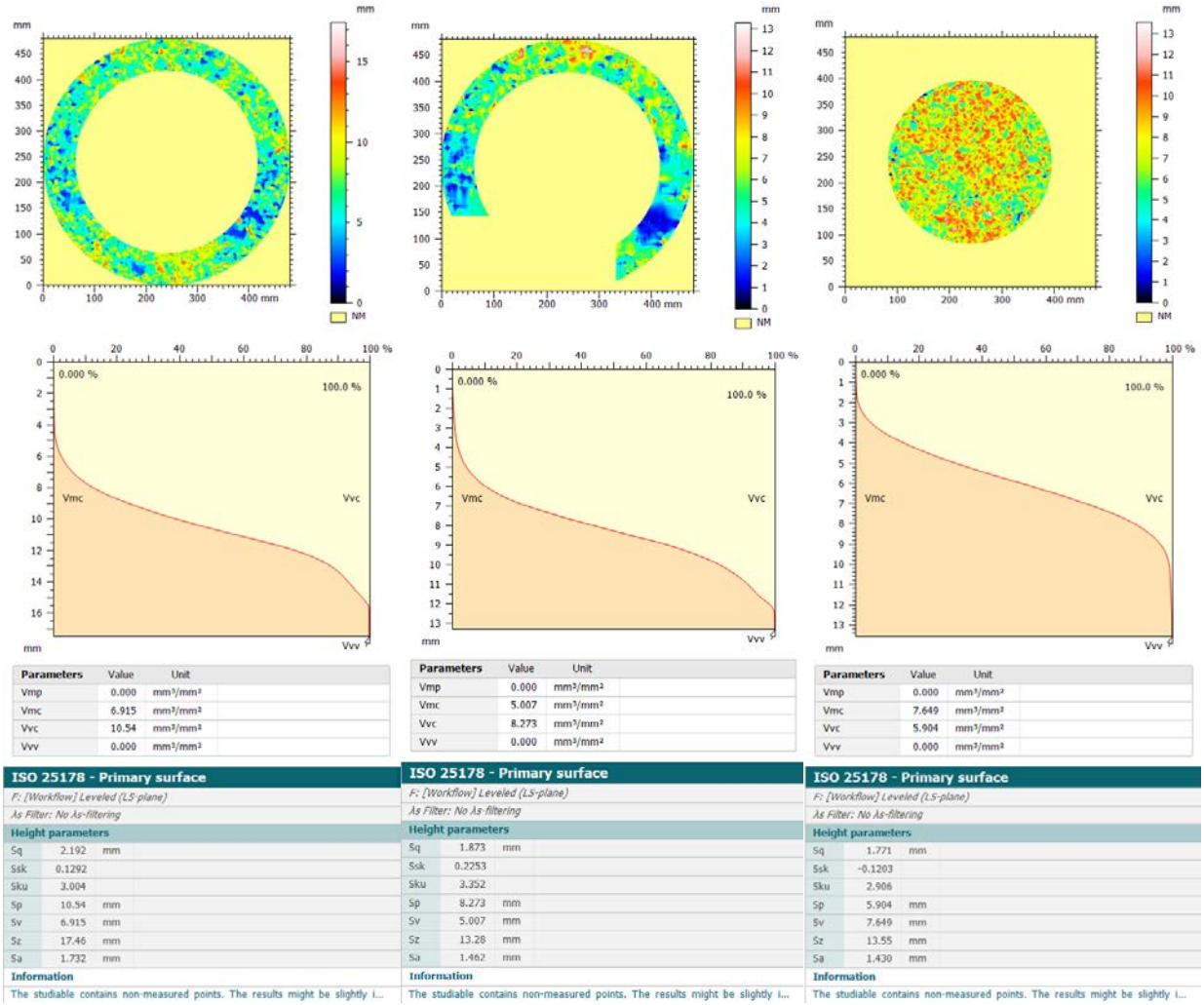

(a) (b) (c)

Fig. E.2 – 25R specimens surface analysis (a) after three snowplow applications, (b) after eight snowplow applications, and (c) outside the snowplow path.

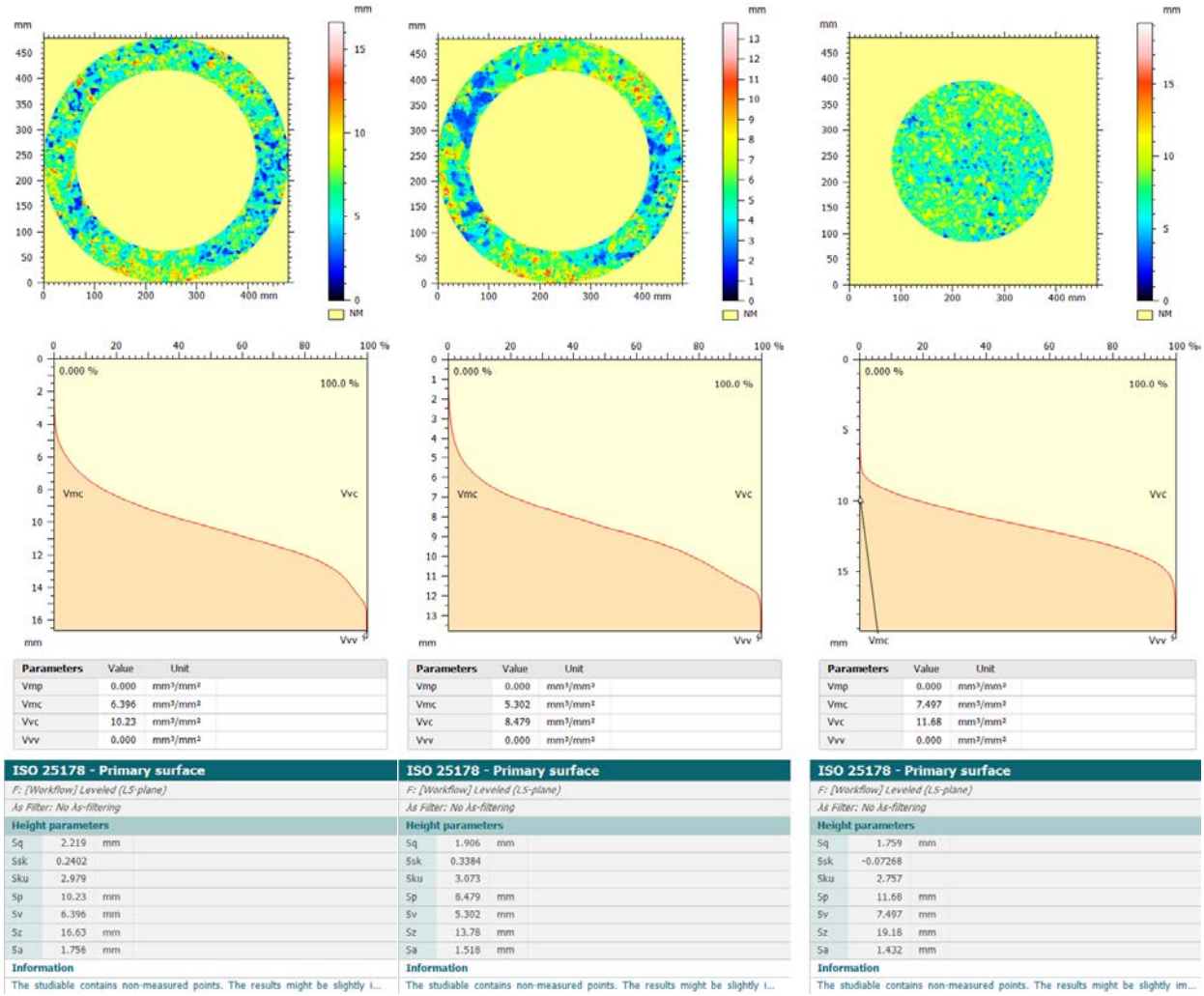

(a) (b) (c)

Fig. E.3 – 50R specimens surface analysis (a) after three snowplow applications, (b) after eight snowplow applications, and (c) outside the snowplow path.

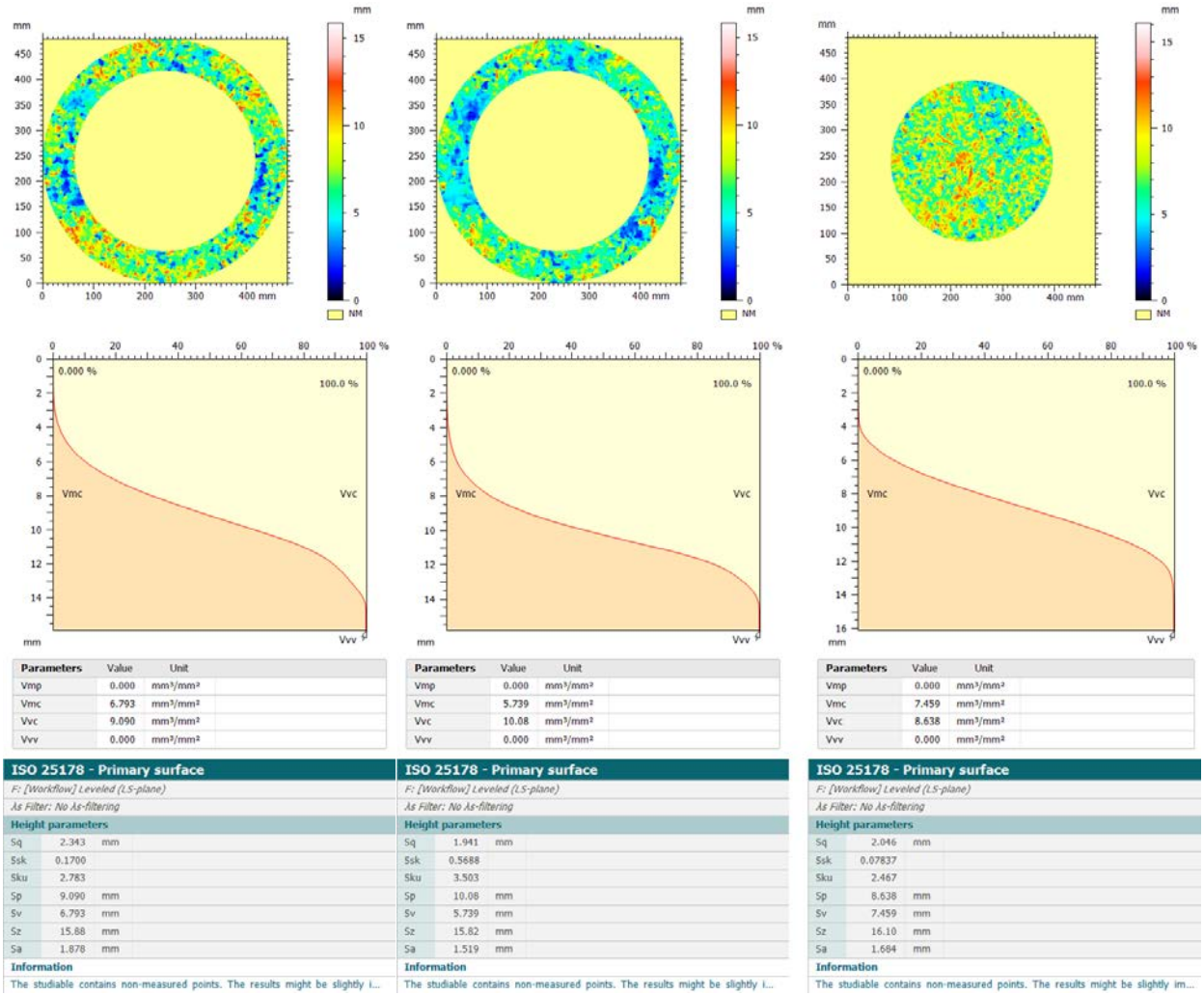

(a) (b) (c)

Fig. E.4 – 100R specimens surface analysis (a) after three snowplow applications, (b) after eight snowplow applications, and (c) outside the snowplow path.

Appendix F: Freezing and Thawing Test Procedure and Results

F.1. Freezing and Thawing Test Procedure

Fig. F.1 – Freezing and thawing test procedure.

F.2. Freezing and Thawing Results

Table F.1 – Volume of Aggregate Loss for Each Test Specimen after Every 5 Cycles.

Cycle	R100	T100	T75		T50	
	Rubber	Trap rock	Trap rock	Rubber	Trap rock	Rubber
	in^3	in^3	in^3		in^3	
5	0.209	0.074	0.104	0.017	0.114	0.124
10	0.220	0.172	0.070	0.045	0.030	0.068
15	0.102	0.038	0.019	0.000	0.055	0.000
20	0.407	0.042	0.076	0.068	0.089	0.153
25	0.017	0.001	0.019	0.028	0.006	0.002
30	0.023	0.016	0.023	0.011	0.001	0.020
35	0.141	0.018	0.039	0.038	0.042	0.002
40	0.122	0.031	0.023	0.010	0.013	0.005
45	0.083	0.079	0.019	0.009	0.013	0.039
50	0.144	0.057	0.065	0.027	0.008	0.075

Cycle	C100	C75		C50	
	Creek Gravel	Gravel	Rubber	Gravel	Rubber
	in^3	in^3		in^3	
5	0.187	0.173	0.011	0.030	0.040
10	0.223	0.262	0.034	0.093	0.062
15	0.216	0.082	0.000	0.057	0.000
20	0.424	0.046	0.011	0.128	0.079
25	0.039	0.020	0.028	0.011	0.006
30	0.052	0.029	0.009	0.021	0.028
35	0.032	0.062	0.016	0.023	0.022
40	0.018	0.029	0.002	0.029	0.050
45	0.315	0.138	0.004	0.137	0.044
50	0.265	0.107	0.009	0.246	0.046

F.3. SWTS Test Results from 3D Scanning

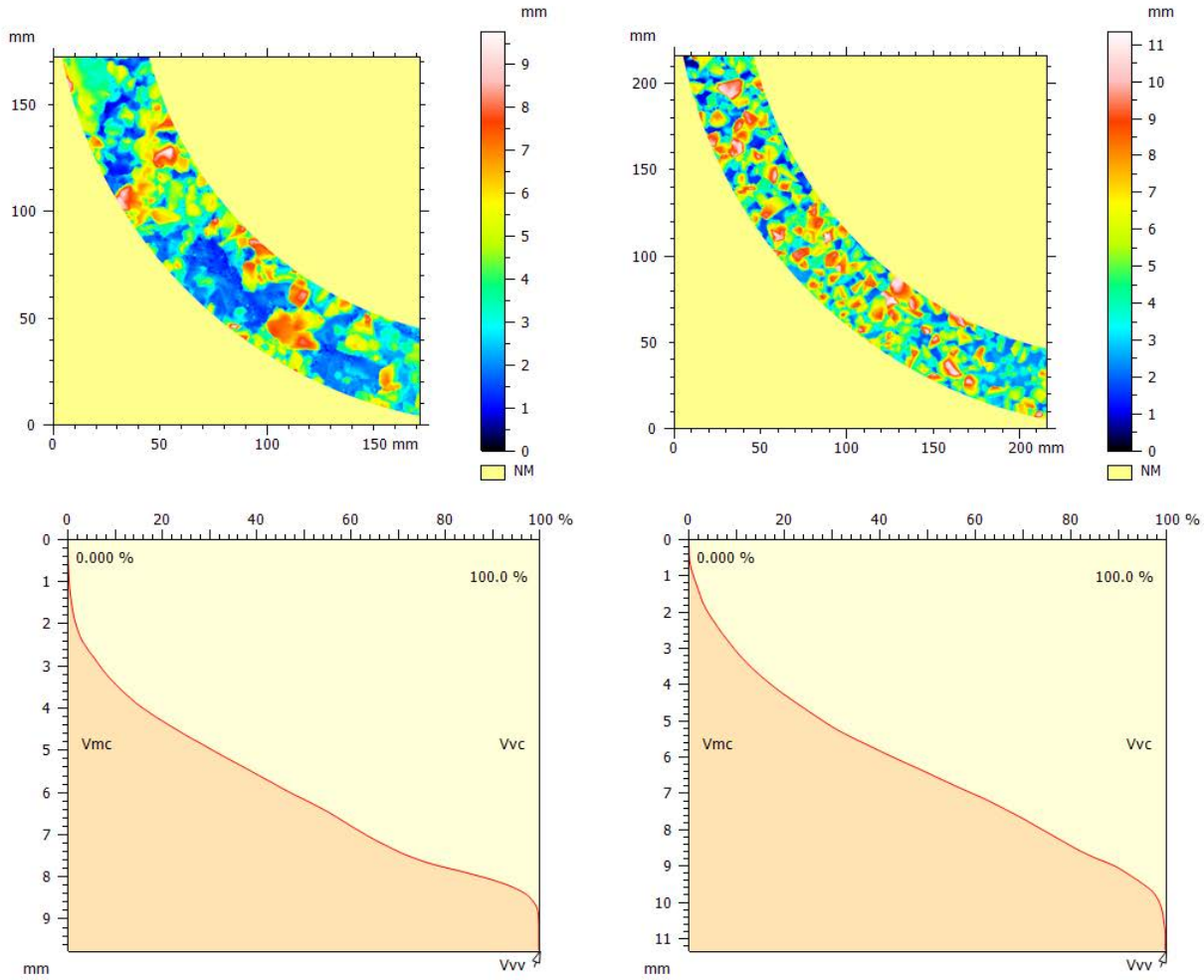

Parameters	Value	Unit
Vmp	0.000	mm³/mm²
Vmc	3.785	mm³/mm²
Vvc	5.982	mm³/mm²
Vvv	0.000	mm³/mm²

Parameters	Value	Unit
Vmp	0.000	mm³/mm²
Vmc	5.076	mm³/mm²
Vvc	6.275	mm³/mm²
Vvv	0.000	mm³/mm²

ISO 25178 - Primary surface		
F: [Workflow] Leveled (LS-plane)		
λs Filter: No λs-filtering		
Height parameters		
Sq	1.798	mm
Ssk	0.4797	
Sku	2.325	
Sp	5.982	mm
Sv	3.785	mm
Sz	9.767	mm
Sa	1.526	mm
Information		

ISO 25178 - Primary surface		
F: [Workflow] Leveled (LS-plane)		
λs Filter: No λs-filtering		
Height parameters		
Sq	2.230	mm
Ssk	0.3652	
Sku	2.412	
Sp	6.275	mm
Sv	5.076	mm
Sz	11.35	mm
Sa	1.837	mm
Information		

Fig. F.2 – SWTS test results for 50C specimen.

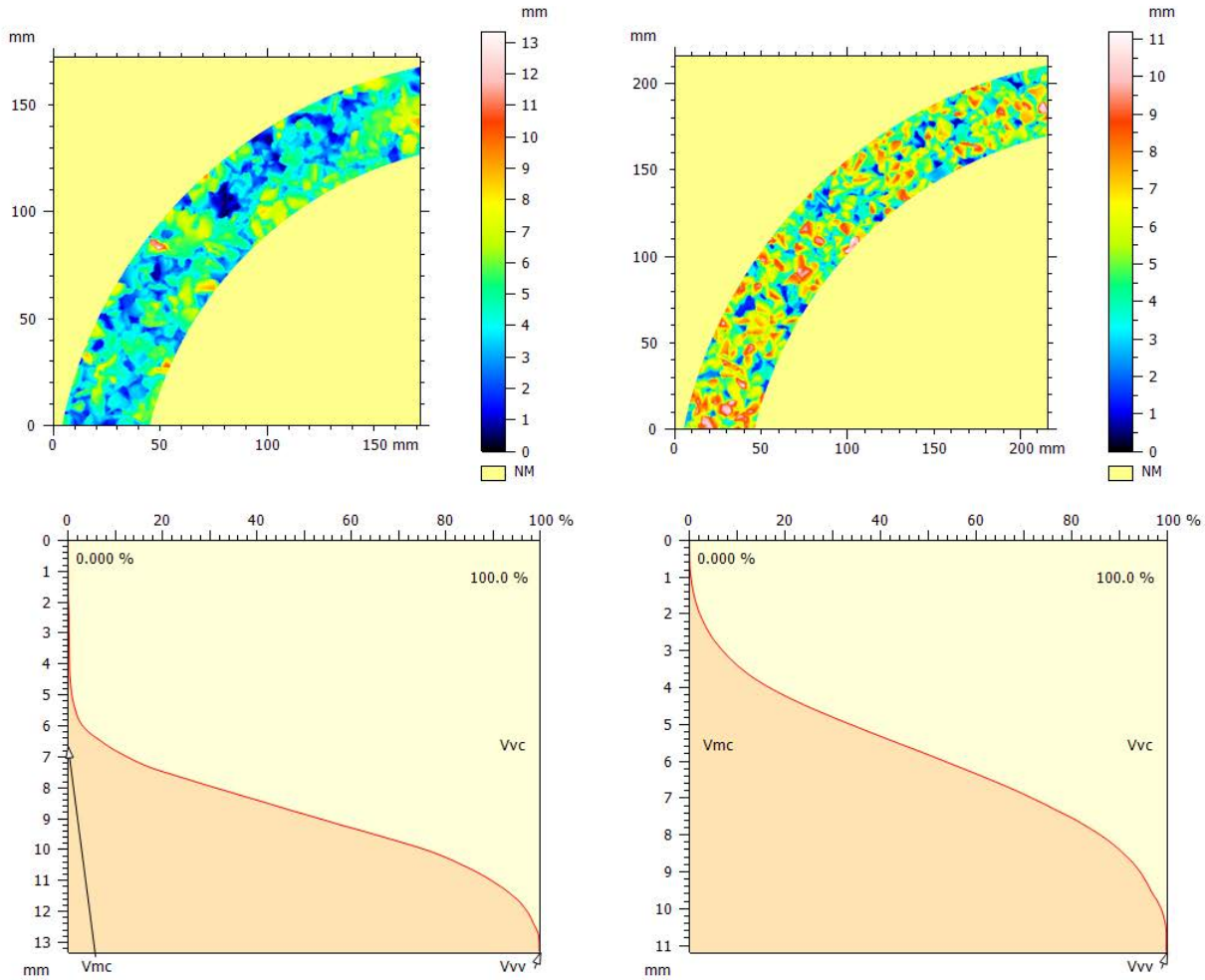

Parameters	Value	Unit
Vmp	0.000	mm³/mm²
Vmc	4.454	mm³/mm²
Vvc	8.877	mm³/mm²
Vvv	0.000	mm³/mm²

Parameters	Value	Unit
Vmp	0.000	mm³/mm²
Vmc	5.331	mm³/mm²
Vvc	5.865	mm³/mm²
Vvv	0.000	mm³/mm²

ISO 25178 - Primary surface		
F: [Workflow] Leveled (LS-plane)		
λs Filter: No λs-filtering		
Height parameters		
Sq	1.633	mm
Ssk	0.1079	
Sku	3.147	
Sp	8.877	mm
Sv	4.454	mm
Sz	13.33	mm
Sa	1.317	mm
Information		

ISO 25178 - Primary surface		
F: [Workflow] Leveled (LS-plane)		
λs Filter: No λs-filtering		
Height parameters		
Sq	1.917	mm
Ssk	-0.001254	
Sku	2.633	
Sp	5.865	mm
Sv	5.331	mm
Sz	11.20	mm
Sa	1.553	mm
Information		

Fig. F.3 – SWTS test results for 50T specimen.

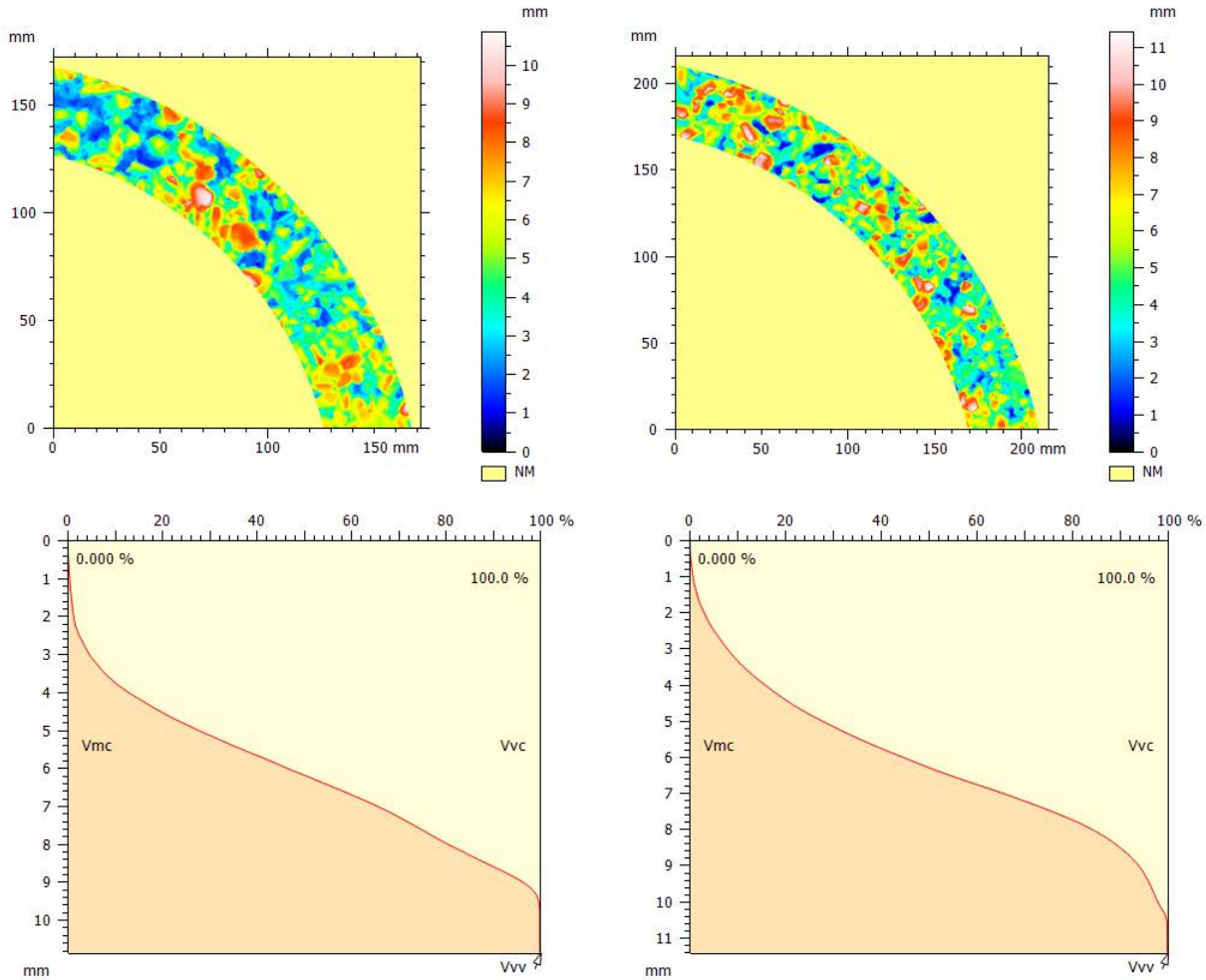

Parameters	Value	Unit
Vmp	0.000	mm³/mm²
Vmc	4.710	mm³/mm²
Vvc	6.154	mm³/mm²
Vvv	0.000	mm³/mm²

Parameters	Value	Unit
Vmp	0.000	mm³/mm²
Vmc	5.322	mm³/mm²
Vvc	6.099	mm³/mm²
Vvv	0.000	mm³/mm²

ISO 25178 - Primary surface		
F: [Workflow] Leveled (LS-plane)		
λs Filter: No λs-filtering		
Height parameters		
Sq	1.820	mm
Ssk	0.2500	
Sku	2.444	
Sp	6.154	mm
Sv	4.710	mm
Sz	10.86	mm
Sa	1.506	mm
Information		

ISO 25178 - Primary surface		
F: [Workflow] Leveled (LS-plane)		
λs Filter: No λs-filtering		
Height parameters		
Sq	1.987	mm
Ssk	0.3007	
Sku	2.788	
Sp	6.099	mm
Sv	5.322	mm
Sz	11.42	mm
Sa	1.594	mm
Information		

Fig. F.4 – SWTS test results for 75C specimen.

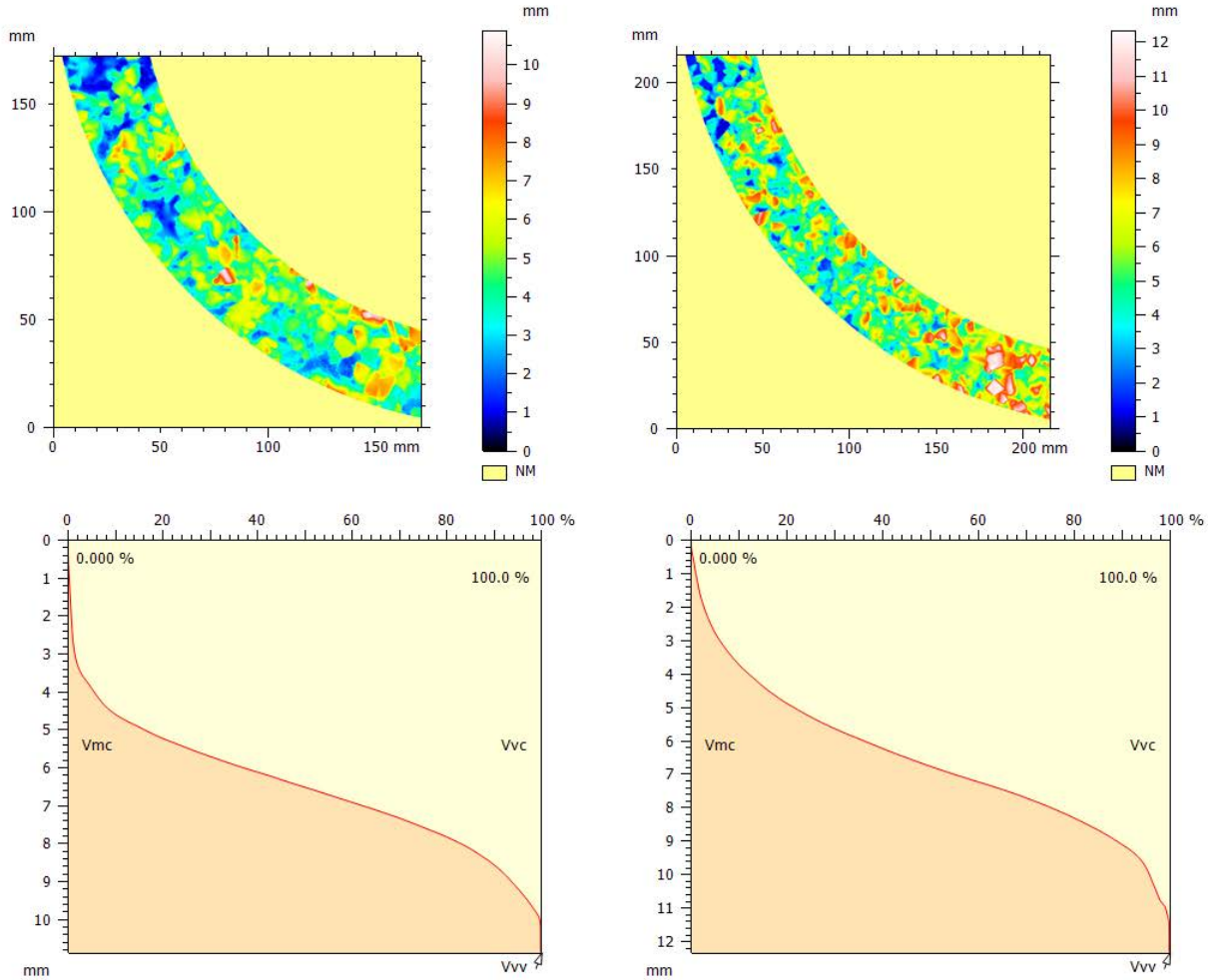

Parameters	Value	Unit
Vmp	0.000	mm³/mm²
Vmc	4.360	mm³/mm²
Vvc	6.523	mm³/mm²
Vvv	0.000	mm³/mm²

Parameters	Value	Unit
Vmp	0.000	mm³/mm²
Vmc	5.757	mm³/mm²
Vvc	6.578	mm³/mm²
Vvv	0.000	mm³/mm²

ISO 25178 - Primary surface		
F: [Workflow] Leveled (LS-plane)		
λs Filter: No λs-filtering		
Height parameters		
Sq	1.564	mm
Ssk	0.1924	
Sku	3.179	
Sp	6.523	mm
Sv	4.360	mm
Sz	10.88	mm
Sa	1.244	mm
Information		

ISO 25178 - Primary surface		
F: [Workflow] Leveled (LS-plane)		
λs Filter: No λs-filtering		
Height parameters		
Sq	2.098	mm
Ssk	0.3696	
Sku	3.046	
Sp	6.578	mm
Sv	5.757	mm
Sz	12.34	mm
Sa	1.659	mm
Information		

Fig. F.5 – SWTS test results for 75T specimen.

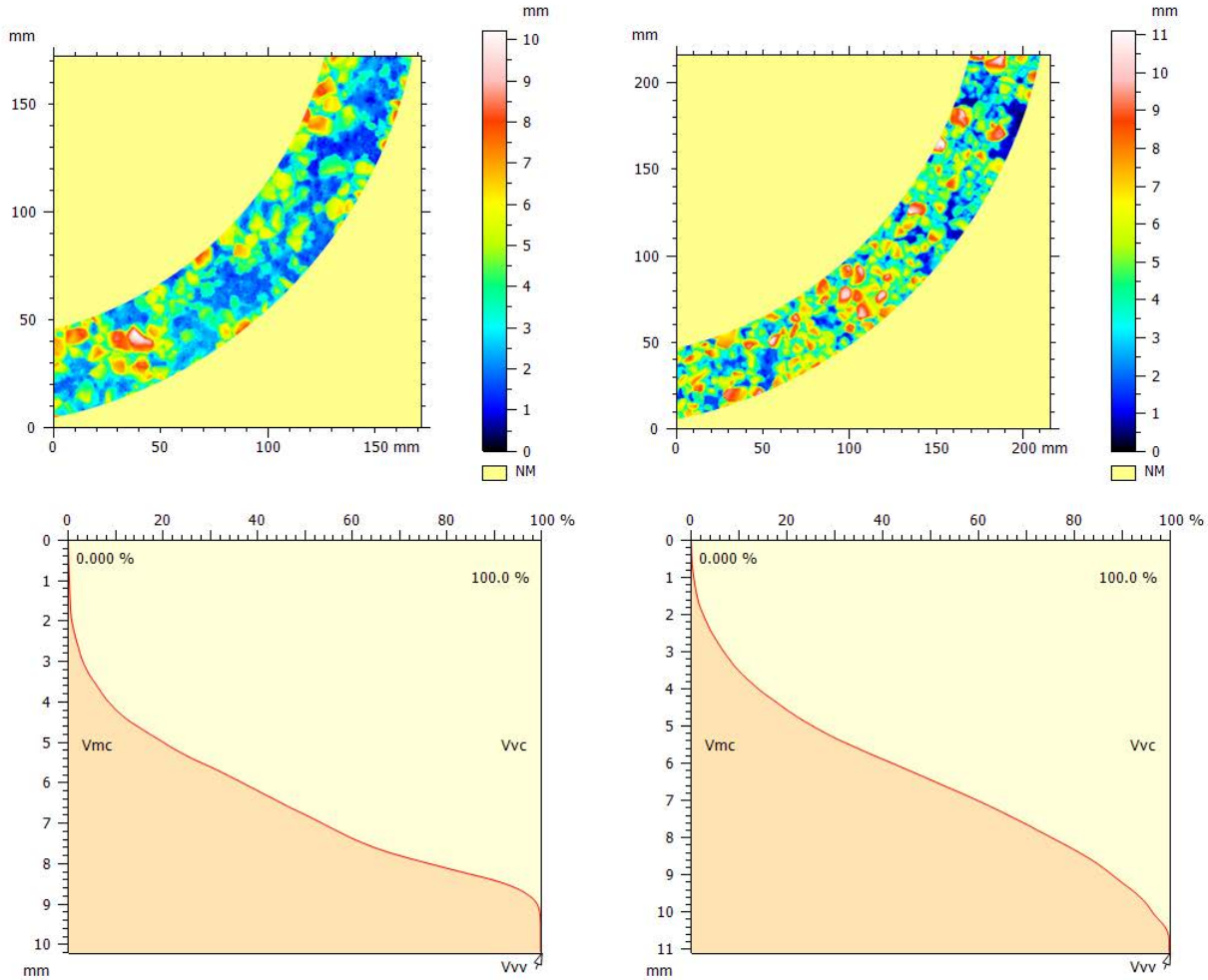

Parameters	Value	Unit
Vmp	0.000	mm³/mm²
Vmc	3.688	mm³/mm²
Vvc	6.525	mm³/mm²
Vvv	0.000	mm³/mm²

Parameters	Value	Unit
Vmp	0.000	mm³/mm²
Vmc	4.710	mm³/mm²
Vvc	6.398	mm³/mm²
Vvv	0.000	mm³/mm²

ISO 25178 - Primary surface		
F: [Workflow] Leveled (LS-plane)		
λs Filter: No λs-filtering		
Height parameters		
Sq	1.689	mm
Ssk	0.6521	
Sku	2.766	
Sp	6.525	mm
Sv	3.688	mm
Sz	10.21	mm
Sa	1.418	mm
Information		

ISO 25178 - Primary surface		
F: [Workflow] Leveled (LS-plane)		
λs Filter: No λs-filtering		
Height parameters		
Sq	2.126	mm
Ssk	0.2356	
Sku	2.547	
Sp	6.398	mm
Sv	4.710	mm
Sz	11.11	mm
Sa	1.730	mm
Information		

Fig. F.6 – SWTS test results for 100C specimen.

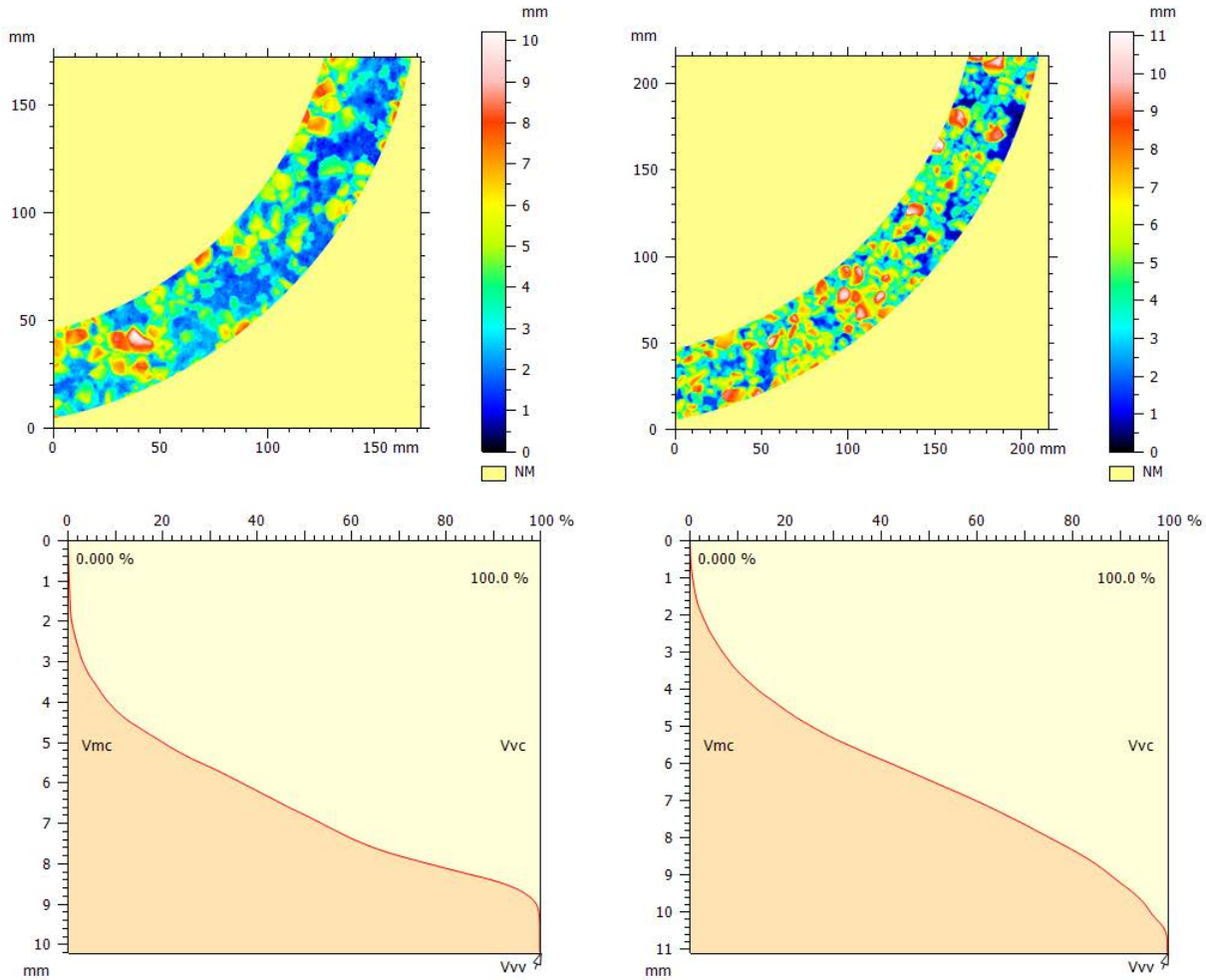

Parameters	Value	Unit
Vmp	0.000	mm³/mm²
Vmc	3.688	mm³/mm²
Vvc	6.525	mm³/mm²
Vvv	0.000	mm³/mm²

Parameters	Value	Unit
Vmp	0.000	mm³/mm²
Vmc	4.710	mm³/mm²
Vvc	6.398	mm³/mm²
Vvv	0.000	mm³/mm²

ISO 25178 - Primary surface		
F: [Workflow] Leveled (LS-plane)		
λs Filter: No λs-filtering		
Height parameters		
Sq	1.689	mm
Ssk	0.6521	
Sku	2.766	
Sp	6.525	mm
Sv	3.688	mm
Sz	10.21	mm
Sa	1.418	mm
Information		

ISO 25178 - Primary surface		
F: [Workflow] Leveled (LS-plane)		
λs Filter: No λs-filtering		
Height parameters		
Sq	2.126	mm
Ssk	0.2356	
Sku	2.547	
Sp	6.398	mm
Sv	4.710	mm
Sz	11.11	mm
Sa	1.730	mm
Information		

Fig. F.7 – SWTS test results for 100T specimen.

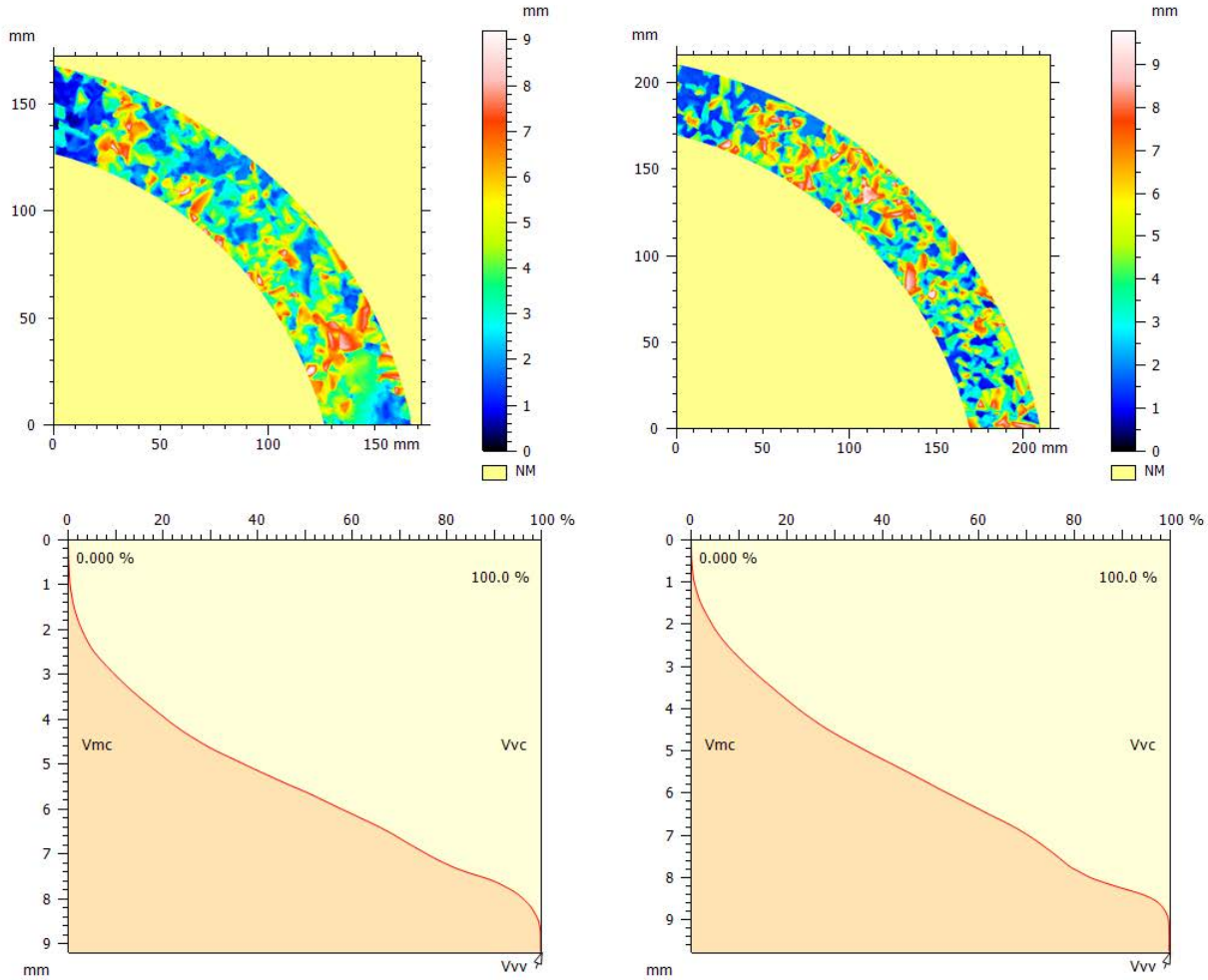

Parameters	Value	Unit
Vmp	0.000	mm³/mm²
Vmc	3.698	mm³/mm²
Vvc	5.500	mm³/mm²
Vvv	0.000	mm³/mm²

Parameters	Value	Unit
Vmp	0.000	mm³/mm²
Vmc	4.110	mm³/mm²
Vvc	5.670	mm³/mm²
Vvv	0.000	mm³/mm²

ISO 25178 - Primary surface		
F: [Workflow] Leveled (LS-plane)		
λs Filter: No λs-filtering		
Height parameters		
Sq	1.726	mm
Ssk	0.4014	
Sku	2.420	
Sp	5.500	mm
Sv	3.698	mm
Sz	9.198	mm
Sa	1.428	mm
Information		

ISO 25178 - Primary surface		
F: [Workflow] Leveled (LS-plane)		
λs Filter: No λs-filtering		
Height parameters		
Sq	2.008	mm
Ssk	0.3278	
Sku	2.209	
Sp	5.670	mm
Sv	4.110	mm
Sz	9.780	mm
Sa	1.681	mm
Information		

Fig. F.8 – SWTS test results for 100R specimen.

Appendix G: Field Implementation Evaluation Procedure and Results

G.1. Construction of The Field Test Sections

Fig. G.1 – Construction of the Rolla field test sections.

VOLVO

GRC

Fig. G.2 – Construction of the Boonville field test sections.

G.2. Field Investigation of Rolla Section

Fig. G.3 – Field investigation visits.

G.3. Sand Patch Test Results of Rolla Section

Table G.1 – Sand Patch Test Results at the Wheel Path

Visit date	Rubber %	V (ml)	V (mm^3)	D1 (mm)	D2 (mm)	D3 (mm)	D Average (mm)	MTD (mm)
9/22/2017	0	124	124000	250	251	253	252	2.50
	25	124	124000	229	231	231	230	2.98
	50	124	124000	223	218	215	219	3.30
12/18/2017	0	124	124000	320	322	325	322	1.52
	25	124	124000	283	289	293	288	1.90
	50	124	124000	279	276	274	276	2.07
1/25/2018	0	124	124000	343	336	331	337	1.39
	25	124	124000	310	305	316	310	1.64
	50	124	124000	280	282	285	282	1.98
5/9/2018	0	124	124000	359	355	350	355	1.26
	25	124	124000	323	334	343	333	1.42
	50	124	124000	315	318	323	319	1.55
6/28/2018	0	124	124000	373	377	378	376	1.12
	25	124	124000	346	333	356	345	1.33
	50	124	124000	324	337	331	331	1.44
10/15/2018	0	124	124000	472	470	465	469	0.72
	25	124	124000	350	358	365	358	1.23
	50	124	124000	353	370	339	354	1.26

Table G.2 – Sand Patch Test Results at the Snowplowing Path

Visit date	Rubber %	V (ml)	V (mm^3)	D1 (mm)	D2 (mm)	D3 (mm)	D Average (mm)	MTD (mm)
9/22/2017	0	124	124000	249	262	253	255	2.43
	25	124	124000	220	223	220	221	3.23
	50	124	124000	227	213	220	220	3.26
12/18/2017	0	124	124000	300	303	300	301	1.74
	25	124	124000	270	275	274	273	2.12
	50	124	124000	264	269	265	266	2.23
1/25/2018	0	124	124000	417	413	412	414	0.92
	25	124	124000	388	393	392	391	1.03
	50	124	124000	383	380	390	384	1.07
5/9/2018	0	124	124000	424	417	420	420	0.89
	25	124	124000	403	410	407	407	0.95
	50	124	124000	390	385	381	385	1.06
6/28/2018	0	124	124000	460	460	463	461	0.74
	25	124	124000	412	430	420	421	0.89
	50	124	124000	395	400	396	397	1.00
10/15/2018	0	124	124000	554	550	553	552	0.52
	25	124	124000	435	430	430	432	0.85
	50	124	124000	405	408	410	408	0.95